Development of a Cross-Section Methodology and a Real-Time Core Model for VVER-1000 Simulator Application

Zur Erlangung des akademischen Grades

Doktor der Ingenieurwissenschaften — Dr.-Ing.

der Fakultät für Maschinenbau

Karlsruher Institut für Technologie (KIT)

genehmigte

Dissertation

von

Emiliya Lyudmilova Georgieva

Tag der mündlichen Prüfung:	6 Juni, 2016
Hauptreferent:	Prof. Dr.- Ing. Robert Stieglitz, Karlsruher Institut für Technologie, Deutschland
Korreferent:	Prof. Dr. Kostadin Ivanov, North Carolina State University, USA

Development of a Cross-Section Methodology and a Real-Time Core Model for VVER-1000 Simulator Application

Emiliya L. Georgieva

A **dissertation** submitted to and approved by
The Department of Mechanical Engineering
Karlsruhe Institute of Technology (KIT)
in fulfilment for the degree of
Doctor of Engineering
(Doktor der Ingenieurwissenschaften — Dr.-Ing.)

Exam date: June 6, 2016

Reviewers: Prof. Robert Stieglitz,
Karlsruhe Institute of Technology, Germany
Prof. Kostadin Ivanov,
North Carolina State University, USA

Table of Contents

Acknowledgments ..... **ix**
Curriculum Vitae ..... **xi**
Declaration of Authorship ..... **xv**
Abstract ..... **xvii**
List of Tables ..... **xix**
List of Figures ..... **xxi**
List of Abbreviations ..... **xxix**
List of Symbols ..... **xxxi**
1. Introduction and background **1**
1.1 Introduction 1
1.2 Background information 1
1.3 Statement of objectives 2
1.4 Thesis outline 3
2. Evolution of fidelity requirements for nuclear power plant simulation **5**
2.1 Early simulators 5
2.2 Simulators for training of nuclear power plant personnel 6
2.2.1 Scope and fidelity of simulation 7
2.2.2 Modelling approaches 7
2.2.3 Core modelling approaches and features 8
2.3 Modern simulators 9
2.3.1 Fidelity of simulation 9
2.3.2 Models and codes 10
2.3.3 Core numerical methods and features 10
2.4 Simulator testing 11
2.5 Conclusions and a concept for tomorrow's simulator 13
3. Description of plant models **15**
3.1 Reactor core 16
3.2 Control rod drives 20
3.3 Thermal-hydraulics 24
3.4 Nuclear instrumentation 27
3.4.1 Ex-core instrumentation 27
3.4.2 Reactimeter 29

3.4.3 In-core monitoring system 30
3.5 Reactor protection and control system 33
3.5.1 Reactor Power Limiter 33
3.5.2 Reactor Power Controller 34
3.5.3 Control rod system 35
3.6 Steam and Power Conversion 35
4. Cross section library 39
4.1 Cross-section representation — an overview 39
4.2 Cross-section generation and modelling 43
4.2.1 Geometry and material composition 45
4.2.2 Instantaneous modelling 45
4.2.3 Burn-up and spectral history modelling 46
4.2.4 Assembly discontinuity factors 49
4.2.5 Four-dimensional look-up tables 49
4.2.6 Other parameters 49
4.2.7 Handling of cross-section tables 49
4.2.8 Accuracy of cross-section representation 50
4.3 Cycle-specific cross-section update procedure 50
4.4 Conclusion 53
5. Kozloduy 6 simulations 55
5.1 Rated power example 55
5.2 Transient example 70
5.3 Conclusion 80
6. Kalinin 3 Coolant Transient benchmark 81
6.1 Cross-section generation and modelling 81
6.1.1 Geometry and material composition 81
6.1.2 Instantaneous modelling 84
6.1.3 Burn-up and spectral history modelling 84
6.1.4 Assembly discontinuity factors 88
6.1.5 Four-dimensional tables 88
6.1.6 Other parameters 88
6.1.7 Handling of cross-section tables 89
6.2 Transient description 91
6.3 Simulation results and discussion 91
6.4 Lessons learnt 110

6.4.1 Primary coolant flow rate 110
6.4.2 Primary pressure 111
6.4.3 Fuel assembly pressure loss 112
6.4.4 Control Rods 112
6.4.5 K-1000-60/3000 turbine and turbine governor 112
6.4.6 ICMS core power reconstruction 113
6.5 Conclusion 116
7. Conclusions and future work 117
7.1 Conclusions 117
7.2 Recommendations for future work 118
8. Bibliography 119
Appendix A. Definitions 127
Appendix B. VVER-1000/V320 general description 131
Appendix C. Kozloduy 6 geometry and material composition 135
Appendix D. Kalinin 3 geometry and material composition 147
Appendix E. Kalinin 3 axial power profile for FAs with SPND 157

Acknowledgments

I would like to express my sincere thanks and appreciation to my advisors, Professor Robert Stieglitz and Professor Kostadin Ivanov for their support and assistance during the course of this work.

I'm thankful to Dr. Yavor Dinkov, Senior expert, Risk Engineering Ltd. who provided expertise which greatly assisted this work.

I would like to express my special gratitude to Mr. George Halev, Director of Nuclear Energy Directorate, Risk Engineering Ltd. for his support.

I thank the staff of the Reactor Core Physics Department of Kozloduy NPP for the expert support during the development and implementation of the VVER-1000 core model into Kozloduy 6 full-scope replica control room simulator.

My sincere thanks are due to the test operators, instructors and engineering staff of the Kozloduy NPP Training Centre for the support in data collection, development and analysis of testing scenarios.

Finally, I wish to thank Yavor and also my parents (Yordanka & Lyudmil) and my sister Gergana for their love, support, and encouragement.

Gergana, I could see the world through your eyes…

Emíliya L. Georgíeva

Curriculum Vitae

PERSONAL DATA

Name: **Emiliya L. Georgieva**

Place of birth: Pleven, Bulgaria

WORK EXPERIENCE

July 2012 to present

Senior Expert, Nuclear Power Engineering

Risk Engineering Ltd., 10 Vihren Str., 1618 Sofia, Bulgaria

March 2007 – January 2010

Nuclear Engineer

Institute for Nuclear Research and Nuclear Energy, Bulgarian Academy of Sciences (INRNE-BAS), 72 Tzarigradsko chausee Blvd., 1784 Sofia, Bulgaria

EDUCATION AND TRAINING

June 2012 – June 2016

PhD - Nuclear Engineering

Department of Mechanical Engineering

Karlsruhe Institute of Technology (KIT), Germany

February 2008 – July 2009

M. Sc. - Nuclear Power Engineering and Technologies

Faculty of Physics

Sofia University ‘St. Kliment Ohridski’, Bulgaria

October 2003 – July 2007

B. Sc. - Nuclear Engineering

Faculty of Physics

Sofia University ‘St. Kliment Ohridski’, Bulgaria

PUBLICATIONS

- Georgieva E., Dinkov Y., Ivanov K., Stieglitz R., Benchmarking the NEM Real-Time Core Model for VVER-1000 Simulator Application – Asymmetric Core, 24th International Conference on Nuclear Engineering (ICONE24), June 2016, Charlotte, North Carolina (USA).
- Georgieva E., Ivanov K., Stieglitz R., Modelling of TVSA Fuel Assemblies with HELIOS Lattice Physics Code in the frame of OECD/NEA Kalinin-3 Coolant Transient Benchmark, Conference Proceedings of TopFuel 2015 – Oral presentations – Part II, pp. 297-306, September 2015, Zurich (Switzerland).
- Georgieva E., Ivanov K., Stieglitz R., Explicit Modeling of a VVER-1000 Radial Reflector by a Ring of Assembly-Size Nodes, Proceedings of ICAPP 2015, pp. 1834–1839, May 2015, Nice (France).
- Georgieva E., Dinkov Y., Ivanov K., A Cycle-Specific Cross-Section Update for Real-Time Simulation of VVER-1000 Core, Progress of Nuclear Energy Journal, Volume 74, pp. 222-231, July 2014.
- Georgieva E., Dinkov Y., A Real-Time Core Model for Kozloduy 6 Full-Scope Replica Control Room Simulator, Proceedings of the 10th International Conference WWER Fuel Performance, Modelling and Experimental Support, pp. 147-153, September 2013, Sandanski (Bulgaria).
- Borisov E., Philipov S., Georgieva E., Donov J., Velev V., Analysis of the Possibility for Boron Dilution in Case of Primary to Secondary Leak for VVER-1000 (V320) Reactors, Proceedings of the XVIII National Scientific Conference with International Participation FPEPM 2013, Vol. I, September 2013, pp. 54-61, Sozopol (Bulgaria) – in Bulgarian.
- Georgieva E., Borisov E., Mancheva K., Dinkov Y., Nuclear Steam Supply System Physics Upgrade of the Kozloduy 6 Full-Scope Replica Control Room Simulator, Science and Technology Journal of the Bulgarian Nuclear Society, Vol. 16, No 2, pp. 2-9, December 2011 – in Bulgarian.
- Stefanova A., Atanasova B., Georgieva E., Groudev P., In-vessel Phase Investigation of SBO Severe Accident for VVER-1000/V320 with ASTEC V1.3R2 Integral Computer Code, Science and Technology Journal of the Bulgarian Nuclear Society, Vol. 14, No 1, pp. 49-53, June 2010 – in Bulgarian.
- Groudev P., Georgieva E., Loss of 'Core cooling' at low power and cold condition of VVER-1000/V320, Progress in Nuclear Energy, Volume 52 Number 2, pp. 229-235, March 2010.

- Georgieva E., Pavlova M., Andreeva M., Groudev P., Investigation of Critical Safety Function 'Core Cooling' in Case of LOCA with Dy 100 mm and Dy 250 mm at Shut down Condition of VVER-1000, Science and Technology Journal of the Bulgarian Nuclear Society, Vol. 13, No 2, pp. 19 – 23, September 2009 – in Bulgarian.
- Georgieva E., Groudev P., VVER – 1000 SBLOCA 60 mm Calculation with ASTEC V1.3 Integral Computer Code, Science and Technology Journal of the Bulgarian Nuclear Society, Vol. 12, No 1, pp. 27 – 33, October 2008 – in Bulgarian.

Declaration of Authorship

I, Emiliya Lyudmilova Georgieva hereby declare, that the work presented in the PhD thesis is my own. I hereby confirm that where I have consulted the published work of others, this is always clearly attributed, where I have quoted from the work of others, the source is always given. I declare that I observed the statutes of the Karlsruhe Institute of Technology (formerly University of Karlsruhe) to ensure good scientific practice in its current version.

Eidesstattliche Erklärung

Hiermit erkläre ich, Emiliya Lyudmilova Georgieva, dass ich die vorliegende Arbeit selbstständigangefertigt und keine anderen als die angegebenen Quellen und Hilfsmittel benutzt sowie die wörtlich und inhaltlich übernommenen Stellen als solche kenntlich gemacht unddie Satzung des Karlsruher Instituts für Technologie (vormals Universität Karlsruhe (TH)) zurSicherung guter wissenschaftlicher Praxis in der jeweils gültigen Fassung beachtet habe.

Date/Datum: September 14, 2016

Signiture/Unterschrift: Emiliya L. Georgieva

Abstract

The full-scope replica control room simulator with the reference unit – Kozloduy 6 (a Russian-style Pressurized Water Reactor VVER-1000/V320 series) is originally supplied with STK-VVER core model for steady-state and transient simulation in real time with 1.5 energy groups in a Hexagonal-Z geometry across the whole reactor core. No cycle specific capability is provided.

While the concept of high-fidelity cycle-specific real-time reactor core simulation became feasible for Pressurized Water Reactor and Boiling Water Reactor operators about year 2000 with commercially available nuclear reactor analysis tools, it was not the case for operators of other plant designs, like VVER.

This PhD work is a response to a necessity for development, implementation, and qualification of an advanced core calculation methodology with cycle-specific capability for VVER-1000 simulator application.

The important novel academic contributions could be summarized as follows.

a. An improved cross-section modelling methodology and a cycle-specific cross-section update procedure are developed to meet fidelity requirements applicable to a cycle-specific reactor core simulation, as well as particular customer needs and practices supporting VVER-1000 operation and safety.
b. An improved real-time version of the Nodal Expansion Method code (NEM) is developed and implemented into Kozloduy 6 full-scope replica control room simulator.

The outcome of this PhD work has been found its direct application in the industry. The core model for VVER-1000 simulator application supplemented with cross-section libraries, tools and procedures for cycle-specific core update is used by Kozloduy NPP personnel with consistently good (accurate and computational efficient in real time) results. Many more steady-state and transient simulations have been performed during rigorous acceptance tests or periodic functional tests of the simulator and the simulator is in routine operation monitored by experienced plant staff. The core model meets all current simulator fidelity requirements. An illustration of steady-state and transient simulation results is presented in this PhD work.

Another phase of validation of the Kozloduy 6 simulator core model, cross-section libraries, tools and procedures for cycle-specific core update with actual plant data from Kalinin 3 (OECD/NEA

Kalinin 3 Coolant Transient Benchmark) is presented in this PhD work. Kalinin 3 transient provides an opportunity to apply the methodology and the core model described in this work to another VVER-1000 unit on a scenario with an asymmetric core load.

The historical sequence is preserved in the presentation of the thesis.

Keywords: VVER, Real-time simulation, Core model, Cross sections.

List of Tables

Table 3.3-1: Thermal-hydraulics nodalization summary of the nuclear steam supply system model for the Kozloduy 6 simulator 24

Table 3.4-1: Operating range of the ex-core neutron flux monitoring system (AKNP-7-02K) 27

Table 3.5-1: Reactor Power Limiter setpoints according to plant configuration 33

Table 4.2-1: Range of values of the feedback parameters and reference values for spectral history used for generation of cross-section library tables 46

Table 4.3-1: Margin of deviations between licensing calculation and ICMS readings.....53

Table 5.1-1: 17^{th} fuel cycle of Kozloduy 6 – Comparison between simulation and plant data (ICMS) – Brief statistics of deviations in assembly power at the BOC, MOC and EOC 56

Table 5.2-1: Time history of the Kozloduy 6 transient of inadvertent MSIV closure and switching off MCP 70

Table 5.2-2: Kozloduy 6 MSIV closure and switching off MCP transient – Comparison between simulation and plant data (ICMS) – Brief statistics of deviations in assembly power at the start and the end of the transient.....73

Table 6.1-1: Range of values of the feedback parameters and reference values for spectral history used for generation of Kalinin 3 cross-section library tables 84

Table 6.1-2: Average exposure per fuel assembly in one-sixth core used in Kalinin 3 cross-section library.....86

Table 6.2-1: Time history of the Kalinin 3 transient 91

Table 6.3-1: Kalinin 3 transient – Comparison between simulation and plant data (ICMS) – Brief statistics of deviations in assembly power during the transient 94

List of Figures

Figure 3.1-1: Scheme of the basic one-sixth building block of the VVER-1000/V320 reactor core model (olive green – FA cells, grey – reflector cells). Numbers indicate nodes in radial (from 1 to 29) and axial plane 19

Figure 3.2-1: Scheme of the fuel assembly cross-section with positions of fuel pins, guide tubes and instrument channel 21

Figure 3.2-2: Scheme of the cluster of absorber elements with spring retainer (vertical view with a partial cut through spring retainer — left; view from above — right). 22

Figure 3.2-3: Vertical cross section of an absorber element (dimensions in mm). 23

Figure 3.3-1: An illustration of Kozloduy 6 model primary thermal-hydraulics nodalization (Reactor pressure vessel and an one primary coolant loop — left; Pressurizer — right; Positive flow directions are shown with arrows).....25

Figure 3.3-2: Scheme of Kozloduy 6 reactor core nodalization (horizontal — left; vertical – right)26

Figure 3.3-3: An illustration of thermal-hydraulics / neutronics coupling scheme for the Kozloduy 6 simulator model (thermal hydraulic sector 1 — heat structure — core). Heat Structure 10401 with 20 heat slabs represents all the fuel elements in one-fourth sector of the core.....26

Figure 3.4-1: Map of Kozloduy 6 ex-core instrument wells locations around reactor core (Andrushechko, 2010) 28

Figure 3.4-2: Map of Kozloduy 6 control rod and in-core instrumentation locations. There are three types of in-core instrumentation assemblies used: (N) SPND array with 7 axial positions; (T) coolant thermocouple above the active part of the fuel assembly; (NT) SPND array with coolant thermocouple, combined.....32

Figure 4.1-1: Scheme of the LWR neutronic core calculation path.....39

Figure 4.2-1: Flowchart of cross-section generation and modelling methodology.....44

Figure 4.2-2: Composition numbers in axial layers by assembly type.....48

Figure 4.3-1: Flowchart of the cycle-specific cross-section update procedure.....52

Figure 5.1-1: 17th fuel cycle pattern of the Kozloduy 6 — an one-sixth symmetry representation with FA type, enrichment and year in the core 55

Figure 5.1-2: 17th fuel cycle of Kozloduy 6 — Comparison between simulation, plant data (ICMS) and core design calculation (BIPR-7A) — Assembly-wise power peaking factors at 5.82 EFPD....57

Figure 5.1-3: 17th fuel cycle of Kozloduy 6 — Comparison between simulation and plant data (ICMS) — Deviation in assembly-wise power peaking factor [%] at 5.82 EFPD (magnitude of deviation is proportional to bubble diameter; coloured — positive, transparent — negative) 58

Figure 5.1-4: 17th fuel cycle of Kozloduy 6 — Comparison between simulation and core design calculation (BIPR-7A) — Deviation in assembly-wise power peaking factor [%] at 5.82 EFPD (magnitude of deviation is proportional to bubble diameter; coloured — positive, transparent — negative).....59

Figure 5.1-5: 17th fuel cycle of Kozloduy 6 — Comparison between plant data (ICMS) and core design calculation (BIPR-7A) — Deviation in assembly-wise power peaking factor [%] at 5.82 EFPD (magnitude of deviation is proportional to bubble diameter; coloured — positive, transparent — negative).....60

Figure 5.1-6: 17th fuel cycle of Kozloduy 6 — Comparison between simulation, plant data (ICMS) and core design calculation (BIPR-7A) — Assembly-wise power peaking factors at 160.72 EFPD61

Figure 5.1-7: 17th fuel cycle of Kozloduy 6 — Comparison between simulation and plant data (ICMS) — Deviation in assembly-wise power peaking factor [%] at 160.72 EFPD (magnitude of deviation is proportional to bubble diameter; coloured — positive, transparent — negative) 62

Figure 5.1-8: 17th fuel cycle of Kozloduy 6 — Comparison between simulation and core design calculation (BIPR-7A) — Deviation in assembly-wise power peaking factor [%] at 160.72 EFPD (magnitude of deviation is proportional to bubble diameter; coloured — positive, transparent — negative).....63

Figure 5.1-9: 17th fuel cycle of Kozloduy 6 — Comparison between plant data (ICMS) and core design calculation (BIPR-7A) — Deviation in assembly-wise power peaking factor [%] at 160.72 EFPD (magnitude of deviation is proportional to bubble diameter; coloured — positive, transparent — negative).....64

Figure 5.1-10: 17th fuel cycle of Kozloduy 6 — Comparison between simulation, plant data (ICMS) and core design calculation (BIPR-7A) — Assembly-wise power peaking factors at 300.58 EFPD65

Figure 5.1-11: 17th fuel cycle of Kozloduy 6 — Comparison between simulation and plant data (ICMS) — Deviation in assembly-wise power peaking factor [%] at 300.82 EFPD (magnitude of deviation is proportional to bubble diameter; coloured — positive, transparent — negative).....66

Figure 5.1-12: 17th fuel cycle of Kozloduy 6 — Comparison between simulation and core design calculation (BIPR-7A) — Deviation in assembly-wise power peaking factor [%] at 300.82 EFPD (magnitude of deviation is proportional to bubble diameter; coloured — positive, transparent — negative).....67

Figure 5.1-13: 17th fuel cycle of Kozloduy 6 — Comparison between plant data (ICMS) and core design calculation (BIPR-7A) — Deviation in assembly-wise power peaking factor [%] at 300.82 EFPD (magnitude of deviation is proportional to bubble diameter; coloured — positive, transparent — negative).....68

Figure 5.2-1: 18th fuel cycle pattern of the Kozloduy 6 — an one-sixth symmetry representation with FA type, enrichment and year in the core 71

Figure 5.2-2: Power excursion (ex-core detectors, power range, linear) and Control Rod Bank Nos. 9 and 10 positions. Plant data are shown with symbols (YC00N_NIK ex-core detectors, average; SZ9A_A position of control rod bank No. 9; SZ10A_A position of control rod bank No. 10). Simulation data are shown with lines (N(RD2) ch 4, ch 5 and ch 6 – power, ex-core detectors, power range, linear, set 2; (9) 14-29 position of control rod 14-29, bank No. 9; (10) 08-35 position of control rod 08-35, bank No. 10).....72

Figure 5.2-3: Kozloduy 6 MSIV closure and switching off MCP transient — Comparison between simulation and plant data (ICMS) — Assembly-wise power peaking factor at the start of the transient.....74

Figure 5.2-4: Kozloduy 6 MSIV closure and switching off MCP transient — Comparison between simulation and plant data (ICMS) — Deviation in assembly-wise power peaking factor [%] at the start of the transient (magnitude of deviation is proportional to bubble diameter; coloured — positive, transparent — negative).....75

Figure 5.2-5: Kozloduy 6 MSIV closure and switching off MCP transient — Comparison between simulation and plant data (ICMS) — Assembly-wise power peaking factor at the end of the transient.....76

Figure 5.2-6: Kozloduy 6 MSIV closure and switching off MCP transient — Comparison between simulation and plant data (ICMS) — Deviation in assembly-wise power peaking factor [%] at the start of the transient (magnitude of deviation is proportional to bubble diameter; coloured — positive, transparent — negative).....77

Figure 5.2-7: Axial power profiles (normalized for rated power conditions, whole core) at 0 s (left), 70 s (middle) and 300 s (right). Data from Kozloduy 6 ICMS are shown with symbols (7-layer power reconstruction).....79

Figure 5.2-8: Kozloduy 6 ICMS thermal power estimation during the transient. Plant data are shown with symbols (YCN_A reactor coolant system thermal power, weighed estimation; YC00N_NIK power, ex-core detectors, average; YAN_S power, primary loop thermal balance; YBN_S power, SG secondary side thermal balance). Simulation data are shown with thick lines (Core Power, NEM; Power (1-2) rate of heat transfer through SG tube bundles, RELAP5-HD).....79

Figure 6.1-1: 1 bis fuel cycle pattern of the Kalinin 3 — an one-sixth symmetry representation with FA type, enrichment and year in the core.....82

Figure 6.1-2: Map of Kalinin 3 control rod and in-core instrumentation locations. There are three types of in-core instrumentation assemblies used: (N) SPND array with 7 axial positions; (T) coolant thermocouple above the active part of the fuel assembly; (NT) SPND array with coolant thermocouple, combined.....83

Figure 6.1-3: RMS error distribution [%] of assembly exposure for each of the 6 sixty-degree core sectors. Error in sector 4 is zero because cross-section set 2 fits exactly this sector. Worst case is sector 5 with RMS deviation of 0.52 %.....87

Figure 6.1-4: RMS error distribution [%] of assembly exposure for each of the 12 thirty-degree core sectors. Error in sector 7 is zero because cross-section set 2 covers whole sector. Worst case is sector 9 with RMS deviation of 0.56 %.....87

Figure 6.1-5: Comparison (cross-section library vs BIPR-8) of the sector-average exposure [MWd/kgU] in 12 thirty-degree core sectors.....88

Figure 6.1-6: Handling of Kalinin 3 cross-section tables. Coloured area is covered by cross-section set 2 while remaining part of the core is covered by set 1. Outermost layer shown is radial reflector 90

Figure 6.3-1: Power excursion (ex-core detectors, power range, linear) and Control Rod Bank Nos. 9 and 10 positions. Plant data are shown with symbols (31YCS00FX005AXQ2 ex-core detector 2; 31YCS00FX005BXQ2 ex-core detector 12; 33YCS00FX006AXQ2 ex-core detector 7; 30YVS00FG013XQ01 position of control rod 14-25, bank No. 9; 30YVS00FG009XQ01 position of control rod 10-23, bank No. 10). Simulation data are shown with lines (N OR2 (linear) ch 1, ch 2 and ch 3 – ex-core detectors, power range, linear, set 1; CR 12-29 (10) control rod 12-29, bank No. 10; CR 08-29 (9) control rod 08-29, bank No. 9) 92

Figure 6.3-2: Axial offset. Data recorded by Kalinin 3 ICMS are shown with symbols (30YQR00FU005XQ01 axial offset of SPND; 30YQR00FU901XQ01 axial offset of the reconstructed 3D power distribution). Simulation data are shown with a tick line 93

Figure 6.3-3: Kalinin 3 transient — Comparison between simulation and plant data (ICMS) — Assembly-wise power peaking factors at the start of the transient 95

Figure 6.3-4: Kalinin 3 transient — Comparison between simulation and plant data (ICMS) — Deviation in assembly-wise power peaking factors [%] at the start of the transient (magnitude of deviation is proportional to bubble diameter; coloured — positive, transparent — negative).....96

Figure 6.3-5: Kalinin 3 transient — Comparison between simulation and plant data (ICMS) — Assembly-wise power peaking factors at 45 s 97

Figure 6.3-6: Kalinin 3 transient — Comparison between simulation and plant data (ICMS) — Deviation in assembly-wise power peaking factors [%] at 45 s (magnitude of deviation is proportional to bubble diameter; coloured — positive, transparent — negative).....98

Figure 6.3-7: Kalinin 3 transient — Comparison between simulation and plant data (ICMS) — Assembly-wise power peaking factors at 90 s 99

Figure 6.3-8: Kalinin 3 transient — Comparison between simulation and plant data (ICMS) — Deviation in assembly-wise power peaking factors [%] at 90 s (magnitude of deviation is proportional to bubble diameter; coloured — positive, transparent — negative).....100

Figure 6.3-9: Kalinin 3 transient — Comparison between simulation and plant data (ICMS) — Assembly-wise power peaking factors 150 s 101

Figure 6.3-10: Kalinin 3 transient — Comparison between simulation and plant data (ICMS) — Deviation in assembly-wise power peaking factors [%] at 150 s (magnitude of deviation is proportional to bubble diameter; coloured — positive, transparent — negative) 102

Figure 6.3-11: Kalinin 3 transient — Comparison between simulation and plant data (ICMS) — Assembly-wise power peaking factors the end of the transient 103

Figure 6.3-12: Kalinin 3 transient — Comparison between simulation and plant data (ICMS) — Deviation in assembly-wise power peaking factors [%] at the end of the transient (magnitude of deviation is proportional to bubble diameter; coloured — positive, transparent — negative) 104

Figure 6.3-13: Kalinin 3 transient — Evolution of sector-average power distribution in 12 thirty-degree core sectors — Simulation data 106

Figure 6.3-14: Kalinin 3 transient — Evolution of sector-average power distribution in 12 thirty-degree core sectors — Kalinin 3 ICMS 106

Figure 6.3-15: RMS deviation [%] of assembly power for each of the 12 thirty-degree core sectors 107

Figure 6.3-16: Axial power profile for FA 27 (12-21) at 0, 45, 90 and 300 s. Data recorded by Kalinin 3 ICMS are shown with symbols — 30YQR04FX027, 30YQR06FX027 (LHR readings normalized to peaking factor). 108

Figure 6.3-17: Axial power profile for FA 30 (12-27) at 0, 45, 90 and 300 s. Data recorded by Kalinin 3 ICMS are shown with symbols — 30YQR04FX030, 30YQR06FX030 (LHR readings normalized to peaking factor). 108

Figure 6.3-18: Axial power profile for FA 81 (08-27) at 0, 45, 90 and 300 s. Data recorded by Kalinin 3 ICMS are shown with symbols — 30YQR04FX081, 30YQR06FX081 (LHR readings normalized to peaking factor). 108

Figure 6.3-19: Axial power profile for FA 96 (07-30) at 0, 45, 90 and 300 s. Data recorded by Kalinin 3 ICMS are shown with symbols — 30YQR04FX096, 30YQR06FX096 (LHR readings normalized to peaking factor). 109

Figure 6.3-20: Axial power profile for FA 134 (04-31) at 0, 45, 90 and 300 s. Data recorded by Kalinin 3 ICMS are shown with symbols — 30YQR04FX134, 30YQR06FX134 (LHR readings normalized to peaking factor). 109

Figure 6.3-21: Axial power profile for FA 150 (02-23) at 0, 45, 90 and 300 s. Data recorded by Kalinin 3 ICMS are shown with symbols — 30YQR04FX150, 30YQR06FX150 (LHR readings normalized to peaking factor). 109

Figure 6.4-1: Reactor pressure vessel coolant mass flow rate — comparison between RELAP5-HD simulation and Kalinin 3 ICMS record. Data recorded by Kalinin 3 ICMS (signal 30YCR10FF903XQ02 in the plant data base) are shown with symbols 114

Figure 6.4-2: An illustration of the magnitude of variation of Kalinin 3 reactor system thermal power during the transient. Kalinin 3 ICMS signals are shown with symbols (30YQR00FX001XQ01 reactor thermal power from SPND; 30YCR00FX001XQ01 ex-core detectors; 30RLR00FX903XQ03 thermal balance of steam generators secondary side; 30YAR00FX001XQ01 primary coolant loop thermal balance). Simulation data are shown with tick lines for comparison (Core thermal power, NEM; SG primary-to-secondary, RELAP5-HD; Power from SPND model) 115

List of Abbreviations

ADF	Assembly Discontinuity Factor
ADV	Atmospheric Dump Valve
BOC	Beginning of Cycle
BOP	Balance of Plant
BWR	Boiling Water Reactor
CFD	Computational Fluid Dynamics
CPU	Central Processing Unit
CR	Control Rod
DNBR	Departure from Nucleate Boiling Ratio
EFPD	Effective Full-Power Days
ENDF	Evaluated Nuclear Data File
EOC	End of Cycle
ESFAS	Engineered Safety Feature Automation System
FA	Fuel Assembly
IAPWS	International Association for the Properties of Water and Steam
ICMS	In-Core Monitoring System
IF	Industrial Formulation
INPO	Institute of Nuclear Power Operations
LHR	Linear Heat Rate
LWR	Light Water Reactor
MSH	Main Steam Header
MCP	Main Coolant Pump
MOC	Middle of Cycle
MSIV	Main Steam Isolation Valve
NEA	Nuclear Energy Agency
NEM	Nodal Expansion Method
NPP	Nuclear Power Plant
OECD	Organization for Economic Cooperation and Development
PhD	Doctor of Philosophy
PWR	Pressurized Water Reactor
RMS	Root-Mean-Square
SCRAM	Safety Control Rods Activator/Actuator Mechanism

SPND	Self-Powered Neutron Detector
TVSA	Alternative Fuel Assembly
TVS-M	Standard Fuel Assembly
VVER	Russian-style PWR (from Russian: *Водо-водяной энергетический реактор*)

List of Symbols

Greek		
β	-	Delayed neutron fractions
γ_{Sm}	-	Yield of Samarium
γ_{Xe}	-	Yield of Xenon
Δt	*[s]*	Time step
$\varkappa$	*[J]*	Energy per fission
λ	*[s^{-1}]*	Decay constant
ν	-	Average number of neutrons released per fission
$\nu\Sigma_f$	*[cm^{-1}]*	Neutron production (nu-fission)
ρ	-	Reactivity
ρ_m	*[kg m^{-3}]*	Moderator density
Σ	*[cm^{-1}]*	Macroscopic cross section
Σ_a	*[cm^{-1}]*	Total absorption macroscopic cross section
Σ_f	*[cm^{-1}]*	Fission macroscopic cross section
Σ_G	*[cm^{-1}]*	Few-group macroscopic cross section
Σ_s	*[cm^{-1}]*	Scattering (fast to thermal group) macroscopic cross section
Σ_t	*[cm^{-1}]*	Total macroscopic cross section
Σ_{tr}	*[cm^{-1}]*	Macroscopic transport cross section
σ_{Xe}	*[10^{-24} cm^2]*	Microscopic cross section of Xenon
σ_{Sm}	*[10^{-24} cm^2]*	Microscopic cross section of Samarium
ϕ	*[cm^{-2} s^{-1}]*	Neutron flux
χ	-	Fission neutron spectrum
Latin		
Bu	*[MWdays/kgU]*	Burn-up
c_B	*[ppm]*	Boron concentration
C	-	Precursor fraction
D	*[cm]*	Diffusion coefficient, $D = 1/(3\Sigma_{tr})$
F_{xy}	-	Power peaking factor

$GEOM$	-	Lattice geometry
k	-	Multiplicative eigenvalue
K_{eff}	-	Effective multiplication factor
l	*[s]*	Prompt-neutron lifetime
n	*[pulse count, current]*	Neutron population
N_f	$[cm^{-3}]$	Number density in a fuel region
N_{f_0}	$[cm^{-3}]$	Initial fuel composition
$N_{Sm,\infty}$	$[cm^{-3}]$	Equilibrium number density of Samarium
$N_{Xe,\infty}$	$[cm^{-3}]$	Equilibrium number density of Xenon
S_{ext}	-	External neutrons source
T_f	*[K]*	Fuel temperature
T_m	*[K]*	Moderator temperature
V	$[cm^3]$	Volume
1/v	$[cm^{-1}\ s]$	Inverse velocity
Indexes		
g	-	Group g
g'	-	Group g'
i	-	Sub-region i
k	-	Current time step
$k-1$	-	Previous time step

1. Introduction and background

1.1 Introduction

A wide range of simulations have to be performed in order to ensure the safe operation of nuclear reactors. None of these calculations is simple or straightforward. Nuclear reactors are complex systems, which require modelling of flow rates and fluids temperature in the system (thermo-hydraulic analysis), as well as the power distribution in the reactor core (core analysis). Feedback between thermal-hydraulics and core condition should be accounted for, thus coupled simulations are required.

Nowadays, the simulator is not only an instrument for training of nuclear power plant personnel, it is also used for safety analysis and design validation before a power plant is build or modernized. Multi-physics simulation is based on best-estimate approach with use of engineering-grade tools like system codes and other thermo-hydraulics, neutronics and severe accident codes. Fidelity of the simulator models is optimized to meet the real-time simulation requirements, however, in a number of cases this fidelity might be equivalent or higher in comparison to the models used in safety analysis applications.

1.2 Background information

Kozloduy 6 full-scope replica control room simulator is commissioned at the beginning of year 2000. The plant-specific simulator is an important instrument for training of Kozloduy Nuclear Power Plant (NPP) personnel. It is employed in process analyses and in the process of validation and verification of plant operation and emergency procedures and guidelines. Expansion of the scope of simulation to a wide range of reference unit conditions corresponds with an augmentation of simulation fidelity requirements. There is a reason for systematic enhancement and modification of the simulator according to the status of the reference unit – Kozloduy 6, which is a VVER-1000/V320 series nuclear steam supply system with a K-1000-60/1500-2 turbine, with a series of extensive upgrades of plant control systems, Engineered Safety Feature Automation System automation, containment and Balance-of-Plant (BOP) equipment, etc. Another important factor for an enhancement of simulators is a forthcoming plant life extension and uprate to a 104 % power.

While the concept of high-fidelity cycle-specific real-time reactor core simulation became feasible for Pressurized Water Reactor (PWR) and Boiling Water Reactor (BWR) operators about year 2000 with commercially available nuclear reactor analysis tools (a popular example is SIMULATE-

3/3K/S3R/GARDEL from Studsvik), it was not the case for operators of other plant designs, like VVER.

There was no off-the-shelf solution available for the purpose of a cycle-specific real-time simulation of a light-water reactor with a hexagonal fuel assembly core. Currently, there are few examples of VVER full-scope simulators equipped with a cycle-specific reactor core model.

1.3 Statement of objectives

The objective of this PhD work is formulated as development, implementation, and qualification of an advanced core calculation methodology for VVER-1000 simulator application.

The steps performed towards achievement of the stated objective are as follows.

a. A two-group macroscopic cross-section modelling methodology for light-water reactors with hexagonal fuel assemblies (Ivanov, 2007a) is enhanced to cover nuclear fuel with sintered Gadolinium Oxide-Uranium Dioxide pellets, Zirconium-alloy structural components and absorber rods with Boron Carbide and Dysprosium-Titanium Oxide.

b. The enhanced two-group macroscopic cross-section modelling methodology is adapted for a VVER-1000 plant-specific full-scope replica control room simulator application.

c. A real-time version of the NEM code is developed and implemented on the Kozloduy 6 full-scope replica control room simulator.

d. A plant-specific reactor core model based on the real-time version of the NEM code is developed to meet all the requirements applicable to a simulator for training of nuclear power plant personnel and implemented on the Kozloduy 6 full-scope replica control room simulator.

e. A cycle-specific cross-section update procedure is developed for and implemented on the Kozloduy 6 full-scope replica control room simulator.

f. A cycle-specific two-group macroscopic cross-section library is developed by application of the above said enhanced methodology for the Kalinin 3 Coolant Transient Benchmark.

g. Adaptation of the Kozloduy 6 plant-specific reactor core model based on the real-time version of the NEM code is developed for a simulation of the Kalinin 3 Coolant Transient Benchmark problem making use of the above said Kalinin 3 cycle-specific two-group macroscopic cross-section library.

1.4 Thesis outline

The evolution of requirements for simulation of a nuclear power plant is summarized in Chapter 2. Main topics considered are as follows.

a. An emergence of a full-scope replica control room simulator.
b. An evolution of simulation requirements for nuclear power plant simulation.
c. Coupled multi-physics (neutronics / thermal-hydraulics) simulation with an emphasis on a real-time full-scope simulation for nuclear power plants.
d. Introduction of a cycle-specific core models coupled with a two-phase non-equilibrium thermo-hydraulic models for light water reactors.

A brief description of the main plant models in the scope of a nuclear power plant simulator (Kozloduy 6 simulator as a plant-specific example) is presented in Chapter 3, as follows.

a. Core (a real-time adaptation of the NEM code with case-specific enhancements);
b. Control rod drives;
c. Thermal-hydraulics;
d. Nuclear instrumentation (ex-core detectors, reactimeters, in-core detectors, power reconstruction);
e. Reactor protection and control system (Reactor Power Limiter, Reactor Power Controller, Control rod system);
f. Balance-of-plant.

Description of plant models is focussed on models, which are in direct interaction with the core model or are strictly necessary for analysis of processes described in the following Chapters. Many plant models are deliberately omitted.

Chapter 4 is focused on cross-section modelling methods and practices. At first, a review of the cross-section modelling methods for light water reactors currently in use is presented. Also, the two-group cross-section generation methodology and the cycle-specific cross-section update procedure for VVER-1000 simulator application are outlined.

The next two chapters are devoted to verification and validation of the cross-section generation methodology and the NEM real-time core model for VVER-1000 simulator application. First, the

methodology and the core model are developed, verified and validated exclusively with Kozloduy 6 plant-specific data. On the next step, verification and validation with actual plant data from Kalinin 3 (OECD/NEA Kalinin 3 Coolant Transient Benchmark) are performed. The historical sequence is preserved in the presentation of the thesis.

Illustrations of the accuracy of simulation using the Kozloduy 6 plant data are presented in Chapter 5, as follows.

a. Rated power – Beginning of Cycle (BOC), Middle of Cycle (MOC) and End of Cycle (EOC);
b. Operational transient of inadvertent closure of a Main Steam Isolation Valve (MSIV) and switching off Main Coolant Pump (MCP) No. 4.

Another illustration of the accuracy of simulation using actual plant data from Kalinin 3 is shown in Chapter 6. The transient of 'Switching-off of One of the Four Operating Main Circulation Pumps at Nominal Reactor Power' is performed at an asymmetric core condition with a range of parameter changes.

Finally, the main findings and conclusions are summarized. Various outstanding issues are identified and suggestions for future research are given in Chapter 7.

Chapter 8, Bibliography completes the main body of this work.

Main terms and definitions employed in this work are presented in Appendix A.

General description of VVER-1000/V320 unit is presented in Appendix B.

Data concerning geometry and material composition of the Kozloduy 6 core model are presented in Appendix C.

Data concerning geometry and material composition of the Kalinin 3 core model are presented in Appendix D.

A large set of Kalinin 3 simulation data are presented in Appendix E.

2. Evolution of fidelity requirements for nuclear power plant simulation

Evolution of nuclear power plant simulators described here is roughly split into three periods. The first period includes all the early (and very early) examples created before the concept of a full-scope replica control room simulator for training of nuclear power plant personnel was established and formalized. The second period covers a large number of plant-specific simulators delivered from late 1970's in time for commissioning of largest number of nuclear power generating plants worldwide and continues at a slower pace into late 1990's or early 2000's. The third period covers the latest developments in simulator technology and operation.

Examples given in this section are deliberately chosen with a focus on PWR simulators in order to comply with the object of this work – the VVER simulator. Actually, the VVER simulators followed the same (or very similar) trends but transition between early-to-mature and mature-to-modern simulator was postponed by about 10 to 15 years in comparison with other light water reactor simulators. The first VVER replica control room simulator for Novovoronezh NPP (VVER-440/V-179) was not strictly plant-specific and technically belonged to a class of very early simulators based on analogue computers. The Loviisa NPP simulator from 1980 was the first VVER full-scope replica control room simulator based on digital computers, soon followed by the Paks NPP simulator. Full-scope replica control room simulators for Balakovo 4 (1992) and Zaporozhye 5 (1993) were the first VVER-1000 simulators in operation.

2.1 Early simulators

During the end of 1960's and early 1970's, when the first computer-based control room simulators were put in operation, the scope and fidelity of plant process models were severely constrained by limited computer capabilities. There were few NPP control room simulators in operation worldwide at the time of the Three Mile Island accident (1979). Their characteristics were as follows (IAEA-TECDOC-1411, 2004).

a. The panel layout and design were not always the same as the reference plant.
b. The thermodynamic models were not plant-specific and the models (for PWR) did not address two-phase flow conditions in the core, associated with accident scenario.
c. The importance of real-time simulation was acknowledged but not always adhered to.
d. The simulators were located at the site of nuclear steam supply system vendor, often quite distant from the reference plant.

e. For initial training, trainees generally had one or two weeks of training on a simulator as part of their training programmes.
f. Licensed/authorized operators might have one week per year of simulator training as part of their refresher training.
g. Simulator instructors were not always familiar with the operating experience of the NPPs for which they provided training.
h. NPP procedures generally could not be used on these simulators, due to design differences, thus operators trained with procedures other than those at their own plant.
i. Prior to authorization, control room operators' competences in responding to abnormal and emergency conditions were generally not formally assessed on a simulator by either the operating organization or the nuclear safety regulator (rather, an assessment in these areas was based upon written and/or oral examinations).

Early 1970's marked another significant shift in simulator technology (Alliston, 1975a). Analogue computers and relay circuits were phased out being gradually superseded by a digital computer (Gregg, 1990). Sophisticated mathematical models were written in high-level programming language (FORTRAN IV) but large amount of assembler code were still present.

2.2 Simulators for training of nuclear power plant personnel

During the 1980's, detailed review of the lessons learned from operating experience caused a re-assessment of the adequacy of training of nuclear power plant personnel, particularly, for control room personnel. As a result of this review, operating organizations and nuclear safety regulators worldwide established more stringent requirements for simulator training of control room personnel (ANSI/ANS-3.5-1985, 1985) as well as other aspects of these training programmes. Other changes were also initiated (IAEA-TECDOC-1411, 2004).

a. Improved (symptom-based) emergency operating procedures;
b. Improved display of safety parameters;
c. Greater reliance on simulator examinations in the qualification/authorization/licensing of control room personnel;
d. Use of the Systematic Approach to Training as the basis for NPP personnel training programmes.

2.2.1 Scope and fidelity of simulation

The scope of simulation was to be defined depending on the required use of the simulator (IAEA-TECDOC-546, 1990). Various systems, sub-systems and components of the plant were either included or left out of the scope of simulation on the basis of assessment of training requirements (extensive scope). The same approach was applied to the scope of plant simulation in terms of mode of plant operation (simulation envelope).

In full-scope simulators, it was important that all the systems the operator has been using for taking the plant through the required evolutions were included into the scope of simulation. It also was necessary to have the whole range of plant operation modes ranging from a cold shutdown to a rated power and including also abnormal and accident (design-basis accident) scenarios, or any sort of emergency caused by malfunction of various components.

An important part in the definition of the modelling requirements consisted of the specification of different physical effects to be seen in the simulation. The systems and transients to be simulated should be described with respect to the phenomena, which should be possible to observe (IAEA-TECDOC-546, 1990). For example, the core should be simulated in such a way that the effects of a new core versus an old core could be seen.

A real-time simulation was a requirement (IAEA-TECDOC-546, 1990).

A typical qualitative requirement was that operator should not be able to observe any difference between the response of the simulator and the reference plant (within the scope of simulation).

2.2.2 Modelling approaches

There were three different kinds of modelling approaches: special purpose models, general solutions and best estimate codes (IAEA-TECDOC-546, 1990).

Special purpose models divided the simulation process according to technological units and every aspect of the given unit was described in the same module. The advantage of this approach was that the model was compact, well documented and easy to replace by a new one. However, this method was not effective with large networks (hydraulic, electrical) involved, because the same element types (like valves) were described in different models many times (and sometimes many ways).

General purpose models described physical phenomena instead of technological units. Typical application areas were as follows.

a. Hydraulic networks (pressure, flow, temperature, concentration)
b. Electrical networks (current, voltage, frequency)
c. Instrumentation and control (interlocks, safety algorithms, analogue or digital controllers)

The advantage of this approach was that it provided a unified solution for every component of the same type and the description of the actual plant topology was easy.

Best estimate codes could be used only on super computers (above 30 MIPS[1] rating, and the ability to vectorize processing). In these codes the simulated process was described as in engineering grade safety analysis tools. This approach provided very accurate results but required extravagance in computing power.

2.2.3 Core modelling approaches and features

Practically, two different kinds of core models were used: coupled point kinetics method and expansion based method. For cores with large physical dimensions, the coupled kinetics method could be better if the nodal structure was fine enough. The major advantage of the expansion-based method in the case of PWR cores was that it provided a fine and realistic flux distribution with less CPU load than the coupled kinetics method. Since the arrangement of a fuel assembly, the control rod movement and the coolant flow in a PWR core were all in axial direction, the expansion based method emphasised the solution in the axial direction and the neutron flux distribution, with different computation rates. However, coupled kinetics methods were widely used with very good results.

Early generation simulator core models often made use of several simplifying assumptions (Alliston, 1975b).

a. One-dimensional axial diffusion theory;
b. Single energy group;
c. One-dimensional coarse-mesh feedback;
d. Generic nuclear data.

Early generation models were relatively easy to update because they required so little data and the expectations on core model fidelity were not so high. The common plant simulator was equipped with a core model able to simulate ‘generic’ core load at BOC, MOC and EOC.

[1] A unit of computing speed equivalent to a million instructions per second.

The data set required to drive a larger, up-to-date core model was much more extensive and the expectations on fidelity were higher. During the 1980's, simulators for training (and later examination) of nuclear power plant personnel were built with a three-dimensional neutron diffusion models, two (or 'one-and-a-half') energy groups, and space-time decomposition (shape function was calculated at larger time-steps, e.g. once every second in comparison with 4 cycles per second for most of the simulation software).

The real-time cycle-specific core model was not yet feasible for simulator applications. Simulation computers were 'mini-computers' soon to be replaced by 'micro-computer' engineering workstations. Computer memory and storage capacity was measured in MBytes.

2.3 Modern simulators

During the last two decades there has been an intensive development of simulation technologies. A modern simulator is no longer based on a philosophy to build a code around the transmitters to produce a desired response. The modern simulator is based on engineering-grade system codes solving systems of differential equations and results are exchanged as feedbacks inside the networks of multi-physics interactions (Romas, 2013). Multiple areas of physics are integrated through best-estimate models predicting very fine phenomena.

Simulators are tested by experienced test engineers and operators and these tests are aimed to assure the quality and reliability of the predictions. After such detailed verification there can be an application of the simulator to predict behaviour of the plant in situations which are abnormal during the operation or, in other words, to perform safety studies.

2.3.1 Fidelity of simulation

The modern simulator is getting close to the state where it can be used not just for training of operators but also for the safety analysis and design validation before a power plant is build or modernized. Fidelity of the simulation models is optimized to meet the real-time simulation requirements, however, in number of cases this fidelity might be equivalent or higher in comparison to the models used in the actual safety analysis applications. The best-estimate real-time simulation models can be switched to finer time steps meeting the safety analysis requirements. The best estimate real-time simulation models are usually derived from and benchmarked against engineering grade models of finer nodalization (Romas, 2013).

2.3.2 Models and codes

Multi-physics simulation is based on best-estimate approach with use of engineering-grade tools like system codes – RELAP5-3D, SIMULATE3-R, MAAP and other thermo-hydraulics, neutronics and severe accident codes.

Codes that are implemented in simulators are aimed to predict behaviour of different phenomena appearing in the actual power plants. Results of the calculations are exchanged between the codes as feedbacks to each other allowing realistic assessment of the events and behaviour of the models in a real-time simulation (Romas, 2013).

Feedbacks between the codes are exchanged in a synchronised manner so that execution of the codes and exchange of the calculation results are happening at the right moments in time.

As an example of such interactivity is a usage of the RELAP5-3D and SIMULATE3-R to model a reactor core. The RELAP5-3D is used to simulate primary thermal-hydraulics while SIMULATE3-R is performing the neutron kinetics calculations (a solution of the system of differential equations based on the two-group diffusion theory). However, these codes cannot perform proper prediction without having knowledge about each other. The SIMULATE3-R needs information about the thermal-hydraulic feedbacks while the RELAP5-3D needs information about the power distribution and magnitude predicted by the SIMULATE3-R. There kinetics results (fission power and decay heat) are passed to the thermal-hydraulics code where heat transfer and flow calculations are performed. The results from the thermal-hydraulics calculations in the form of water and steam density, coolant and fuel temperature, void, and boron concentration are passed back to the neutron kinetics code.

2.3.3 Core numerical methods and features

Recommendation 6 of INPO's SOER 96-02 to provide cycle-specific simulator training made a shift in simulator operation and core model fidelity requirements.

Core design numerical methods, along with measured plant data, provide the basis for assessment of the simulator model. All modern core design software employs an advanced nodal method of some sort. Some simplifications to core design models and practices are usually required to allow real-time execution on the training simulator. The following premises guided the simplifications made, and not made, in the development of the engineering grade core model (Borkowski, 2003).

a. Explicit modelling of all radial assemblies is required to model radial tilts, asymmetric rod insertion, and instrumentation readings.
b. Assembly power predictions are strongly influenced by local fuel temperature and moderator density variations. Axial-average feedback parameters cannot reproduce core design accuracy in general.
c. One-group energy models can be shown to introduce significant errors in the local neutron flux.
d. The more detailed the core model, the more effort is required for updating the core.

Advanced engineering grade core models are being applied to real-time training simulators. The motivation for such an upgrade is increased fidelity to core design methodology and measured plant data. A further expectation is that the core model uses cycle-specific data such that training is performed on the cycle actually loaded (Borkowski, 2003).

2.4 Simulator testing

According to the American national standard 'Nuclear Power Plant Simulators for Use in Operator Training and Examination' (ANSI/ANS-3.5-2009, 2009),

> *'... Verification, validation, and performance testing shall be performed to ensure that no noticeable differences exist between the simulator control room or simulated systems when evaluated against the control room or systems of the reference unit.*
>
> ***Simulator verification testing***
>
> *Simulator verification testing is a form of software development testing. Simulator verification testing shall be conducted by comparison of simulated component or system software design to the original requirements to ensure that each step in the software development process completely incorporates all requirements of the previous step.*
>
> ***Simulator validation testing***
>
> *Simulator validation testing is a form of software development testing. Simulator validation testing shall be conducted by comparison of simulated component or system test results against actual or predicted reference unit performance data in a stand-alone or integrated fashion.*

Simulator performance testing

Simulator performance testing comprises operability testing, scenario-based testing, reactor core performance testing, and post-event simulator testing. Simulator performance testing shall be performed in a fully integrated mode of operation.

Simulator operability testing

Simulator operability testing shall be conducted to confirm overall simulator model completeness and integration by testing the following:

- *Simulator steady-state performance;*
- *Simulator transient performance for a benchmark set of transients.*

Simulator scenario-based testing

Scenario-based testing shall be conducted to ensure the simulator is capable of producing the expected reference unit response to satisfy predetermined learning or examination objectives by utilizing the existing training and examination scenario validation process.

As a minimum, the following types of simulator scenarios shall undergo scenario-based testing:

- *Initial License Examination scenarios;*
- *Licensed Operator Requalification annual examination scenarios;*
- *Scenarios used for reactivity control manipulation experience.*

Additional scenario-based testing should be considered for other operator training scenarios.

Simulator reactor core performance testing

Simulator reactor core performance testing shall be conducted to confirm that the simulator nuclear and thermal-hydraulic models replicate the reference unit core response within the scope of simulation.

Post-event simulator testing

Certain reference unit events provide the opportunity to acquire relevant reference unit performance data. For such data, post-event simulator testing should be conducted to confirm that the simulator is capable of reproducing the response of relevant reference unit parameters within the scope of simulation…'

2.5 Conclusions and a concept for tomorrow's simulator

A problem of real-time simulation of coupled primary thermal-hydraulics and neutron kinetics for light-water reactors is a discrepancy between coarse-mesh representation of the core in a two-phase multi-component non-equilibrium thermal-hydraulics model and much more detailed core nodalization in a two-group kinetics model, as follows.

a. **Primary thermal-hydraulics model —** Few segments (e.g. between 4 and 12) in a horizontal plane and few axial layers (e.g. 5 or 10 layers with 2 or 4 heat slabs per node).
b. **Two-group neutron kinetics model —** One node per fuel assembly in a horizontal plane with about 20 or more axial layers (plus one layer each of bottom, top and radial reflector nodes).

In order to solve such a discrepancy in terms of thermal-hydraulics feedback, an intermediate layer is introduced usually as a part of the core model, often called 'core mapping' scheme. The coarse-mesh thermal-hydraulics model provides boundary conditions for an algorithm handling reconstruction of thermal-hydraulic feedback variables per each of fine-mesh kinetics model nodes. Necessarily, such a reconstruction is based on simplifications concerning flow distribution between fuel assemblies mapped to a single coarse-mesh node, cross-flow between fine-mesh nodes and, usually, phase equilibrium.

A logical step for further development in near future will be to introduce a more comprehensive treatment of fuel assembly thermal-hydraulics in the form of a sub-channel code (e.g. COBRA-TF like) as an intermediate layer between coarse-mesh model of the whole nuclear steam supply system and finer-mesh core kinetics model using one or more nodes per fuel assembly.

Another problem not properly addressed yet is integration of severe accident models into a full-scope replica control room simulator. There are few early examples but no common technical approach is established and no formal requirements are defined by nuclear regulators worldwide.

3. Description of plant models

Kozloduy 6 full-scope replica control room simulator is commissioned in the beginning of year 2000. The plant-specific simulator is an important instrument for training of Kozloduy NPP personnel. It is employed in process analyses and in the process of validation and verification of plant operation and emergency procedures and guidelines. Expansion of the scope of simulation to a wide range of reference unit conditions corresponds with an augmentation of simulation fidelity requirements (ANSI/ANS-3.5-2009, 2009); (IAEA-TECDOC-1500, 2006). There is a reason for systematic enhancement and modification of the simulator according to the status of the reference unit, Kozloduy 6.

Kozloduy 6 consists of a VVER-1000/V320 series nuclear steam supply system and a K-1000-60/1500-2 turbine, with a series of extensive upgrades of plant control systems, ESFAS hardware and algorithms, containment and BOP equipment, etc. General description of VVER-1000/V320 unit is presented in Appendix B.

Another factor contributing to a series of changes in simulator configuration is forthcoming plant life extension and 104 % power uprate. Both procedures require significant effort on the side of the plant for license extension and re-qualification or replacement of equipment and procedures. Necessarily, this process affects the simulator design data base. Power uprate is achieved mostly by re-assessment of equipment operating limits and tolerances, or by implementation of new components or equipment.

Almost all the plant systems are included in the scope of simulation, that is, all the plant system controlled or just monitored from the main control room.

All of the plant automation concerning systems of normal operation is handled by an extensive Ovation digital control system. Quite common problem in implementation of complex digital control systems on simulators, including nuclear power plant simulators, is the right choice of approach. There are three approaches: simulation, emulation and stimulation (IAEA-TECDOC-1500, 2006). A hybrid solution with an emulation of Ovation controllers and stimulation of Westinghouse workstations are implemented.

Kozloduy 6 ESFAS are based on ‘Radiy’ Field Programmable Gates Array technology. Simulation of the controllers and stimulation of the graphics user interface is implemented. Stimulation of graphics user interface means that part of the original software package is used on the simulator for visualisation of data supplied by the simulation computer.

The description of plant systems and simulator models is given here as per plant configuration of 2015.

3.1 Reactor core

The Nodal Expansion Method code (NEM) has been initially developed by the Pennsylvania State University, and later improved, verified and validated by the Reactor Dynamics and Fuel Modelling Group at North Carolina State University. In this work 'NEM' refers to the code, not the method. NEM is a multi-group code – up to 70 energy groups can be simulated (Eq. 3.1-1). It is a three-dimensional transient nodal core model. Stand-alone version provides for three geometry-modelling options: Cartesian, Hexagonal-Z and Cylindrical (*R-θ-Z*). NEM is based on the transverse integration procedure and it has been recently updated to utilize semi-analytical transverse integrated flux representation and an improved transverse leakage approximation (NEM Theory Manual, 2009).

$$\frac{1}{\nu_g}\frac{\partial \phi_g}{\partial t} - \nabla \cdot \left(D_g \nabla \phi_g\right) + \Sigma_{t,g}\phi_g = \\ = \sum_{g'=1}^{G} \Sigma_{s,g'\to g}\phi_{g'} + \frac{\chi_g}{k}\sum_{g'=1}^{G} \nu\Sigma_{f,g'}\phi_{g'} + S_{ext,g} \qquad \text{Eq. 3.1-1}$$

$$\Sigma_{t,g} = \Sigma_{a,g} + \sum_{g'=1}^{G} \Sigma_{s,g\to g'}$$

$$g = 1 \ldots G$$

where

- ϕ_g - Neutron flux in group g;
- ν_g - Average number of neutrons released by a group g fission event;
- D_g - Diffusion coefficient in group g;
- $\Sigma_{t,g}$ - Total macroscopic cross section in group g;
- $\Sigma_{a,g}$ - Absorption macroscopic cross section in group g;
- $\Sigma_{s,g'\to g}$ - Probability of a neutron scattering from group g' into group g;
- χ_g - Fission neutron spectrum in group g;
- k - Multiplicative eigenvalue;
- $\nu\Sigma_{f,g'}$ - Nu-fission macroscopic cross section in group g';
- $S_{ext,g}$ - External neutrons source in group g.

For the purpose of VVER-1000 real-time application, NEM code is further developed. With this version of the code, steady-state and transient simulation in real time is performed with 2 energy groups in a Hexagonal-Z geometry across the whole reactor core. Therefore, Eq. 3.1-2 ÷ Eq. 3.1-5 are the basis of the code. Various other NEM code options (Cartesian/Cylindrical geometry, core symmetry, number of energy groups, etc.) are disabled for this particular application (REL-786-DD-002-02, 2012).

The two-group diffusion equations, without up-scattering (energy group cut-off point of 0.625 eV), in a typical form for Light Water Reactor (LWR) applications are shown below.

$$\frac{1}{\mathrm{v}_1}\frac{\partial \phi_1}{\partial t} - \nabla \cdot (D_1 \nabla \phi_1) + \left(\Sigma_{a,1} + \Sigma_{s,1\to 2} - \frac{\chi_1}{k}\nu\Sigma_{f,1}\right)\phi_1 = \frac{\chi_1}{k}\nu\Sigma_{f,2}\phi_2 + S_{ext,1} \qquad \text{Eq. 3.1-2}$$

$$\frac{1}{\mathrm{v}_2}\frac{\partial \phi_2}{\partial t} - \nabla \cdot (D_2 \nabla \phi_2) + \left(\Sigma_{a,2} - \frac{\chi_2}{k}\nu\Sigma_{f,2}\right)\phi_2 == \Sigma_{s,1\to 2}\phi_1 + \frac{\chi_2}{k}\nu\Sigma_{f,1}\phi_1 + S_{ext,2} \qquad \text{Eq. 3.1-3}$$

In the case of a fission neutron spectrum defined as $\chi_1 = 1$, $\chi_2 = 0$ the fast and thermal group equations are further simplified, as follows.

$$\frac{1}{\mathrm{v}_1}\frac{\partial \phi_1}{\partial t} - \nabla \cdot (D_1 \nabla \phi_1) + \left(\Sigma_{a,1} + \Sigma_{s,1\to 2} - \frac{1}{k}\nu\Sigma_{f,1}\right)\phi_1 = \frac{1}{k}\nu\Sigma_{f,2}\phi_2 + S_{ext,1} \qquad \text{Eq. 3.1-4}$$

$$\frac{1}{\mathrm{v}_2}\frac{\partial \phi_2}{\partial t} - \nabla \cdot (D_2 \nabla \phi_2) + \Sigma_{a,2}\phi_2 = \Sigma_{s,1\to 2}\phi_1 + S_{ext,2} \qquad \text{Eq. 3.1-5}$$

Vacuum boundary conditions are applied on the outer surface of each reflector node.

The two-group neutron diffusion equations are solved at each node for each time step, as follows.

a. Two-group neutron fluxes, using node-specific energy per fission ($\varkappa$) and inverse velocities (1/v);
b. Xenon, Iodine, Samarium and Promethium concentrations;
c. Six delayed neutron groups, using node-specific effective delayed neutron fractions (β) and decay constants (λ);
d. Decay heat and neutron source strength.

Fuel burn-up, plutonium build-up and depletion of burnable poisons are accounted for at the cycle-specific library generation stage. It is not yet practical to include such calculations in a real-time

simulation when the duration of a common simulator session is less than 6 hours. This may not always be the case, however.

The core consists of hexagonal cells with a pitch of 23.6 cm, each cell corresponding to one fuel assembly (FA), plus an external layer of radial reflector cells of the same size. There are a total of 211 cells, of which 163 FA and 48 radial reflector cells.

An axial core nodalization comprising 20 layers, with a height of 17.75 cm each, is used. Their count starts from the bottom, adding up to a total active core height of 355 cm. The number of axial layers for kinetic calculations is twice the number of axial layers in the cross-section library. The height of both bottom and top axial reflector layers is 23.6 cm.

The basic one-sixth building block of the Kozloduy 6 VVER-1000/V320 reactor core model is shown in Figure 3.1-1. The same one-sixth core symmetry sector numbering is used as in the cross-section libraries. Although a full core model, one-sixth core representation is employed for cross-section handling. The symmetry in data arrays is common (and desirable) feature. This approach contributes to a small decrease in computer resource requirements and more efficient procedures for core model updates but asymmetric configurations can be handled too (Chapter 6).

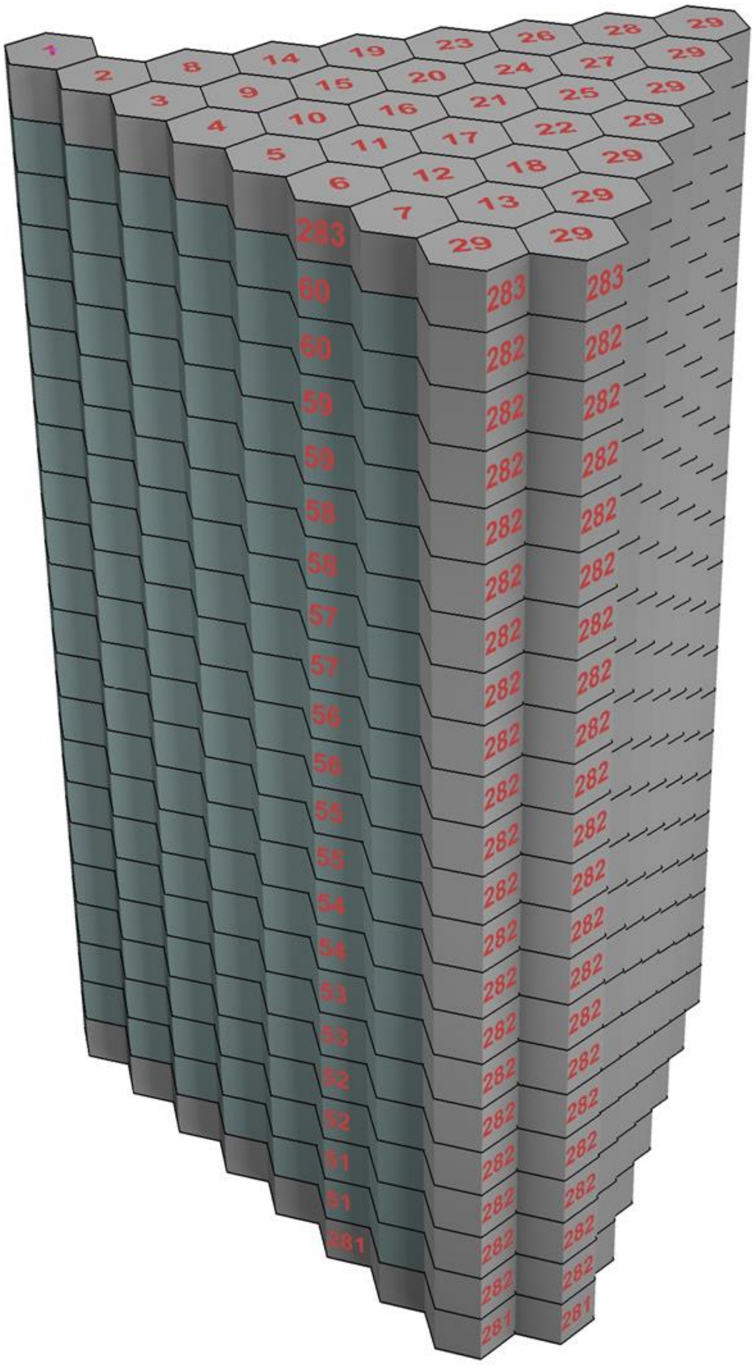

Figure 3.1-1: Scheme of the basic one-sixth building block of the VVER-1000/V320 reactor core model (olive green – FA cells, grey – reflector cells). Numbers indicate nodes in radial (from 1 to 29) and axial plane

3.2 Control rod drives

There are 61 control rod drives, each equipped with a cluster (Figure 3.2-1) of 18 absorber elements (Figure 3.2-2). Absorber material is Boron Carbide, B_4C except in a lower section of the element (300 mm) which contains Dysprosium-Titanium oxide, $Dy_2O_3 \cdot TiO_2 -$ as illustrated in Figure 3.2-3, (Andrushechko, 2010). The effect of absorber elements in the core is accounted for through material compositions (rodded and unrodded).

Movement of control rods and function of control rod position indicators is handled by another model, Control Rod System (Section 3.5.3).

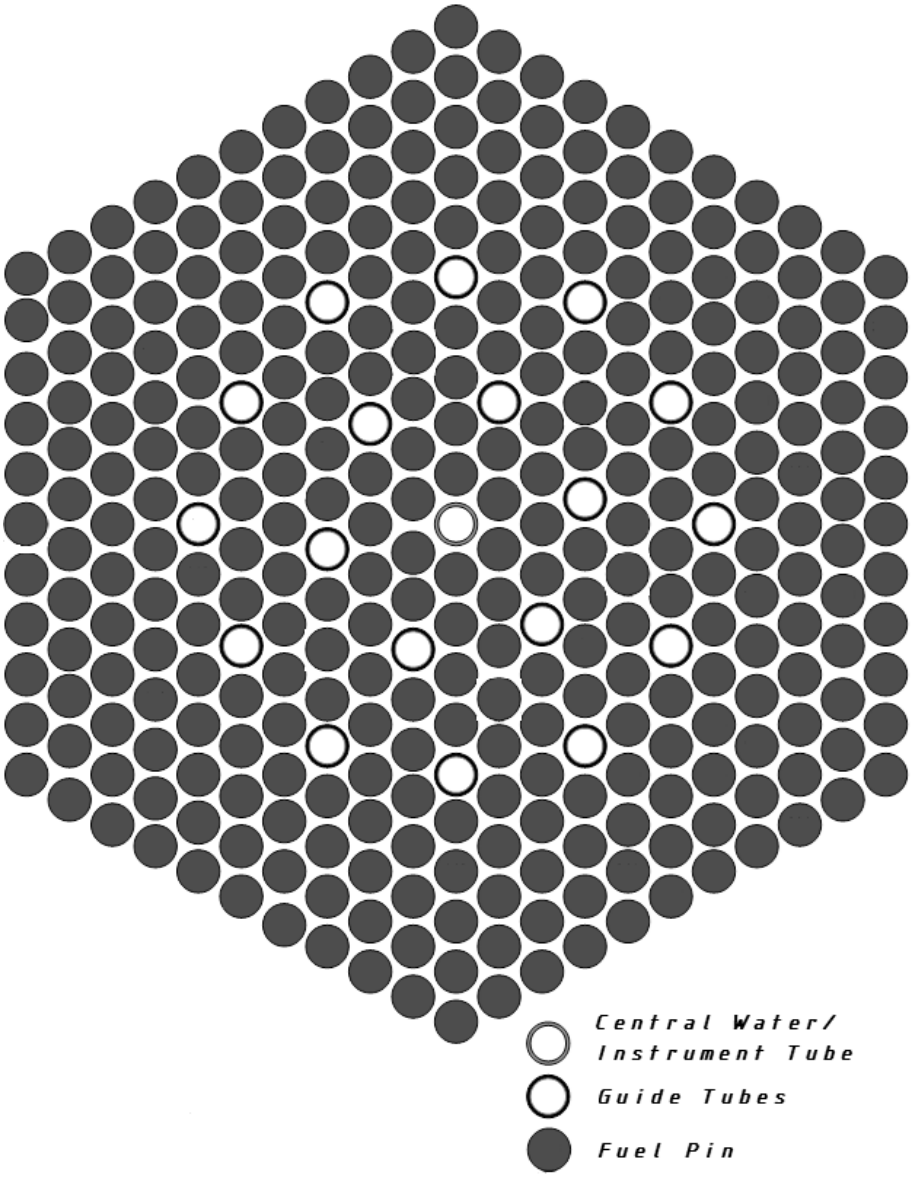

Figure 3.2-1: Scheme of the fuel assembly cross-section with positions of fuel pins, guide tubes and instrument channel

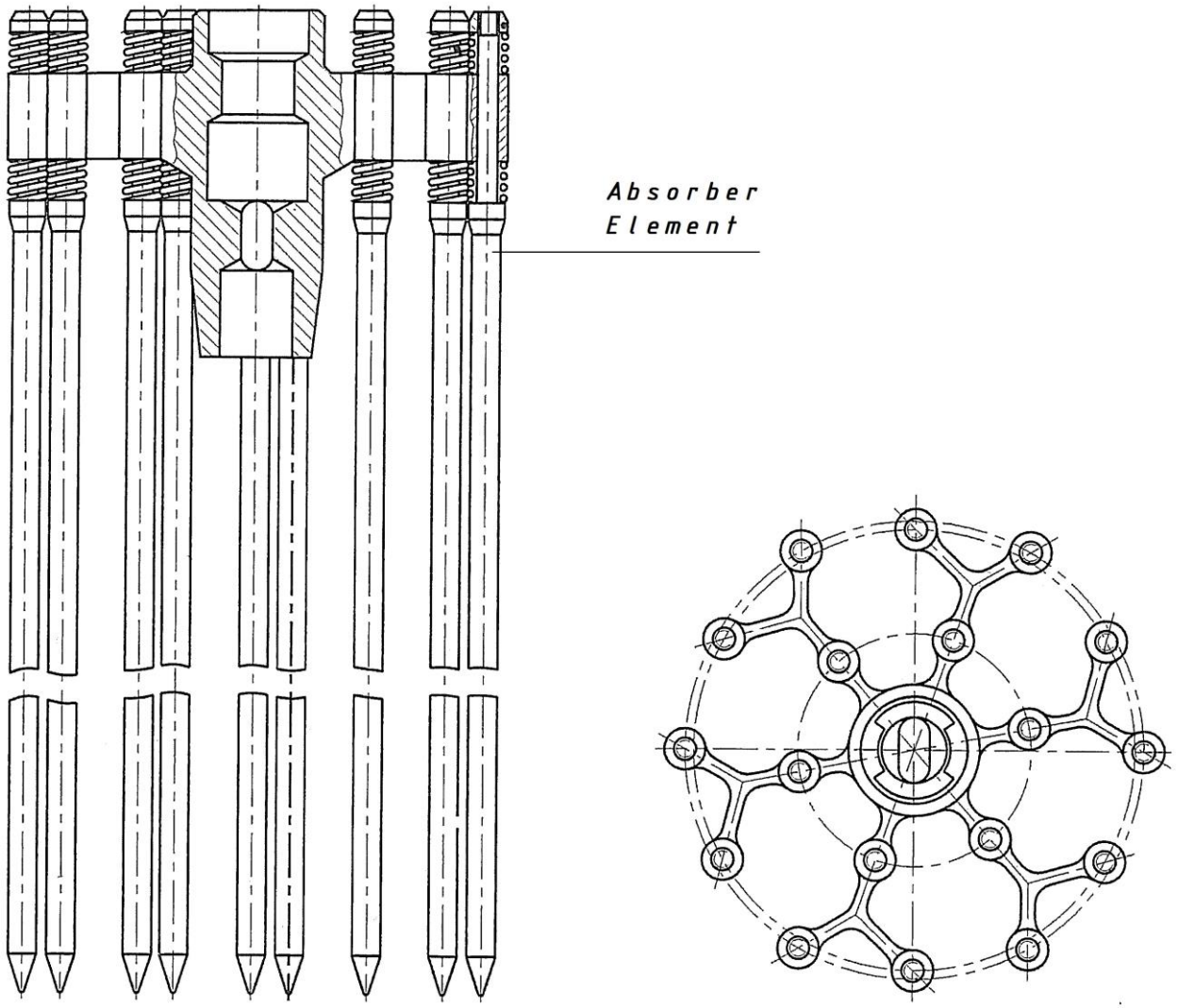

Figure 3.2-2: Scheme of the cluster of absorber elements with spring retainer (vertical view with a partial cut through spring retainer — left; view from above — right).

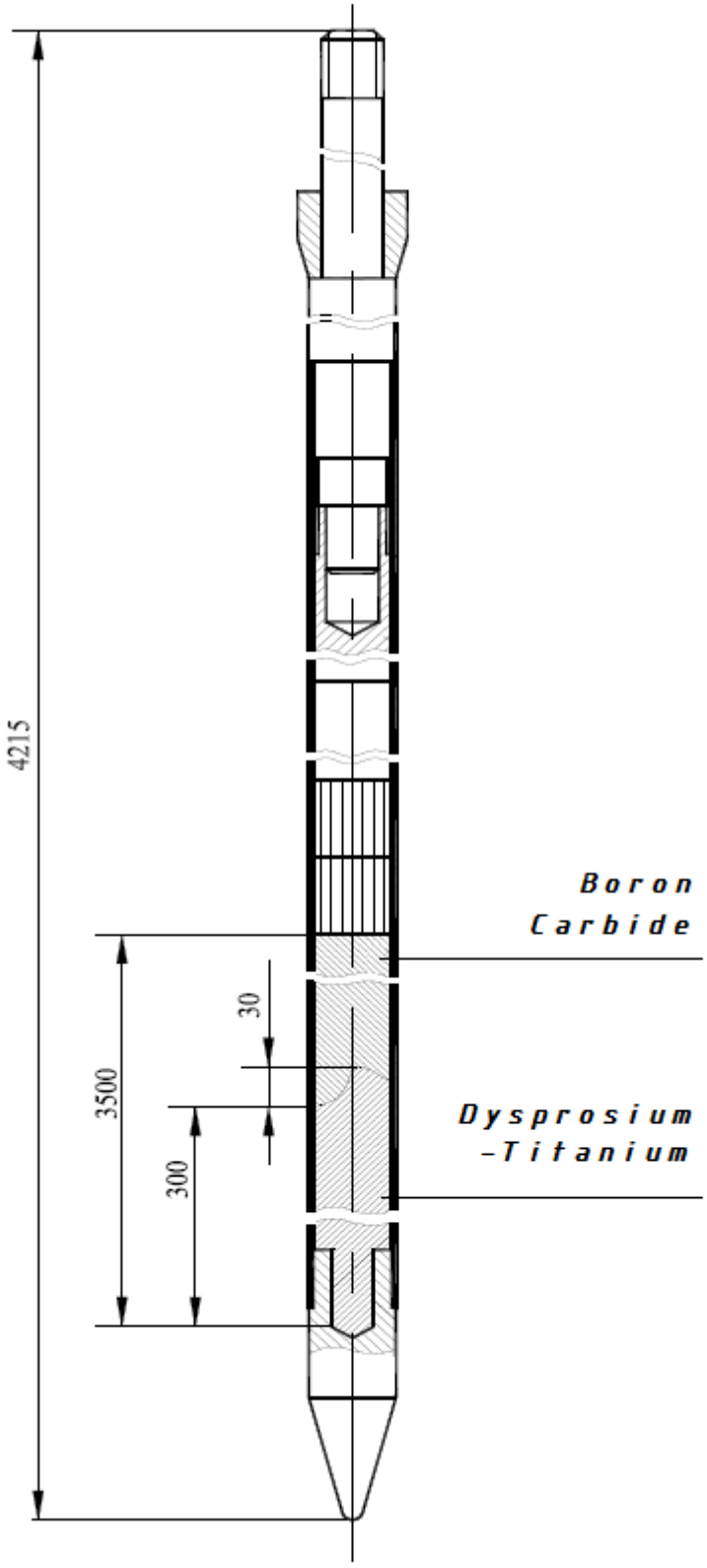

Figure 3.2-3: Vertical cross section of an absorber element (dimensions in mm).

3.3 Thermal-hydraulics

The input deck for RELAP5-HD™ (RELAP5-3D compatible) contains the following major components (RELAP5-HD™ Verification Report, 2011); (REL-786-DD-003-01, 2012).

a. Reactor vessel and internals;
b. Main circulation pipelines including main circulation pumps;
c. Pressurizer surge line and pressurizer vessel;
d. Steam generators primary and secondary side, including steam pipes and steam collector.

All of these major parts include hydrodynamics input, heat structures input and boundary conditions for external systems. Nodalization summary is presented in Table 3.3-1. Illustration of the primary thermal-hydraulics nodalization is shown in Figure 3.3-1.

Table 3.3-1: Thermal-hydraulics nodalization summary of the nuclear steam supply system model for the Kozloduy 6 simulator

Item	Nodes
Primary and Secondary (Total)	316
• Primary	240
• Secondary (Steam generators)	76 (4 x 19)
Reactor Pressure Vessel (RPV)	72
Pressurizer	11
Loop Hot / Cold Legs	57 (3 x 14 + 15)
Steam Generators Primary Side	100 (4 x 25)

In the reactor core nodalization 5 axial nodes are used, but core heat structures for each sector with 20 axial slabs and 10 radial mesh points are referred to them (Figure 3.3-2). This is done in order to ensure compatibility with the NEM core model. General scheme of the RELAP5-HD™ and NEM interface through the respective heat structure is given in Figure 3.3-3. For the other core sectors the same configuration is used.

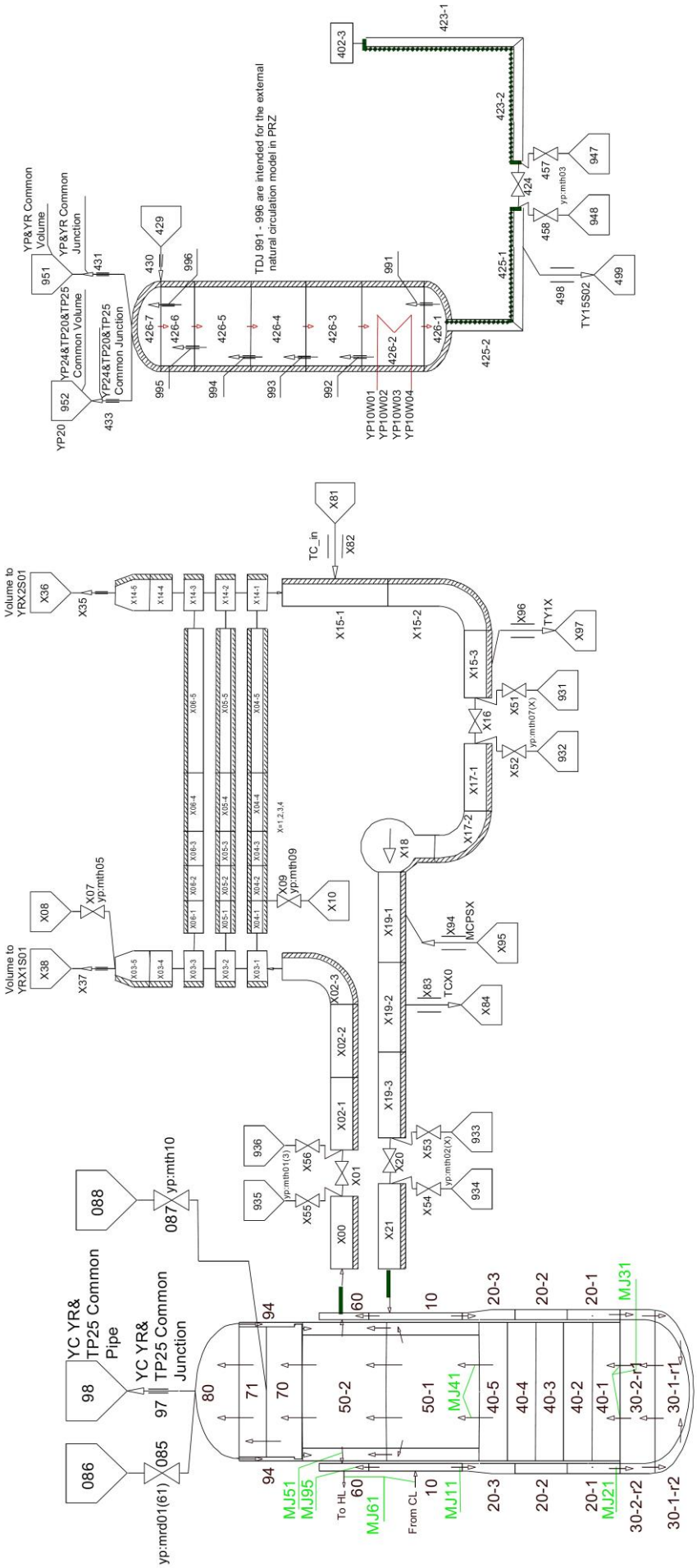

Figure 3.3-1: An illustration of Kozloduy 6 model primary thermal-hydraulics nodalization (Reactor pressure vessel and an one primary coolant loop — left; Pressurizer — right; Positive flow directions are shown with arrows)

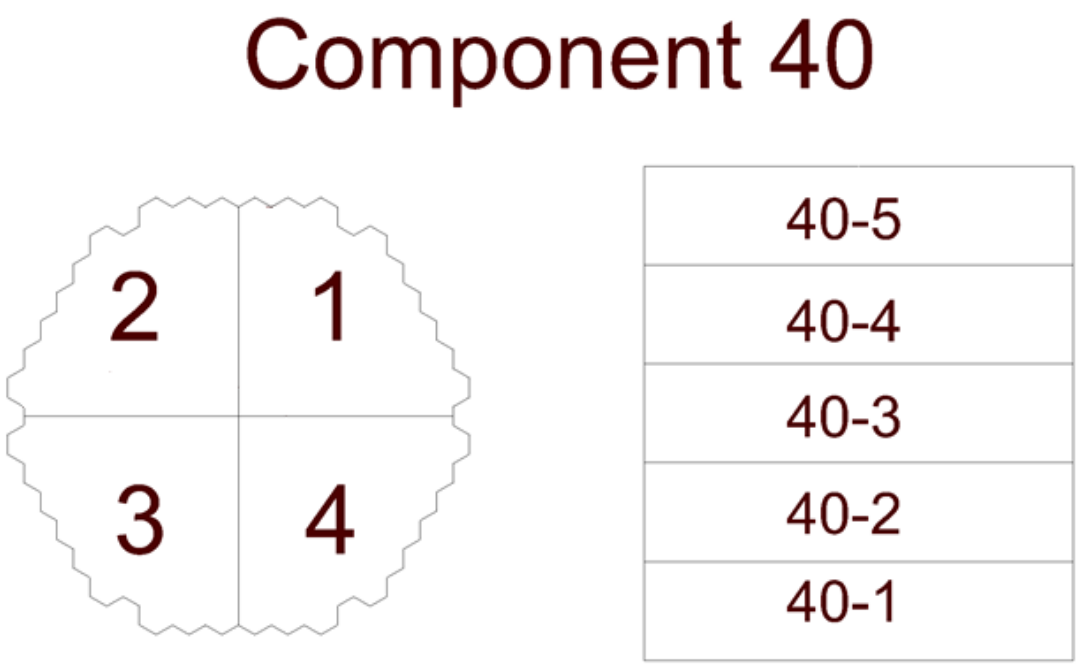

Figure 3.3-2: Scheme of Kozloduy 6 reactor core nodalization (horizontal — left; vertical – right)

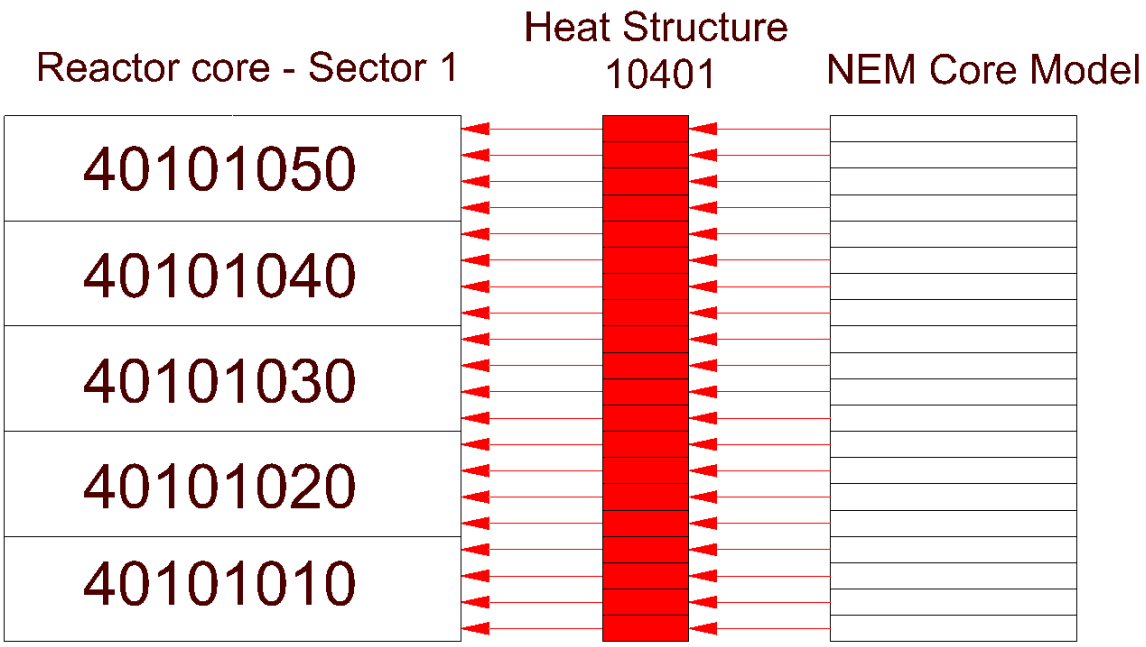

Figure 3.3-3: An illustration of thermal-hydraulics / neutronics coupling scheme for the Kozloduy 6 simulator model (thermal hydraulic sector 1 — heat structure — core). Heat Structure 10401 with 20 heat slabs represents all the fuel elements in one-fourth sector of the core

3.4 Nuclear instrumentation

3.4.1 Ex-core instrumentation

Ex-core Neutron Flux Monitoring System (AKNP-7-02K) monitors the reactor power by means of thermal neutron flux ex-core detectors located in instrument wells adjacent to the reactor vessel. The system provides indication, control and alarm signals for reactor operation (Andrushechko, 2010). There are three Neutron Flux Monitoring System sets – two sets for the main control room and the third set for the emergency control room. Each set consists of 3 equivalent channels. Each channel is equipped with start-up range and power range detectors ─ ion chambers (Figure 3.4-1) with overlapping ranges (Table 3.4-1). Start-up range and power range detectors occupy 9 instrument wells.

Table 3.4-1: Operating range of the ex-core neutron flux monitoring system (AKNP-7-02K)

Range	Power, %	Neutron flux (Φ), neutrons·m^{-2}·s^{-1}	Measurement error, %
Start-up	1×10^{-8} — 1.5×10^{-3}	3×10^{-1} — 5×10^{4}	±30 % of the measured value (10^{-7} – 10^{-6} %) ±10 % of the measured value (10^{-6} – 10^{-1} %)
Power, logarithm	1.5×10^{-5} — 120	5×10^{2} — 4×10^{9}	±30 % of the measured value (10^{-3} – 10^{-2} %) ±10 % of the measured value (10^{-2} – 120 %)
Power, linear	0.1 — 120	3×10^{6} — 4×10^{9}	±1 % of the rated power (1 – 120 %)

This system provides also monitoring of the range rate (period) in start-up range and in power range in the interval from 1 to 999 s (measurement error ±10 % of the measured value). Range rate protection setpoints are 10 – 20 – 40 s (SCRAM, preventive protection 1 and 2 respectively).

Shutdown and Refuelling Monitoring System (SKP) provides source range monitoring in shutdown and refuelling operation mode (10^{-10} – 10^{-6} %). There are two duplicate sets. Each set comprises of three channels. Strings of three source range detectors occupy 6 instrument wells. Range of operation is from $3\cdot10^{-4}$ to $3\cdot10^{2}$ neutrons·m^{-2}·s^{-1}. Shutdown and Refuelling Monitoring System detectors are positioned at the bottom of the wells during power operation. Detectors can be raised to an elevation of the core 72 hours after reactor shutdown. Detectors can be used (in top position) during unit start-up up to a power of 10^{-6} %.

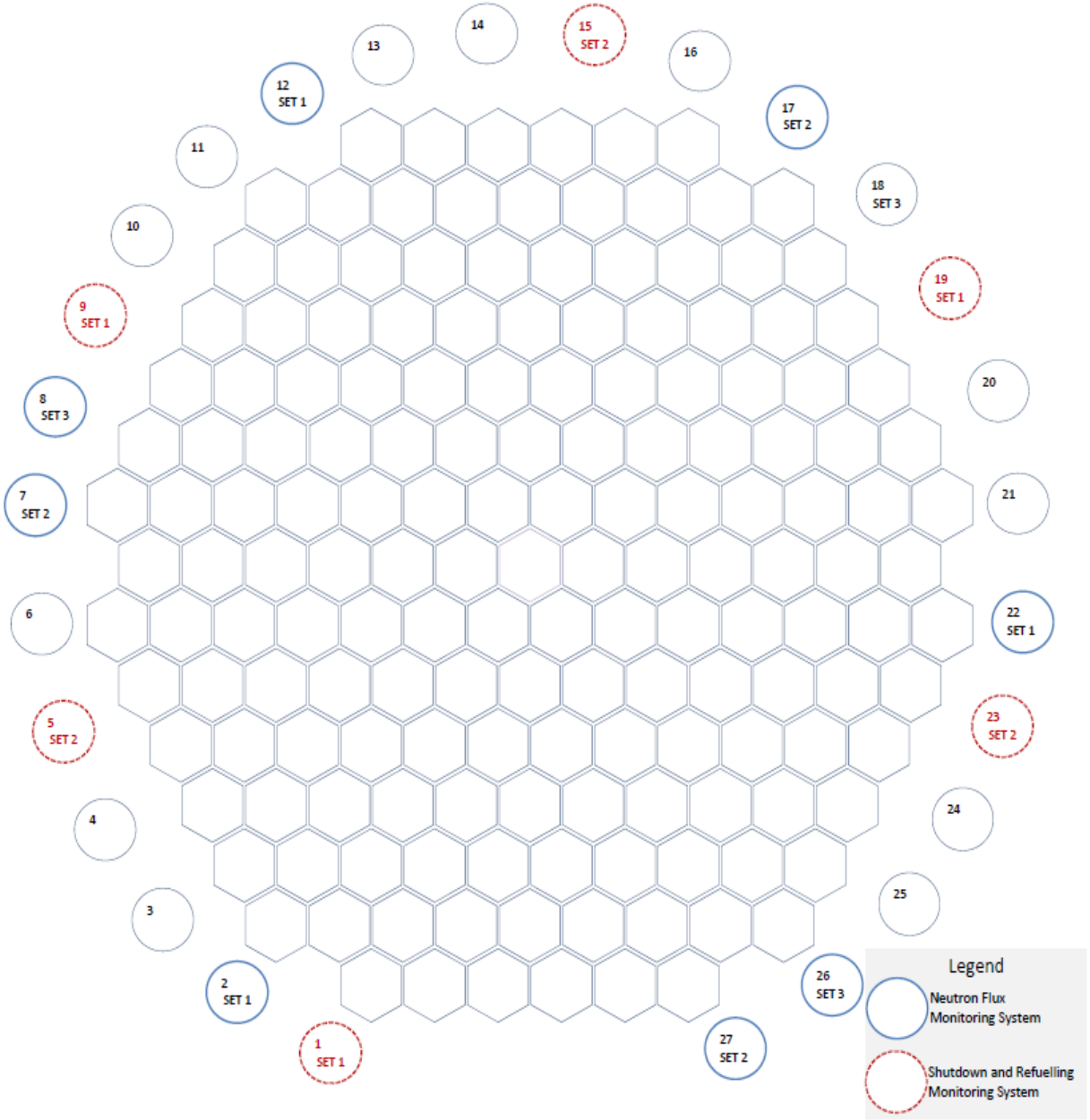

Figure 3.4-1: Map of Kozloduy 6 ex-core instrument wells locations around reactor core (Andrushechko, 2010)

3.4.2 Reactimeter

Three sets of reactimeters use input signals from ex-core detectors, Neutron flux monitoring system or Shutdown and refuelling monitoring system (Section 3.4.1).

The digital reactimeter, and the reactimeter model, calculates the margin with respect to the critical state (reactivity). The reactivity is continuously calculated based on the signals of the neutron flux monitoring system (ex-core detectors), knowledge of the composition of the fissile material in the fuel and point kinetics equations according to the Eq. 3.4-1 and Eq. 3.4-2.

$$\rho_k = \left(\sum_{i=1}^{6} \beta_i\right) + \frac{l}{n_k}\left(\frac{n_k - n_{k-1}}{\Delta t} - \sum_{i=1}^{6} \lambda_i \, C_{i,k}\right). \qquad \text{Eq. 3.4-1}$$

$$C_{i,k} = C_{i,k-1} \cdot e^{-\lambda_i \Delta t} + \frac{\beta_i n_{k-1}}{\lambda_i l}\left(1 - e^{-\lambda_i \Delta t}\right), \qquad \text{Eq. 3.4-2}$$

$$i = 1 \ldots 6 .$$

where

ρ	-	Reactivity
β_i	-	Delayed neutron fraction
l	-	Prompt-neutron lifetime, [s]
Δt	-	Time step, [s]
n	-	Neutron population (pulse count, current)
λ_i	-	Decay constant, [s^{-1}]
$C_{i,k}$	-	Precursor fraction
k	-	Current time step (index)
$k-1$	-	Previous time step (index)

The reactimeter model requires a core average (flux-weighed) set of delayed neutron fractions, decay constants and prompt-neutron lifetime.

3.4.3 In-core monitoring system

In-core monitoring system (SVRK-M) performs an evaluation of the reactor thermal power on the basis of 5 methods, as follows (Andrushechko, 2010).

a. Primary loop thermal balance;
b. Steam generator secondary side thermal balance;
c. High-pressure feedwater heater thermal balance;
d. Core power reconstruction (in-core detectors);
e. Ex-core detector readings.

Reactor system thermal power is a weighed estimation from the results of the five methods listed. Different sets of weighting coefficients can be used. Primary loop thermal balance is based on loop flow rate and loop coolant ΔT. Loop flow rate is calculated as a function of MCP head and frequency of the bus providing electric power to the motor. Secondary side thermal balance is based on measured secondary pressure and feedwater flow for each steam generator. Heat losses are interpolated from a set of values according to the plant condition. Another method of secondary thermal balance is based on main steam line pressure and feedwater flow through high-pressure feedwater heaters.

Core coolant inlet temperature is calculated on the basis of cold leg thermocouple and resistance thermometer readings and estimated (not measured) loop flow rate.

In-core monitoring system combines measured data and reactor physics calculations (BIPR-5 code) for reconstruction of core power distribution and monitors the compliance with the fuel thermal limits (in terms of the linear heat rate and the DNBR) according to the Kozloduy 6 Technical Specification requirements.

Core power reconstruction is based on the following instrument readings (Mitin, 2006).

a. 64 Rhodium Self-Power Neutron Detector (SPND) strings (7 axial positions) located in the central instrument tube of 64 fuel assemblies;
b. 95 thermocouples for coolant temperature located in fuel assembly top nozzles;
c. 3 thermocouples for coolant temperature in upper plenum;
d. 16 thermocouples and 8 resistance thermometers for coolant temperature in loop hot and cold legs;

e. Control rods positions (from control rod system), boron concentration in primary coolant, primary and secondary pressure, MCP head and feedwater flow rate;
f. Equipment line-up (e.g. open / closed position of various valves; on / off status of electric motors, pressurizer heaters, etc.).

Arrangement of SPND strings and thermocouples is shown in Figure 3.4-2.

ICMS model into the Kozloduy 6 full-scope replica control room simulator collects ‘measured’ signals from the simulated plant systems, including SPND current readings, and employs shape functions provided from NEM core model in place of BIPR-5 core simulator.

At the end, the in-core monitoring system model displays computed results via the original graphics user interface as follows.

a. Parameter distributions (in 2D slices);
b. Margins for peaking factors, linear power and DNBR;
c. Heat balance;
d. Nuclear steam supply system power;
e. Axial offset, etc.

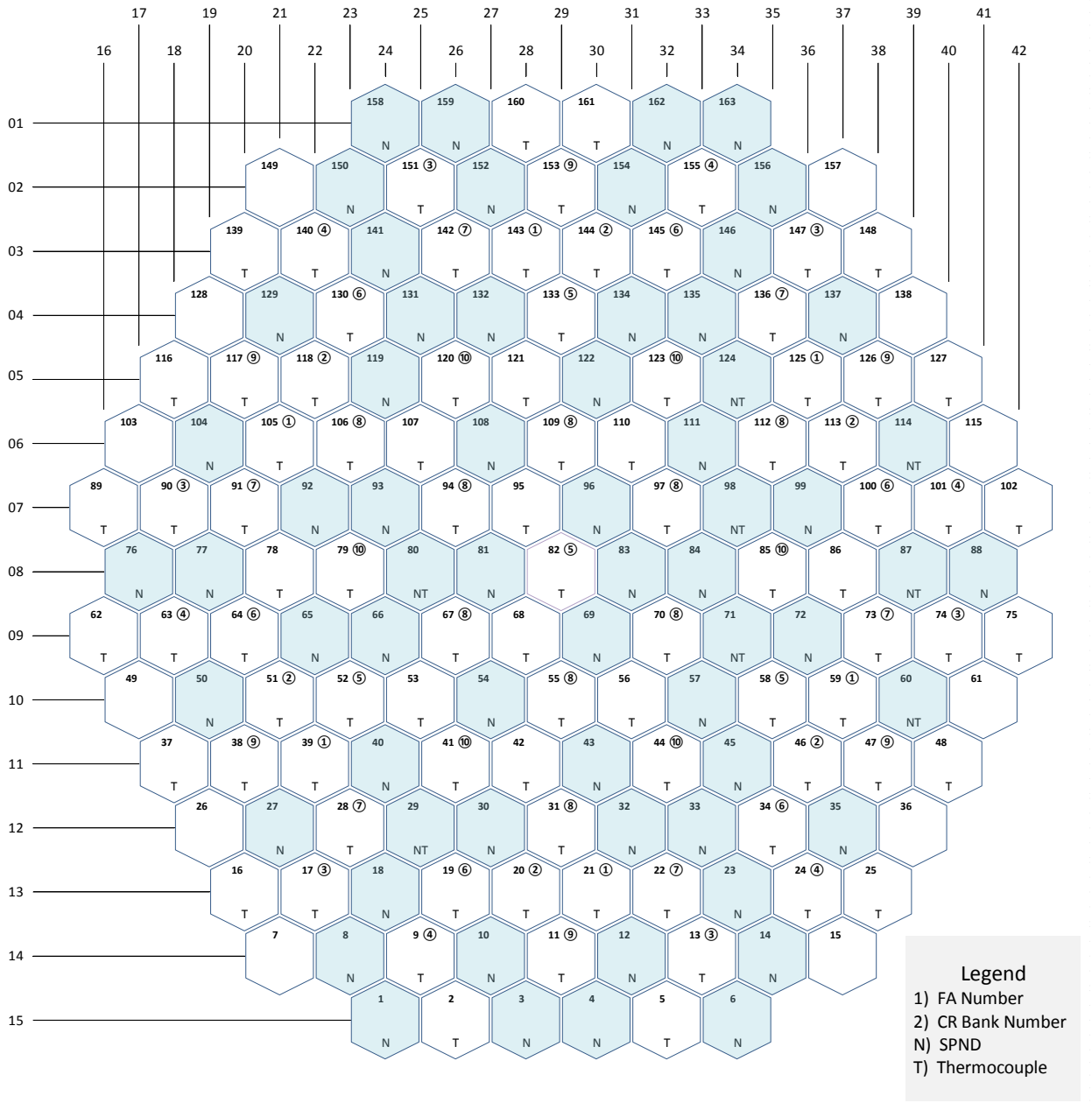

Figure 3.4-2: Map of Kozloduy 6 control rod and in-core instrumentation locations. There are three types of in-core instrumentation assemblies used: (N) SPND array with 7 axial positions; (T) coolant thermocouple above the active part of the fuel assembly; (NT) SPND array with coolant thermocouple, combined

3.5 Reactor protection and control system

Reactor protection and control system performs SCRAM, preventive protection, accelerated power decrease and reactor power control functions. Only information necessary for analysis of examples given in the following chapters is included here. Description of other reactor protection and control system functions like reactor SCRAM, preventive protection and accelerated power decrease can be found elsewhere (Yastebenetsky, 2014).

3.5.1 Reactor Power Limiter

Reactor Power Limiter (AROM-04R) monitors status of equipment and unit mode of operation and performs adjustment of nuclear steam supply system power setpoints. There are two duplicate sets. Each set comprises of three identical channels acting through 2-out-of-3 voting logic.

Nuclear steam supply system power setpoint defaults to 100 % if no deviation from normal mode of operation is present. Setpoint limitation (decrease) is performed as follows.

Table 3.5-1: Reactor Power Limiter setpoints according to plant configuration

Condition	Power setpoint
Normal operation	100 % (or lower value selected)
1-out-of-4 MCP Off	67 %
2-out-of-4 MCP Off (opposite sides of RPV)	50 %
2-out-of-4 MCP Off (neighbours)	40 %
1-out-of-2 Main Feedwater Pumps Off	50 %
Second Stage Condensate Pump Malfunction	50 %
2-out-of-4 Turbine Stop Valve Closed	40 %
Turbo-generator Off	40 %
2-out-of-2 Main Feedwater Pumps Off	6 %
Turbine by-pass Failure	6 %

In case of 3-out-of-4 MCP buss frequency less than 49 Hz the resulting setpoint is further decreased by a factor of 0.94 (Note: bus frequency of 49 Hz setpoint indicates partial degradation, not a loss of AC power. Setpoint for loss of AC power to the MCP motor is buss frequency of less than 46 Hz).

Reactor Power Limiter performs evaluation of thermal power of the nuclear steam supply system on the basis of mean coolant ΔT signals from the coolant loops in operation. Reactor Power Limiter calculates 'corrected' core power on the basis of neutron flux signals with adjustment to thermal power of the nuclear steam supply system.

Reactor Power Limiter compares 'corrected' core power with setpoint and produces a preventive protection signal for decrease of nuclear steam supply system power in case of deviation exceeding 2 %. Power rundown signal is sent to control rod system, which performs insertion of control rod bank designated for power control with a rate of one step per second as long as signal is active and there are control rod banks still in position above lower end switch (Section 3.5.3).

3.5.2 Reactor Power Controller

The reactor power controller (ARM-04R) is designed to perform automatic adjustment of reactor power to match the turbine power or to maintain nuclear steam system power at a pre-selected level (setpoint). There are two duplicate sets. Usually, one of the two sets is selected by reactor operator (through a three-position switch) and the other set is in stand-by mode. Each ARM-04R set comprises of three identical channels acting through 2-out-of-3 voting logic.

The reactor power controller performs in four modes of operation.

a. Mode T – Constant steam pressure upstream turbine control valves in the range from about 10 to 102 % rated power (±0.05 MPa).
b. Mode N – Constant core power (neutron flux) in the range from 3 to 102 % rated power (±0.5 %).
c. Stand-by – Powered up, on-line monitoring reactor power and steam pressure.
d. Mode S – Stand-by decreasing power through insertion of control rod bank in case of steam pressure increase of 0.2 MPa above setpoint.

Automatic change to Mode N is performed in following cases.

a. Core power rise above the prescribed setpoint (or above maximum setpoint of 102 %);
b. Any preventive protection (PZ) signal.

Automatic change to Mode T is performed when steam pressure is more than 0.15 MPa above setpoint unless prohibition of transition from Mode N to Mode T is active.

Prohibition for extraction of control rod banks by reactor power controller is performed as follows.

a. Core power above the prescribed setpoint (or above maximum setpoint of 102 %);
b. Reactor range rate (period) less than 40 s;
c. Any preventive protection (PZ) signal.

Prohibition for insertion of control rod banks by reactor power controller is prompted by primary pressure decrease below 15.3 MPa unless higher-priority protection signals are present.

3.5.3 Control rod system

The control rods are grouped into 10 banks. Arrangement of control rods into banks is shown in Figure 3.4-2. When the reactor is operated at rated power, all control rods are at the top position (above the lower limit switch), except Control Rod Bank No. 10. Usually, Control Rod Bank No. 10 position is 80 - 90 % (above the lower limit switch). Bank No. 10 is used to compensate small changes of reactivity due to variations of coolant temperature, boron concentration, etc.

The Control Rod System provides collective (banks) and individual control of control rod drives in automatic or manual mode. All control rods perform SCRAM and preventive protection function. When a SCRAM signal occurs all control rods are dropped into the core and the time necessary to reach the bottom position is less than 4 s.

Accelerated power decrease signal (URB) causes a drop of a designated control rod bank, No. 5.

Signals of preventive protection (PZ-1) cause sequential insertion of control rod banks with a speed of one step (2 cm) per second. Automatic sequence starts with the bank selected for power control (e.g. No. 10) and continues with other banks in decreasing order (Nos. 9, 8, etc.) with an overlap of 20 % (movement of the next bank begins when current bank position decreases below 20 % above the lower limit switch).

Preventive protection (PZ-2) signal enforces a prohibition of control rod withdrawal.

3.6 Steam and Power Conversion

The turbine-generator is designed for base-load operation with a restricted load follow operation capability. The steam generated in the four steam generators is supplied to the high-pressure turbine by the main steam system. After expansion through the high-pressure turbine, the steam passes through the four moisture separator/reheaters and is then admitted to the three low-pressure turbines. A portion of the steam is extracted from the high- and low-pressure turbines for seven stages of regenerative feedwater heating.

Exhaust steam from the low-pressure turbines is condensed and deaerated in the main condenser. The heat rejected in the main condenser is removed by the circulating water system. The first-stage condensate pumps take suction from the condenser hotwell and deliver the condensate through condensate polishing unit and ejector coolers to the suction of the second-stage condensate pumps. The second-stage condensate pumps deliver the condensate through four stages of low-pressure feedwater heaters (shell-and-tube heat exchangers) to the fifth stage, deaerating heater. Condensate then flows to the suction of the steam generator feedwater booster pump and is discharged to the suction of the main feedwater pump. The steam generator feedwater pumps discharge the feedwater through two stages of high-pressure feedwater heating to the four steam generators.

The turbine-generator has an output of approximately 1025 MWe for the nuclear steam supply system thermal output of 3000 MW(t). The K-1000-60/1500-2 turbine (Troyanovsky, 1985) is tandem-compound 6-flow layout, 1.45 m last stage blade, 1500 rpm operating speed. Rated pressure is 5.88 MPa, rated steam flow 1632 kg/s, maximum steam moisture 0.5 %. There is a single high-pressure turbine (2 x 7 stages; exhaust pressure 1.2 MPa) and three low-pressure turbines (3 x 2 x 7 stages), total length of 50.6 m and total mass of 3 280 000 kg (without condensers).

The single direct-driven generator (TVV-1000-4 UZ) is hydrogen / de-ionized water cooled, rated 1111 MVA at 0.9 power factor, 24 kV, total mass of 680,000 kg.

In the event of turbine trip, fresh steam is bypassed to the condenser via the turbine bypass valves and, if required, to the atmosphere via the atmospheric relief valves. Steam relief permits energy removal from the reactor coolant system.

Pilot-operated safety valves are provided on the four main steam lines. The pressure relief capacity of the safety valves is such that the energy generated at the high-flux reactor trip setting can be dissipated through this system.

The two start-up feedwater pumps provide feedwater to the steam generators for the removal of sensible and decay heat whenever main feedwater flow (the two turbine-driven booster / main feedwater pumps) is interrupted.

The three emergency feedwater pumps provide feedwater from three dedicated storage tanks to the steam generators for the removal of sensible and decay heat whenever feedwater from the two feedwater deaerator tanks is unavailable, including loss of offsite electric power.

Under normal operating conditions, there are no significant radioactive contaminants present in the steam and power conversion system. However, it is possible for the system to become contaminated through steam generator tube leakage. In this event, radiological monitoring of the main condenser air removal system, the steam generator blowdown system, and the main steam lines will detect contamination and alarm high radioactivity concentrations.

4. Cross section library

4.1 Cross-section representation — an overview

The established methodology for performing reactor calculations during the last 20 years is based on a two-step process (Figure 4.1-1). First, a lattice physics calculation is performed on a fuel assembly basis using reflective boundary conditions (infinite lattice calculation). The resultant neutron spectrum is used to collapse and homogenize the cross-sections to few-group cross-sections over the entire fuel assembly. Such a lattice physics calculation has to be performed for each fuel assembly type in the core. In order to cover all possible core conditions numerous sets of cross-sections for each fuel assembly type at various values of thermal-hydraulic parameters (such as fuel temperature, moderator temperature, moderator density, etc.), control feedback parameters (rodded, unrodded compositions) as well as exposure should be generated. The generation of such a cross-section set is achieved by performing numerous base depletion and 'branch' lattice calculations. At the end of this step all cross-section values are tabulated in a huge parameterized cross-section library. The second step in the process is to utilize this cross-section library by using different methods in order to analyse the reactor core. Traditionally, in the second step, a few-group diffusion theory is used for performing reactor core calculations. This approach is proven to be quite satisfactory for the current LWR cases (Ivanov, 2007a).

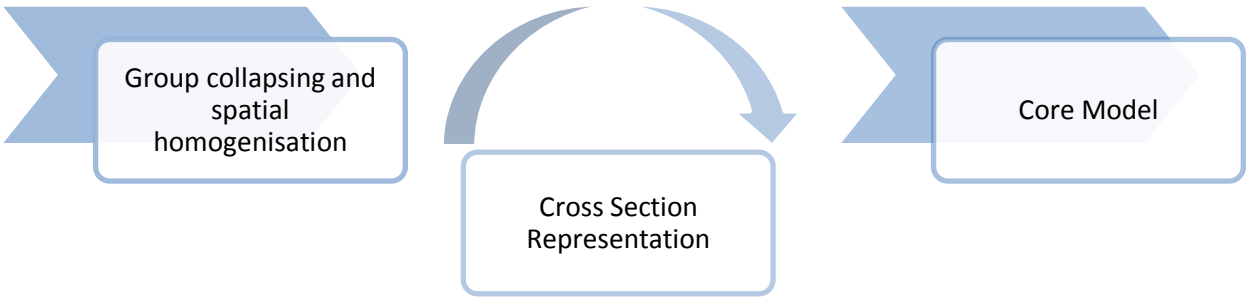

Figure 4.1-1: Scheme of the LWR neutronic core calculation path

The basis of the methodology, outlined above, is a crude simplification by the assumption of an infinite lattice neglecting the impact of the ambient conditions. Therefore, much better way to calculate homogenized cross-sections would be embedding the lattice solution in the core solution in order to use the exact environment conditions in the core. This adds the cost of repeated transport calculations every time a core simulation is performed (Kosaka, 2000). Ad-hoc approaches such as the utilization of Assembly Discontinuity Factors (ADFs) are efficient techniques to correct for environmental approximations (Smith, 1986).

Macroscopic cross section, Σ expresses the probability of neutron interaction in a macroscopic chunk of material (Duderstadt, 1976). In a lattice physics calculation, a few-group macroscopic cross section is calculated by

$$\Sigma_G = \frac{\sum_i^{i\in N} V_i \sum_g^{g\in G} \Sigma_{g,i}\phi_{g,i}}{\sum_i^{i\in N} V_i \sum_g^{g\in G} \phi_{g,i}}, \qquad \text{Eq. 4.1-1}$$

where $\Sigma_{g,i}$ is an effective macroscopic cross section, and $\phi_{g,i}$ a neutron flux of a fine group g in a sub-region i with a volume V_i (Sato, 2010).

In a PWR case, the data specifications necessary for such a lattice physics calculation are as follows.

a. Lattice geometry, $GEOM$
b. Number density in a fuel region, N_f
c. Moderator density, ρ_m
d. Fuel temperature, T_f
e. Moderator temperature, T_m
f. Boron concentration, c_B

To obtain an effective macroscopic cross section for each region, which is necessary for a spatial neutron flux calculation, a resonance calculation is performed.

The effective macroscopic cross section of fuel region $\Sigma_{g,f}$ is calculated based on a resonance calculation of each nuclide, and it depends on lattice geometry, number density of fuel region, fuel temperature and moderator density. Thus, the dependency of $\Sigma_{g,f}$ to the fuel assembly specifications can be expressed as,

$$\Sigma_{g,f} = f_1\left(GEOM; N_f; T_f; \rho_m\right). \qquad \text{Eq. 4.1-2}$$

Moderator density and boron concentration affect the effective macroscopic cross section of moderator region $\Sigma_{g,m}$. Furthermore, the moderator temperature influences the thermal scattering data of hydrogen, so the dependency of $\Sigma_{g,m}$ to the calculation specifications can be expressed as,

$$\Sigma_{g,m} = f_2(\rho_m;\ T_m; c_B). \qquad \text{Eq. 4.1-3}$$

By using the above effective macroscopic cross section, a heterogeneous assembly transport calculation is performed to obtain a spatial neutron flux $\phi_{g,i}$. Thus, the neutron flux depends on the calculation geometry and the effective macroscopic cross section. The dependency of $\phi_{g,i}$ from the calculation specifications is expressed as follows.

$$\phi_{g,f} = f_3\left(GEOM; \Sigma_{g,f}; \Sigma_{g,m}\right). \quad \text{Eq. 4.1-4}$$

$$\phi_{g,m} = f_4\left(GEOM; \Sigma_{g,f}; \Sigma_{g,m}\right). \quad \text{Eq. 4.1-5}$$

As shown by Eq. 4.1-1, a few group macroscopic cross sections for a core model are generated by collapsing and homogenizing the effective macroscopic cross sections with spatial neutron flux. So, the dependency of a few-group macroscopic cross-section Σ_G to the fuel assembly specifications can be expressed as follows.

$$\Sigma_G = f_5\left(GEOM; \Sigma_{g,i}; \phi_{g,i}\right) = f_6\left(GEOM; \Sigma_{g,f};\ \Sigma_{g,m}; \phi_{g,f}; \phi_{g,m}\right). \quad \text{Eq. 4.1-6}$$

By substituting the Eq. 4.1-4 and Eq. 4.1-5 into Eq. 4.1-6 the dependency of Σ_G can be rewritten as,

$$\begin{aligned}\Sigma_G &= f_7\left(GEOM; \Sigma_{g,f}; \Sigma_{g,m}; f_3\left(GEOM; \Sigma_{g,f}; \Sigma_{g,m}\right); f_4\left(GEOM; \Sigma_{g,f}; \Sigma_{g,m}\right)\right) \\ &= f_8\left(GEOM; \Sigma_{g,f}; \Sigma_{g,m}\right).\end{aligned} \quad \text{Eq. 4.1-7}$$

By substituting Eq. 4.1-2 and Eq. 4.1-3 into Eq. 4.1-7, the dependency of Σ_G can be rewritten as,

$$\begin{aligned}\Sigma_G &= f_9\left(GEOM; f_1\left(GEOM;\ N_f\ ; T_f\ ; \rho_m\right), f_2\left(\rho_m;\ T_m\ ; c_B\ \right)\right) \\ &= f_{10}\left(GEOM; N_f; T_f\ ; \rho_m; T_m\ ; c_B\ \right).\end{aligned} \quad \text{Eq. 4.1-8}$$

The number density of fuel region N_f can be expressed as

$$\mathrm{N}_f = f_{11}\left(N_{f_0}\ ; Bu\right). \quad \text{Eq. 4.1-9}$$

where N_{f_0} is an initial fuel composition and Bu is an assembly burn-up.

By substituting the Eq. 4.1-9 into Eq. 4.1-8, the dependency of Σ_G can be rewritten as

$$\Sigma_G = f_{12}\left(GEOM; N_{f_0}; Bu; C_B; T_f\ ; \rho_m; T_m\ \right). \quad \text{Eq. 4.1-10}$$

Although the seven physical terms of Eq. 4.1-10 correspond to the parameters in the lattice physics calculation, assuming the typical state in core calculation, $GEOM$, N_{f_0} and Bu for each assembly is uniquely specified. Otherwise, T_f, ρ_m, T_m and c_B depend on core calculation conditions.

The two groups of parameters above, on which the cross-sections greatly depend are so called instantaneous parameters and history parameters. Most of the instantaneous parameters are the local thermal-hydraulic parameters: moderator temperature and density, fuel temperature, and boron (Müller, 2007). Branch-off calculations are performed with a lattice code for all of the possible combinations of the instantaneous parameters.

The history dependence is a burn-up dependence and the history parameters include exposure, control history, and spectral history. History parameters are introduced in order to capture the impact of previous changes in the reactor on the current reactor state (Dufek, 2011a).

The control history in a PWR is often treated as a burnable poison history but this is a simplification. Control rod history is usually neglected as the control rods are rarely used during the fuel cycle of electric power generating units but it is not exactly the case in nuclear propulsion installations. Furthermore, control rod history is not known at the stage of core design and can only be accounted for in an on-line core monitoring application or post-event analysis.

Another factor often neglected is the migration of a fuel assembly throughout the core in successive fuel loads, e.g. 'in-in-out' strategy applied in a pursuit of more uniform power distribution and better fuel economy. This simplification is a trade-off between some loss of accuracy and quite significant reduction in complexity, man-power and computer resources necessary to take into account detailed spectral history. The price of this simplification will be discussed in the following chapters of this work.

As a conclusion, there are usually several independent parameters that may influence a few-group neutron cross-sections, both instantaneous and history parameters. At the end of the process, all cross-sections are tabulated in a multi-dimensional parameterized table. The table is built on a finite set of samples taken at regular or irregular intervals for each parameter.

There are traditionally two ways for recovering few-group cross section – approximation and interpolation.

Approximation is done via standard regression (Dufek, 2011b), step-wise regression (Zimin, 2005) and via quasi-regression (Bokov, 2007). All of these approaches can be implemented on arbitrary samples (Bokov, 2007).

The simplest form of interpolation is a table representation of the samples with a rule for interpolating with low-order functions between them (Watson, 2002), (Fujita, 2010). This method is simple to implement, to reconstruct from and the library is easily readable and interpretable, since it contains the explicit cross section values calculated at particular value of independent parameter with a rule for interpolation.

A refined method is multi-linear interpolation on a sparse grid. The sparse grid method is based on Smolyak's construction. This construction is a special way of combining tensor products of one-dimensional linear functionals (e.g. interpolants, quadratures, etc.) with the objective of optimizing their convergence rate for certain classes of functions. Multi-dimensional discretization meshes, resulting from this process, are called sparse grids (Botes, 2011). Higher-order polynomials could be used (Dufek, 2011b), or trigonometric functions, or a mixture of different basis functions in different directions (Guimarães, 2009), or interpolation with higher order Lagrange polynomials and quasi-regression with higher-order Legendre polynomials (Bokov, 2012).

If the difference between the neutron spectrum in the true environment and in the infinite medium is relevant, these averaged values do not permit to represent true reaction rates. For example, the error induced is not negligible with neighbouring assemblies with different compositions. So, there are methods determining a homogenization correction to multi-group cross sections, corresponding to the difference between a realistic neighbourhood environment, asymmetric and non-uniform, and infinite medium spectrum, (Dall'Osso, 2010).

4.2 Cross-section generation and modelling

Cross-section modelling methodology employed in this work (Georgieva, 2014) is a further development of the methodology outlined in (Watson, 2002) and (Ivanov, 2007a). The HELIOS-1.9 lattice code (HELIOS Methods, 2003) is used to calculate cross-section data tables.

HELIOS-1.9 is based on ENDF/B-VI evaluated neutron data library. IAPWS Industrial Formulation 1997 for the thermodynamic properties of water and steam is employed for calculation of coolant properties.

A summary of the cross-section modelling methodology is presented in Figure 4.2-1.

At the first step, various HELIOS models for fuel assemblies and reflectors are developed accounting for geometry and material composition.

Second, a complete set of cross-section data is generated. Cross-section data are tabulated per multiple instantaneous parameters, depletion points, and spectral history points. All of these parameters are assumed to be the same for all the cross-section sub-sets, both fuel assemblies and reflectors.

Third, a cycle-specific cross-section library is generated by linear interpolation over the whole set of cross-section data according to exposure and moderator temperature history values of interest.

Fourth, block data files are produced and uploaded into a real-time simulation environment, and new simulator initial condition is created.

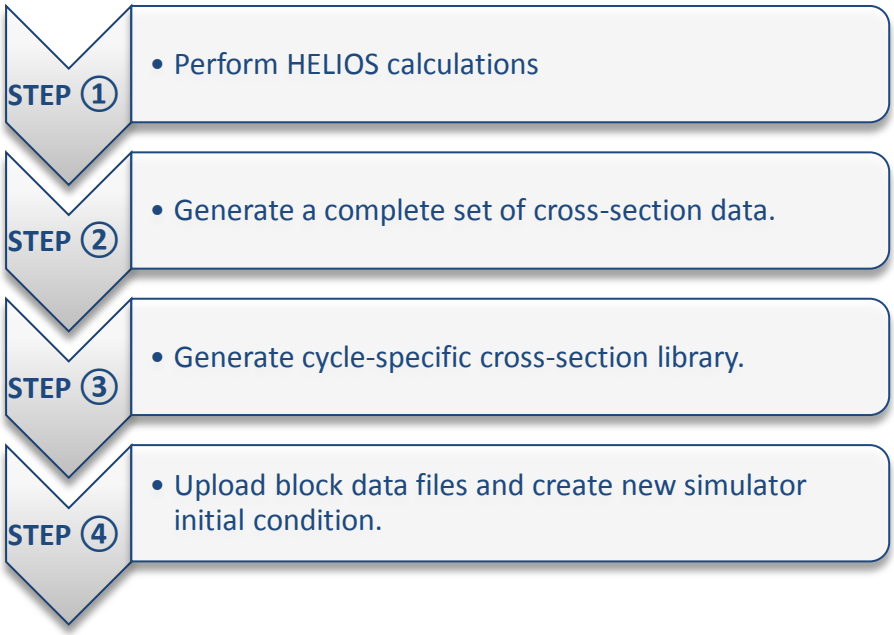

Figure 4.2-1: Flowchart of cross-section generation and modelling methodology

Such an approach for cross-section generation and modelling, as outlined above, was developed and tested several years ago at the Pennsylvania State University (Ivanov, 2007a). This approach has been further developed in this work for the purpose of a cycle-specific real-time simulation of a light-water reactor with a hexagonal fuel assembly core. Currently, there are few examples of VVER full-scope simulators equipped with a cycle-specific reactor core model.

4.2.1 Geometry and material composition

Fuel assembly types present in the reactor core are most often distinguished by a variation in pin fuel composition (fuel enrichment, burnable poison, etc.). Each fuel assembly type is represented as a single fuel assembly in an infinite lattice physics HELIOS calculation. There are two HELIOS base input models per fuel assembly type: one handling a fuel assembly without control rods, another for a fuel assembly with control rods inserted.

Three reflector models are used: bottom, top and radial. Two-group reflector cross-sections are generated by performing a two-dimensional colour-set lattice physics transport calculations, including the next fuel region. Hence, the feedback of fuel temperature on the reflector region is modelled. The value of the fuel temperature is taken from the neighbouring fuel region for both axial and radial reflectors (Ivanov, 2006). This is a very simple approach, because a single fuel composition is used for each of the reflector models. Such kind of model is used at present in order to minimize time consuming lattice physics calculations.

Fuel assembly geometry and material composition data, as well as data for reactor vessel internals, relevant to the Kozloduy 6 examples are given in some detail in Appendix A. Modelling assumptions used for the calculations are presented, too.

4.2.2 Instantaneous modelling

The instantaneous dependence model of the cross-sections is based on four thermal-hydraulic variables: fuel temperature, moderator temperature, moderator density and boron (boric acid) concentration. These variables are the feedback parameters, calculated by RELAP5-HD™. A linear interpolation over four-dimensional look-up tables is used.

For the purpose of a full-scope replica control room simulator an extremely wide range of all the four feedback parameters is necessary. The scope of simulation shall cover the whole range of plant operation modes ranging from cold shutdown (depressurized) to rated power, as well as deviations from normal operating modes and even beyond-design basis accidents (ANSI/ANS-3.5-2009, 2009). Ranges of fuel and moderator temperature shall be consistent with ranges of parameters of properties of water and steam and other material properties used.

The expected scope is covered by the selection of an adequate range of the independent variables (*i.e.* feedback parameters), as follows.

a. 300 ÷ 3100 K for fuel temperature;
b. 300 ÷ 1500 K for moderator (coolant) temperature;
c. 0.1 ÷ 1000 kg/m^3 for moderator (coolant) density;
d. 5 ÷ 2933.33 ppm boron concentration (0.029 ÷ 16.8 g/kg boric acid) in the primary coolant.

An important consideration is how to cover the above mentioned range with number of points in order to find a reasonable compromise between library size and accuracy of the interpolation. Taking into account manpower and computer resources available, the selection is to use a 300-point template for the four-dimensional macroscopic cross-section look-up tables, as follows.

a. 5 points for (node-average) fuel temperature;
b. 5 points for (node-average) moderator (coolant) temperature;
c. 6 points for (node-average) moderator (coolant) density;
d. 2 points for boron (boric acid) concentration.

Values for each of the four feedback parameters are shown in Table 4.2-1.

Table 4.2-1: Range of values of the feedback parameters and reference values for spectral history used for generation of cross-section library tables

Parameter	Instantaneous modelling interpolation values	History modelling reference value
Fuel temperature, K	300 – 800 – 1200 – 2700 – 3100	1000
Moderator temperature, K	300 – 600 – 900 – 1200 – 1500	577.15
Moderator density, kg/m^3	0.1 – 100 – 300 – 600 – 800 – 1000	718.85
Boron concentration, ppm	5 – 2933.33	800

4.2.3 Burn-up and spectral history modelling

The cross-section tables generated by lattice calculations contain a full set of cross-section data for each type of fuel assembly. One unrodded and two rodded (Boron Carbide and Dysprosium-Titanium) compositions are accounted for. Cross-section data are tabulated per multiple depletion points and per multiple spectral history points. As an example, a set of 32 non-equidistant depletion points and burn-up up to 75 MWd/kgU are common, as well as one (core average) or three (inlet, average and outlet) moderator temperature points.

The cycle-specific cross-section library is designed for ten axial layers containing fission material (Figure 3.1-1 and Figure 4.2-2). Single layer is used for bottom, top and radial reflectors. Exposure for each node is usually obtained from BIPR-7A load design calculations. This is a simple way to

create an initial condition for a selected fuel cycle and core effective full-power days. The initial condition is benchmarked with the data from Kozloduy 6 ICMS and from BIPR-7A calculations.

There are three options for moderator temperature history models studied.

a. core-average coolant temperature;
b. a linear interpolation between three moderator temperature points - one point corresponding to the highest (outlet) temperature, one point for the core-average coolant temperature, and the final point representing the lowest temperature (inlet);
c. a linear interpolation based on prescribed three-dimensional node-by-node coolant temperature distribution.

The use of core-average coolant temperature is a simple approach, which is the least expensive in terms of manpower and computer resources necessary for lattice calculations. The two other models with increased complexity produce a noticeable effect on axial power distribution within the core but the results are not always consistent when compared with the axial profile reconstructed by Kozloduy 6 ICMS on the basis of rhodium self-powered neutron detector readings. Possible explanation for the lack of improvement is the fact that ever the last model (item ‘c’) is not comprehensive enough to reflect spectrum variations throughout core life. A further investigation is necessary in order to justify the potential improvement, if any against the necessary effort. The basic, single temperature approach is employed for the present methodology.

Axial layer	Assembly																												
	1	**2**	**3**	**4**	**5**	**6**	**7**	**8**	**9**	**10**	**11**	**12**	**13**	**14**	**15**	**16**	**17**	**18**	**19**	**20**	**21**	**22**	**23**	**24**	**25**	**26**	**27**	**28**	**29**
Top Reflector																													
12	*283*	*283*	*283*	*283*	*283*	*283*	*283*	*283*	*283*	*283*	*283*	*283*	*283*	*283*	*283*	*283*	*283*	*283*	*283*	*283*	*283*	*283*	*283*	*283*	*283*	*283*	*283*	*283*	*283*
11	10	20	30	40	50	60	70	80	90	100	110	120	130	140	150	160	170	180	190	200	210	220	230	240	250	260	270	280	*282*
10	9	19	29	39	49	59	69	79	89	99	109	119	129	139	149	159	169	179	189	199	209	219	229	239	249	259	269	279	*282*
9	8	18	28	38	48	58	68	78	88	98	108	118	128	138	148	158	168	178	188	198	208	218	228	238	248	258	268	278	*282*
8	7	17	27	37	47	57	67	77	87	97	107	117	127	137	147	157	167	177	187	197	207	217	227	237	247	257	267	277	*282*
7	6	16	26	36	46	56	66	76	86	96	106	116	126	136	146	156	166	176	186	196	206	216	226	236	246	256	266	276	*282*
6	5	15	25	35	45	55	65	75	85	95	105	115	125	135	145	155	165	175	185	195	205	215	225	235	245	255	265	275	*282*
5	4	14	24	34	44	54	64	74	84	94	104	114	124	134	144	154	164	174	184	194	204	214	224	234	244	254	264	274	*282*
4	3	13	23	33	43	53	63	73	83	93	103	113	123	133	143	153	163	173	183	193	203	213	223	233	243	253	263	273	*282*
3	2	12	22	32	42	52	62	72	82	92	102	112	122	132	142	152	162	172	182	192	202	212	222	232	242	252	262	272	*282*
2	1	11	21	31	41	51	61	71	81	91	101	111	121	131	141	151	161	171	181	191	201	211	221	231	241	251	261	271	*282*
1 *Bottom Reflector*	*281*	*281*	*281*	*281*	*281*	*281*	*281*	*281*	*281*	*281*	*281*	*281*	*281*	*281*	*281*	*281*	*281*	*281*	*281*	*281*	*281*	*281*	*281*	*281*	*281*	*281*	*281*	*281*	*281*

Figure 4.2-2: Composition numbers in axial layers by assembly type

4.2.4 Assembly discontinuity factors

ADFs quantify the ratio between the homogenized nodal flux solution and the actual heterogeneous transport solution at the boundary of the node/assembly. The simplified 2D ADFs are calculated with HELIOS-1.9 and are treated as the rest of the cross-sections with instantaneous dependencies and spectral history. ADFs are implicitly incorporated into cross-sections (i.e. by dividing the cross-section value by the ADF value for each energy group).

4.2.5 Four-dimensional look-up tables

The macroscopic cross-sections are tabulated in four-dimensional look-up tables: diffusion coefficient, $1/(3\Sigma_{tr})$; total absorption, Σ_a; fission, Σ_f; neutron production (nu-fission), $\nu\Sigma_f$; and scattering (fast to thermal), Σ_s.

A standard linear interpolation in four-dimensional tables is used. The advantage of using a linear interpolation scheme is that it is fast. The disadvantage is a loss in accuracy when linear interpolation is used due to the non-linearity of the cross-section behaviour. The error is dependent on the non-linearity of cross-sections with respect to the different feedback parameters and the distance between tabulated points.

4.2.6 Other parameters

There are parameters tabulated per each fuel composition and exposure only, as follows.

a. Two-group *Xe* and *Sm* microscopic cross sections, equilibrium number densities and yields (σ_{Xe}; $N_{Xe,\infty}$; γ_{Xe}; σ_{Sm}; $N_{Sm,\infty}$; γ_{Sm}), and neutron fluxes (ϕ);
b. Two-group energy per fission ($\varkappa$), and inverse neutron velocity (1/v);
c. Six-group precursors' parameters (delayed neutron fractions, β; and decay constants, λ).

4.2.7 Handling of cross-section tables

While the library generation is a process, performed independently and optimized to cover (hopefully) a wide spectrum of cycle-specific libraries, the process of extraction of values of macroscopic cross-sections from look-up tables for kinetic calculations is performed at each time step (e.g. 10 times per second) for each spatial node according to the local thermal-hydraulic feedback. The computer resources necessary for cross-section determination are of the same

magnitude as the resources consumed by kinetics calculations. This is another important consideration for real-time calculations.

A reactor core is designed for symmetry and this feature is used in handling of cross-section tables. If the symmetric exposure of fuel compositions is preserved, a description of one-sixth of the hexagonal core is sufficient. The assumption of circumferential symmetry is used only to optimize data storage and handling. In the case of asymmetric core, however, another set of data is loaded into desired sector using the same one-sixth format. The same procedure can be performed several times for different sectors, if necessary.

4.2.8 Accuracy of cross-section representation

Large intervals between interpolation points present in Table 4.2-1 cause much concern particularly about non-linear effects of moderator density and moderator temperature on cross-section values (Ivanov, 2007a). Interpolation over such a large interval causes an error with a magnitude of couple of per cent. A review of steady-state and transient results presented in Chapter 5 and Chapter 6 naturally points to an increase of deviations in local core parameters with increase of intervals between interpolation points. Situation is not dramatic because errors remain within allowable margins. An on-going project aims to find a technique for better accuracy of cross-section reconstruction without too extravagant increase of computer resources necessary. A technique for multi-parameter interpolation of few-group neutron cross-sections on sparse grids proposed by Prof. Pavel M. Bokov and Danniëll Botes (NECSA, The South African Nuclear Energy Corporation SOC Ltd.) is under investigation (Bokov, 2012), (Botes, 2011). At this stage it can be said the necessary algorithms are incorporated into simulation software for testing. Work in progress is the development and testing of higher-order polynomial representations with improved accuracy on large parameter ranges.

4.3 Cycle-specific cross-section update procedure

The cross sections library tables are prepared as block data files with specific format for one-sixth of the core. There are three block data files: one for unrodded fuel compositions (283, including reflectors); and two for rodded fuel compositions (110 each).

Flowchart of the cycle-specific cross-section update procedure is shown in Figure 4.3-1.

The core model is in a steady-state mode. Time-dependent terms in the diffusion equations are cancelled and equilibrium Xenon-Iodine and Promethium-Samarium concentrations are used.

Simulation of some plant control systems is disabled in order to avoid additional complications from control rod movement or other automatic actuation functions. A snapshot is recorded.

In the case of asymmetric fuel loading pattern, a further set of block data files is loaded and data stored in the desired sector. A snapshot is recorded and process returns back to the first step. This cycle can be repeated for as many data sets as necessary.

The next step is to obtain K_{eff} and/or define the critical boron (boric acid) concentration (K_{eff} = 1). This step is usually performed at rated power state of the reference unit; optionally hot or cold zero power conditions can be selected for testing of the models. The radial power distribution (F_{xy}) and the critical boron (boric acid) concentration values are compared with ICMS data and BIPR-7A calculations. The acceptance criteria used (Table 4.3-1) are the same as applied to deviations between licensing calculation (BIPR-7A) and Kozloduy 6 ICMS (Kozloduy 6 TechSpec, 2006). As much as simulator fidelity requirements put emphasis on information displayed in front of a plant control room operator, simulator customer is concerned about deviations between simulation and ICMS records.

The calculated critical boron (boric acid) concentration has to be used to initialize the RELAP5-HD^{TM} and other hydraulic system models (primary coolant system, primary coolant make-up and blowdown tanks and pipes, etc.). Then NEM is switched to a transient mode. After about 5 minutes, when reactor power is settled to a steady-state value, the simulation could be switched to the full configuration.

Final examination of boron (boric acid) concentration, power distribution and control rod worth are performed against data from reference plant transients or BIPR-7A calculations.

The final step is to update the simulator ICMS data base. Data from Kozloduy 6 ICMS archive are used, if applicable. Otherwise, ICMS configuration files have to be developed from scratch for simulation of core loads without analogue in history of the reference plant.

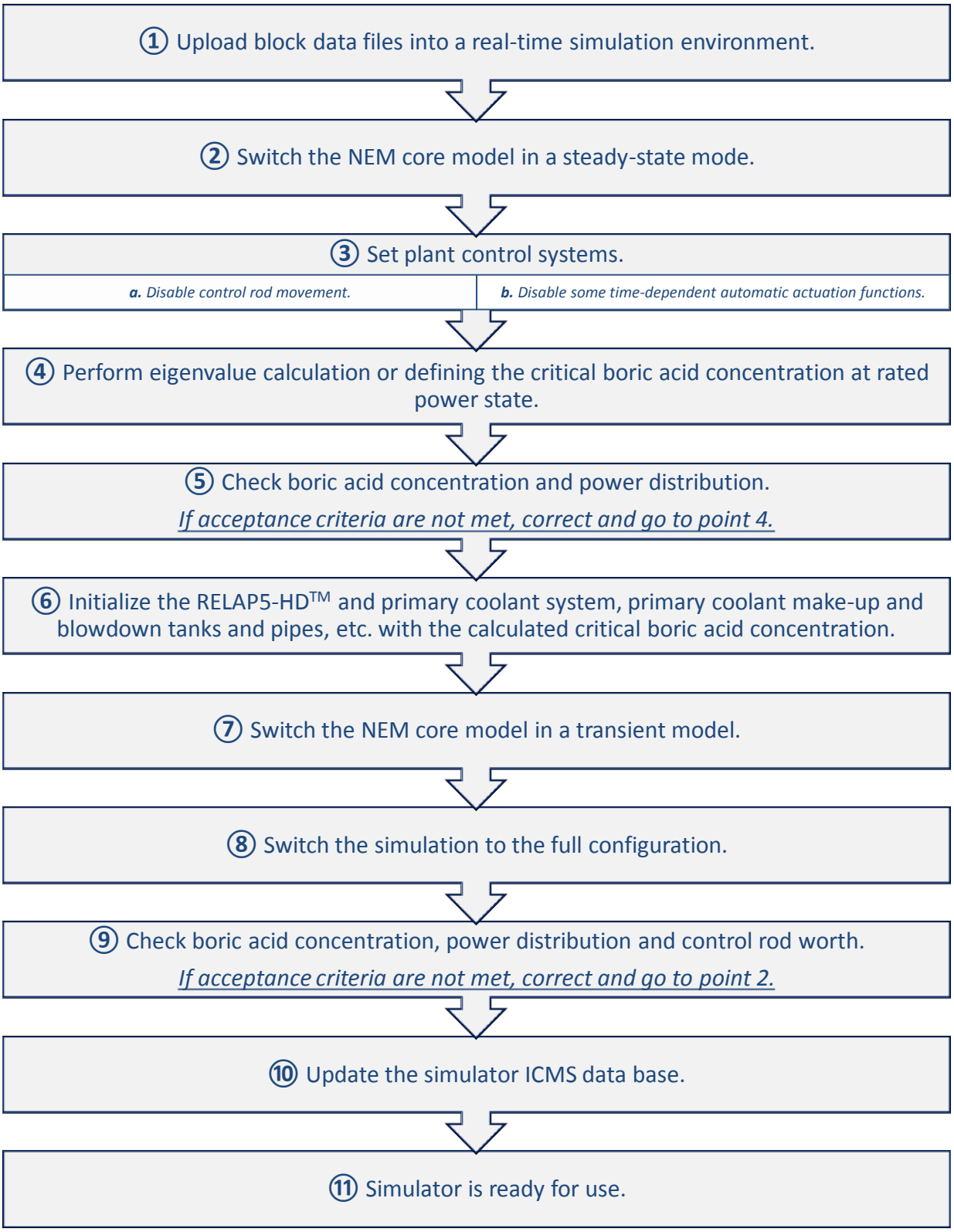

Figure 4.3-1: Flowchart of the cycle-specific cross-section update procedure

Table 4.3-1: Margin of deviations between licensing calculation and ICMS readings

Parameter	Criteria
Boric acid concentration (at the start of the fuel cycle)	± 0.3 g/kg (± 50 ppm boron)
Length of the fuel cycle, EFPD	± 3 %
Worth of control rod bank used for power control (usually control rod bank Bank No. 10)	± 20 %
Power of FA located in central part of the core	± 5 %
Power of FA located in core periphery	± 10 %
Power of FA with burn-up more than 30 MWd/kgU located in core periphery (low leakage core design)	± 15 %
Maximum local (three-dimensional) power peaking factor	± 10 %

4.4 Conclusion

An account of the simplifications introduced in the methodology of macroscopic cross-section generation presented in this chapter is given as follows.

a. The methodology of cross-section generation is based on a two-dimensional infinite lattice calculation with HELIOS-1.9 (ENDF/B-VI evaluated neutron data library; IAPWS-IF 97 for the thermodynamic properties of water and steam). Impact of ambient conditions is neglected.
b. The two-dimensional model of a large heterogeneous object (a fuel assembly) uses the best available data for geometry and material composition. A large step in both radial and axial direction is used. Because of the large step in axial direction some details, e.g. spacer grids, are ‘dissolved’ into the coolant. Also, as much as the outer diameter of the instrument tube is larger than the axis-to-axis distance between fuel pins, the tube is shrunk to fit inside the cell while volume and mass of material is preserved.
c. It is not necessary to postulate symmetry in the model. As a rule, however, the symmetry of the object as designed is exploited further for simplification of the model and small irregularities are neglected.
d. The two-dimensional model of a reflector node introduces simplifications similar to these listed in previous points. Small construction details are lumped into material compositions divided in a small number of layers. One and the same approach is used for all the reflector nodes.
e. Series of infinite lattice calculations is performed over a wide range of independent variables. Necessarily, the wide range for each of the independent variables is split into few intervals.

f. Burn-up calculation is performed with constant values of the history parameters and a set of homogenized macroscopic cross-sections is produced.
g. Homogenization is performed for two energy groups over a large heterogeneous object, a fuel assembly. Two dimensional ADF is generated by the same infinite calculation as a ratio between homogenized nodal flux solution at the boundary of the node (fuel assembly) and the heterogeneous transport solution at the boundary of the node (fuel assembly).
h. At the end, a large library is created containing entries for all the objects with geometry and material composition with all the macroscopic cross-sections tabulated per value of independent variable and per burn-up step.
i. Exposure from a load design calculations is used in the process of creation of a cycle-specific library at desired effective full-power days. There are simplifications involved in the calculation of this exposure. The exposure is averaged over a large node and used to create a cycle-specific library by linear interpolation of macroscopic cross-section values for a selected material composition between burn-up points.
j. A linear interpolation is used over a large interval between interpolation points in four-dimensional tables for macroscopic cross-section reconstruction.

A review of steady-state and transient results presented in Chapter 5 and Chapter 6 naturally points to an increase of deviations in local core parameters with increase of intervals between interpolation points. Situation is not dramatic because errors remain within allowable margins.

The macroscopic cross-section modelling methodology described in this chapter is used to produce the cycle-specific cross-section library for the participants of the Kalinin 3 Coolant Transient Benchmark (Pasichnyk, 2014). The same set of HELIOS models and cross-section data is used to develop the a version of this library in a form, compatible with the Kozloduy 6 simulator, as described in Chapter 6.

5. Kozloduy 6 simulations

Simulations presented here illustrate a full-scope plant model. No boundary conditions are used except grid voltage and frequency, condenser cooling water temperature and atmosphere pressure and temperature. Small sets of simulation results are selected with a focus of core model performance.

5.1 Rated power example

Loading pattern of the 17th fuel cycle (2011/12) of Kozloduy 6 is shown in Figure 5.1-1. There are 5 different types of TVSA fuel assemblies used.

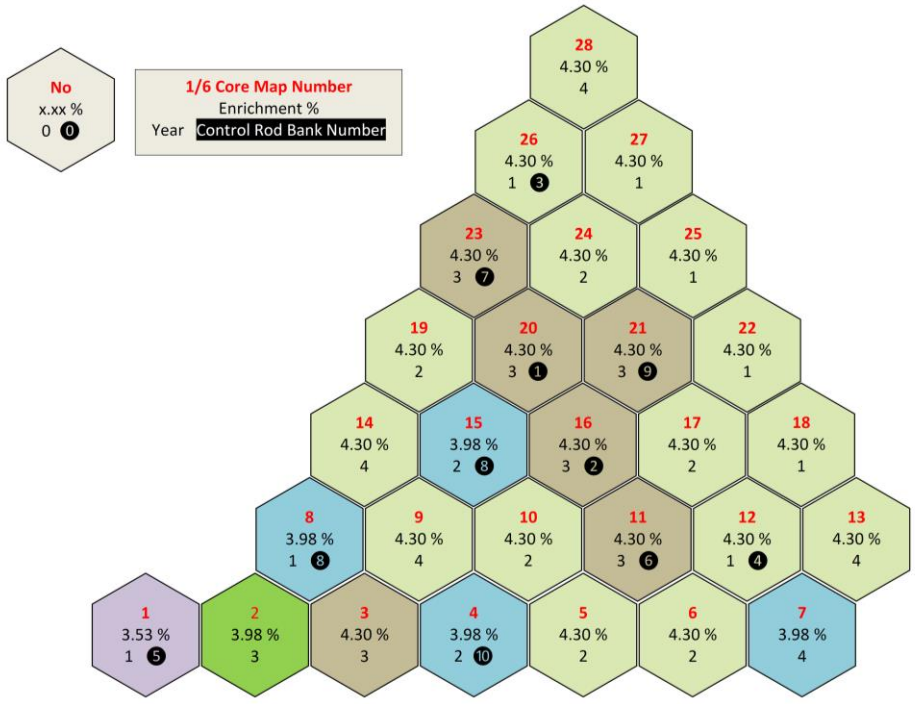

Figure 5.1-1: 17th fuel cycle pattern of the Kozloduy 6 — an one-sixth symmetry representation with FA type, enrichment and year in the core

An example of simulated rated power conditions throughout the 17th fuel cycle is shown in Figure 5.1-2, Figure 5.1-6 and Figure 5.1-10. The acceptance criteria used are the same as applied for monitoring deviations between licensing calculation (BIPR-7A) and Kozloduy 6 ICMS (Kozloduy 6 TechSpec, 2006). Deviations in comparison with Kozloduy 6 ICMS records and BIPR-7A calculations are fairly consistent and remain within acceptance limits throughout the core life, as shown in Table 5.1-1. Deviations are calculated as follows.

$$Deviation\,,\% = \left(F_{xy,\ Simulation} - F_{xy,\ ICMS}\right) \times 100\,. \qquad \text{Eq. 5.1-1}$$

$$Deviation\,,\% = \left(F_{xy,\ Simulation} - F_{xy,\ BIPR-7A}\right) \times 100\,. \qquad \text{Eq. 5.1-2}$$

This particular form of Eq. 5.1-1 and Eq. 5.1-2 corresponds to the approach used at the plant. Because only high values of F_{xy} cause much concern, normalization to unity is chosen as more conservative.

As much as simulator fidelity requirements put emphasis on information displayed in front of a plant control room operator, simulator customer is concerned about deviations between simulation and ICMS records.

Table 5.1-1: 17th fuel cycle of Kozloduy 6 – Comparison between simulation and plant data (ICMS) – Brief statistics of deviations in assembly power at the BOC, MOC and EOC

Core Life	Maximum Deviation				RMS Deviation	
					whole core	FA with SPND
EFPD	%	FA (position)	%	FA (position)	%	%
5.82	-6.50	103 (06-17)	+4.46	31 (12-29)	2.18	2.18
160.72	-4.73	103 (06-17)	+4.27	159 (01-26)	2.17	2.57
300.58	-3.68	50 (10-19)	+5.52	160 (01-28)	2.20	2.18

Comparison between simulation and Kozloduy 6 ICMS at the start of the 17th fuel cycle (Figure 5.1-3) indicates pronounced tilt in ICMS data – negative deviations in upper left part of the core and positive deviations in lower right part – while simulation results are fairly symmetric. The effect cannot be observed later during the fuel cycle (Figure 5.1-7 and Figure 5.1-11).

At the start of the fuel cycle (Figure 5.1-3) there are very small deviations in the central part, while larger absolute value deviations are later more uniformly distributed between the central part and the periphery of the core.

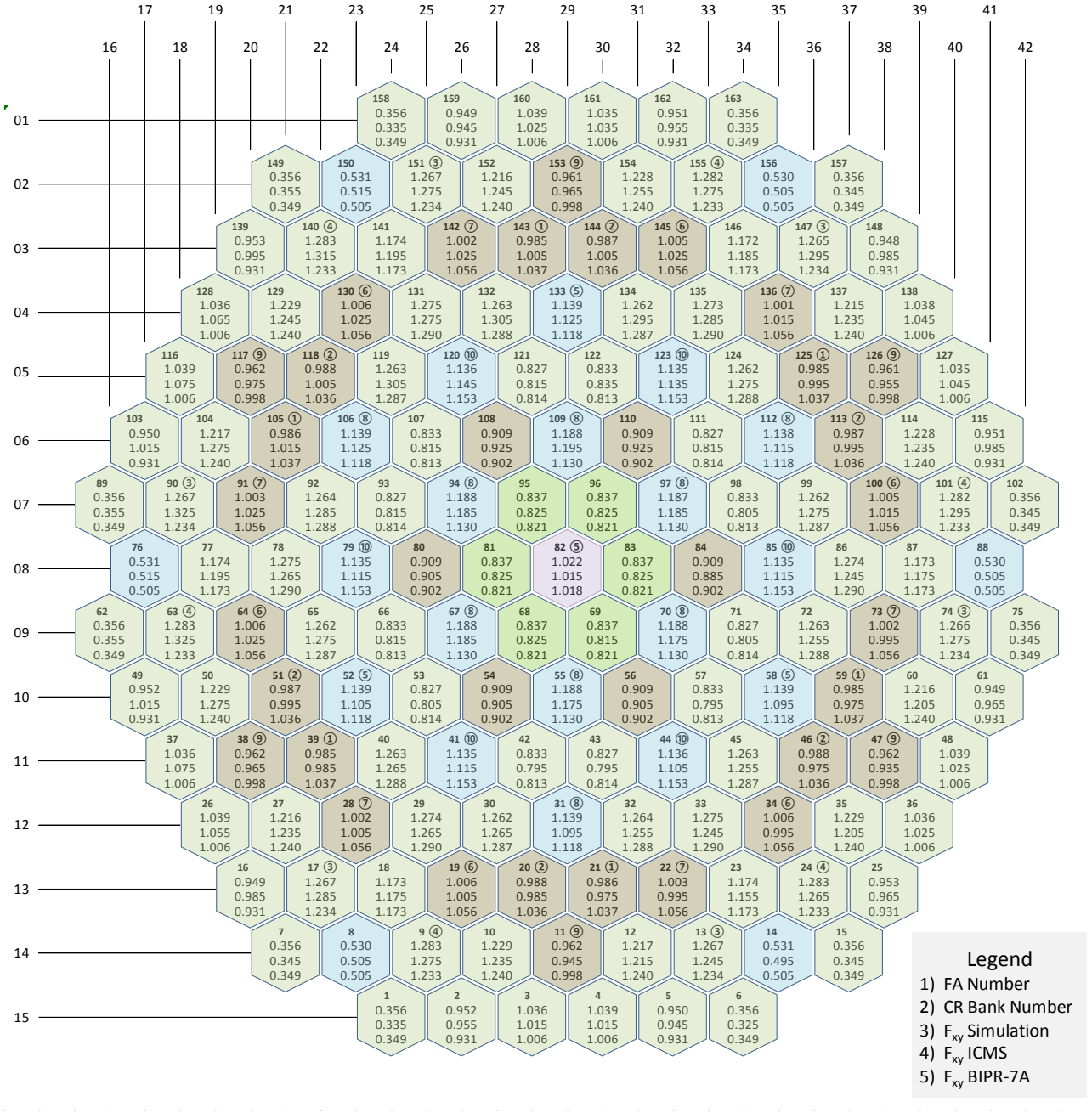

Figure 5.1-2: 17th fuel cycle of Kozloduy 6 — Comparison between simulation, plant data (ICMS) and core design calculation (BIPR-7A) — Assembly-wise power peaking factors at 5.82 EFPD

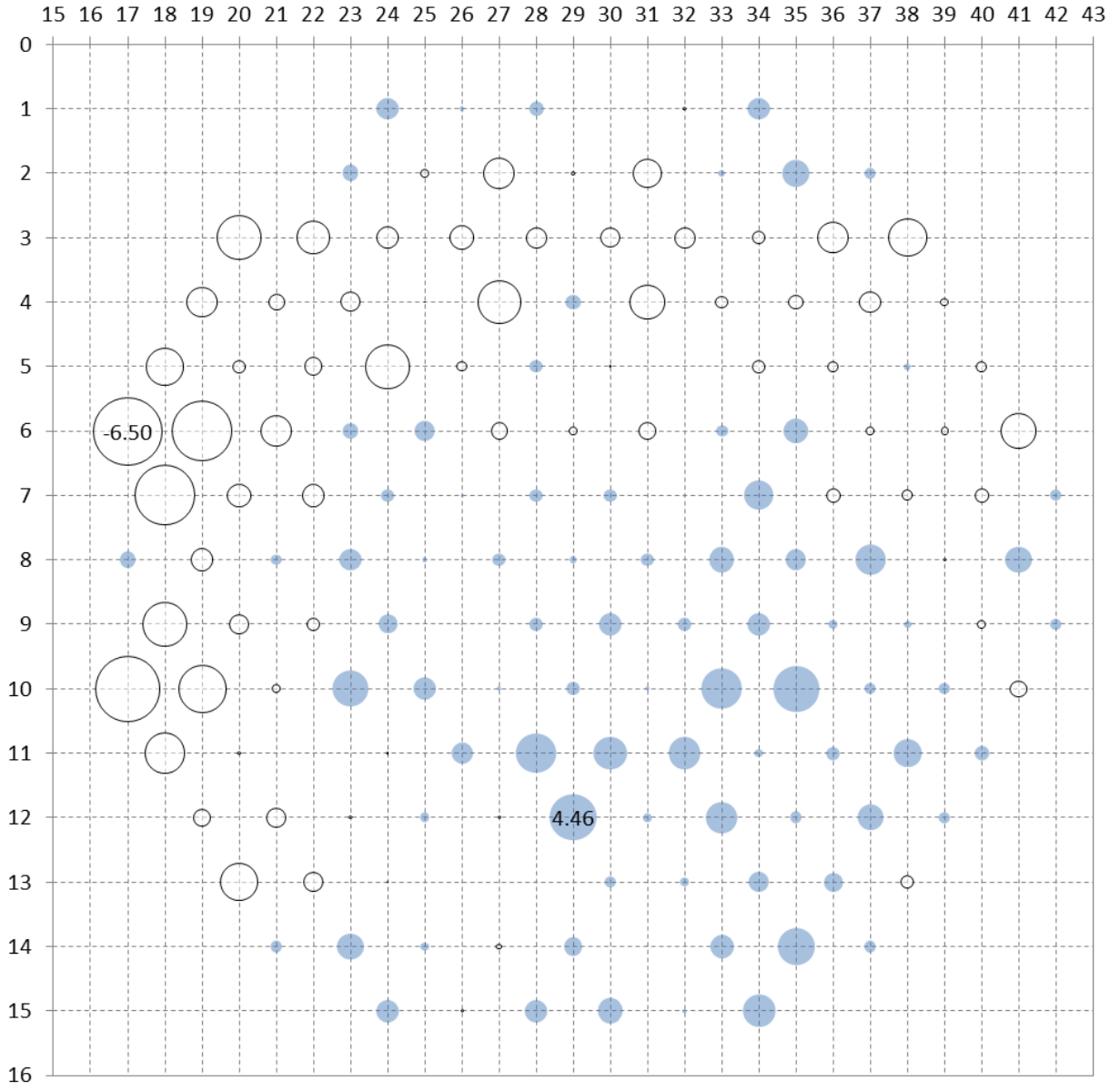

Figure 5.1-3: 17th fuel cycle of Kozloduy 6 — Comparison between simulation and plant data (ICMS) — Deviation in assembly-wise power peaking factor [%] at 5.82 EFPD (magnitude of deviation is proportional to bubble diameter; coloured — positive, transparent — negative)

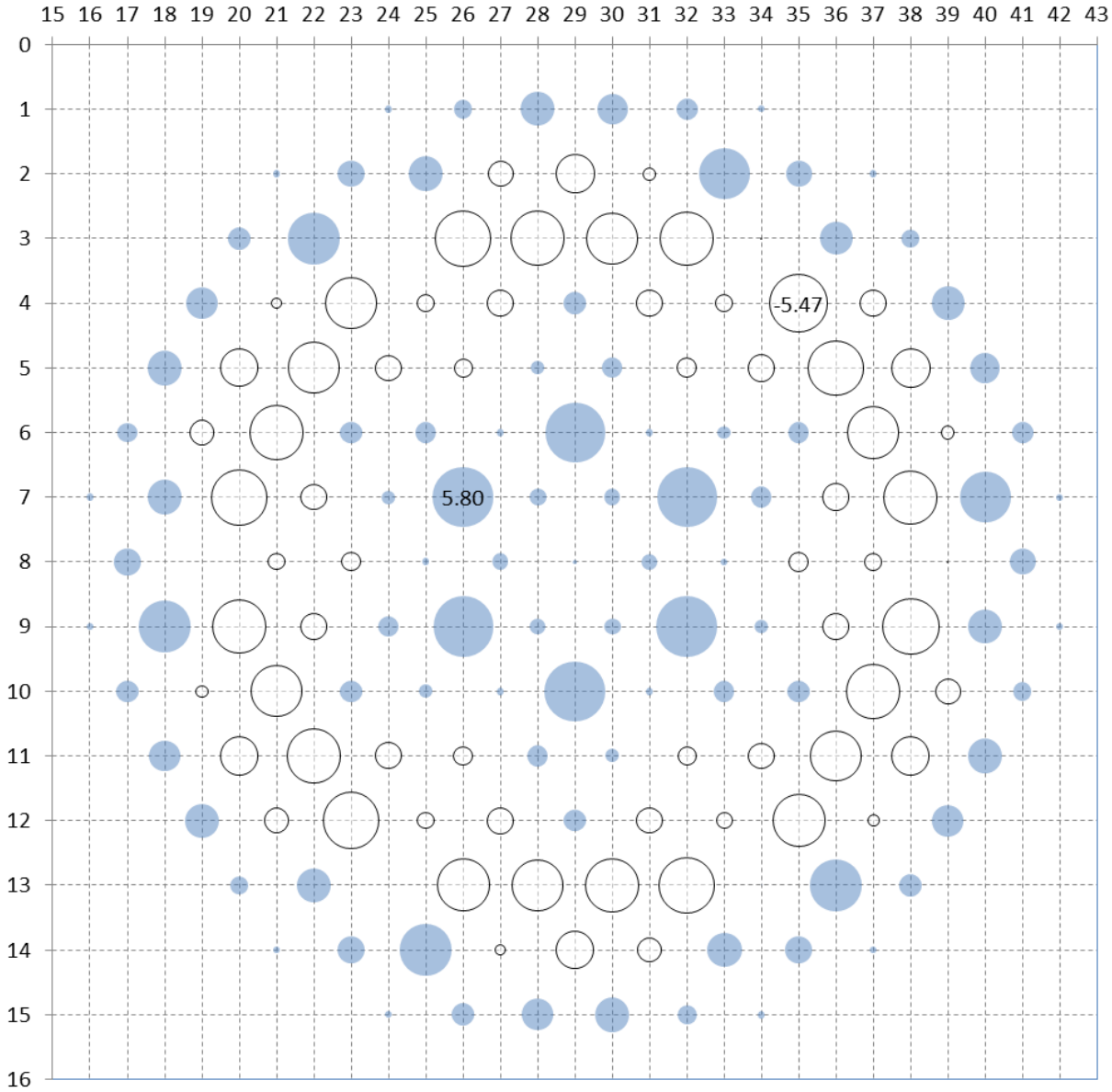

Figure 5.1-4: 17th fuel cycle of Kozloduy 6 — Comparison between simulation and core design calculation (BIPR-7A) — Deviation in assembly-wise power peaking factor [%] at 5.82 EFPD (magnitude of deviation is proportional to bubble diameter; coloured — positive, transparent — negative)

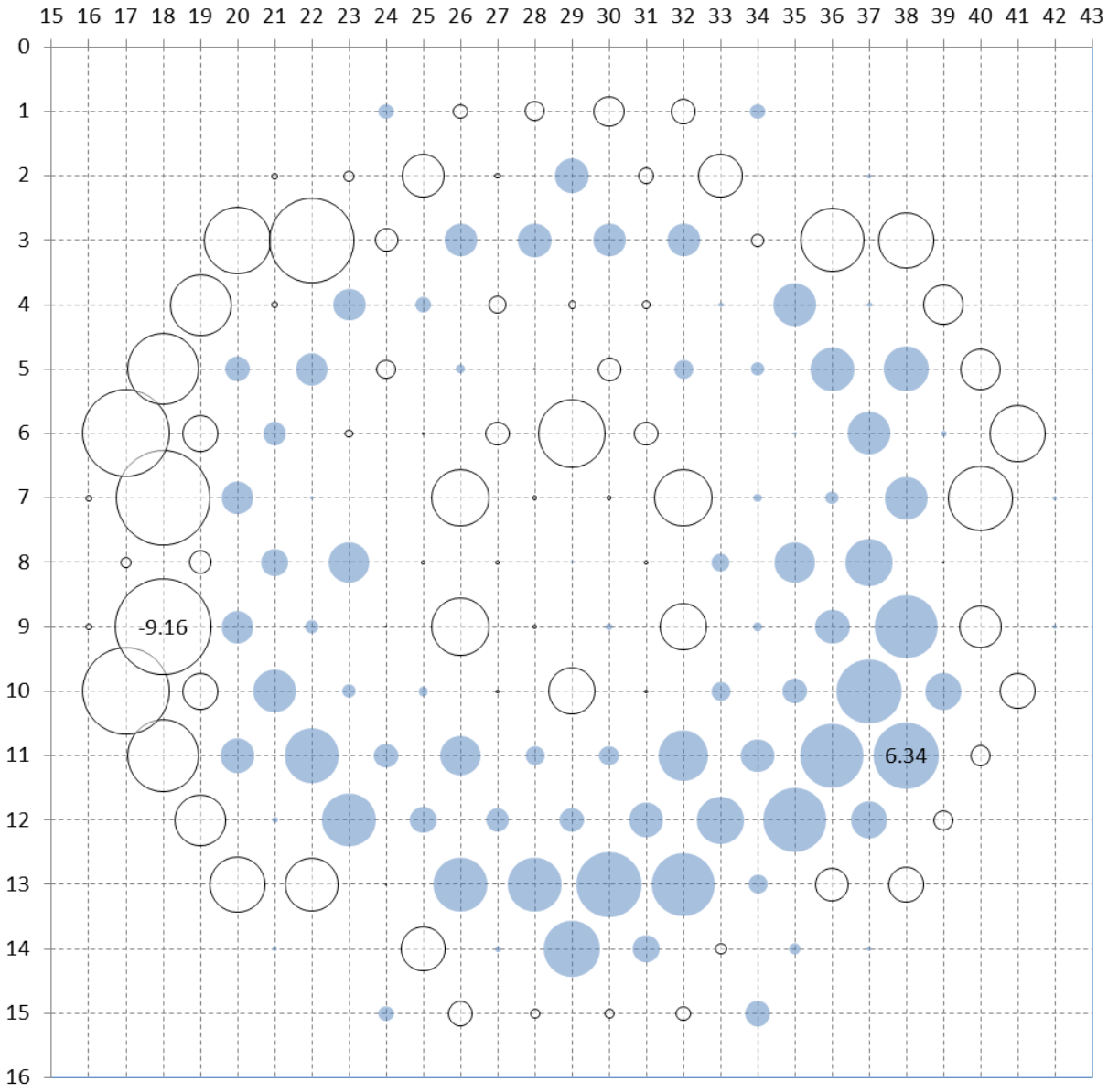

Figure 5.1-5: 17th fuel cycle of Kozloduy 6 — Comparison between plant data (ICMS) and core design calculation (BIPR-7A) — Deviation in assembly-wise power peaking factor [%] at 5.82 EFPD (magnitude of deviation is proportional to bubble diameter; coloured — positive, transparent — negative)

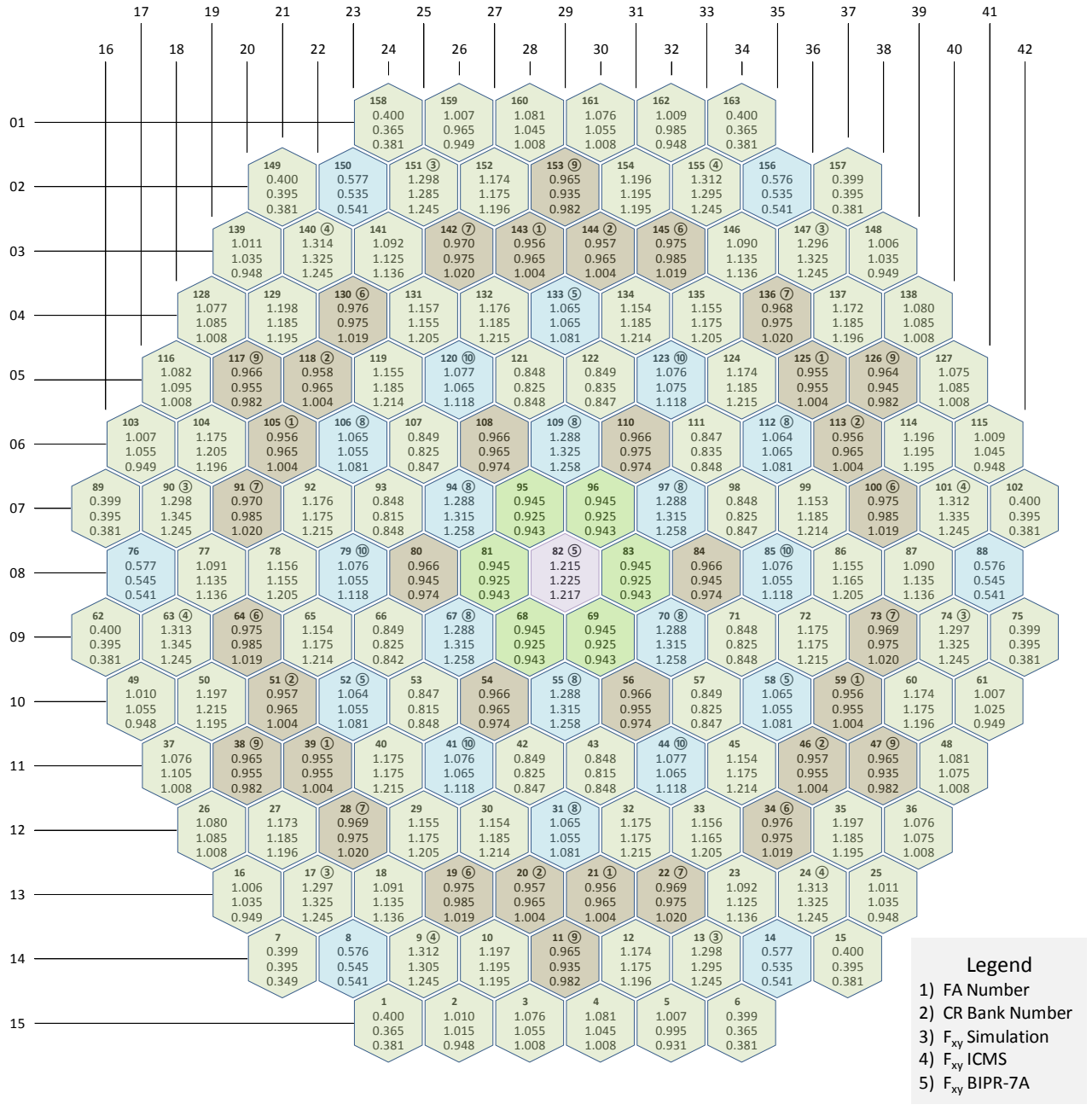

Figure 5.1-6: 17th fuel cycle of Kozloduy 6 — Comparison between simulation, plant data (ICMS) and core design calculation (BIPR-7A) — Assembly-wise power peaking factors at 160.72 EFPD

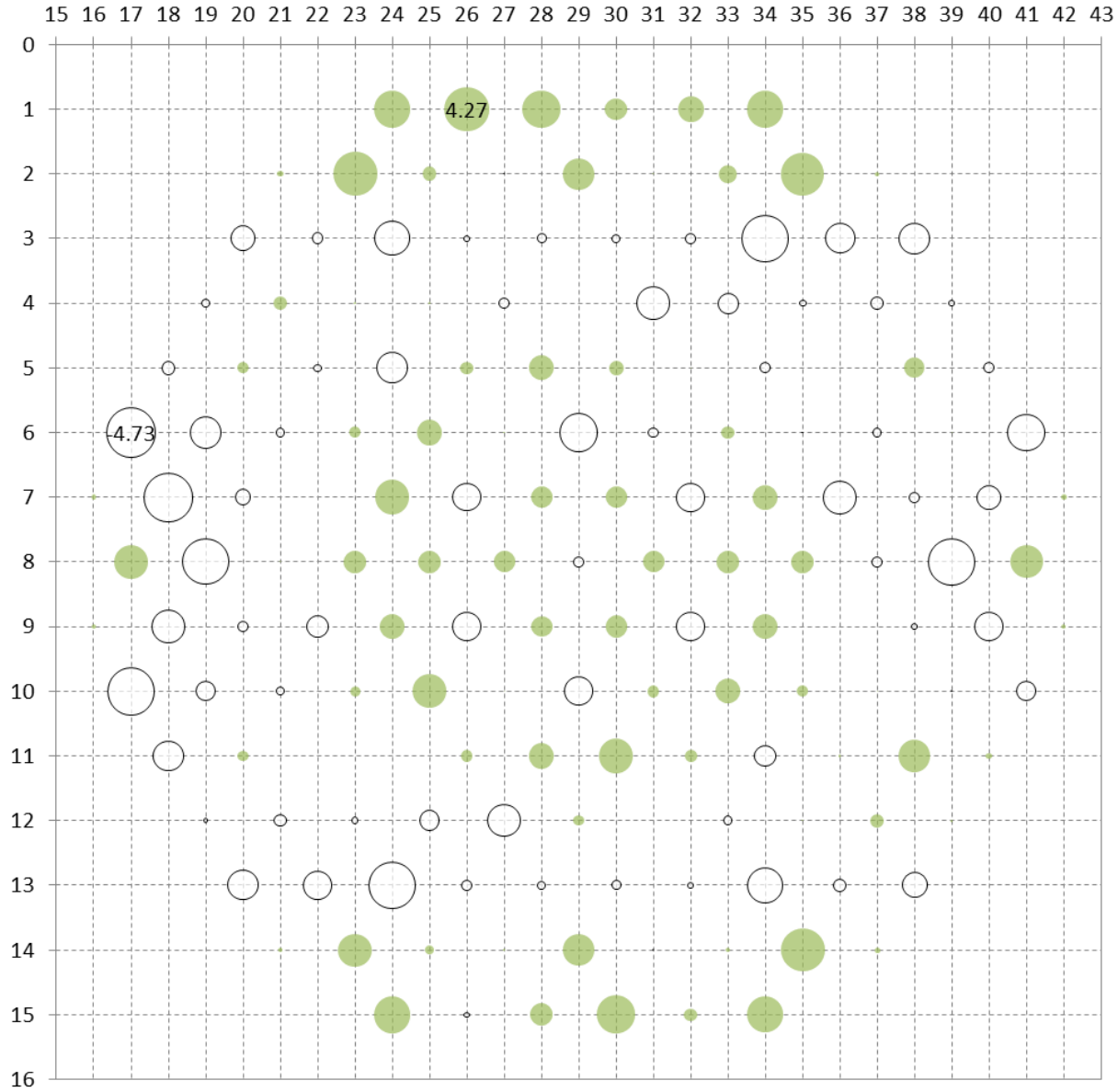

Figure 5.1-7: 17th fuel cycle of Kozloduy 6 — Comparison between simulation and plant data (ICMS) — Deviation in assembly-wise power peaking factor [%] at 160.72 EFPD (magnitude of deviation is proportional to bubble diameter; coloured — positive, transparent — negative)

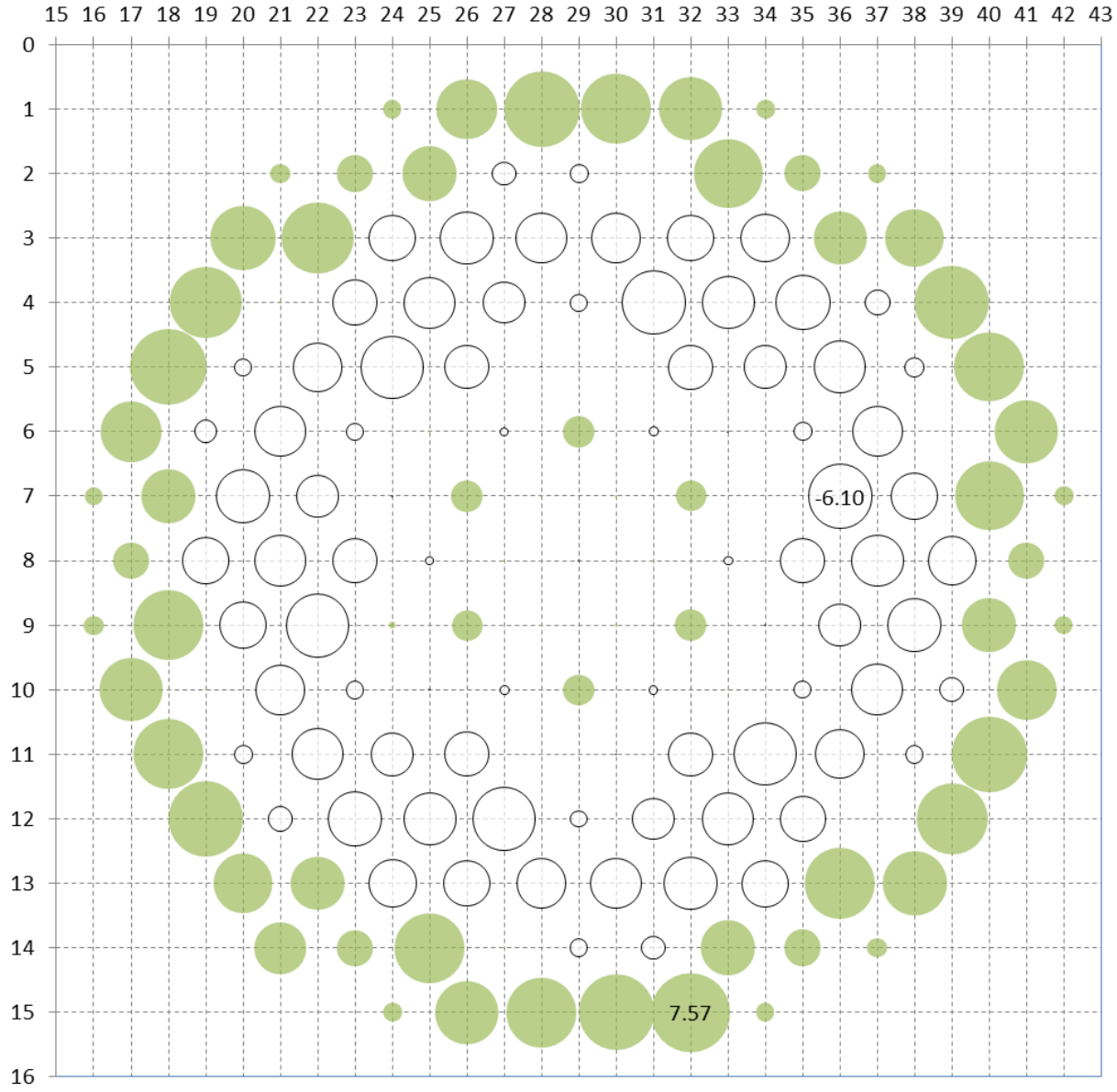

Figure 5.1-8: 17th fuel cycle of Kozloduy 6 — Comparison between simulation and core design calculation (BIPR-7A) — Deviation in assembly-wise power peaking factor [%] at 160.72 EFPD (magnitude of deviation is proportional to bubble diameter; coloured — positive, transparent — negative)

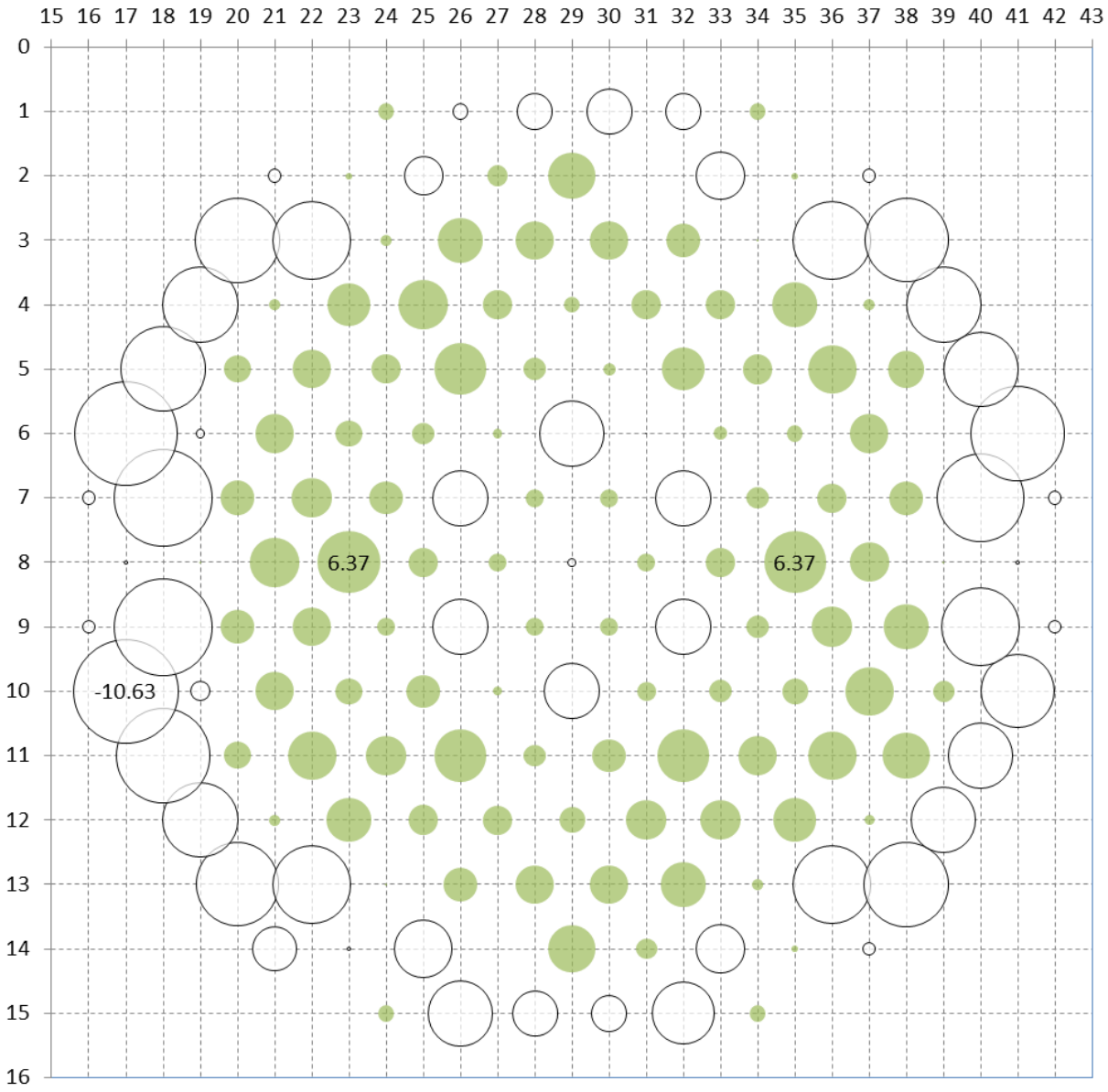

Figure 5.1-9: 17th fuel cycle of Kozloduy 6 — Comparison between plant data (ICMS) and core design calculation (BIPR-7A) — Deviation in assembly-wise power peaking factor [%] at 160.72 EFPD (magnitude of deviation is proportional to bubble diameter; coloured — positive, transparent — negative)

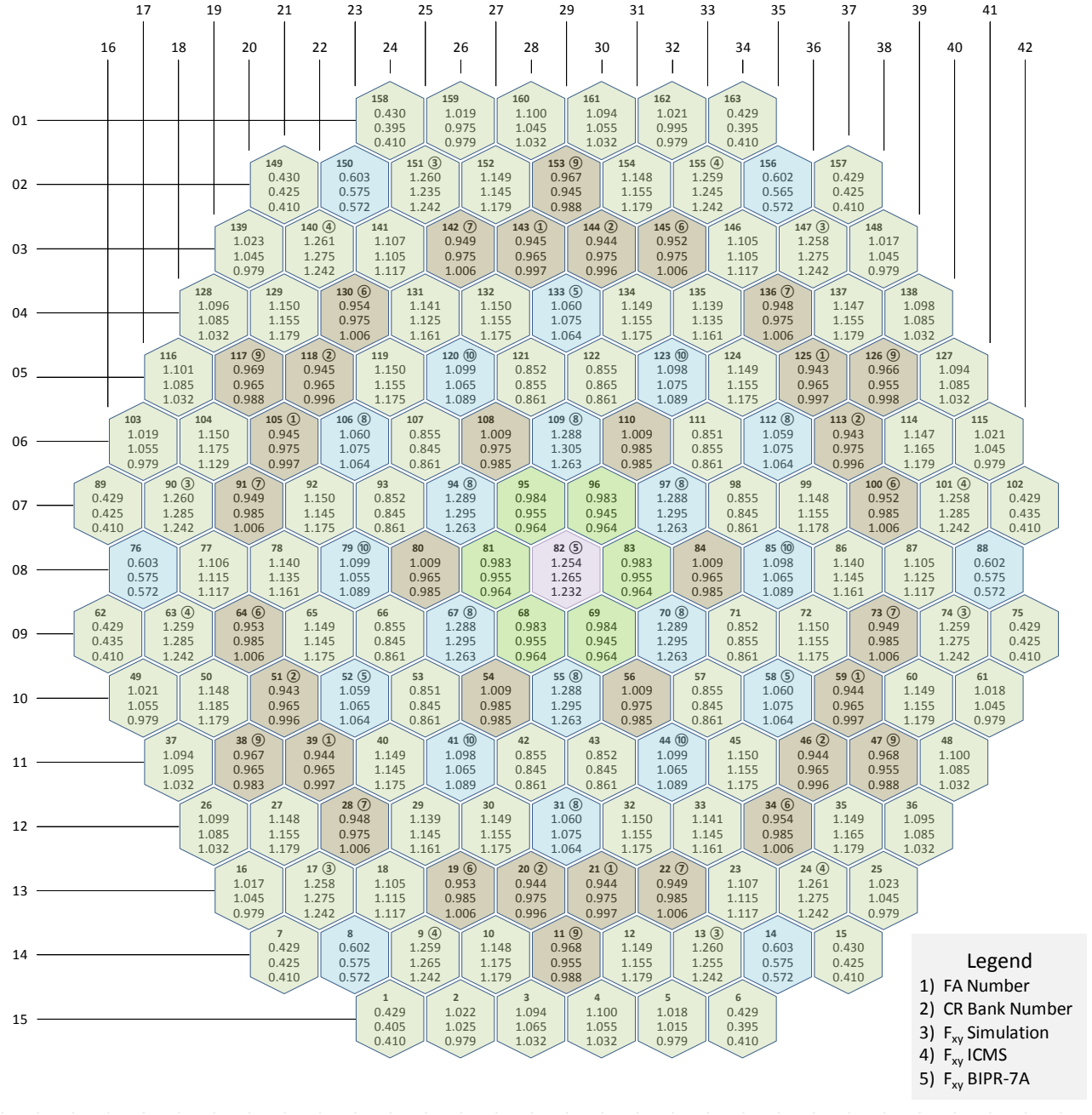

Figure 5.1-10: 17th fuel cycle of Kozloduy 6 — Comparison between simulation, plant data (ICMS) and core design calculation (BIPR-7A) — Assembly-wise power peaking factors at 300.58 EFPD

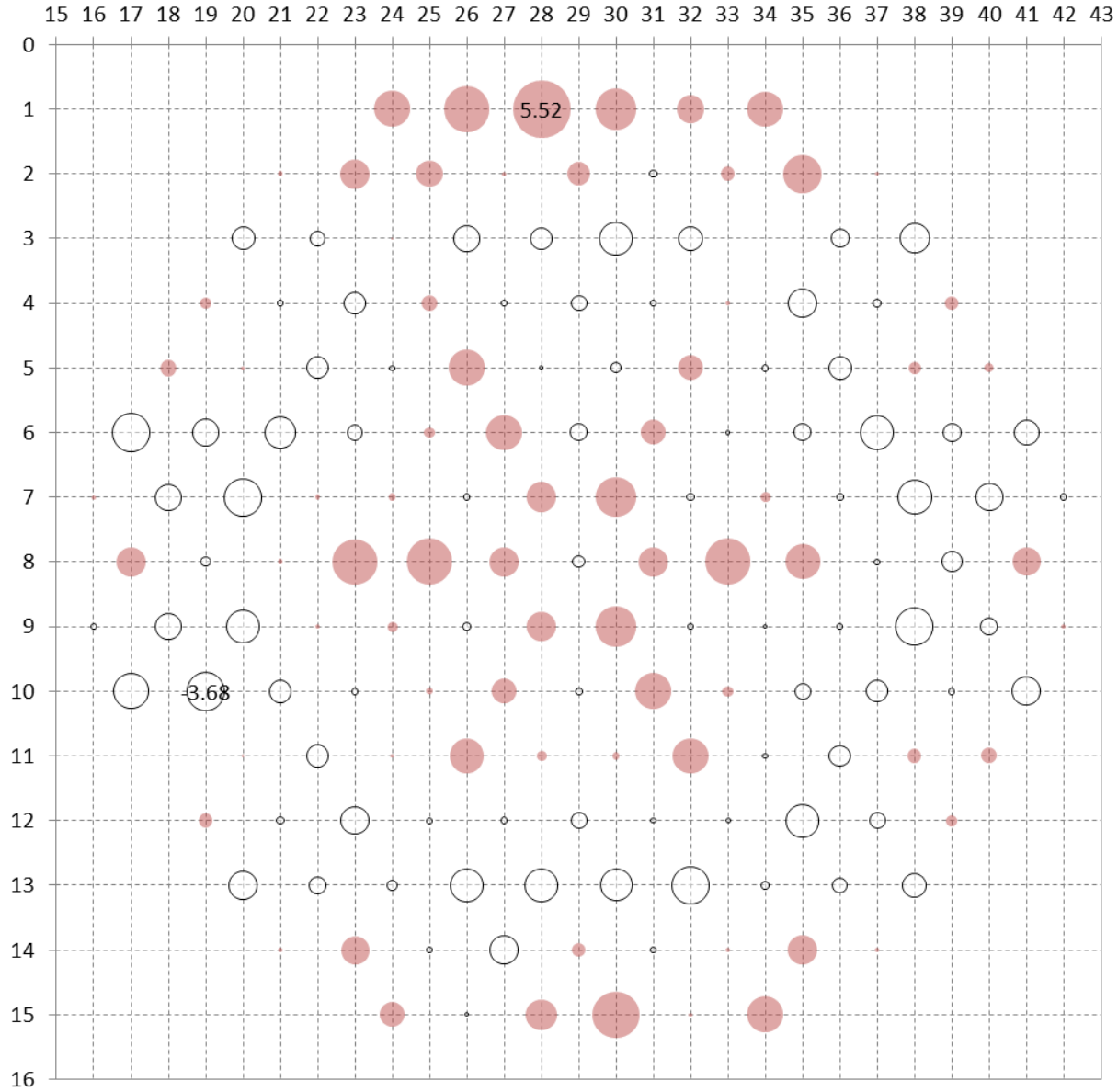

Figure 5.1-11: 17th fuel cycle of Kozloduy 6 — Comparison between simulation and plant data (ICMS) — Deviation in assembly-wise power peaking factor [%] at 300.82 EFPD (magnitude of deviation is proportional to bubble diameter; coloured — positive, transparent — negative)

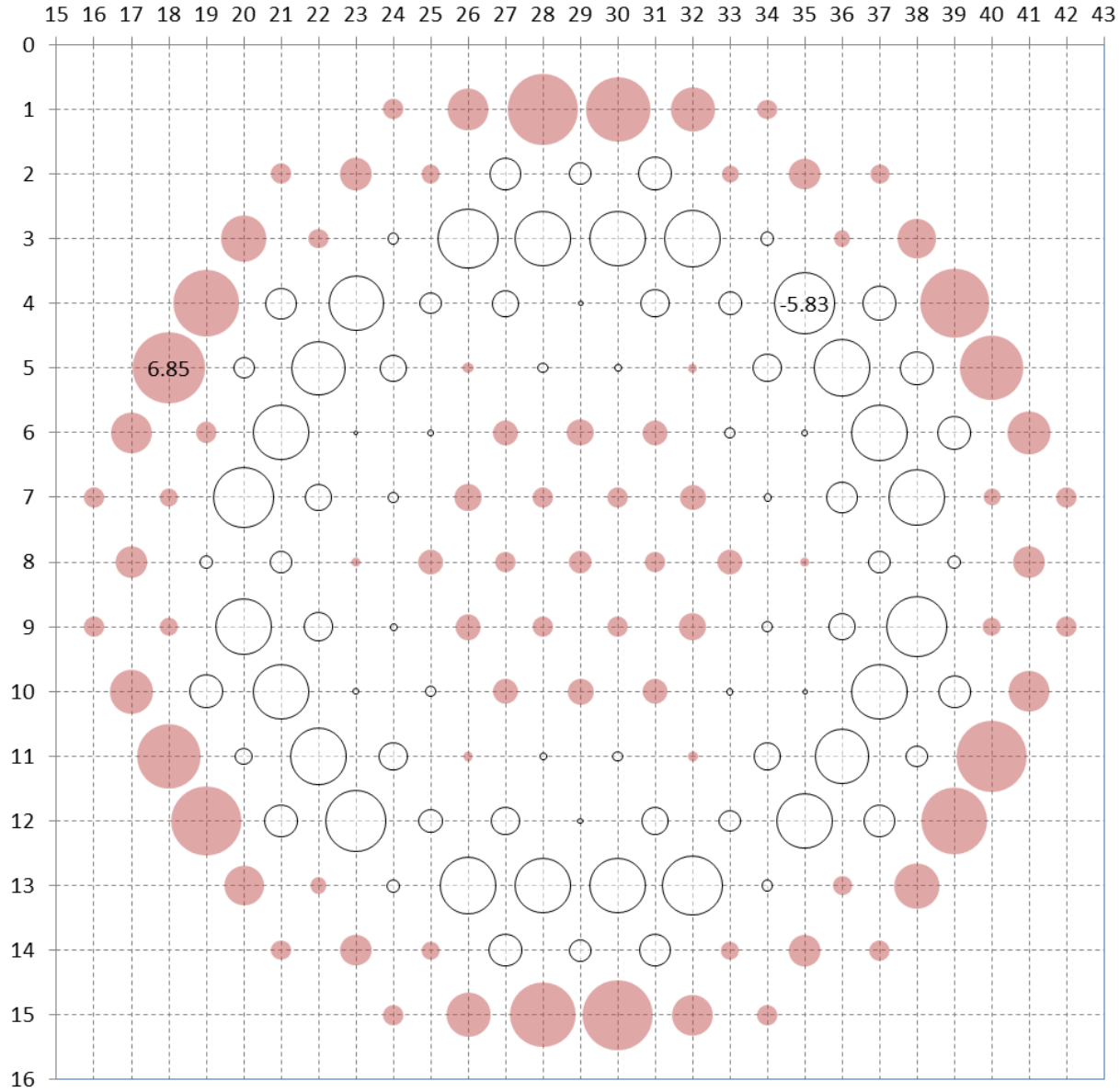

Figure 5.1-12: 17th fuel cycle of Kozloduy 6 — Comparison between simulation and core design calculation (BIPR-7A) — Deviation in assembly-wise power peaking factor [%] at 300.82 EFPD (magnitude of deviation is proportional to bubble diameter; coloured — positive, transparent — negative)

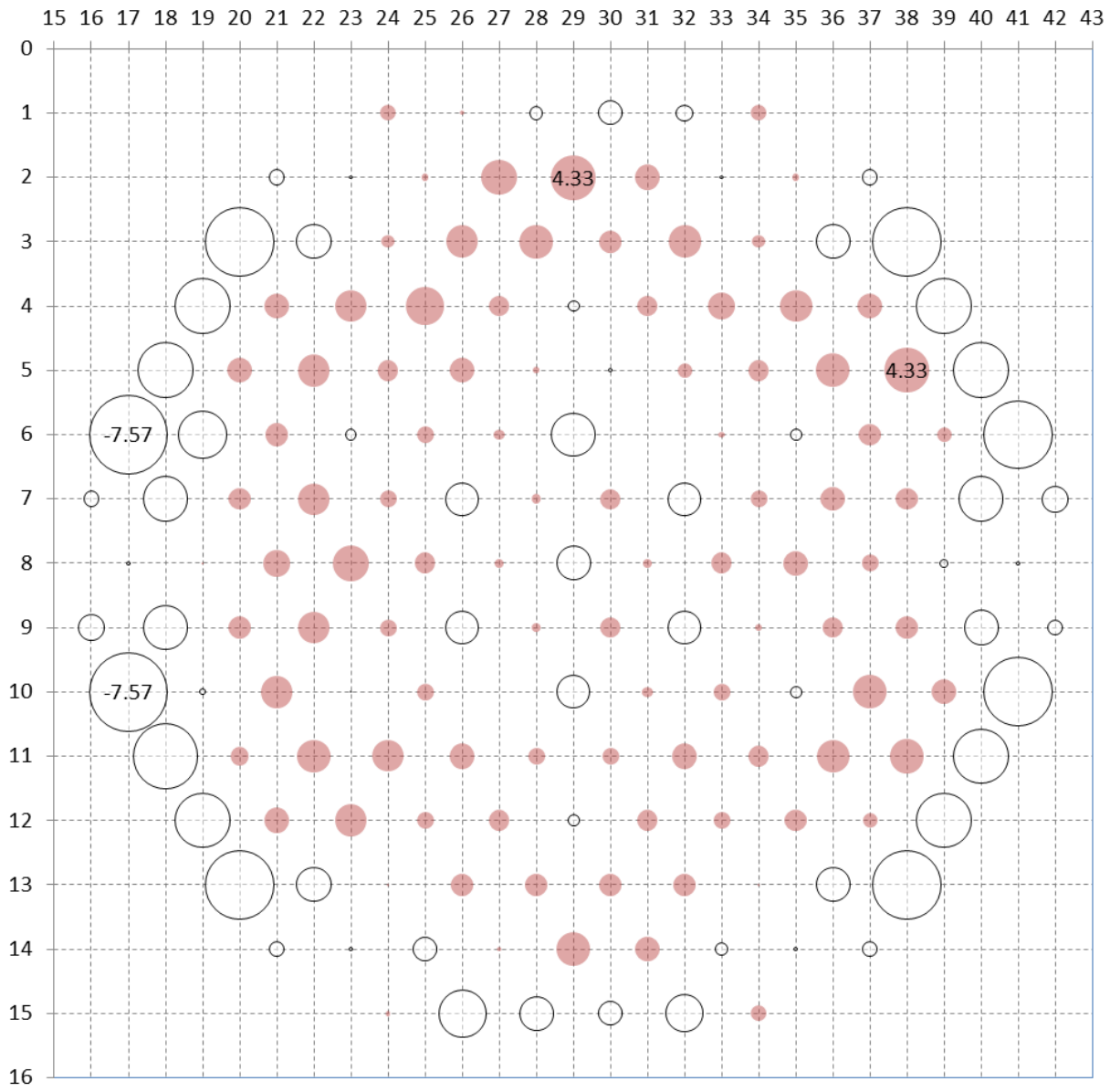

Figure 5.1-13: 17th fuel cycle of Kozloduy 6 — Comparison between plant data (ICMS) and core design calculation (BIPR-7A) — Deviation in assembly-wise power peaking factor [%] at 300.82 EFPD (magnitude of deviation is proportional to bubble diameter; coloured — positive, transparent — negative)

Significant part of both the RMS error value and the maximum deviation observed is, most probably, an asymmetric effect caused by a different loop coolant temperatures and flow rates. Review of history of Kozloduy 6 ICMS records show a combination of high loop coolant flow and high coolant ΔT in loop No. 4 and low loop coolant flow and low loop coolant ΔT in loop No. 1. Estimated thermal power of loop No. 1 is about 1.9 ÷ 3.2 % below average and estimated thermal power of loop No. 4 is about 1.6 ÷ 2.9 % above average. For comparison, thermal power of loop No. 2 is about 0.6 % below average and for loop No. 3 is 0.9 ÷ 1.1 % above average. Unfortunately, there is no reliable data about history of error in measured loop coolant temperatures (accuracy of ±0.5 °C is required by plant specification).

Comparisons between simulation and BIPR-7A calculations show positive deviations in the outermost orbit of the core and negative deviations in the middle orbit throughout the fuel cycle (Figure 5.1-4, Figure 5.1-8 and Figure 5.1-12). At the start of the 17th fuel cycle there is large positive deviation in the third orbit which diminishes towards the middle of the cycle. Throughout the fuel cycle comparison between simulation and BIPR-7A calculations show positive deviations in the central part, negative deviations in the middle orbits and positive deviations in the outermost orbit.

Comparison between BIPR-7A and ICMS (reconstruction based on BIPR-5) show similar trend (Figure 5.1-5, Figure 5.1-9 and Figure 5.1-13). Interestingly, BIPR-7A results for all the fresh fuel assemblies in the outermost layer show significant deviations in comparison with both simulation (NEM core model) and ICMS throughout the fuel cycle. The deviations are much smaller for the fuel assemblies at the edges in the outermost orbit but with high burn-up (4^{th} year in the core). Unfortunately, the author does not have detailed information concerning radial reflector model used in BIPR-7A or ICMS.

RMS deviation over the whole core between simulation and Kozloduy 6 ICMS, as illustrated for 17^{th} fuel cycle, rated power, is smaller (about 2.2 % throughout) than the RMS deviation between BIPR-7A calculations and ICMS (3.5; 4.6; 2.9 % respectively).

5.2 Transient example

An operational transient of inadvertent closure of a MSIV and switching off MCP No. 4 of Kozloduy 6 (Operational Event Report, 12 February 2013) is used to illustrate the accuracy of simulation provided by the core model, as described in Section 3.

At the start of the transient, 14:03:22 on 9 February 2013, Kozloduy 6 is operated at rated power, 3026.1 MW(t) at 109.8 EFPD. Control Rod Bank No. 10 position is 85.8 % (above the lower limit switch). Generator power is 1025.1 MW(e). Description of the transient is presented in Table 5.2-1.

Table 5.2-1: Time history of the Kozloduy 6 transient of inadvertent MSIV closure and switching off MCP

Time		Event description
s	hh:mm:ss	
0	14:03:22	A spurious signal causes opening of a MSIV pilot valve. Steam-actuated MSIV on a steam line of Steam Generator No 4 is forced to close.
1	14:03:23	An interlock trips MCP No 4 in order to prevent overheating of the affected steam generator.
3	14:03:25	Trip of 1 (out of 4) MCPs causes automatic reactor power decrease and shifts setpoints of reactor protection system channels down to 67 %. Control rod bank No 10 insertion starts. Main steam pressure is decreasing and Turbine Governor starts to close turbine control valves in order to maintain main steam pressure (constant pressure mode).
4	14:03:26	MSIV is closed within four seconds. Decreasing core coolant flow causes primary pressure to increase.
10	14:03:32	Steam pressure in the affected steam generator reaches setpoint for atmospheric steam dump. Atmospheric Dump Valve (ADV) starts to open.
23	14:03:45	ADV reaches 67.4 % position. Primary pressure starts to decrease following decrease of reactor power caused by control rod insertion.
28	14:03:50	About this time circulation in affected loop No 4 is reversed, although MCP shaft speed is still above 400 rpm.
36	14:03:58	ADV is closed.
38	14:04:00	Pressurizer heaters on (Bank No 2).
79	14:04:41	MCP No 4 coast down complete.
122	14:05:24	Control Rod Bank No 10 is down to 20 %. Control Rod Bank No 9 insertion started.
129	14:05:31	Reactor power below 67 % (ex-core detectors). Control Rod Bank No 10 position is 15 %. Control Rod Bank No 9 position is 95 %. Reactor power controller is on, mode N (power). Primary pressure reaches lowest point and then starts to increase. Main steam pressure is increasing slowly towards nominal value.

The loading pattern of the 18th fuel cycle (2012/13) of Kozloduy 6 is shown in Figure 5.2-1. There are 4 different types of TVSA fuel assemblies used.

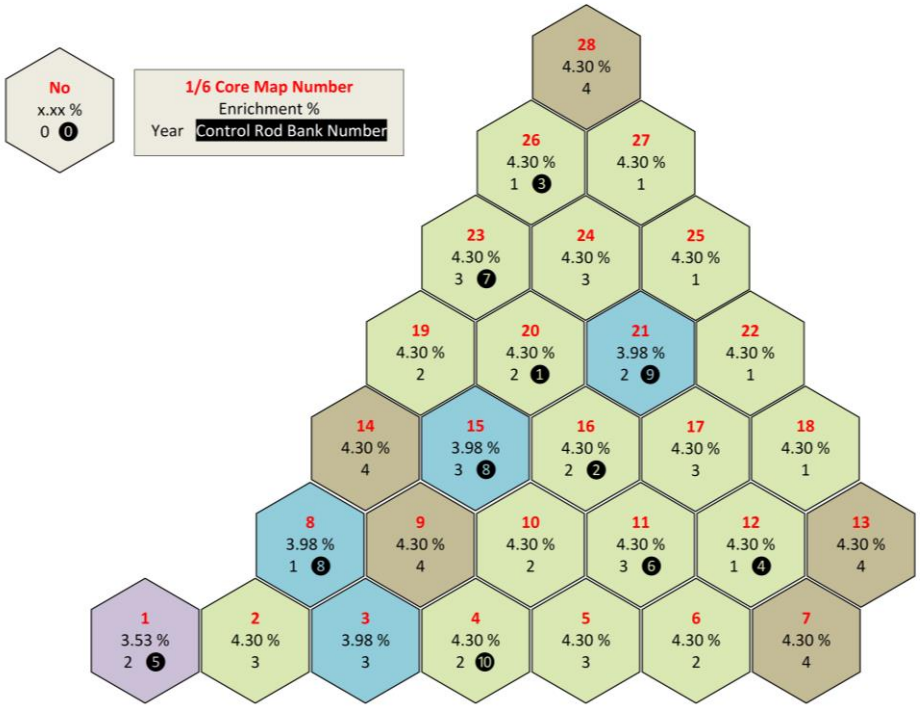

Figure 5.2-1: 18th fuel cycle pattern of the Kozloduy 6 — an one-sixth symmetry representation with FA type, enrichment and year in the core

The core thermal power (ex-core detectors, power range) and Control Rod Bank Nos. 9 and 10 positions are shown in Figure 5.2-2. At the end of the transient, Control Rod Bank No. 10 position is 15.34 % (above the lower limit switch), the same position as recorded by ICMS. Control Rod Bank No. 9 position in the simulation is 94.89 % (above the lower limit switch), just one step off the ICMS record, 95.45 %. There is a very small deviation in the core power according to ex-core detectors, too. Core thermal power estimated by Kozloduy 6 ICMS is 2.4 % lower in comparison with the simulation.

Agreement between simulation and ICMS records concerning reactor coolant system power, control rod movements and ex-core detector readings is very good.

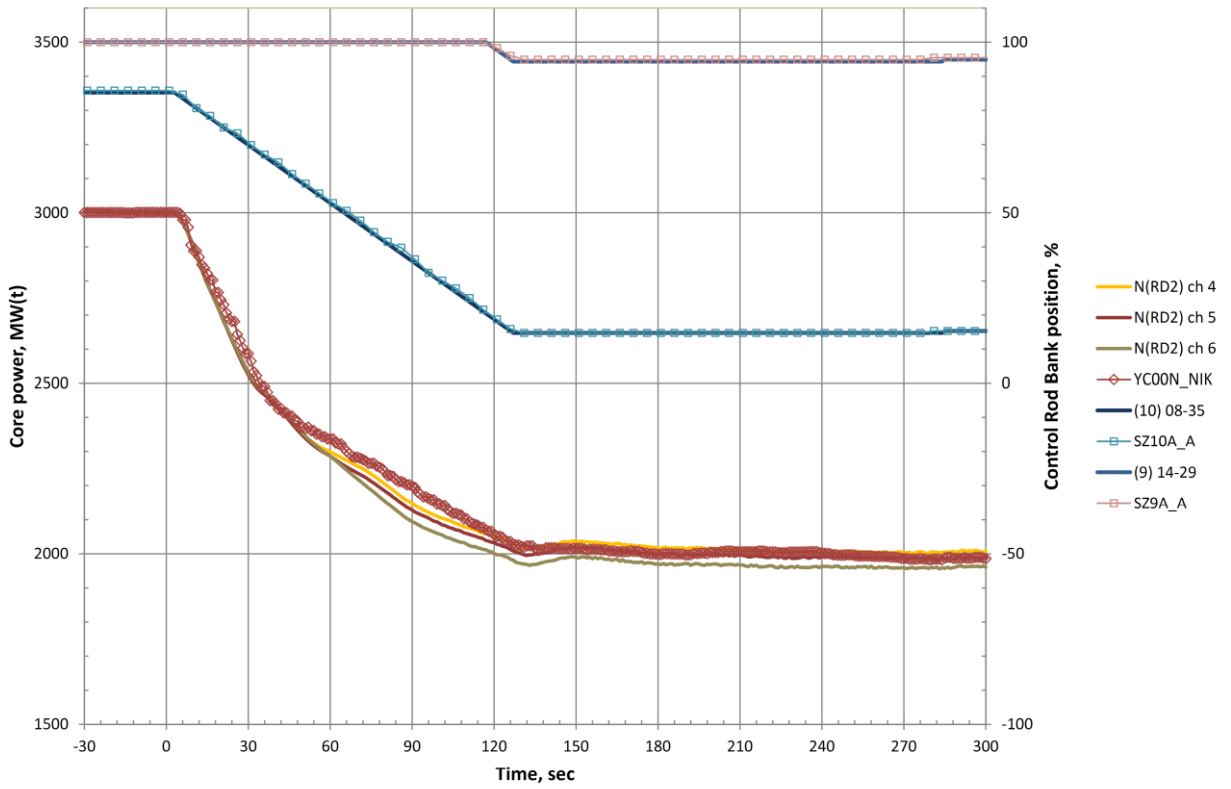

Figure 5.2-2: Power excursion (ex-core detectors, power range, linear) and Control Rod Bank Nos. 9 and 10 positions. Plant data are shown with symbols (YC00N_NIK ex-core detectors, average; SZ9A_A position of control rod bank No. 9; SZ10A_A position of control rod bank No. 10). Simulation data are shown with lines (N(RD2) ch 4, ch 5 and ch 6 – power, ex-core detectors, power range, linear, set 2; (9) 14-29 position of control rod 14-29, bank No. 9; (10) 08-35 position of control rod 08-35, bank No. 10)

Assembly-wise power peaking factor distribution at the start of the transient is shown in Figure 5.2-3. Magnitude of deviations is plotted on Figure 5.2-4. Deviation is calculated as follows.

$$Deviation\ ,\% = \left(F_{xy,\ Simulation} - F_{xy,\ ICMS}\right) \times 100 \qquad \text{Eq. 5.2-1}$$

Assembly-wise power peaking factor distribution at the end of the transient is shown in Figure 5.2-5, as well as magnitude of corresponding deviations in Figure 5.2-6. There are no BIPR-7A data available for comparison with the transient simulation.

Maximum amplitude deviations and RMS are summarized in Table 5.2-2.

Table 5.2-2: Kozloduy 6 MSIV closure and switching off MCP transient – Comparison between simulation and plant data (ICMS) – Brief statistics of deviations in assembly power at the start and the end of the transient

Time	Maximum Deviation				RMS Deviation	
					whole core	FA with SPND
s	%	FA (position)	%	FA (position)	%	%
0	-5.01	49 (10-17)	+6.28	4 (15-30)	2.10	2.05
300	-7.09	49 (10-17)	+8.35	85 (08-35)	3.05	2.65

Note: Core life at the time of transient is 109.8 EFPD.

Although agreement in the power of fuel assemblies is quite good across the whole core, there is a significant deviation in the fuel assemblies with Control Rod Banks Nos. 9 and 10 (Figure 5.2-6). Deviation in core thermal power, mentioned above, is not sufficient to provide explanation for the deviation of 8.35 % (0.7345 vs 0.651) in FA No. 85 (08-35, bank No. 10). There is a pronounced deviation in assemblies with Control Rod Bank No. 9, too. Obviously, the simulation overestimates the power of fuel assemblies with control rods inserted as is the case with Control Rod Bank No. 10, +7.8 % (average). It was -2.92 % (average) at the start of the transient with Control Rod Bank No. 10 at 85.8 % (above the lower limit switch). In the case of Control Rod Bank No. 9, which is inserted just about 10 cm into the core, overestimation is +3.75 % (average). It was +2.4 % (average) at the start of the transient with Control Rod Bank No. 9 at the upper end switch.

Looking further into Kozloduy 6 ICMS data for fuel assemblies with Control Rod Bank No. 9 at the end of the transient, a very large variation in fuel assembly power can be seen on Figure 5.2-5, ranging from 1.224 in FA No. 153 to 1.298 in FA No. 38. Variation in ICMS data of such magnitude within a symmetry group of fuel assemblies is not unusual for a transient of switching off 1-out-of-4 MCPs in various VVER-1000 units (Tereshonok, 2008). This kind of variation clearly corresponds with the variation of recorded loop cold leg coolant temperatures, ranging from 283.6 °C in loop 1, to 285.1 °C in loop 2 and 285.5 °C in loop 3 at the end of the transient.

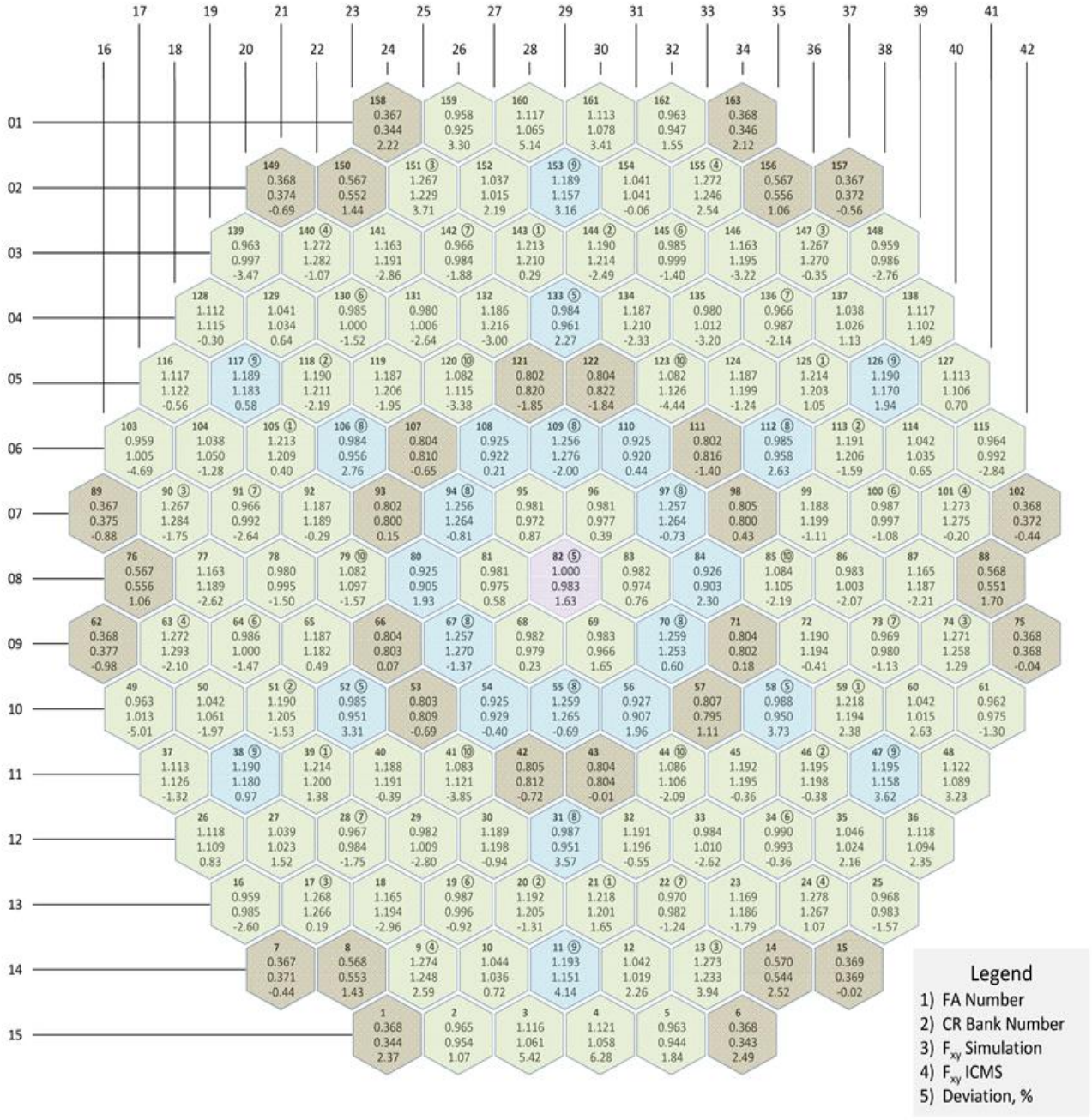

Figure 5.2-3: Kozloduy 6 MSIV closure and switching off MCP transient — Comparison between simulation and plant data (ICMS) — Assembly-wise power peaking factor at the start of the transient

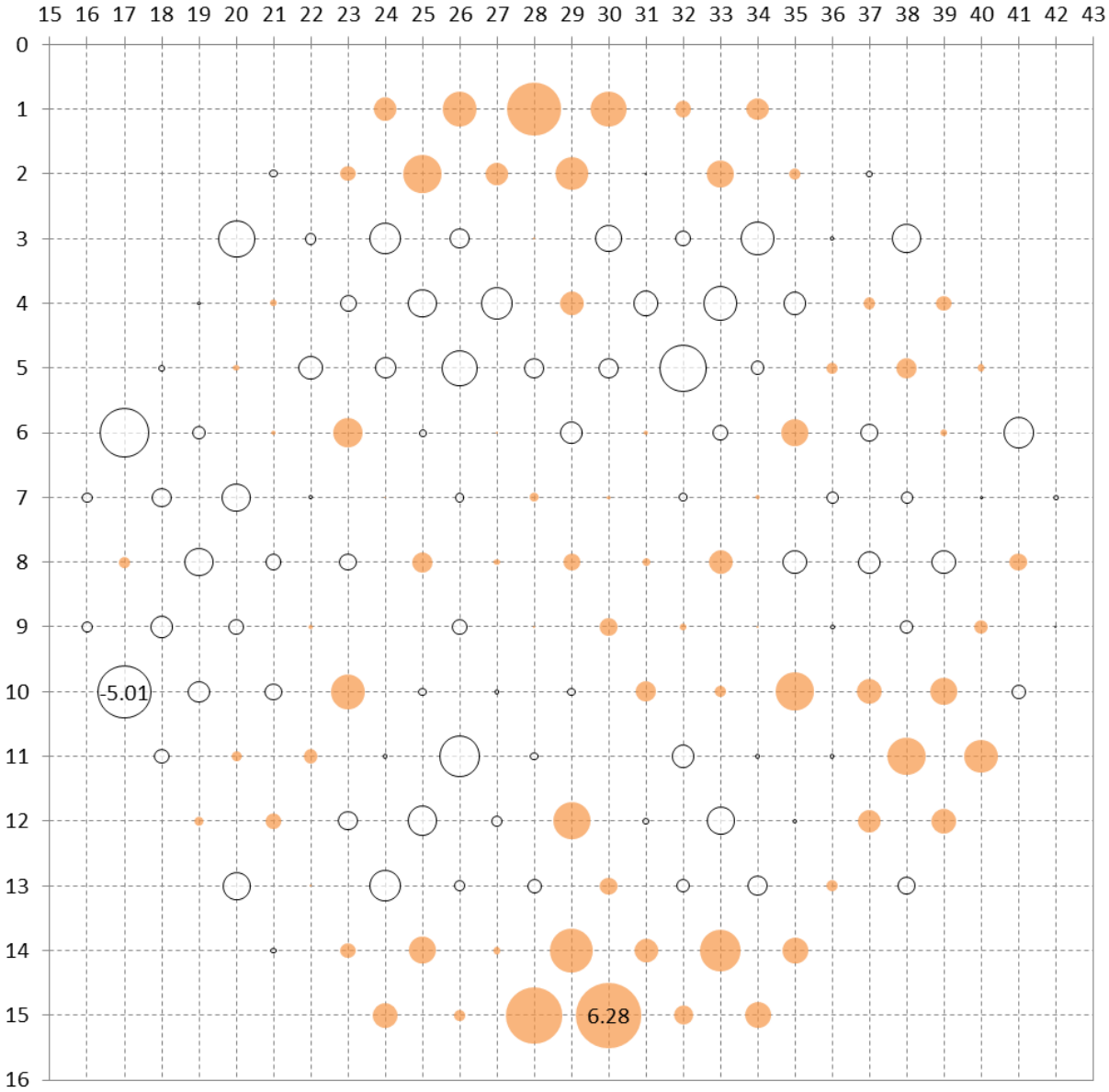

Figure 5.2-4: Kozloduy 6 MSIV closure and switching off MCP transient — Comparison between simulation and plant data (ICMS) — Deviation in assembly-wise power peaking factor [%] at the start of the transient (magnitude of deviation is proportional to bubble diameter; coloured — positive, transparent — negative)

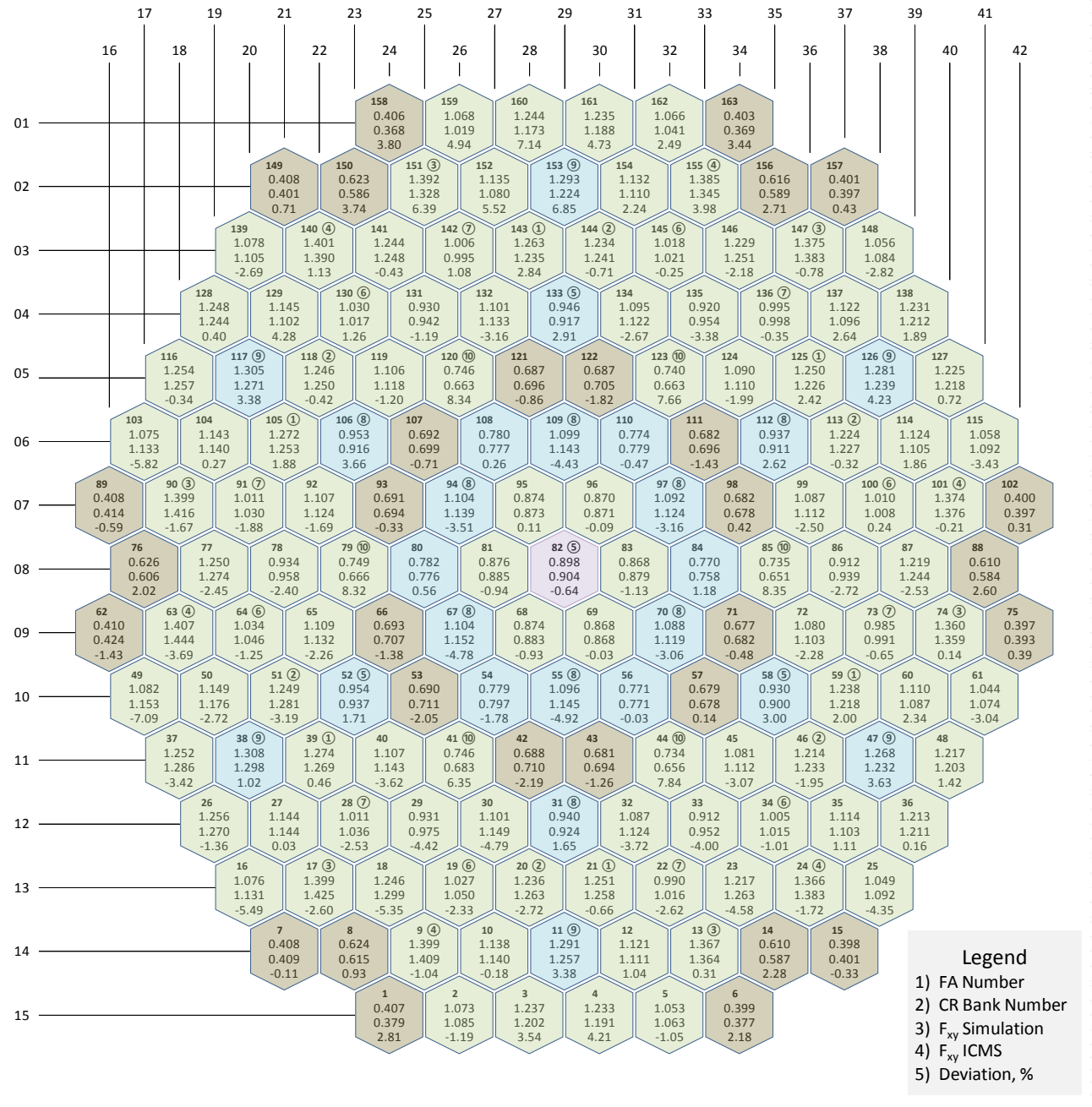

Figure 5.2-5: Kozloduy 6 MSIV closure and switching off MCP transient — Comparison between simulation and plant data (ICMS) — Assembly-wise power peaking factor at the end of the transient

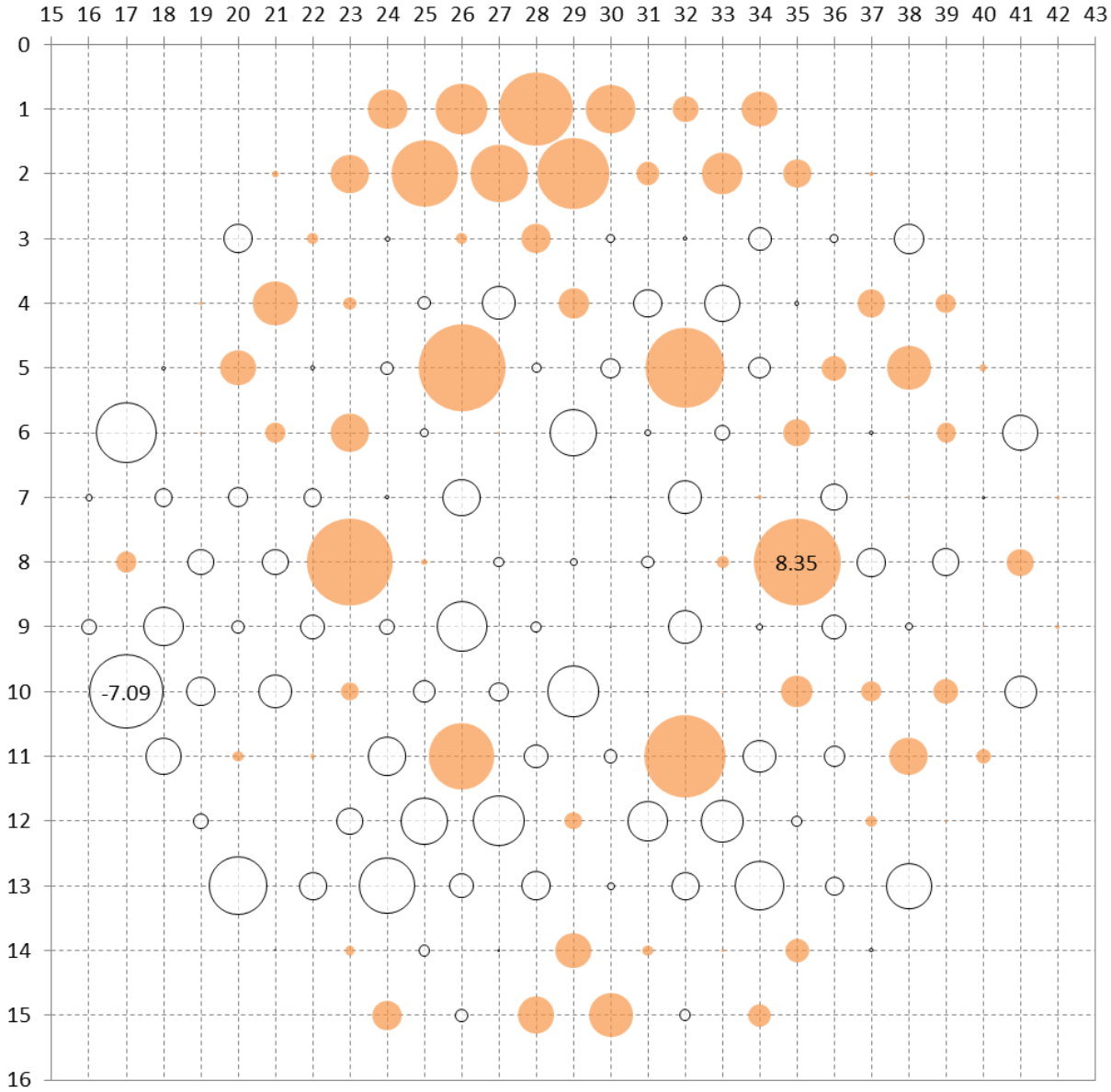

Figure 5.2-6: Kozloduy 6 MSIV closure and switching off MCP transient — Comparison between simulation and plant data (ICMS) — Deviation in assembly-wise power peaking factor [%] at the start of the transient (magnitude of deviation is proportional to bubble diameter; coloured — positive, transparent — negative)

There are no SPNDs in fuel assemblies with control rods (Figure 3.4-2). For assemblies without SPND, ICMS provides an estimation of power distribution using readings from nearby detectors and a shape function calculated by BIPR-5. The author can see three effects as possible contributing factors for the substantial deviations in some fuel assemblies at the end of the transient.

a. In comparison with simulation (NEM), ICMS (BIPR-5) predicts very strong effect on fuel assembly with control rod inserted and smaller influence on nearby fuel assemblies. The method of solving the diffusion equation in hexagonal geometry in the NEM code can be prone to inaccuracies in case of strong neutron flux gradients in the vicinity of nodes with rodded compositions (Ivanov, 2006). The deviations in the neighbour fuel assemblies are, however, not large. Furthermore, it will be discussed in Chapter 6, the same control rod model applied to a similar transient does not produce such a large deviations.

b. The model of absorber rods used for ICMS power reconstruction (at the time of transient in February 2013) does not take into account different material composition in the lower part of the absorber rods ($Dy_2O_3 \cdot TiO_2$ instead of B_4C). Such a simplification in ICMS, however, can explain only part of the deviation.

c. Difference in coolant temperature distribution at the inlet of fuel assemblies estimated in the simulation and the Kozloduy 6 ICMS, as much as this is the most probable explanation for the asymmetry observed.

Evolution of the axial power profile (normalized for rated power conditions, whole core) is shown in Figure 5.2-7. Agreement between simulation and ICMS concerning axial power profile is quite good too with a slight underprediction in the middle and more pronounced humps below and above centre of the core. Worth of Control Rod Bank No. 10 in simulation is in excellent agreement with records (Figure 5.2-2). There is no indication that axial shape of power distribution in the core is a reason for the deviations described above. At present time, the exact cause of significant deviation observed in the power of fuel assemblies with Control Rod Banks Nos. 9 and 10 at the end of the transient remains undetermined.

There is a reason to discuss some peculiarities of Kozloduy 6 ICMS power reconstruction during the transient. ICMS data concerning ex-core detectors (ion chambers), primary and secondary thermal balance are plotted on Figure 5.2-8.

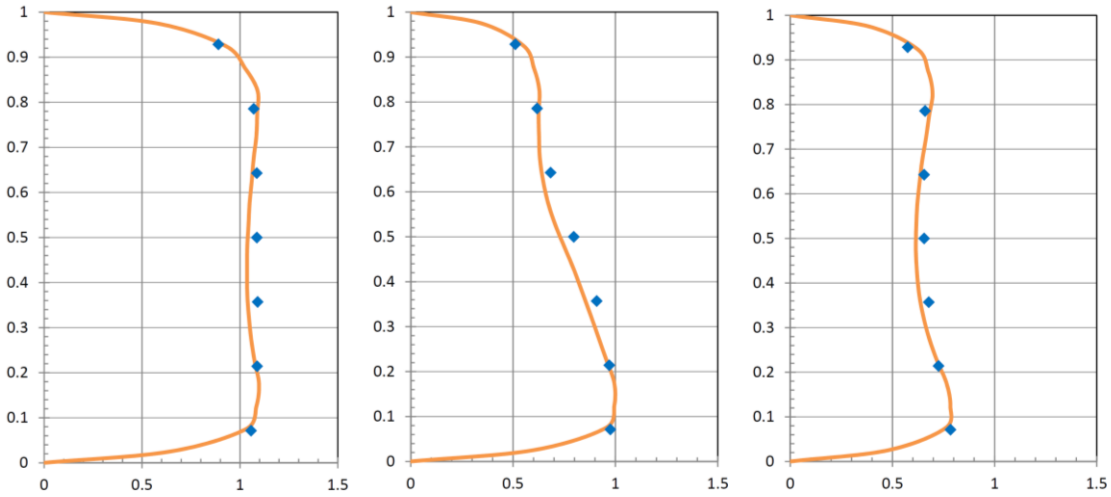

Figure 5.2-7: Axial power profiles (normalized for rated power conditions, whole core) at 0 s (left), 70 s (middle) and 300 s (right). Data from Kozloduy 6 ICMS are shown with symbols (7-layer power reconstruction)

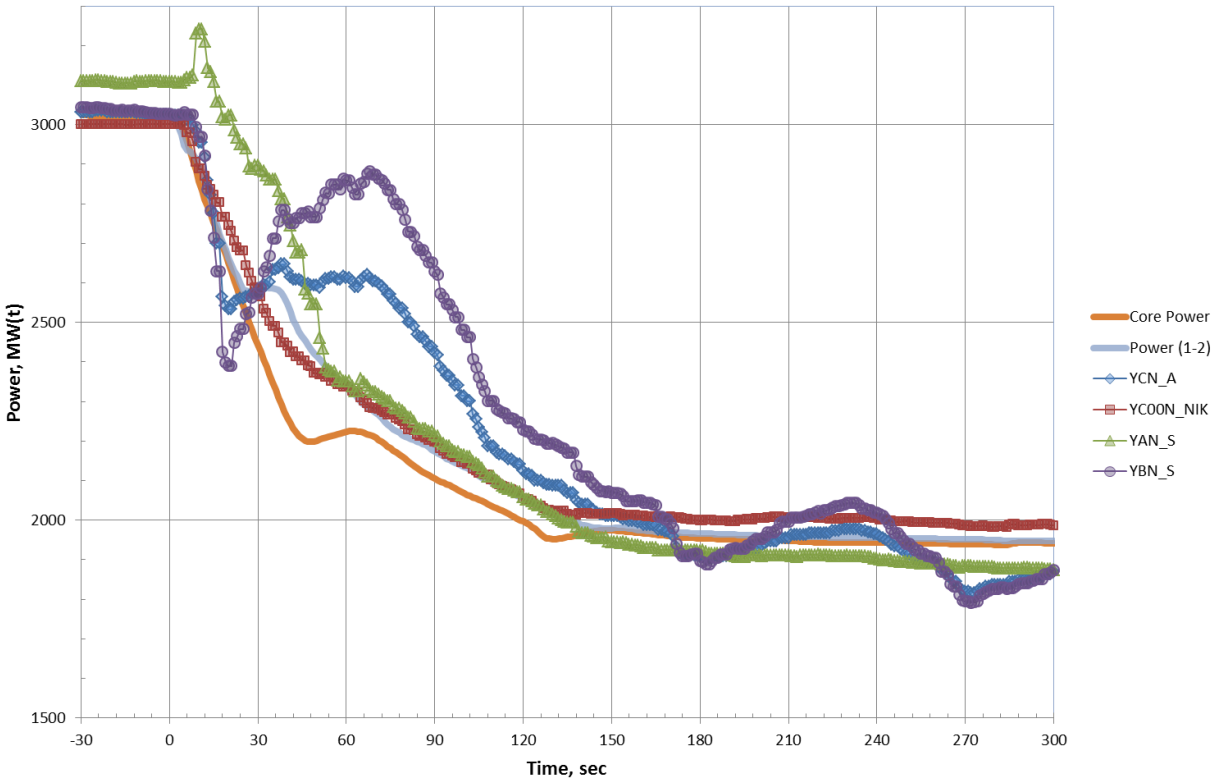

Figure 5.2-8: Kozloduy 6 ICMS thermal power estimation during the transient. Plant data are shown with symbols (YCN_A reactor coolant system thermal power, weighed estimation; YC00N_NIK power, ex-core detectors, average; YAN_S power, primary loop thermal balance; YBN_S power, SG secondary side thermal balance). Simulation data are shown with thick lines (Core Power, NEM; Power (1-2) rate of heat transfer through SG tube bundles, RELAP5-HD)

Simulated core thermal power and rate of heat transfer through steam generator tube bundles are included in Figure 5.2-8 just for illustration of dynamic response of plant instrumentation. Spreading of values of reactor coolant system thermal power estimated by primary or secondary thermal balance is worth mentioning. Estimated thermal power is used to calculate coolant and fuel temperature and in this way is essential for cross-section reconstruction in the ICMS core model. At the end, thermal power estimated by different methods, as well as three-dimensional power distribution in the core is essential for the accuracy of the ICMS power reconstruction. Power estimation by secondary heat balance data, as shown on Figure 5.2-8, is based on feedwater flow. However, due to peculiarities of steam generator dynamics during this kind of transient, feedwater flow is not equal to the steam flow. The difference is caused by a significant decrease in void fraction in steam generator tube bundle during power run-down. Discussion of this effect continues in Section 6.4.6.

5.3 Conclusion

The core model performance is evaluated on the basis of comparison between simulation results, core design calculations and plant records. The main parameters used for the comparison are assembly-wise power peaking factors. In general, deviations between simulation, core design calculations (BIPR-7A) and plant data (ICMS) remain within the margin of error. Special emphasis is placed on substantial deviations (albeit within the margin of error) in rodded fuel assemblies at the end of the presented Kozloduy 6 transient. At present time there is no definitive explanation for the root cause of these deviations.

The core model for VVER-1000 simulator application (Chapter 3) complete with cross-section libraries, tools and procedures for cycle-specific core update (Chapter 4) is used by the Kozloduy NPP personnel from the spring of 2012 with consistently good results. Many more steady-state and transient simulations were performed during rigorous acceptance tests or periodic functional tests of the simulator and the simulator is in routine operation monitored by experienced plant staff. The core model meets all current simulator fidelity requirements. An illustration of steady-state and transient simulation results is given in this Chapter. There is no way to compare this model with the old one as much as the old model had no capability to provide cycle-specific simulation.

6. Kalinin 3 Coolant Transient benchmark

Several benchmarks have been designed in order to verify and validate the capability of the coupled thermal-hydraulic and neutron kinetics code systems to analyse complex transients with significant neutronic / thermal-hydraulic interactions for different types of reactors.

The Nuclear Energy Agency (NEA) of the Organization for Economic Cooperation and Development (OECD) has completed a two-part VVER-1000 Coolant Transient Benchmark (V1000CT-1 and V1000CT-2; 2002 through 2007) for evaluation of coupled codes by simulation of plant transients at Kozloduy NPP unit 6.

A continuation of the above activities is defined as a coupled code benchmark problem for validation of thermal-hydraulics system codes for application to VVER-1000 reactors based on actual plant data from Kalinin 3 (Tereshonok, 2009). The transient of 'Switching-off of One of the Four Operating Main Circulation Pumps at Nominal Reactor Power' is performed at an asymmetric core condition with a range of parameter changes.

6.1 Cross-section generation and modelling

Cross-section modelling methodology is outlined in Section 4.2. The HELIOS-1.9 lattice code is used to calculate cross-section data tables.

6.1.1 Geometry and material composition

The loading pattern of the Kalinin 3 reactor core after 96 EFPD is shown in Figure 6.1-1. The fuel cycle is described as '1 bis' or '2' in various sources. There are five different 'alternative' fuel assembly (TVSA) types and one 'standard' fuel assembly (TVS-M) type used.

Control rods re-distributed between banks according to Kalinin 3 arrangement are shown in Figure 6.1-2.

The geometry and material composition data are presented in detail in Appendix D.

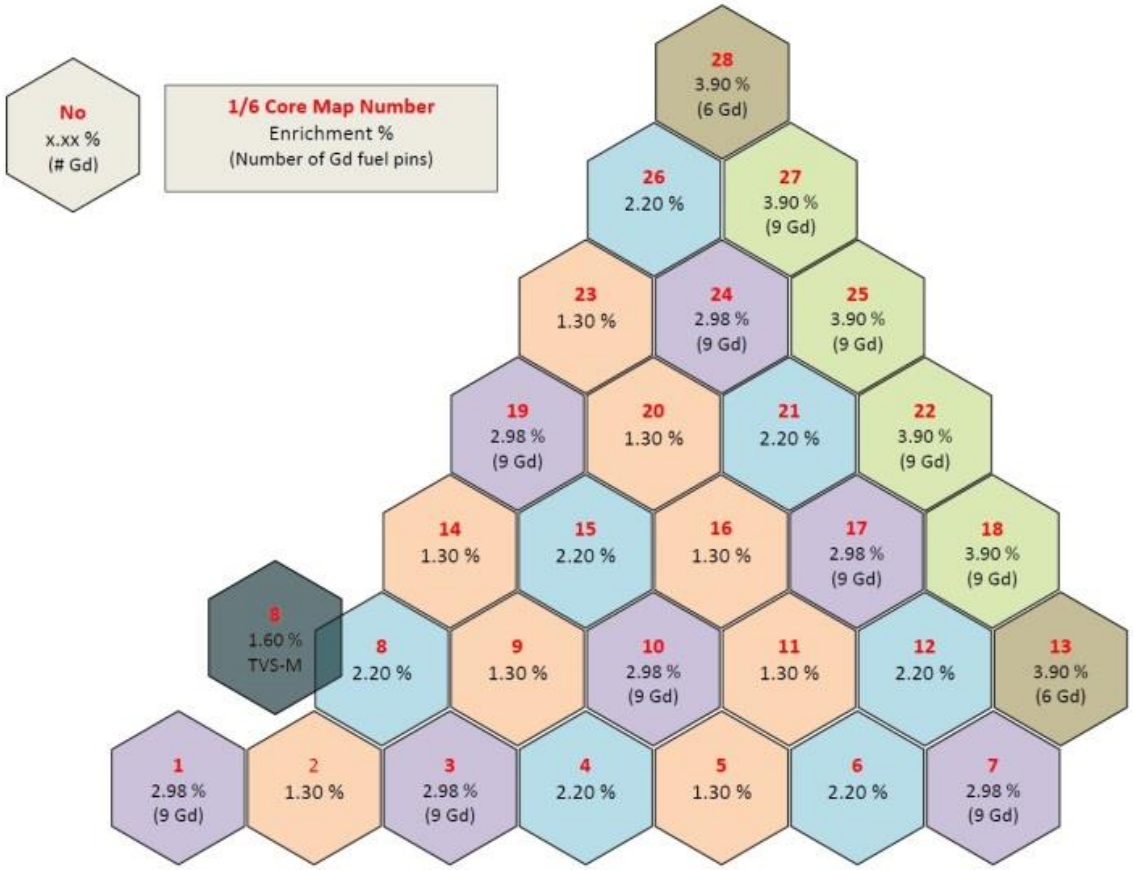

Figure 6.1-1: 1 bis fuel cycle pattern of the Kalinin 3 — an one-sixth symmetry representation with FA type, enrichment and year in the core

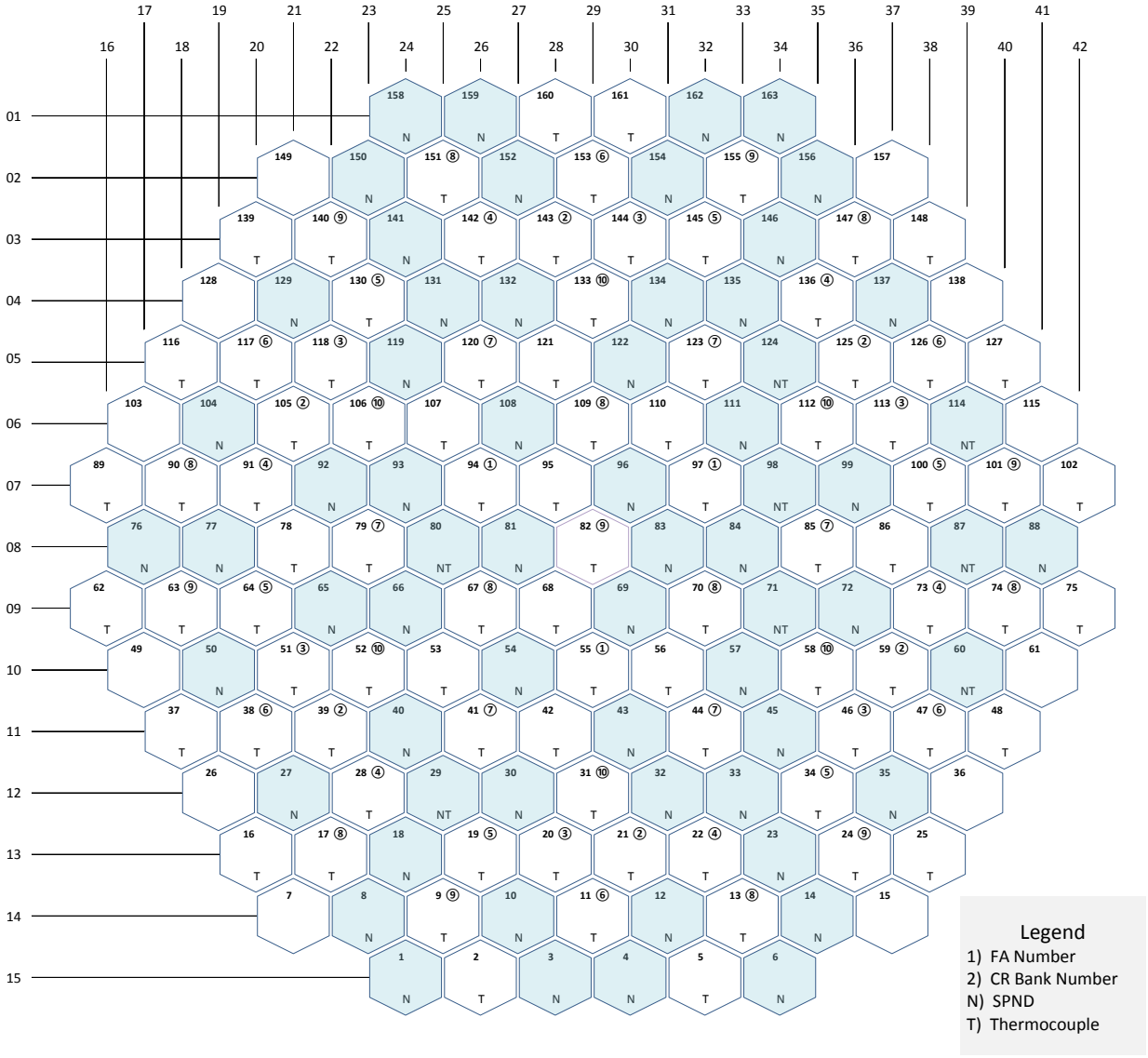

Figure 6.1-2: Map of Kalinin 3 control rod and in-core instrumentation locations. There are three types of in-core instrumentation assemblies used: (N) SPND array with 7 axial positions; (T) coolant thermocouple above the active part of the fuel assembly; (NT) SPND array with coolant thermocouple, combined

6.1.2 Instantaneous modelling

The expected scope is covered by a range of the independent variables (*i.e.* feedback parameters) according to Kalinin 3 Coolant Transient benchmark specification, as follows.

a. 540 ÷ 1700 K for fuel temperature, 4 points.
b. 540 ÷ 600 K for moderator (coolant) temperature, 4 points.
c. 660 ÷ 790 kg/m^3 for moderator (coolant) density, 4 points.
d. 630 ppm boron concentration (3.6 g/kg boric acid) in the primary coolant (presumed constant).

Current version of the VVER-1000 core model is designed to use larger four-dimensional look-up tables. Additional points outside of the expected range are added in order to use a 300-point template for the four-dimensional macroscopic cross-section look-up tables (as described in Section 4.2.2).

Values for each of the four feedback parameters are shown in Table 6.1-1.

Table 6.1-1: Range of values of the feedback parameters and reference values for spectral history used for generation of Kalinin 3 cross-section library tables

Parameter	Instantaneous modelling interpolation values *	History modelling reference value
Fuel temperature, K	540 – 900 – 1300 – 1700 – *2300*	850
Moderator temperature, K	540 – 560 – 580 – 600 – *620*	577.15
Moderator density, kg/m^3	660 – 700 – 740 – 790 – *830 – 890*	718.85
Boron concentration, ppm	*5.0 – 2933.33*	630

** Note: Values in Italic are points added outside of the range of the Kalinin 3 Coolant Transient benchmark specification (Tereshonok, 2009).*

6.1.3 Burn-up and spectral history modelling

The cycle-specific cross-section library is designed for ten axial layers containing fission material. Exposure for each node is obtained from BIPR-8 results (Core Design Calculations, 2013) provided by Kurchatov Institute (available for benchmark participants but not included in published specification).

At the time when design of the cross-section library was established, it was decided to develop library with two sets of data. Set 2 makes use of exposure calculation results provided for the sector with a replacement fuel assembly No 97 (07-32), sector 4 in the notation used here. Set 1 uses

average exposure over 5 out of 6 sixty degree core sectors (1, 2, 3, 5 and 6). Each set contains 283 unrodded compositions, 110 rodded compositions for Boron Carbide absorber part control rods, and 110 rodded compositions for Dysprosium-Titanium absorber part of control rods. Average exposure per fuel assembly is shown in Table 6.1-2. The RMS deviation of assembly exposure over 6 and 12 core sectors is shown in Figure 6.1-3 and Figure 6.1-4, respectively. A comparison between sector-averaged exposures used in the cross-section library and BIPR-8 data is presented in Figure 6.1-5. Worst case deviation is +1.52 % in FA No. 110 (06-31). The deviation is well within below error in estimated fuel assembly exposure. Results shown in Section 6.3 do not indicate any significant effect caused by this simplification.

Table 6.1-2: Average exposure per fuel assembly in one-sixth core used in Kalinin 3 cross-section library

Assembly index (in one-sixth)	Assembly Type		Exposure, MWd/kgU *(set 1)*	Exposure, MWd/kgU *(set 2)*
	Enrichment ^{235}U, %	Number of Gd pins		
1	2.98	—	5.82	5.82
2	1.3	—	4.41	4.36
3	2.98	9	6.69	6.60
4	2.2	—	6.19	6.14
5	1.3	—	4.57	4.54
6	2.2	—	6.08	6.06
7	2.98	9	5.54	5.52
8	2.2 | 1.6	—	6.01	1.25
9	1.3	—	4.71	4.62
10	2.98	9	6.49	6.43
11	1.3	—	4.62	4.60
12	2.2	—	5.99	5.97
13	3.9	6	4.35	4.34
14	1.3	—	4.72	4.62
15	2.2	—	5.81	5.74
16	1.3	—	4.60	4.57
17	2.98	9	6.72	6.69
18	3.9	—	5.35	5.34
19	2.98	9	6.50	6.43
20	1.3	—	4.61	4.57
21	2.2	—	6.20	6.18
22	3.9	9	5.59	5.57
23	1.3	—	4.63	4.60
24	2.98	9	6.72	6.69
25	3.9	9	5.60	5.57
26	2.2	—	5.99	5.97
27	3.9	9	5.36	5.34
28	3.9	6	4.36	4.34
29	Reflector	—	—	—
Sector-average exposure:			**5.50**	**5.29**

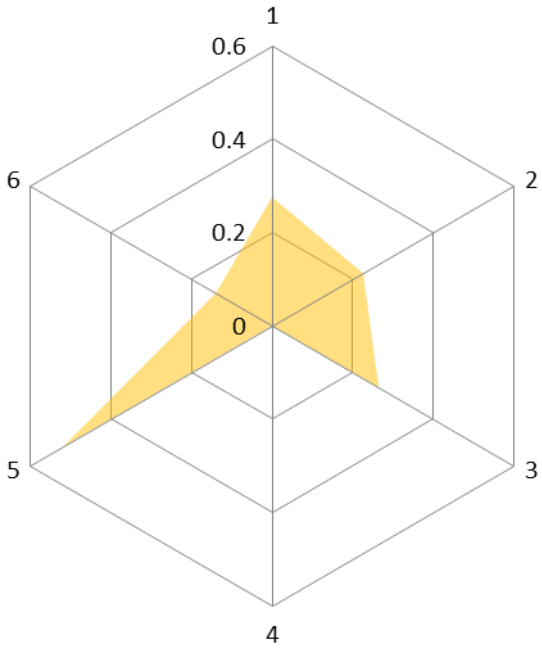

Figure 6.1-3: RMS error distribution [%] of assembly exposure for each of the 6 sixty-degree core sectors. Error in sector 4 is zero because cross-section set 2 fits exactly this sector. Worst case is sector 5 with RMS deviation of 0.52 %

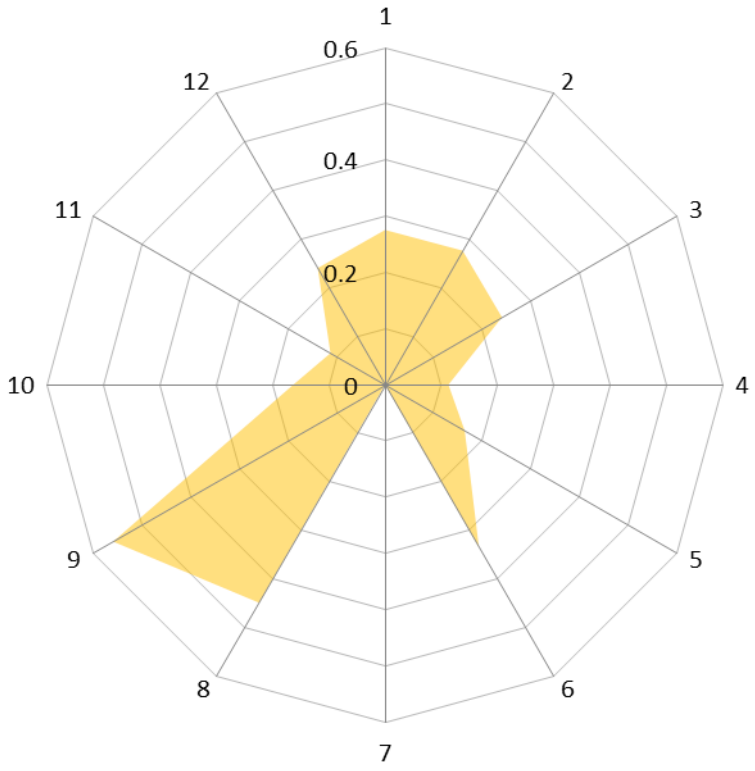

Figure 6.1-4: RMS error distribution [%] of assembly exposure for each of the 12 thirty-degree core sectors. Error in sector 7 is zero because cross-section set 2 covers whole sector. Worst case is sector 9 with RMS deviation of 0.56 %

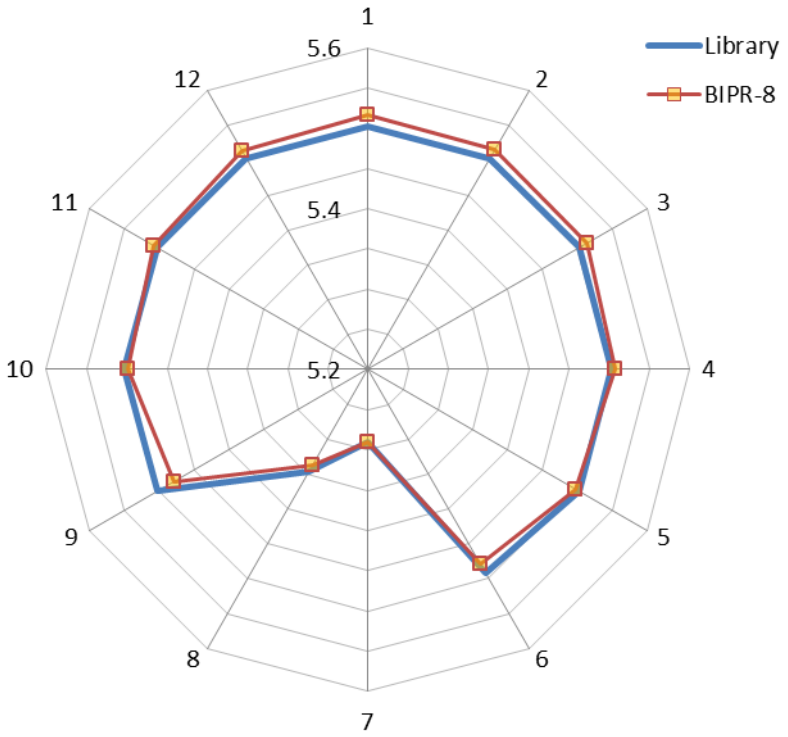

Figure 6.1-5: Comparison (cross-section library vs BIPR-8) of the sector-average exposure [MWd/kgU] in 12 thirty-degree core sectors

6.1.4 Assembly discontinuity factors

ADFs are preserved the same as described in Section 4.2.4.

6.1.5 Four-dimensional tables

The four-dimensional look-up tables are preserved the same as described in Section 4.2.5.

6.1.6 Other parameters

The parameters tabulated per each fuel composition and exposure only are preserved the same as described in Section 4.2.6.

Two-group *Xe* and *Sm* microscopic cross sections, equilibrium number densities and yields (σ_{Xe}; $N_{Xe,\infty}$; γ_{Xe}; σ_{Sm}; $N_{Sm,\infty}$; γ_{Sm}), and neutron fluxes (ϕ) are included into cross-section library but these parameters are not required in Kalinin 3 Coolant Transient benchmark specification (Tereshonok, 2009).

6.1.7 Handling of cross-section tables

A reactor core is designed for symmetry and this feature is used in handling of cross-section tables. If the symmetric exposure of fuel compositions is preserved, description of one-sixth of the hexagonal core is enough. The assumption of symmetry is used only to optimize data storage and handling. In the case of Kalinin 3 asymmetric core, another set of data is provided to be loaded into desired sector using the same format (Figure 6.1-6).

Concerning current version of the VVER-1000 core model, the cross-section library tables are prepared as block data files with specific format for one-sixth of the core. There are two sets with three block data files each: one for unrodded fuel compositions (283, including reflectors); and for two rodded (110 each) fuel compositions. These are uploaded to the simulation environment as any other block data file. In the case of asymmetric fuel loading pattern, a further set of block data files is loaded in the desired sector.

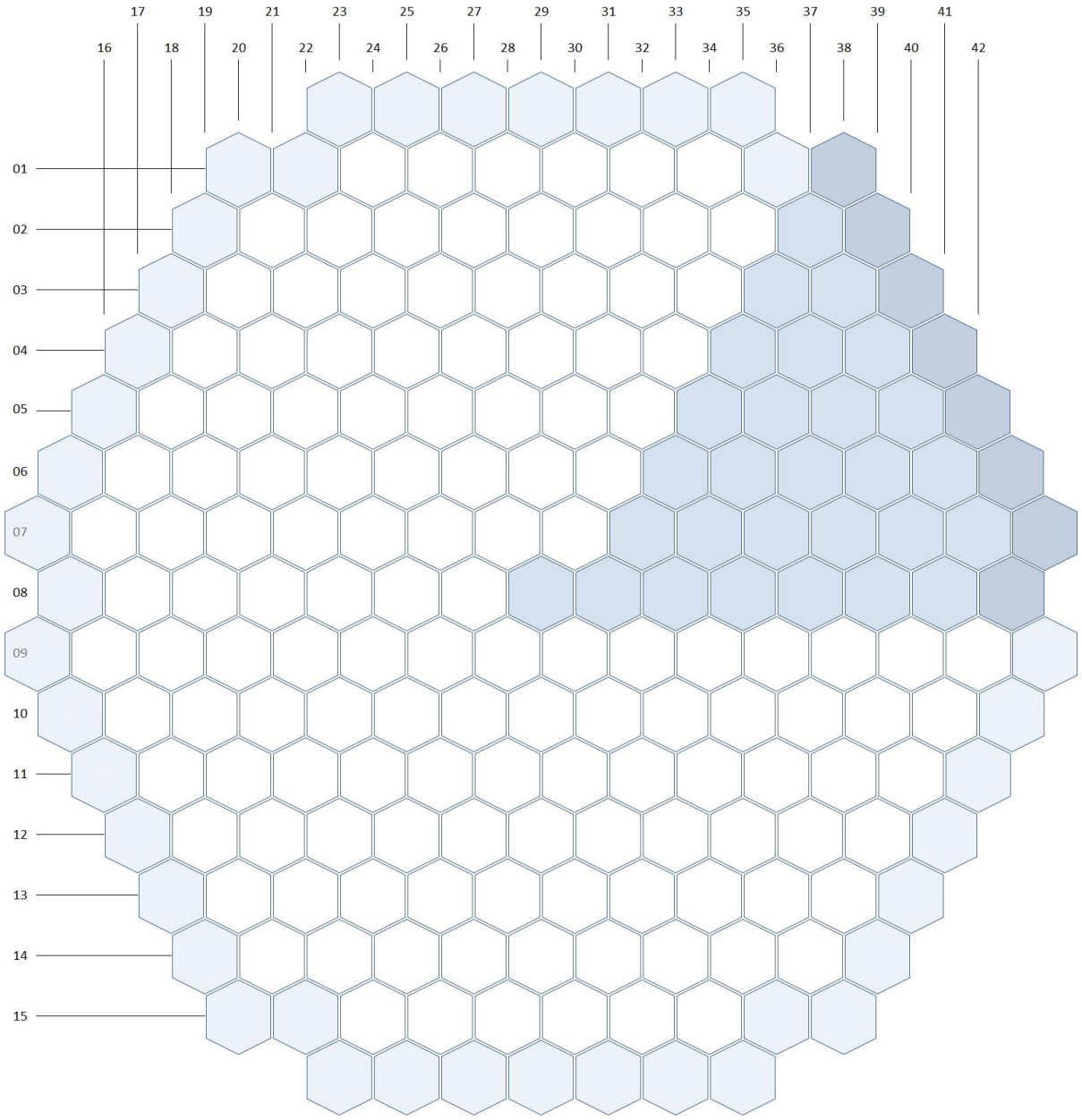

Figure 6.1-6: Handling of Kalinin 3 cross-section tables. Coloured area is covered by cross-section set 2 while remaining part of the core is covered by set 1. Outermost layer shown is radial reflector

6.2 Transient description

At the start of the transient, 20:30:02 on 2 October 2005, Kalinin 3 is operated at 2965 MW(t) at 128.5 EFPD. Control Rod Bank No. 10 position is 82.95 % (above the lower end switch). Transient is described in Table 6.2-1 (Tereshonok, 2009).

Table 6.2-1: Time history of the Kalinin 3 transient

Time		Event description
s	**hh:mm:ss**	
0	20:30:02	A manual trip of MCP #1 from the main control room.
1	20:30:03	Trip of 1 (out of 4) MCPs causes automatic reactor power downturn and shifts set-points of reactor protection system channels down to 67 %. Control rod bank No 10 insertion starts. Reactor power controller stand-by, switch-over from mode T (constant steam pressure) to mode N (constant core power).
60	20:31:02	Control Rod Bank No 10 is down to 50 % above lower limit switch. Control Rod Bank No 9 insertion started.
71	20:31:23	Reactor power below 67.2 % (ex-core detectors). Control Rod Bank No 10 position is 43.4 % (70 steps below position at the start of the transient). Control Rod Bank No 9 position is 93.1 %. Reactor power controller is on, mode N (constant core power). Primary pressure reaches lowest point and then starts to increase. Main steam pressure is increasing slowly towards nominal value.
180	20:33:02	Manual extraction of Control Rod Bank No 9 (one step per second).

6.3 Simulation results and discussion

Simulation presented here illustrates a full-scope plant model. No boundary conditions are used except grid voltage and frequency, condenser cooling water temperature and atmosphere pressure and temperature. A set of simulation results is selected with a focus of core model performance.

The core thermal power (ex-core detectors, power range) and Control Rod Bank Nos. 9 and 10 positions are shown in Figure 6.3-1. Axial offset is shown in Figure 6.3-2. These two figures provide an overall picture of the transient. The maximum in axial power profile is shifted towards the bottom of the core due to the insertion of Control Rod Bank Nos. 9 and 10.

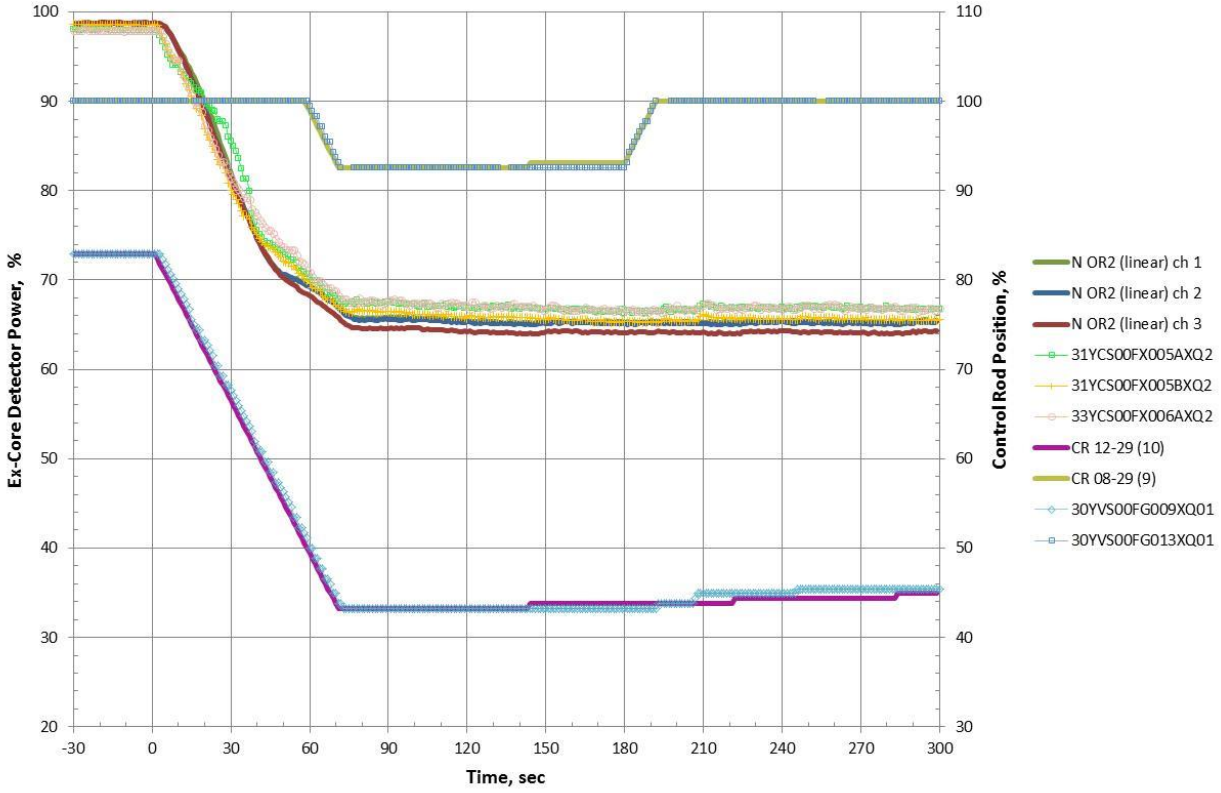

Figure 6.3-1: Power excursion (ex-core detectors, power range, linear) and Control Rod Bank Nos. 9 and 10 positions. Plant data are shown with symbols (31YCS00FX005AXQ2 ex-core detector 2; 31YCS00FX005BXQ2 ex-core detector 12; 33YCS00FX006AXQ2 ex-core detector 7; 30YVS00FG013XQ01 position of control rod 14-25, bank No. 9; 30YVS00FG009XQ01 position of control rod 10-23, bank No. 10). Simulation data are shown with lines (N OR2 (linear) ch 1, ch 2 and ch 3 – ex-core detectors, power range, linear, set 1; CR 12-29 (10) control rod 12-29, bank No. 10; CR 08-29 (9) control rod 08-29, bank No. 9)

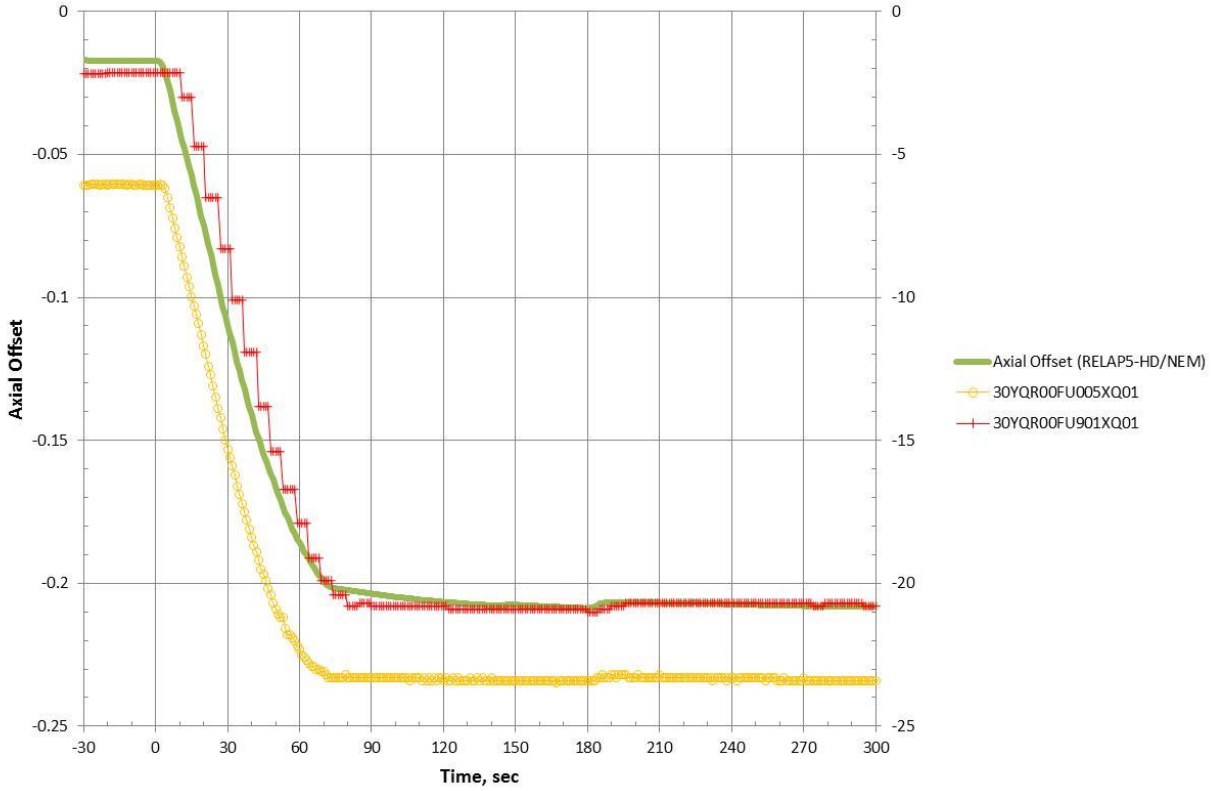

Figure 6.3-2: Axial offset. Data recorded by Kalinin 3 ICMS are shown with symbols (30YQR00FU005XQ01 axial offset of SPND; 30YQR00FU901XQ01 axial offset of the reconstructed 3D power distribution). Simulation data are shown with a tick line

Results of the simulation are illustrated with five sets of data: start of the transient, 0 s; 45 s; 90 s; 150 s; end of the transient, 300 s.

Assembly power distribution at the start of the transient is shown in Figure 6.3-3. Deviation is calculated as follows.

$$Deviation\,,\% = \left(F_{xy}Simulation - F_{xy}ICMS\right) \times 100 \qquad \text{Eq. 6.3-1}$$

Magnitude and radial distribution of deviations at the start of the transient is plotted on Figure 6.3-4. Summary of deviations in assembly power during the transient are presented in Table 6.3-1.

Table 6.3-1: Kalinin 3 transient – Comparison between simulation and plant data (ICMS) – Brief statistics of deviations in assembly power during the transient

Time,	Maximum Deviation				RMS Deviation	
					whole core	FA with SPND
s	%	FA (position)	%	FA (position)	%	%
0	-3.77	134 (04-31)	+2.51	95 (07-28)	1.36	1.71
45	-4.01	134 (04-31)	+2.69	81 (08-27)	1.32	1.78
90	-4.47	30 (12-27)	+3.72	150 (02-23)	1.70	2.01
150	-4.62	27 (12-21)	+3.74	150 (02-23)	1.76	2.04
300	-4.19	30 (12-27)	+3.61	150 (02-23)	1.66	2.00

At the start of the transient, simulation slightly overestimates power of fuel assemblies in the central part of the core and underestimates power of fuel assemblies in the middle orbits in comparison with Kalinin 3 ICMS records. At the start of the transient all the deviations in assembly-wise power peaking factors remain within measurement error margin.

Assembly-wise power peaking factor distribution at 45 s is shown in Figure 6.3-5. Magnitude and radial distribution of deviations at 45 s is plotted on Figure 6.3-6.

At 45 s after the start of the transient there is still no significant change in the distribution of assembly-wise power peaking factors, as well as in the deviations between simulation and ICMS records.

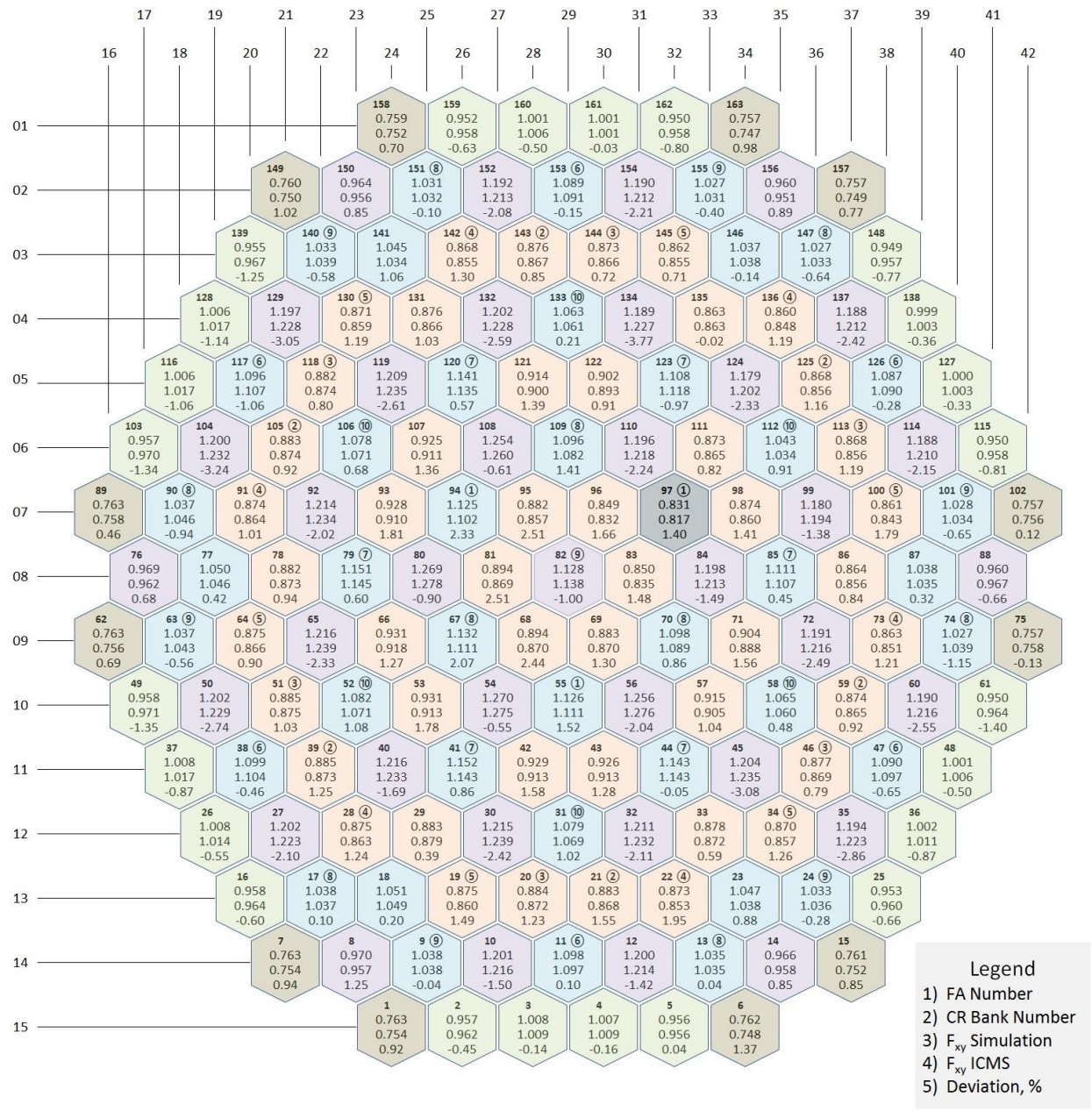

Figure 6.3-3: Kalinin 3 transient — Comparison between simulation and plant data (ICMS) — Assembly-wise power peaking factors at the start of the transient

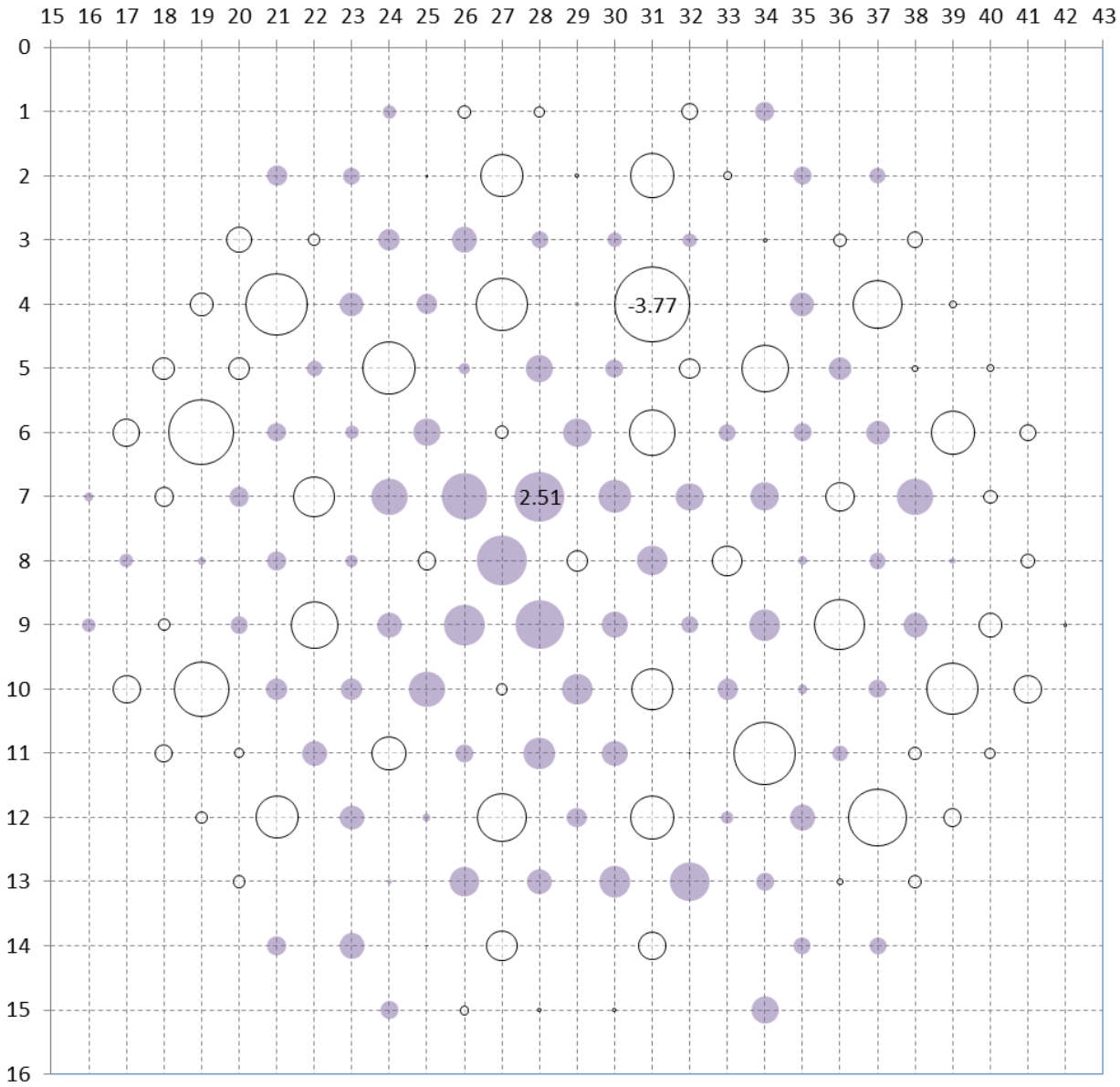

Figure 6.3-4: Kalinin 3 transient — Comparison between simulation and plant data (ICMS) — Deviation in assembly-wise power peaking factors [%] at the start of the transient (magnitude of deviation is proportional to bubble diameter; coloured — positive, transparent — negative)

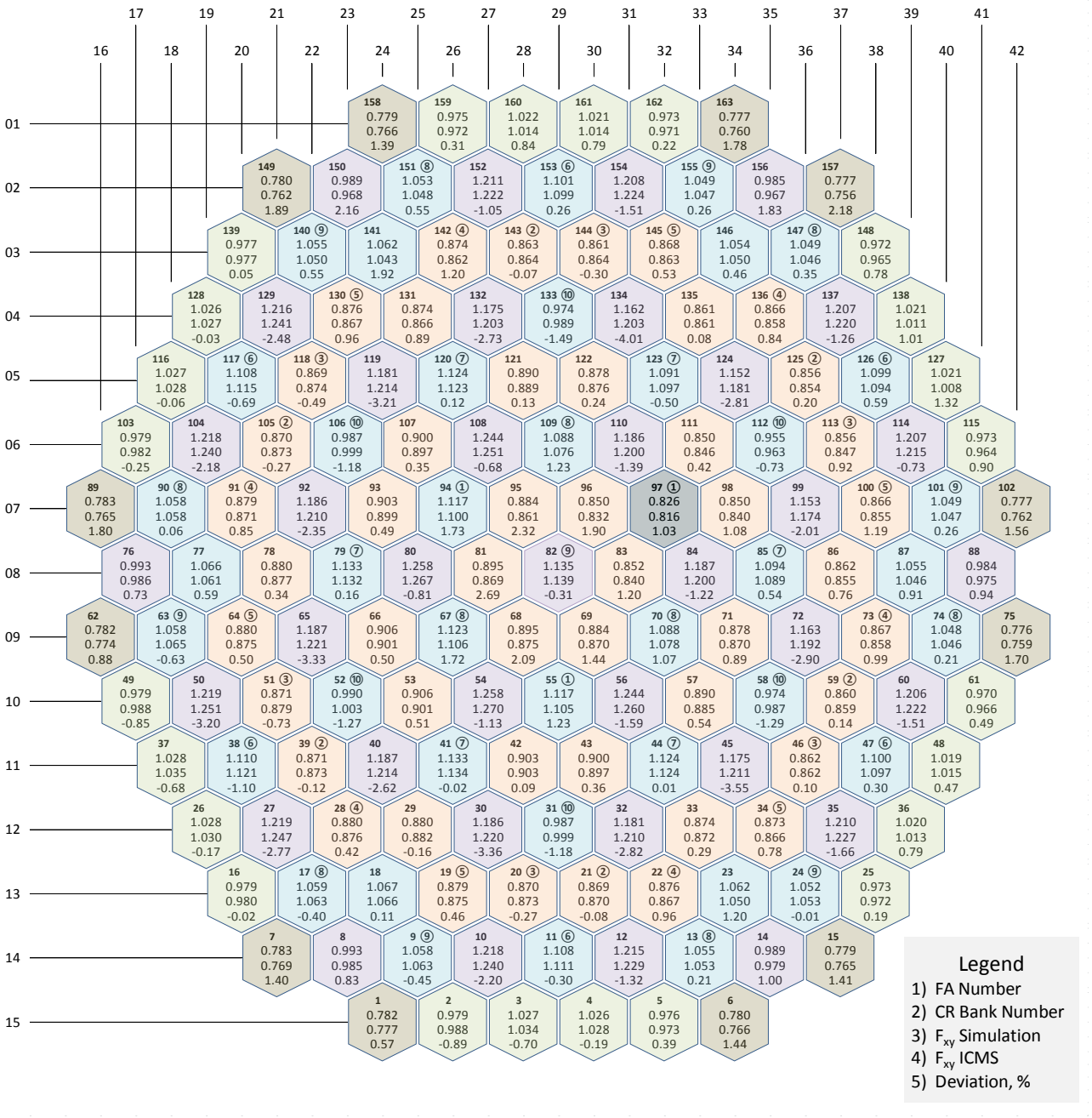

Figure 6.3-5: Kalinin 3 transient — Comparison between simulation and plant data (ICMS) — Assembly-wise power peaking factors at 45 s

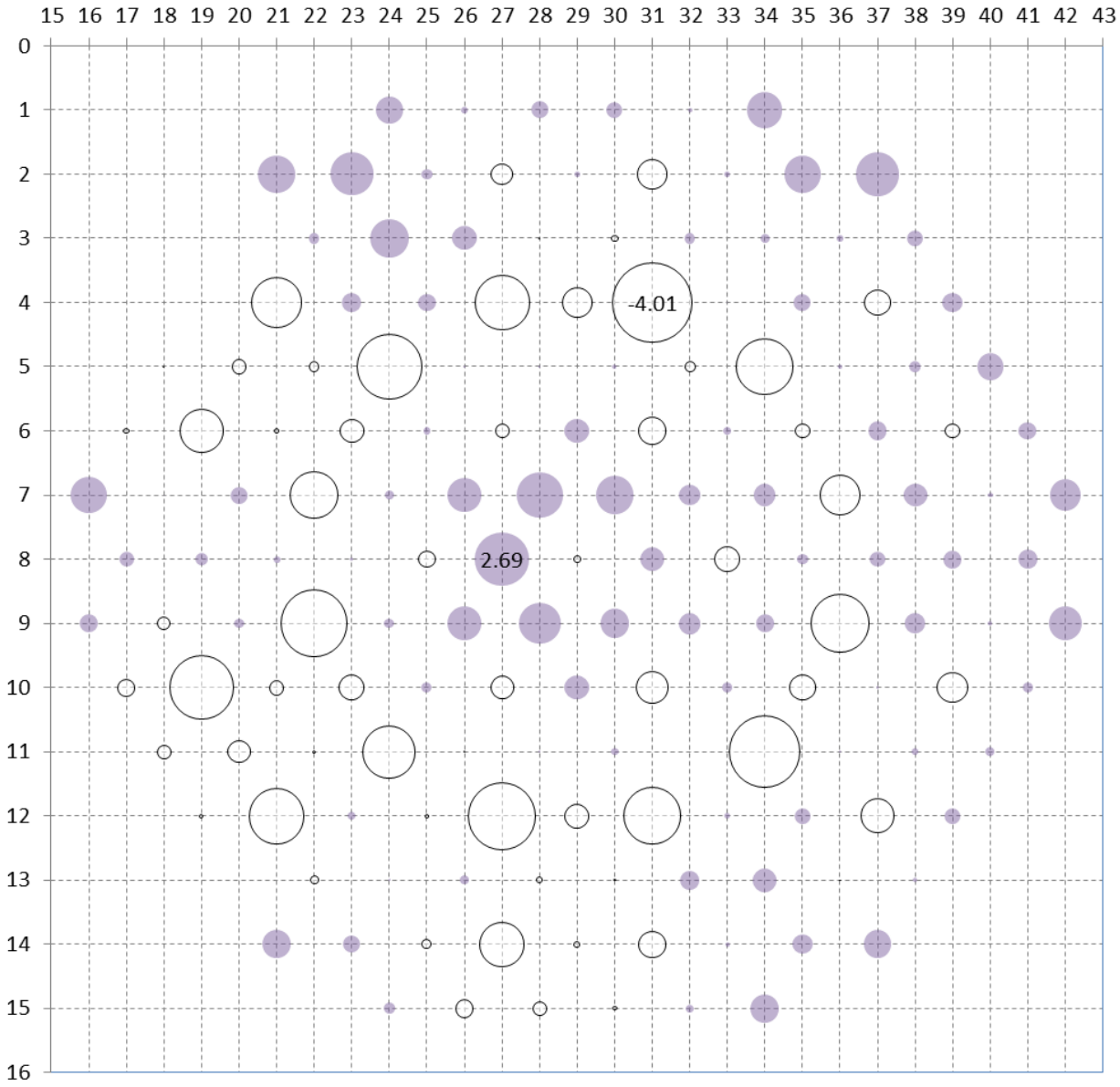

Figure 6.3-6: Kalinin 3 transient — Comparison between simulation and plant data (ICMS) — Deviation in assembly-wise power peaking factors [%] at 45 s (magnitude of deviation is proportional to bubble diameter; coloured — positive, transparent — negative)

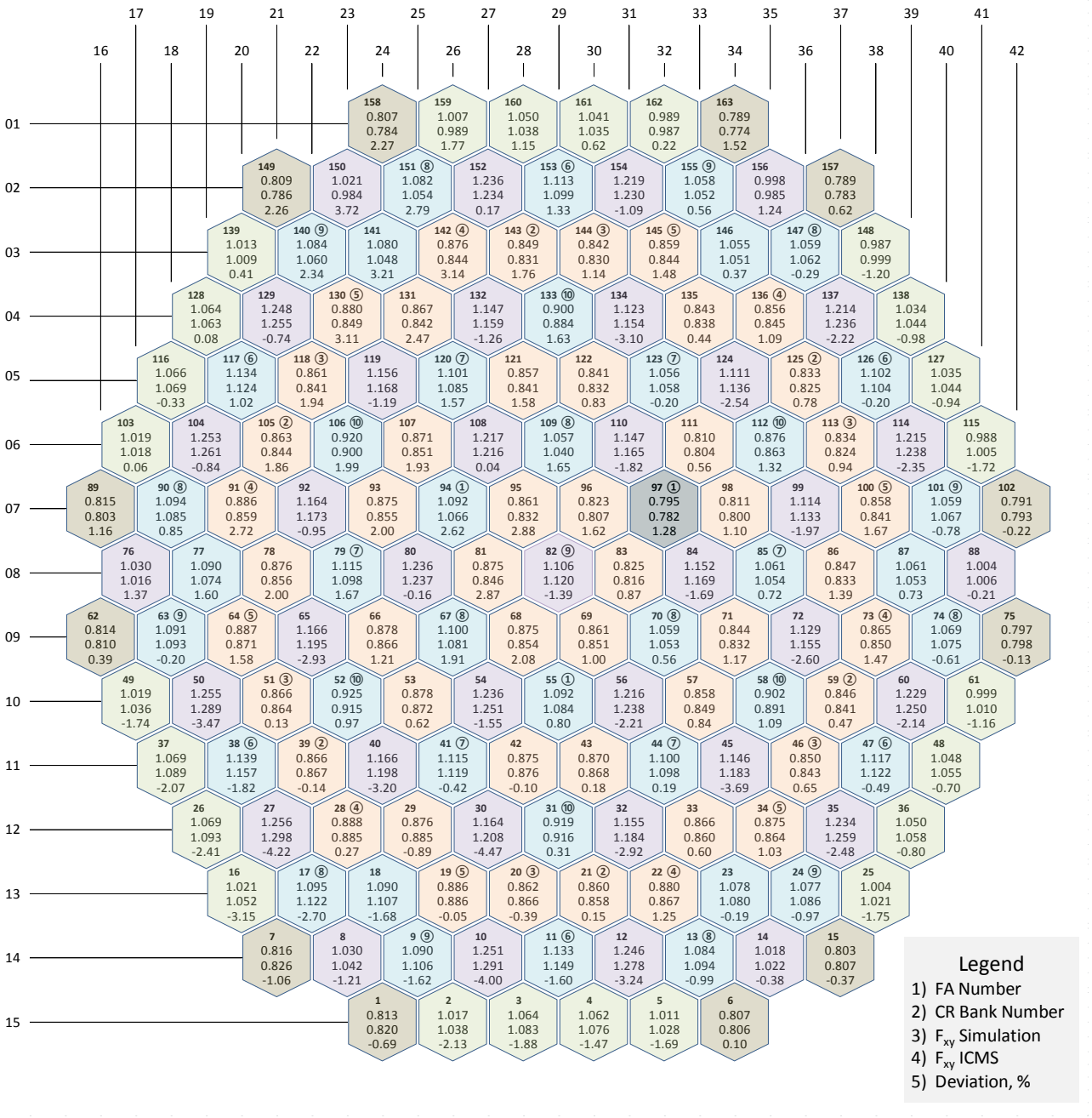

Figure 6.3-7: Kalinin 3 transient — Comparison between simulation and plant data (ICMS) — Assembly-wise power peaking factors at 90 s

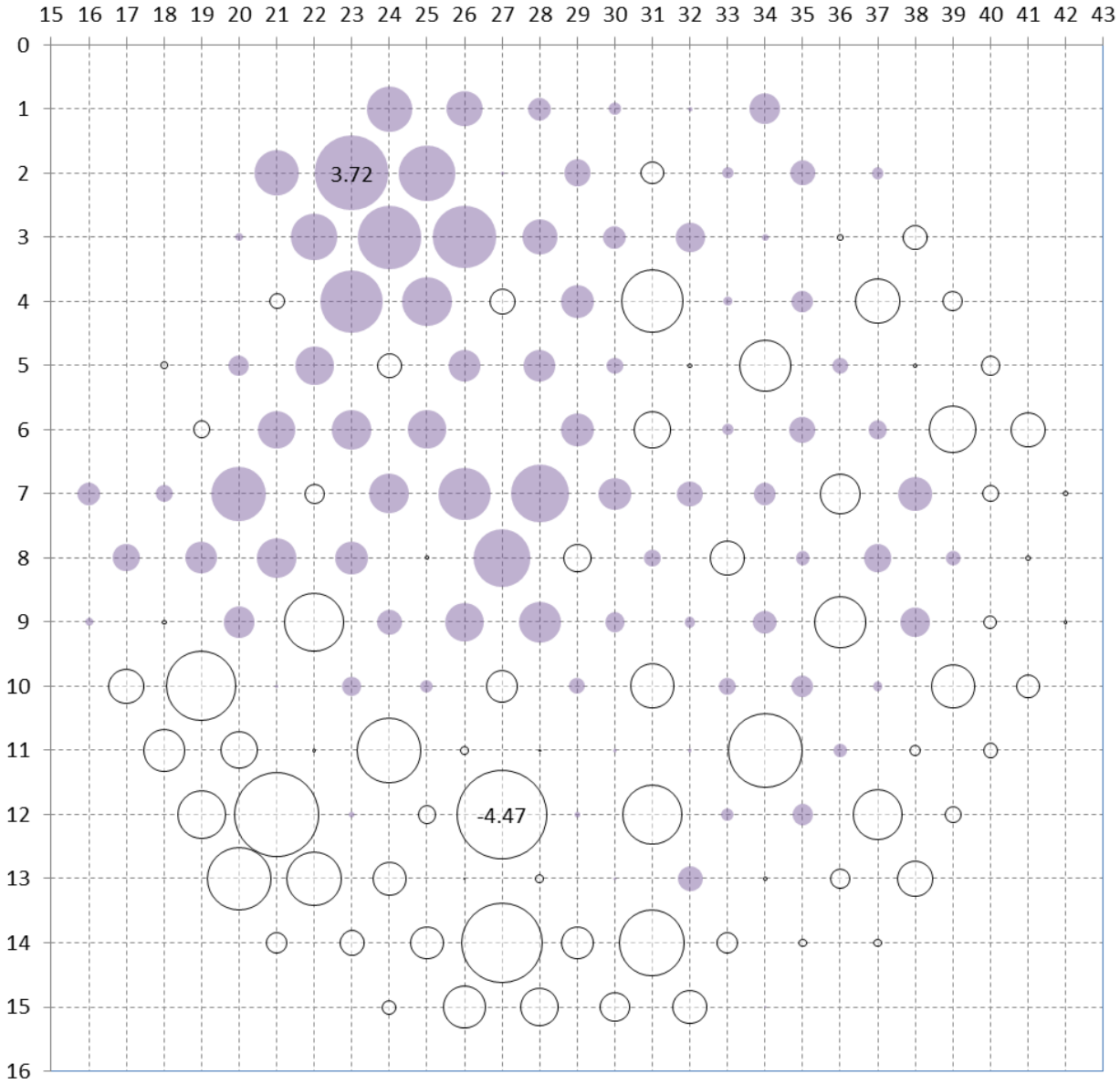

Figure 6.3-8: Kalinin 3 transient — Comparison between simulation and plant data (ICMS) — Deviation in assembly-wise power peaking factors [%] at 90 s (magnitude of deviation is proportional to bubble diameter; coloured — positive, transparent — negative)

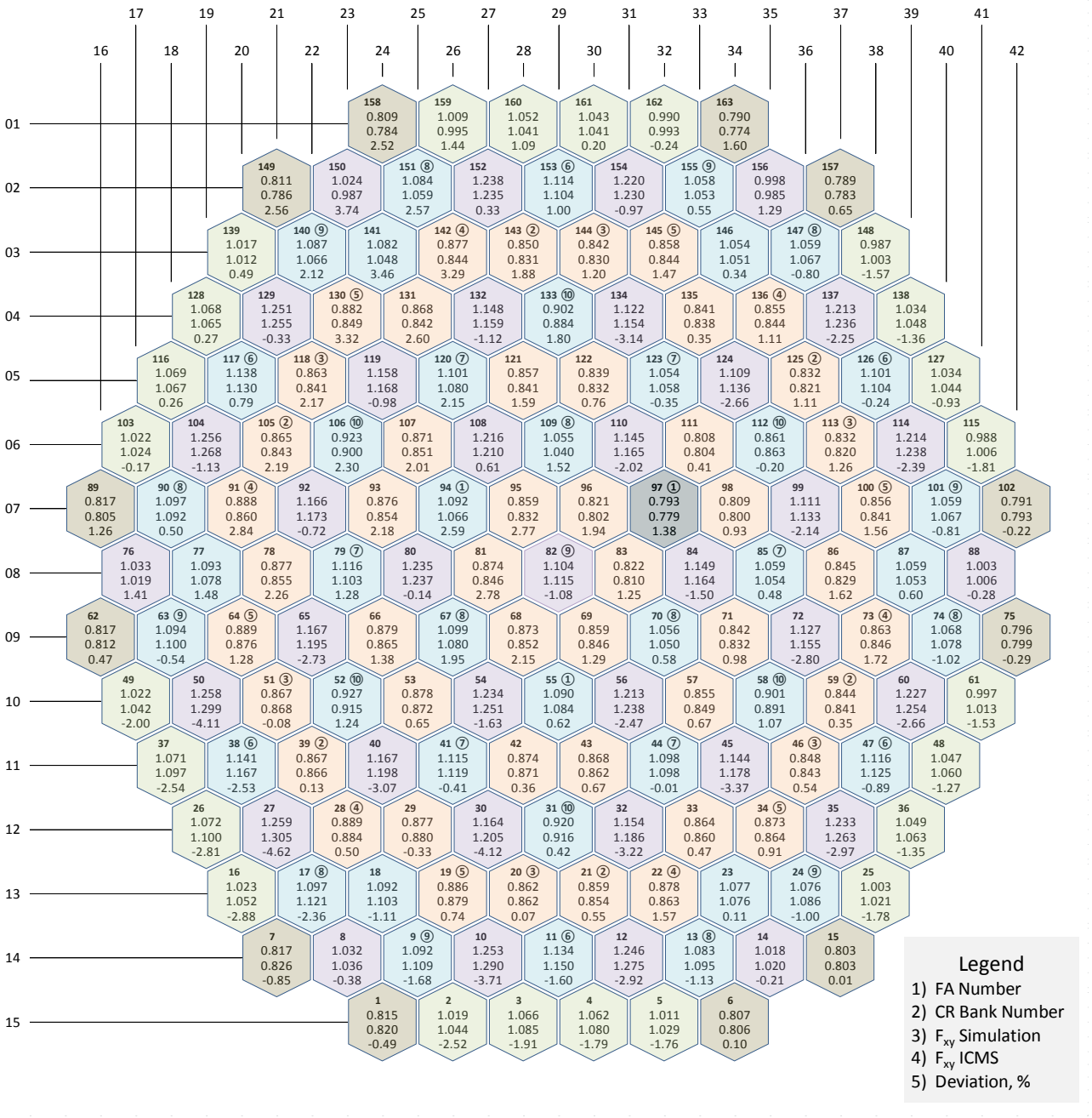

Figure 6.3-9: Kalinin 3 transient — Comparison between simulation and plant data (ICMS) — Assembly-wise power peaking factors 150 s

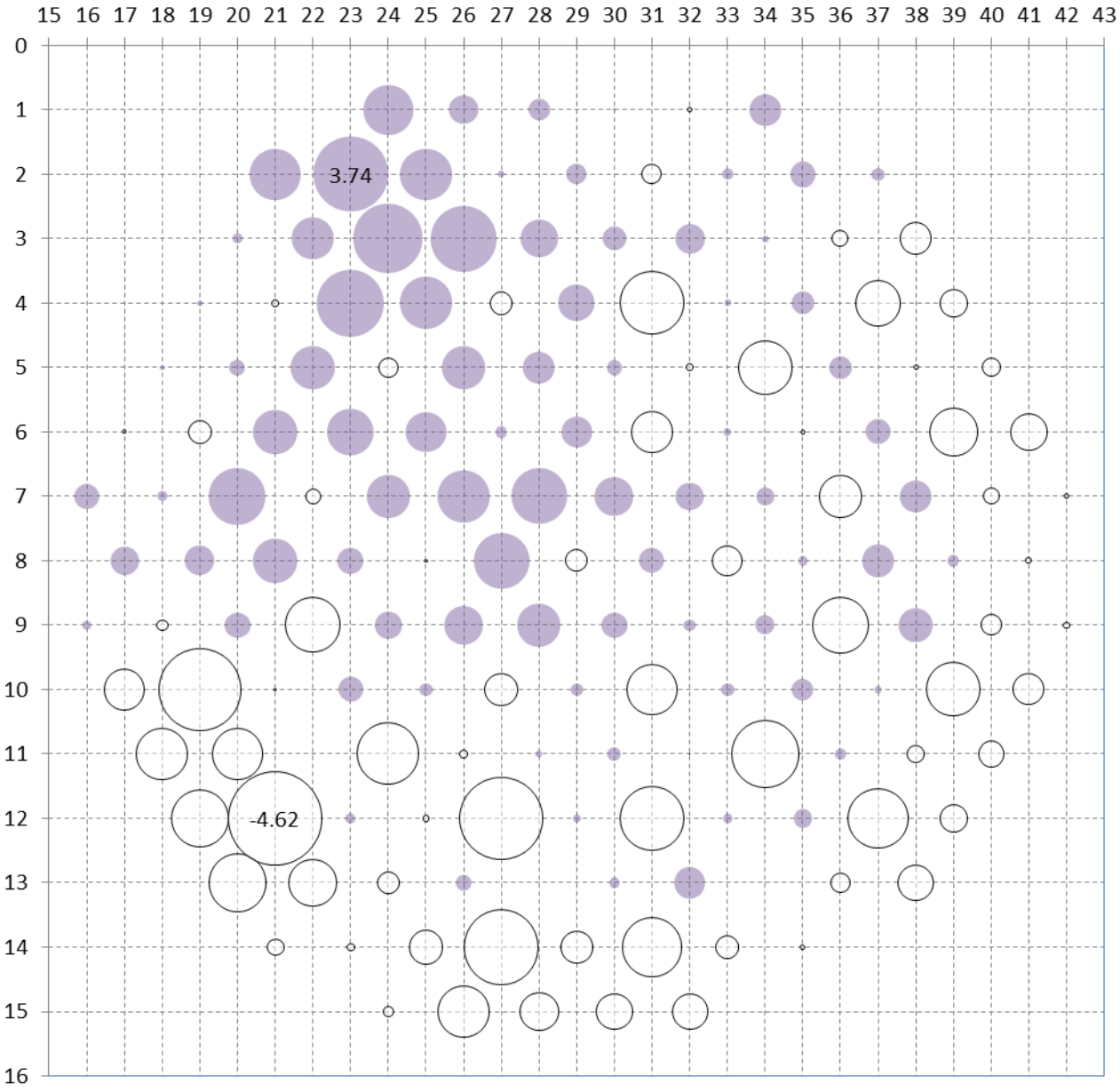

Figure 6.3-10: Kalinin 3 transient — Comparison between simulation and plant data (ICMS) — Deviation in assembly-wise power peaking factors [%] at 150 s (magnitude of deviation is proportional to bubble diameter; coloured — positive, transparent — negative)

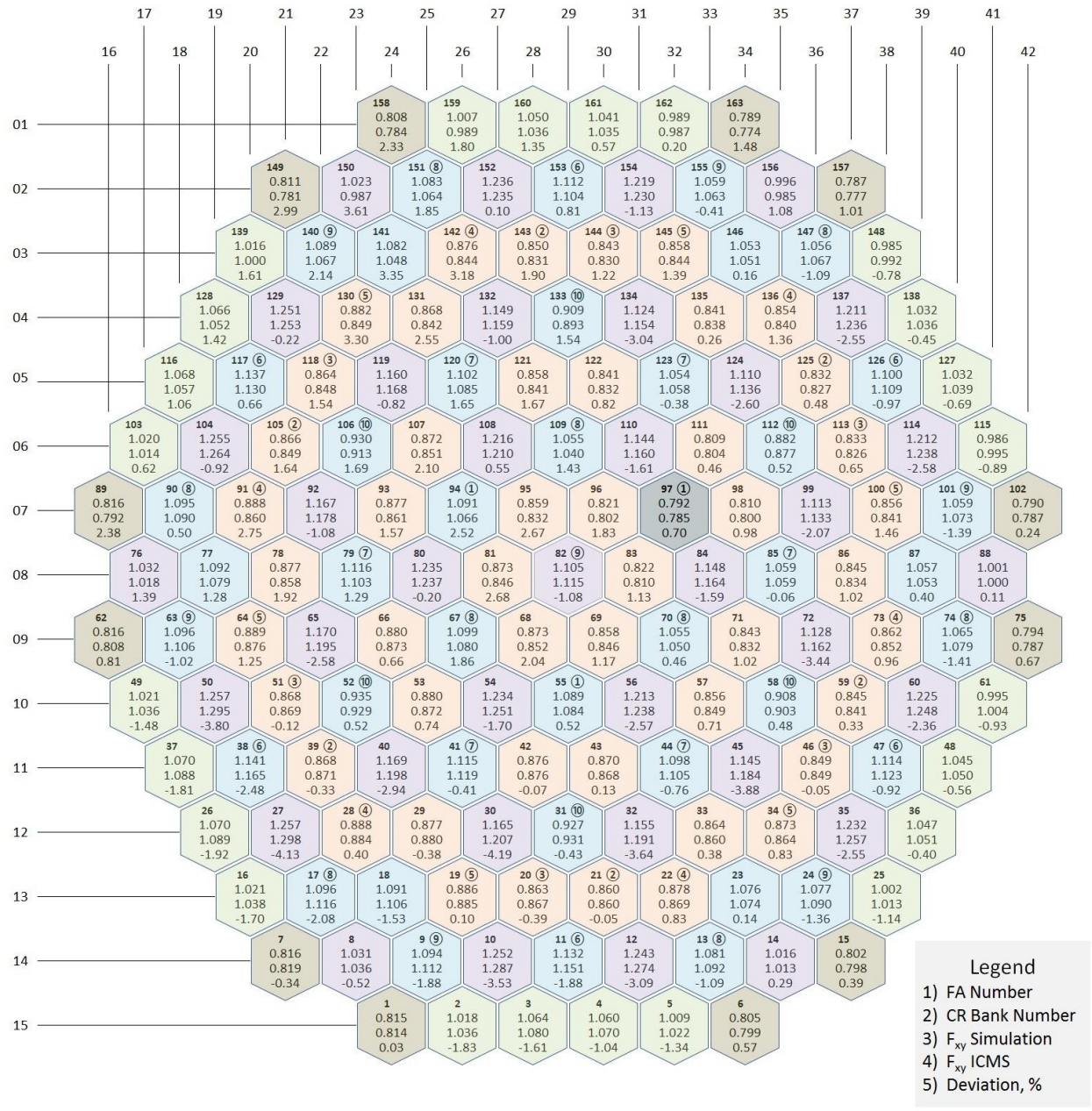

Figure 6.3-11: Kalinin 3 transient — Comparison between simulation and plant data (ICMS) — Assembly-wise power peaking factors the end of the transient

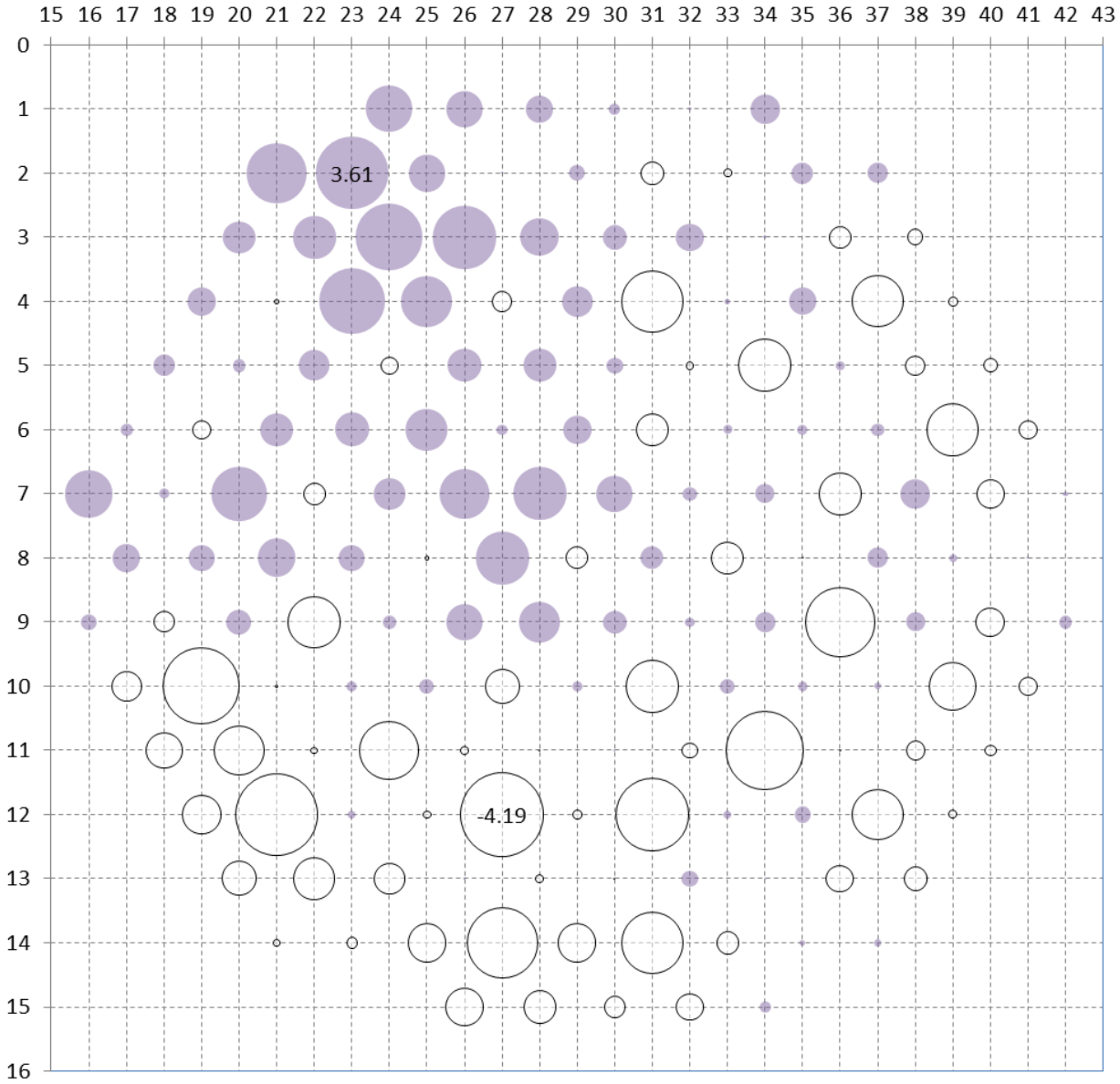

Figure 6.3-12: Kalinin 3 transient — Comparison between simulation and plant data (ICMS) — Deviation in assembly-wise power peaking factors [%] at the end of the transient (magnitude of deviation is proportional to bubble diameter; coloured — positive, transparent — negative)

Assembly-wise power peaking factor distribution at 90 s is shown in Figure 6.3-7. Magnitude and radial distribution of deviations at 90 s is plotted on Figure 6.3-8. At 90 s after the start of the transient more significant changes in the distribution of assembly-wise power peaking factors are present, as well as some increase of deviations between simulation and ICMS records. There is a change in distribution of deviations, too.

Assembly-wise power peaking factor distribution at 150 s is shown in Figure 6.3-9. Magnitude and radial distribution of deviations at 150 s is plotted on Figure 6.3-10. The parameters show little change from the condition at 90 s.

Assembly-wise power peaking factor distribution at the end of the transient is shown in Figure 6.3-11. Magnitude and radial distribution of deviations at the end of the transient is plotted on Figure 6.3-12. Again, the parameters show little change from the condition at 90 s and 150 s, although towards the end of the power excursion deviations decrease slightly.

Evolution of simulated sector-average power distribution in 12 thirty-degree core sectors is plotted on Figure 6.3-13. Data from Kalinin 3 ICMS are given for comparison in Figure 6.3-14. These two figures provide an explanation for the distribution of deviations shown in Figure 6.3-8, Figure 6.3-10 and Figure 6.3-12. In the simulation, the hydraulic characteristics of the two neighbour loops No. 1 and No. 4 are quite similar. Kalinin 3 records in Figure 6.3-14 indicate something different. When coolant flow loop No. 4 replaces coolant from loop No. 1 power in sectors Nos. 11 decreases, and this decrease is compensated by a strong increase in sector No. 2. Variations in cold leg coolant temperature between loops Nos. 1 and 4 cause this effect.

Evolution of RMS deviation of assembly-wise power peaking factor for each of the 12 thirty-degree core sectors is shown in Figure 6.3-15. This figure can be compared with Figure 6.1-4. There is no correlation between errors in assembly exposure and in assembly-wise power peaking factors.

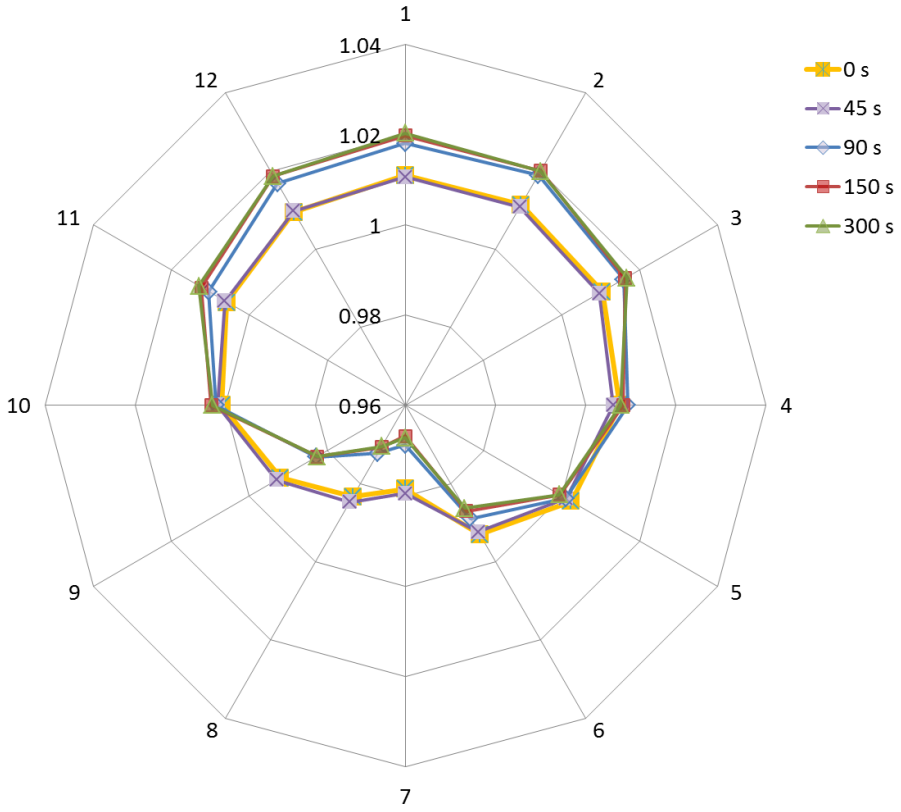

Figure 6.3-13: Kalinin 3 transient — Evolution of sector-average power distribution in 12 thirty-degree core sectors — Simulation data

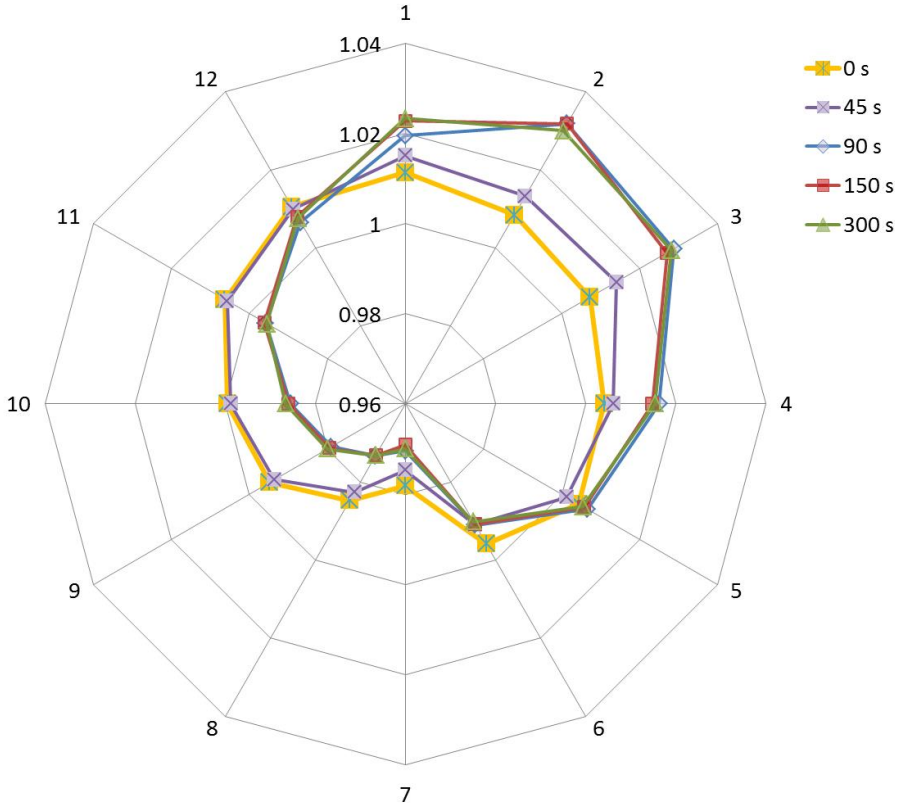

Figure 6.3-14: Kalinin 3 transient — Evolution of sector-average power distribution in 12 thirty-degree core sectors — Kalinin 3 ICMS

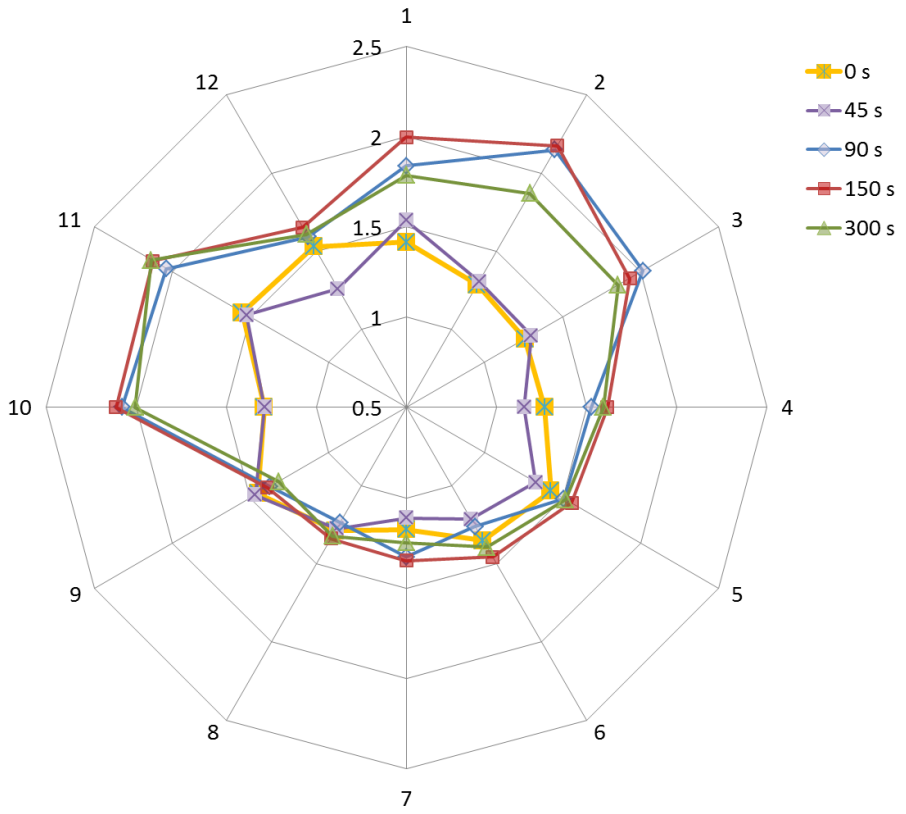

Figure 6.3-15: RMS deviation [%] of assembly power for each of the 12 thirty-degree core sectors

Evolution of the axial power profile for FA with largest deviations in assembly-wise power peaking factor – Nos. 27, 30, 81, 96 (neighbour with FA No 95), 134 and 150 – is shown in Figure 6.3-16, Figure 6.3-17, Figure 6.3-18, Figure 6.3-19, Figure 6.3-20 and Figure 6.3-21. Evolution of the axial power profile for all fuel assemblies with SPND is shown in 0.

Peaking factor data from Kalinin 3 ICMS (30YQR04FXnnn, where 'nnn' is assembly number, 001 to 163) reflect position of detector strings and are slightly different for each one. Estimated error in axial peaking factor is about 10 %. Linear Heat Rate (LHR) data from Kalinin 3 ICMS (30YQR06FXnnn) are estimated in seven uniformly distributed layers positioned symmetrically about the centre. For the purpose of comparison, LHR records are reduced to peaking factor through reverse application of ICMS algorithm on the basis core thermal power (recorded) and clad surface. A small error in the conversion of LHR data is introduced by variations in pin power distribution along the fuel assembly. This error is not significant.

Axial power peaking factor results shown are very good in comparison with ICMS records throughout the transient taking in account response time of SPND and power reconstruction algorithms.

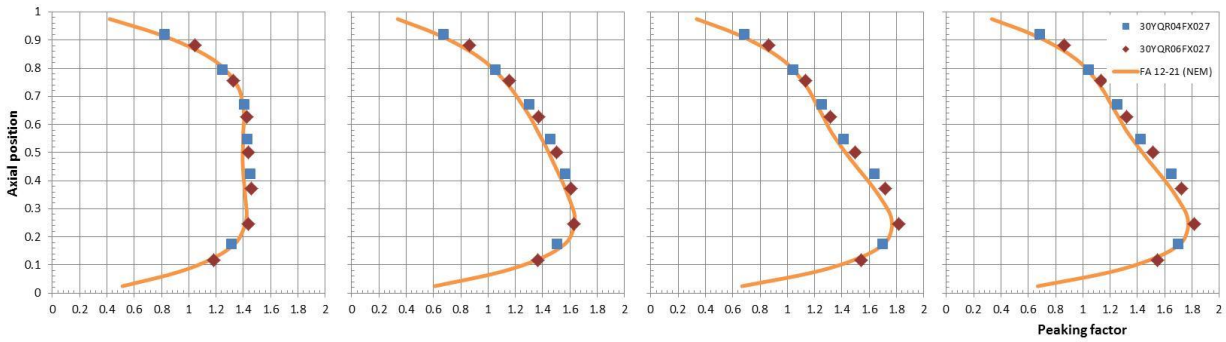

Figure 6.3-16: Axial power profile for FA 27 (12-21) at 0, 45, 90 and 300 s. Data recorded by Kalinin 3 ICMS are shown with symbols — 30YQR04FX027, 30YQR06FX027 (LHR readings normalized to peaking factor).

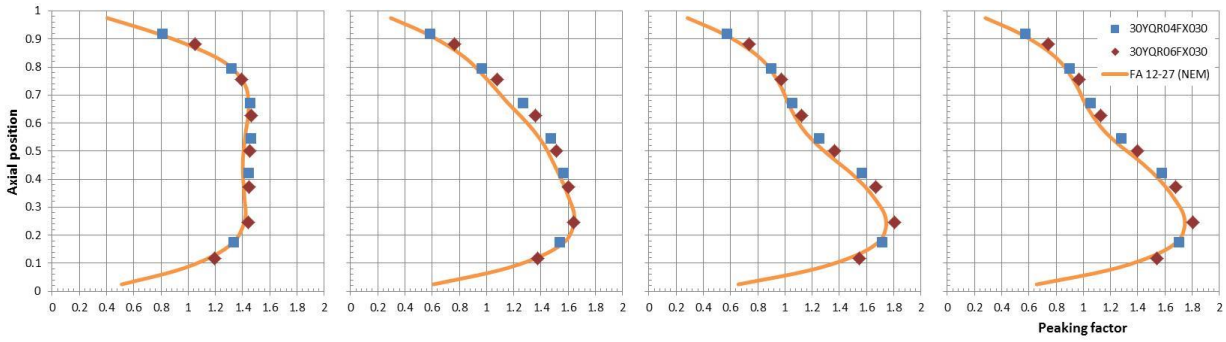

Figure 6.3-17: Axial power profile for FA 30 (12-27) at 0, 45, 90 and 300 s. Data recorded by Kalinin 3 ICMS are shown with symbols — 30YQR04FX030, 30YQR06FX030 (LHR readings normalized to peaking factor).

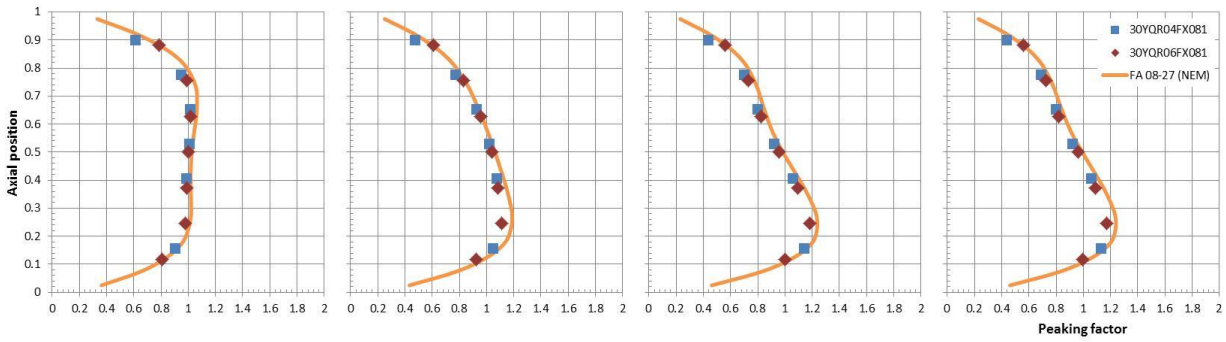

Figure 6.3-18: Axial power profile for FA 81 (08-27) at 0, 45, 90 and 300 s. Data recorded by Kalinin 3 ICMS are shown with symbols — 30YQR04FX081, 30YQR06FX081 (LHR readings normalized to peaking factor).

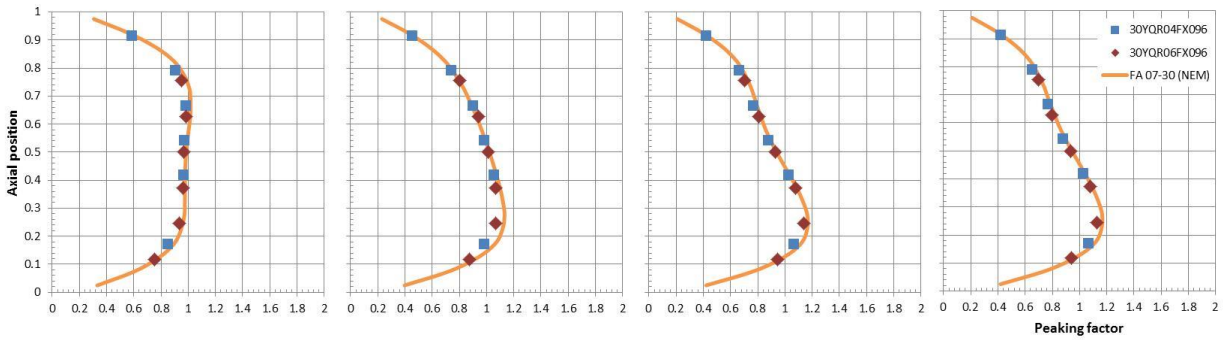

Figure 6.3-19: Axial power profile for FA 96 (07-30) at 0, 45, 90 and 300 s. Data recorded by Kalinin 3 ICMS are shown with symbols — 30YQR04FX096, 30YQR06FX096 (LHR readings normalized to peaking factor).

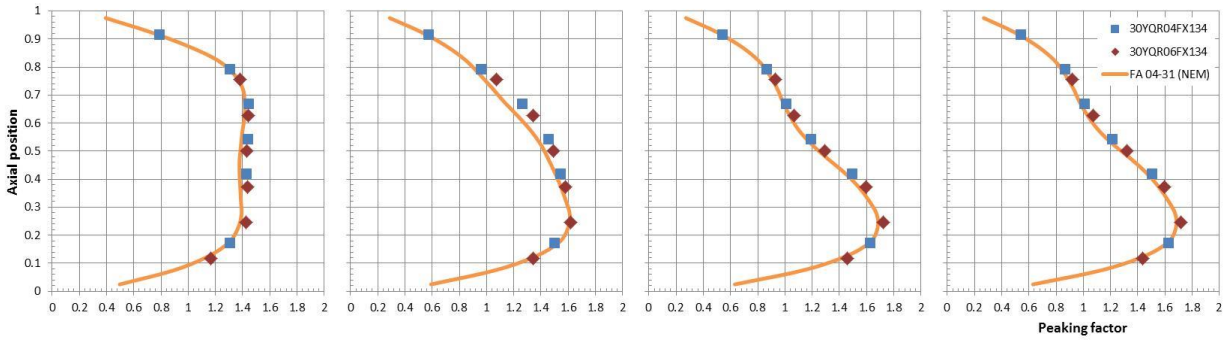

Figure 6.3-20: Axial power profile for FA 134 (04-31) at 0, 45, 90 and 300 s. Data recorded by Kalinin 3 ICMS are shown with symbols — 30YQR04FX134, 30YQR06FX134 (LHR readings normalized to peaking factor).

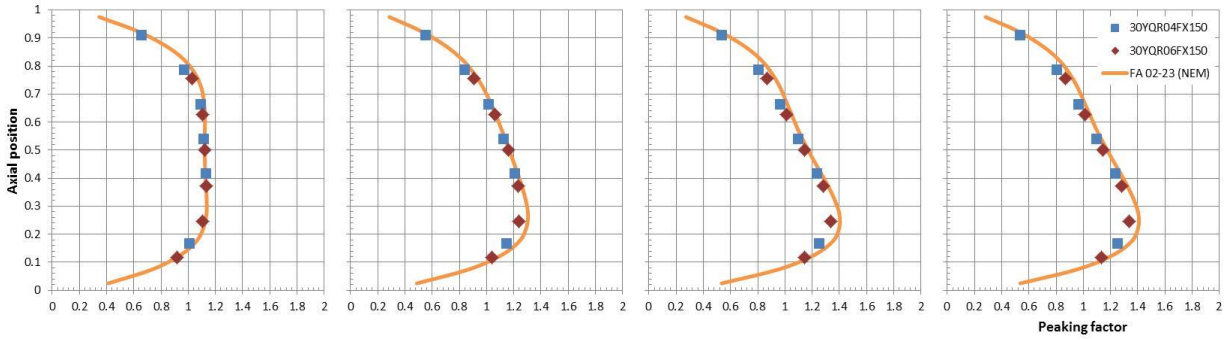

Figure 6.3-21: Axial power profile for FA 150 (02-23) at 0, 45, 90 and 300 s. Data recorded by Kalinin 3 ICMS are shown with symbols — 30YQR04FX150, 30YQR06FX150 (LHR readings normalized to peaking factor).

6.4 Lessons learnt

While Kalinin 3 benchmark specification (Tereshonok, 2009) contains very good description of the transient, as well as record of many parameters of the unit, the document provides only superfluous description of the reference unit. The only meaningful approach in a case when plant-specific data are incomplete is to fill the necessary gaps with 'generic' data from other VVER-1000/V320 plants. As there are always differences in the construction of individual power generating units, even if such units belong to a one-and-the-same series, such an approach, by default, introduces deviations which are difficult to quantify.

Kalinin 3 benchmark specification makes reference to V1000CT-1 benchmark specification (Ivanov, 2002) for plant description. The analysis, however, indicates important differences in plant characteristics. There are several examples which require quantification.

6.4.1 Primary coolant flow rate

Kalinin 3 records demonstrate marked difference in coolant mass flow rate in comparison with the Kozloduy 6 plant-specific model. While Kozloduy 6 model reproduces reasonably well the Kozloduy 6 ICMS data, Kalinin 3 ICMS primary coolant flow estimation shows a significant difference in loop flow rates both before and after pump switching off. As a result, Reactor Pressure Vessel (RPV) mass flow rate for the simulation presented here is 3 % less at the start of the transient and about 5 % less at the end (Figure 6.4-1).

The same Figure 6.4-1 illustrates another problem – there is no reliable estimation of core and loop coolant flow rates during the transient. ICMS loop coolant flow estimation is based on two algorithms. The first one is a second-degree polynomial approximation of flow-versus-head curve of the MCP with pump motor on (taking into account pump suction pressure and temperature for estimation of coolant density, as well as bus frequency for the pump motor). The second algorithm is applicable only for reverse flow after complete pump coast-down. The first algorithm is used until detection of MCP loss-of-power condition. Once MCP is de-energized, loop flow rate is assumed to decrease in proportion with decrease of MCP head as long as measured loop coolant heat-up is positive – an assumption, which is neither physically sound nor conservative. Switchover to the reverse flow algorithm in Kalinin 3 ICMS is performed about 40 s after de-energizing of the pump motor (for the sake of comparison, this period is about 45 s in the Kozloduy 6 ICMS, mostly due to a difference in response time of thermo-couples used). An abrupt change in recorded value can be seen on Figure 6.4-1. At the time of switchover, however, both algorithms are out of their

respective application range. There is no reliable estimation of the affected loop flow rate for a period of about 90 s after trip of the pump motor until steady reverse flow is established at zero pump rotation speed.

Partial explanation for the deviations in F_{xy} between present simulation and ICMS readings (Table 6.3-1) is far from perfect prediction of flow and coolant temperature in loops Nos. 1 and 4. Part of the problem is lack of Kalinin 3 loop-specific pump characteristics.

Another part of the problem is non-uniform coolant temperature in the hot leg of the coolant loop. Magnitude of such a non-uniformity varies along the length of the hot leg being large at the reactor vessel nozzle and gradually decreasing towards steam generator. Also, fine-mesh CFD simulations show change in position of hot and cold spots in coolant temperature distribution at various cross-sections along the hot leg. Available data from various VVER-1000 units confirm significant spreading of hot leg coolant temperature readings from sensors located at different positions in the hot leg. Last but not least, magnitude of coolant temperature non-uniformity varies between VVER-1000 units.

Plant-specific data at various modes of operation (ranging from cold shutdown to rated power, both steady state and transient; operation with incomplete number of MCP; natural circulation test; etc.) are necessary for proper adjustment of pressure loss coefficients of the whole primary coolant system. The same applies for proper tuning of the response of simulated resistance thermometers and thermocouples. Lack of a representative set of Kalinin 3 data prevents introduction of changes to the present thermal hydraulics model, which is validated through an extensive set of Kozloduy 6 documents.

6.4.2 Primary pressure

Kalinin 3 records show primary pressure at the start of the transient of 15.5 MPa. Kozloduy 6 primary pressure at rated power is higher, 15.7 MPa. Measurement error margin for primary pressure is ± 0.25 MPa. The difference in plant primary pressure at rated power conditions remains unexplained and is not accounted for in the simulation presented here because it affects function of primary pressure controller (e.g. set-points for actuation of pressurizer spray valves and pressurizer heaters). Luckily, the difference is not so significant and causes only small changes in coolant density and specific heat capacity.

6.4.3 Fuel assembly pressure loss

TVS-M type fuel assembly used at position 07-32 (No 97) differs considerably from remaining TVSA type (alternative) fuel assemblies in the core. Generic data for fuel assembly pressure loss coefficient (in the form of a dimensionless multiplier to the dynamic pressure at the inlet of fuel assembly) show 12.1 for TVS-M in comparison with 11.5 for TVSA (+5.2 % difference). Simple calculation (square root of the product of density and pressure difference) results in 2.5 % less coolant mass flow rate through TVS-M fuel assembly.

The core model was modified with an introduction of individual fuel assembly pressure loss coefficient (array of 163 elements; values assigned per assembly type as given above) and variation in coolant flow is accounted for in calculation of coolant density and temperature.

6.4.4 Control Rods

Control rods bank overlap is increased from 20 % to 50 %, as is the case in Kalinin 3. Otherwise, the Kozloduy 6 algorithm is left without change, so there is simultaneous withdrawal of banks Nos. 9 and 10. Presumed 'Operator action' causes extraction of CR Bank No 9 after 180 s. Not so obvious but very important is necessary adjustment of control rod movement to the elevation of the Kalinin 3 core.

6.4.5 K-1000-60/3000 turbine and turbine governor

Kozloduy 6 plant-specific model is based on a modified Kharkov (KhTGZ) K-1000-60/1500-2 turbine while Kalinin 3 is equipped with a K-1000-60/3000 turbine. Although both turbines and related balance-of-plant equipment are designed for compatibility with a VVER-1000/V320 nuclear steam supply system there are marked differences in turbine dynamics and turbine governor response.

One of the important differences is steam pressure at moisture separator and steam reheat. Separator-reheater units are placed between high-pressure and low-pressure turbines. Pressure after high-pressure turbine at rated power is about 0.55 MPa for K-1000-60/3000 turbine and about 1 MPa for K-1000-60/1500-2 turbine. The type of main-feedwater-pump turbine is selected according to the same pressure, etc. Rotating mass of K-1000-60/1500-2 turbine is much larger.

Turbine governor response is consistent with differences in turbine design and vendor. In the case of Kalinin 3, turbine governor reaction is within 20 s from the start of the transient (steam pressure

decreases from 6.02 to 5.9 MPa). Main steam header (MSH) pressure returns swiftly back to normal value in 32 s ('swiftly' in relative terms – by default, turbine control is designed to avoid abrupt changes in steam pressure). MSH pressure is allowed to decrease again later (64 s). Pressure remains low, at 5.9 MPa, for the following 2 min (about 200 s) then slowly returns back to normal value (6 MPa at 255 s). A note about an unspecified deviation from the expected response of secondary pressure controller is mentioned at the conclusion of transient analysis in the Kalinin 3 benchmark specification (Tereshonok, 2009).

K-1000-60/1500-2 turbine governor allows larger MSH pressure excursion at the start of the transient (down to 5.75 MPa) and then steadily pushes MSH pressure back to normal value (about 6 MPa within 180 s). Faster secondary pressure recovery in present simulation affects cold leg coolant temperature and causes faster recovery of primary pressure.

Lack of plant-specific turbine and turbine governor data prevents implementation of any significant changes to the balance of plant models.

6.4.6 ICMS core power reconstruction

Although ICMS version of Kalinin 3 differs in some details from Kozloduy 6 ICMS both systems are similar enough and the following comments are applicable to both units. Just in this particular case there are more data recorded and available for comparison.

Core coolant inlet temperature in ICMS is assumed uniform across the whole core. It is calculated on the basis of cold leg thermocouple and resistance thermometer readings and estimated loop flow rate (Section 6.4.1). Transport time between position of temperature sensors in the cold legs and core inlet and response time of sensors itself is not accounted for. This simplification is unimportant in steady state but affects accuracy of power reconstruction during the transient.

Reactor system thermal power is a weigthed estimation through five methods. One of the five methods – primary loop thermal balance – is based on estimated loop flow rate and coolant temperature difference. In the case of pump coast-down, an estimation of loop flow rate (and thermal power) on the basis of measured pump head in the affected loop is very crude (Figure 6.4-1). Furthermore, this method is prone to the same kind of errors as described in the previous paragraph.

Two methods out of five are based on feedwater flow rate readings. On the secondary side, measurement of feedwater flow is quite reliable but it does not reflect actual core thermal power

during the transient. It depends upon assumption of equilibrium between steam production and feedwater supply. Again, such an assumption is correct in steady state but there is no such equilibrium during a significant stage of the transient.

All the five methods produce results spreading away from each other during the first two minutes of the transient (Figure 6.4-2).

Shape functions used for power reconstruction in ICMS are calculated on the basis of core coolant flow, inlet coolant temperature, boron, reconstructed three-dimensional coolant temperature and density distribution, control rod position and estimated thermal power. Shape functions are updated (re-calculated) every two to five seconds but not at exactly the same time for all nodes in the core (163 x 16 array for high-level core model and 163 x 7 array for handling SPND readings by lower-level algorithms). Accuracy of estimation of local power peaking factor in any part of the core in steady state is about 10 %. Error margin for ICMS power reconstruction during the period of pump coast down and quick load reduction increases considerably.

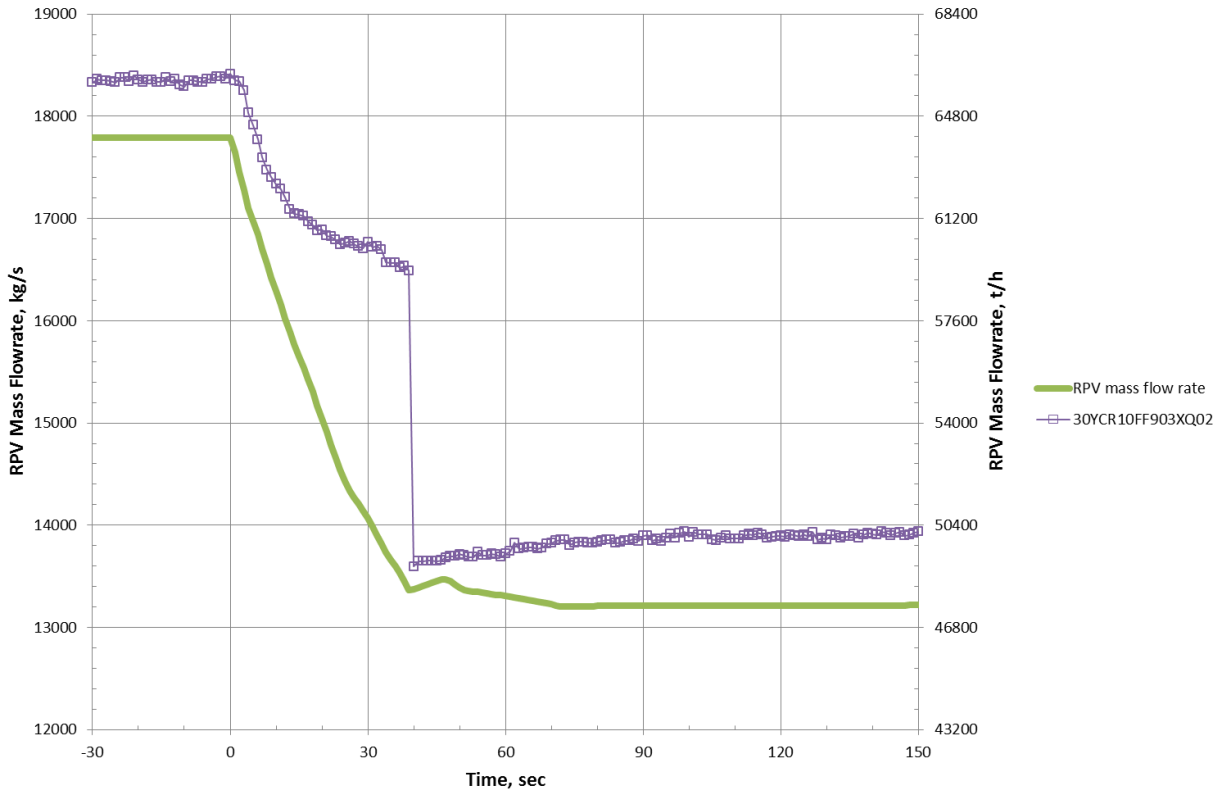

Figure 6.4-1: Reactor pressure vessel coolant mass flow rate — comparison between RELAP5-HD simulation and Kalinin 3 ICMS record. Data recorded by Kalinin 3 ICMS (signal 30YCR10FF903XQ02 in the plant data base) are shown with symbols

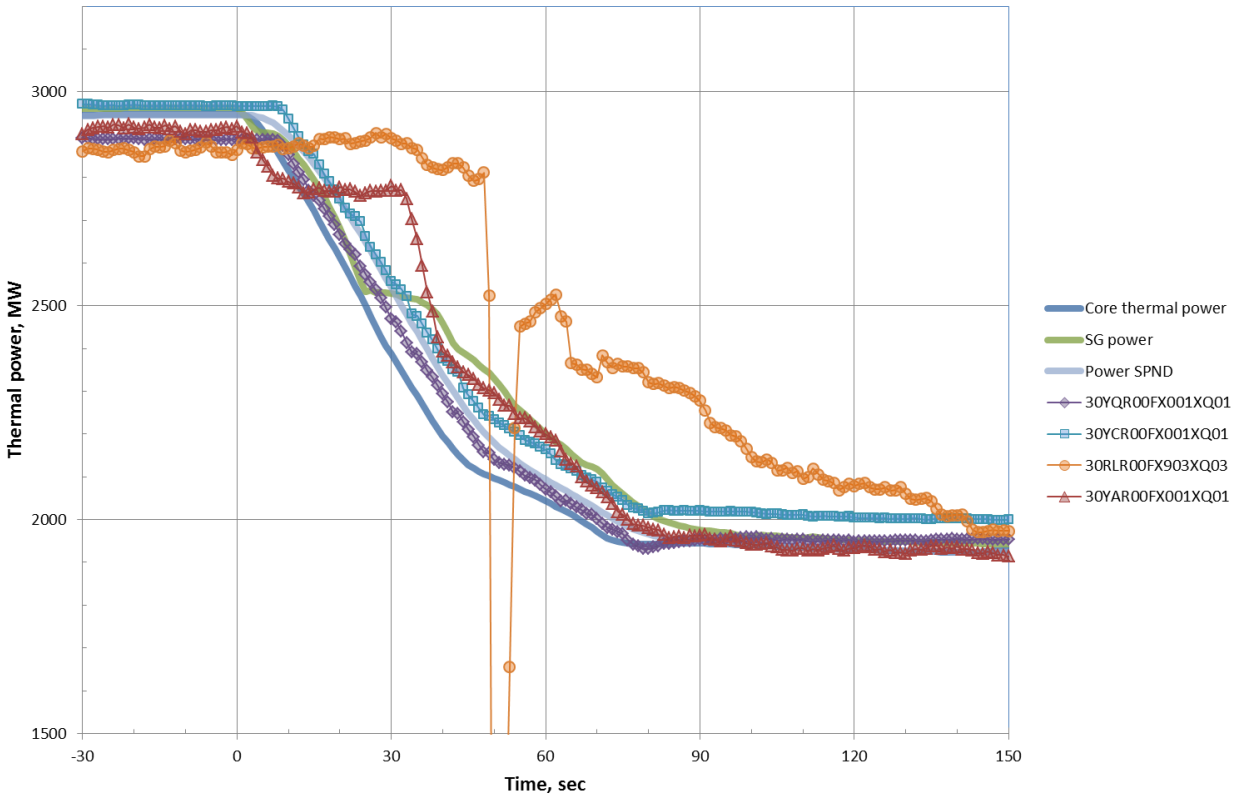

Figure 6.4-2: An illustration of the magnitude of variation of Kalinin 3 reactor system thermal power during the transient. Kalinin 3 ICMS signals are shown with symbols (30YQR00FX001XQ01 reactor thermal power from SPND; 30YCR00FX001XQ01 ex-core detectors; 30RLR00FX903XQ03 thermal balance of steam generators secondary side; 30YAR00FX001XQ01 primary coolant loop thermal balance). Simulation data are shown with tick lines for comparison (Core thermal power, NEM; SG primary-to-secondary, RELAP5-HD; Power from SPND model)

6.5 Conclusion

Another phase of validation of the Kozloduy 6 simulator core model complete with cross-section libraries, tools and procedures for cycle-specific core update with actual plant data from Kalinin 3 (OECD/NEA Kalinin 3 Coolant Transient Benchmark) is quite successful.

Kalinin 3 transient simulation is in very good agreement with ICMS records although several important differences between model and plant characteristics are identified and necessary generic data filled-in.

The core model performance is evaluated on the basis of comparison between simulation results and plant records as follows.

a. assembly-wise power peaking factors;
b. axial profiles of three-dimensional power peaking factors.

In general, deviations between simulation and ICMS records remain within the margin of error. There is no correlation between errors in assembly exposure, introduced through a simplification in cross-section library handling, and in assembly-wise power peaking factors.

Cause of a substantial part of the deviations observed is identified as small variations in the characteristics of plant equipment, particularly reactor pressure vessel and coolant loops (friction coefficients), main coolant pumps (four-quadrant homologous curves) and steam generators (heat transfer and friction coefficients).

7. Conclusions and future work

7.1 Conclusions

The original contribution of this PhD work is the development, implementation, and qualification (verification and validation) of an advanced core calculation methodology for VVER-1000 simulator application.

The important novel features are as follows.

a. The two-group macroscopic cross-section modelling methodology for light-water reactors with hexagonal fuel assemblies (Ivanov, 2007a) is enhanced to cover nuclear fuel with sintered Gadolinium Oxide-Uranium Dioxide pellets, Zirconium-alloy structural components and absorber rods with Boron Carbide and Dysprosium-Titanium Oxide.

b. The enhanced two-group macroscopic cross-section modelling methodology is adapted for a VVER-1000 plant-specific full-scope replica control room simulator application.

c. A real-time version of the NEM code is developed with author's participation and implemented on the Kozloduy 6 full-scope replica control room simulator.

d. A plant-specific reactor core model based on the real-time version of the NEM code is developed with author's participation to meet all the requirements applicable to a simulator for training of nuclear power plant personnel and implemented on the Kozloduy 6 full-scope replica control room simulator.

e. A cycle-specific cross-section update procedure is developed for and implemented on the Kozloduy 6 full-scope replica control room simulator. The procedure is designed to meet specific customer requirements and practices.

f. A cycle-specific two-group macroscopic cross-section library is developed by application of the above said enhanced methodology for use by the participants of the Kalinin 3 Coolant Transient Benchmark.

g. Adaptation of the Kozloduy 6 plant-specific reactor core model based on the real-time version of the NEM code is developed with author's participation for a simulation of the Kalinin 3 Coolant Transient Benchmark problem making use of the above said Kalinin 3 cycle-specific two-group macroscopic cross-section library.

These novel features are demonstrated in through comparison with a steady-state plant specific data from Kozloduy 6 and transient records from Kozloduy 6 and Kalinin 3 as described in Chapter 5 and Chapter 6.

The Kalinin 3 two-group cycle-specific cross-section library have been produced and used by the participants of the Kalinin 3 Coolant Transient Benchmark (Pasichnyk, 2014). The library has been used with PARCS, NESTLE, DYN3D, KIKO-3D and COBAYA (Perin, 2012); (Gonzalez, 2012); (Parisi, 2012); (Hádek, 2012); (Keresztúri, 2013); (Calleja, 2013).

7.2 Recommendations for future work

Today (2016), the Kozloduy 6 full-scope replica control room simulator is still a not so common example of a VVER full-scope simulators equipped with a cycle-specific reactor core model. The core model, in combination with an enhanced thermal-hydraulics, containment and Instrumentation (I&C) models in the scope of Kozloduy 6 full-scope replica control room simulator is a high-fidelity simulation tool, which is extensively used for operator training and various other applications.

The simulation models of the Kozloduy 6 full-scope replica control room simulator or any other training simulator should meet the real-time simulation requirements at first. Expansion of the scope of simulation to a wide range of reference unit conditions corresponds with an augmentation of simulation fidelity requirements.

Special emphasis should be put on the available measured plant data and analysis of the measurements. Introduction of an up-to-date digital data acquisition and control systems to a power plants being prepared for life extension and power uprate provide an opportunity for accumulation of extensive plant history records. Availability of extensive plant data is a necessary condition for reduction of the uncertainty in the models and can provide evidence of phenomena currently unaccounted for.

This work could be continued with improvements of the cross-section generation methodology, as follows.

a. More detailed modelling (reflectors, boundary conditions).
b. More precise discontinuity factors parameterization.
c. Pin power reconstruction parameters parameterization.
d. Techniques for better cross-section representation and reconstruction.

The NEM core model for VVER-1000 simulator application should be enhanced simultaneously in order to present the cross-section generation methodology improvements. The real-time requirement should be accounted at each improvement effort.

8. Bibliography

(Alliston, 1975a) Alliston W., United States Patent 3,919,720, Nuclear Power Plant Training Simulator Modeling Organization and Method, November 11, 1975.

(Alliston, 1975b) Alliston W., Czerniejewski F., Mutafelija B., United States Patent 3,916,444, Training Simulator for Nuclear Power Plant Reactor Monitoring, October 28, 1975.

(Andrushechko, 2010) Anrushechko S., Afrov A., Vassilev B., Generalov V., Kosourov K., Semchenkov Y., Uraintsev V., Nuclear power generating stations with a VVER-1000 reactor : From reactor physics to evolution of the design, Logos, Moscow, Russia, 2010. (Russian language: *Андрушечко С., Афров А., Васильев Б., Генералов В., Косоуров К., Семченков Ю., Украинцев В., АЭС с реактором типа ВВЭР-1000: От физических основ эксплуатации до эволюции проекта, Логос, Москва, Россия, 2010*).

(ANSI/ANS-3.1-2014, 2014) ANSI/ANS-3.1-2014, Selection, Qualification, and Training of Personnel for Nuclear Power Plants, American Nuclear Society, La Grange Park, Illinois, 2014.

(ANSI/ANS-3.5-1985, 1985) ANSI/ANS-3.5-1985, Nuclear Power Plant Simulators for Use in Operator Training, American Nuclear Society, La Grange Park, Illinois, 1985.

(ANSI/ANS-3.5-1993, 1993) ANSI/ANS-3.5-1993, Nuclear Power Plant Simulators for Use in Operator Training, American Nuclear Society, La Grange Park, Illinois, 1993.

(ANSI/ANS-3.5-1998, 1998) ANSI/ANS-3.5-1998, Nuclear Power Plant Simulators for Use in Operator Training and Examination, an American National Standard, American Nuclear Society, La Grange Park, Illinois, 1998.

(ANSI/ANS-3.5-2009, 2009) ANSI/ANS-3.5-2009, Nuclear Power Plant Simulators for Use in Operator Training and Examination, an American National Standard, American Nuclear Society, La Grange Park, Illinois, 2009.

(Core Design Calculations, 2013) BIPR-8 Core Design Calculations of Kalinin NPP, unit 3 – Exposure per Fuel Assembly, NRC Kurchatov Institute, July 2013.

(Bokov, 2012) Bokov P., Botes D., Zimin V., Pseudospectral Chebyshev Representation of Few-Group Cross Sections on Sparse Grids, Advances in Reactor Physics Linking Research, Industry, and Education (PHYSOR 2012), Knoxville, Tennessee, USA, April 15-20, 2012.

(Bokov, 2007) Bokov P., Prinsloo R., Cross-Section Parameterization Using Quasi-Regression Approach, Joint International Topical Meeting on Mathematics & Computation and Supercomputing in Nuclear Applications (M&C + SNA 2007), Monterey, California, April 15-19, 2007.

(Borkowski, 2003) Borkowski J., Belblidia L., Core Model Performance for Training Simulators, Advances in Nuclear Fuel Management III (ANFM 2003), Hilton Head Island, South Carolina, USA, October 5-8, 2003.

(Botes, 2011) Botes D., Bokov P., Hierarchical Multilinear Representation of Few-group Cross Sections on Sparse Grids, International Conference on Mathematics and Computational Methods Applied to Nuclear Science and Engineering (M&C 2011), Rio de Janeiro, Brazil, May 8-12, 2011.

(Calleja, 2013) Calleja M., Jiménez J., Sanchez V., KIT Results for the exercise 2 of Kalinin3 Benchmark, Fifth Workshop of OECD Kalinin-3 Benchmark, Paris, France, 2013.

(Dall'Osso, 2010) Dall'Osso A., Tomatis D., Du Y., Improving Cross Sections via Spectral Rehomogenization, Advances in Reactor Physics to Power the Nuclear Renaissance (PHYSOR 2010), Pittsburgh, Pennsylvania, USA, May 9-14, 2010.

(Duderstadt, 1976) Duderstadt J., Hamilton L., Nuclear Reactor Analysis, John Wiley & Sons, Inc., New York, USA, 1976.

(Dufek, 2011a) Dufek J., Complex Models of Nodal Nuclear Data, International Conference on Mathematics and Computational Methods Applied to Nuclear Science and Engineering (M&C 2011), Rio de Janeiro, RJ, Brazil, May 8-12, 2011.

(Dufek, 2011b) Dufek J., Building the Nodal Nuclear Data Dependences in a Many-Dimensional State-Variable Space, Annals of Nuclear Energy, Volume 38, Issue 7, pp. 1569-1577, July 2011.

(Fujita, 2010) Fujita T., Tada K., Yamamoto A., Yamane Y., Kosaka S., Hirano G., Investigation on Macroscopic Cross Section Model for BWR Pin-by-pin Core Analysis, Advances in Reactor Physics to Power the Nuclear Renaissance (PHYSOR 2010), Pittsburgh, Pennsylvania, USA, May 9-14, 2010.

(Gregg, 1990) Gregg G., Putman R., Gomola J., United States Patent 4,977,529, Training Simulator for a Nuclear Power Plant, December 11, 1990 (*Publication of this patent was postponed 17 years after original application.*).

(Georgieva, 2014) Georgieva E., Dinkov Y., Ivanov K., A Cycle-Specific Cross-Section Update for Real-Time Simulation of VVER-1000 Core, Progress of Nuclear Energy Journal, Volume 74, pp. 222-231, July 2014.

(Georgieva, 2013) Georgieva E., Dinkov Y., A Real-Time Core Model for Kozloduy 6 Full-Scope Replica Control Room Simulator, Proceedings of the 10th International Conference WWER Fuel Performance, Modelling and Experimental Support, pp. 147-153, September 7-14, 2013, Sandanski (Bulgaria).

(Georgieva, 2011) Georgieva E., Borisov E., Mancheva K., Dinkov Y., Nuclear Steam Supply System Physics Upgrade of the Kozloduy 6 Full-Scope Replica Control Room Simulator, Science and Technology Journal of the Bulgarian Nuclear Society, Vol. 16, No 2, pp. 2-9, December 2011, (in Bulgarian);

(Gonzalez, 2012) Gonzalez R., Petruzzi A., D'Auria F., GRNSPG/UNIPI activities on K-3 Benchmark, Forth Workshop of OECD Kalinin-3 Benchmark, Karlsruhe, Germany, 2012.

(Guimarães, 2009) Guimarães P., Müller E., Parameterization of Two-Group Nodal Cross Section Data for POLKA-T BWR Transient Applications, International Conference on Mathematics, Computational Methods & Reactor Physics (M&C 2009). Saratoga Springs, New York May 3-7, 2009.

(Hádek, 2012) Hádek J., ÚJV Řež Solution of the Kalinin-3 Benchmark Exercise 2 and 3, Fifth Workshop of OECD Kalinin-3 Benchmark, Paris, France, 2013.

(HELIOS Methods, 2003) HELIOS Methods, Studsvik Scandpower, November 2003 (proprietary).

(IAEA-TECDOC-443, 1987) IAEA-TECDOC-443, Experience With Simulator Training for Emergency Conditions (Report of a Technical Committee Meeting, Vienna, 15-19 September 1986), International Atomic Energy Agency, Vienna, Austria, 1987.

(IAEA-TECDOC-546, 1990) IAEA-TECDOC-546, Common Modelling Approaches for Training Simulators for Nuclear Power Plants (Final Report of a Co-ordinated Research Programme, January 1985 - November 1988), International Atomic Energy Agency, Vienna, Austria, 1990.

(IAEA-TECDOC-995, 1998) IAEA-TECDOC-995, Selection, Specification, Design and Use of Various Nuclear Power Plant Training Simulators, International Atomic Energy Agency, Vienna, Austria, 1998.

(IAEA-TECDOC-1411, 2004) IAEA-TECDOC-1411, Use of Control Room Simulators for Training of Nuclear Power Plant Personnel, International Atomic Energy Agency, Vienna, 2004.

(IAEA-TECDOC-1500, 2006) IAEA-TECDOC-1500, Guidelines for Upgrade and Modernization of Nuclear Power Plant Training Simulators, International Atomic Energy Agency, Vienna, Austria, 2006.

(IAEA-TECDOC-1502, 2006) IAEA-TECDOC-1502, Authorization of Nuclear Power Plant Control Room Personnel - Methods and Practices with Emphasis on the Use of Simulators, International Atomic Energy Agency, Vienna, Austria, 2006.

(Ivanov, 2002) Ivanov B., Ivanov K., Groudev P., Pavlova M., Hadjiev V., VVER-1000 Coolant Transient Benchmark, Phase 1 (V1000CT-1) Vol. I: Main Coolant Pump (MCP) Switching On – Final Specifications, NEA/NSC/DOC(2002)6, OECD 2002.

(Ivanov, 2006) Ivanov B., Aniel S., Siltanen P., Royer E., Ivanov K., Impact of Cross-Section Generation Procedures on the Simulation of the VVER-1000 Pump Start-up Experiment in the OECD/DOE/CEA V1000CT Benchmark by Coupled 3-D Thermal-Hydraulics / Neutron Kinetics Models, Progress in Nuclear Energy, Vol. 48, Number 8, pp. 746-763, November 2006.

(Ivanov, 2007a) Ivanov B., Methodology for Embedded Transport Core Calculation, Ph. D. Thesis, The Pennsylvania State University, University Park, PA 16802, USA, December 2007.

(Ivanov, 2007b) Ivanov B., Ivanov K., VVER-1000 Coolant Transient Benchmark Phase 1 (V1000CT-1) Vol. 3: Summary Results of Exercise 2 on Coupled 3-D Kinetics / Core Thermal-hydraulics. NEA/NSC/DOC(2007)18, NEA No. 6201, pp. 51-59, OECD 2007.

(Keresztúri, 2013) Keresztúri A., Trosztel I., Elter Zs., Hegyi Gy., Calculation of the OECD NEA Kalinin-3 benchmark (Exercise 2) by the ATHLET-KIKO3D code system, Fifth Workshop of OECD Kalinin-3 Benchmark, Paris, France, 2013.

(Kosaka, 2000) Kosaka S., Saji E., Transport Theory Calculation for a Heterogeneous Multi-Assembly Problem by Characteristics Method with Direct Neutron Path Linking Technique, Journal of Nuclear Science and Technology, Volume 37, No 12, pp. 1015-1023, December 2000.

(Kozloduy 6 TechSpec, 2006) Kozloduy 6 VVER-1000/V-320 Technical Specification, 36.ОБ.00.Р.01/1, Kozloduy NPP, 2006 (confidential, only in Bulgarian).

(Mitin, 2006) Mitin V., Alekseev A., Golovanov M., Zorin A., Kalinushkin A., Kovel A., Milto N., Musikhin A., Tikhonova N., Filatov V., Advanced In-core Monitoring System for High-power Reactors, 16th Symposium of AER on VVER Reactor Physics and Safety, Bratislava, Slovakia, September 25-29, 2006.

(Müller, 2007) Müller E., Mayhue L., Zhang B., Reactor Physics Methods Development at Westinghouse, Proceedings of the International Conference Nuclear Energy for New Europe 2007, Portorož, Slovenia, September 10-13, 2007.

(NEM Input Manual, 2008) NEM Input Manual, Reactor Dynamics and Fuel Management Group (RDFMG), Department of Mechanical & Nuclear Engineering, The Pennsylvania State University, USA, 2008 (proprietary).

(NEM Theory Manual, 2009) NEM Theory Manual, Reactor Dynamics and Fuel Management Group (RDFMG), Department of Mechanical & Nuclear Engineering, The Pennsylvania State University, USA, 2009 (proprietary).

(Operational Event Report, 12 February 2013) Operational Event Report, Closing of a Fast Acting Steam Isolation Valve and Automatic Trip of Main Circulation Pump, Events in Nuclear Facilities, Nuclear Regulatory Agency, Sofia, Bulgaria, 12 February 2013.

(Parisi, 2012) Parisi C., Negrenti E., Sepielli M., ENEA Activities on Kalinin-3 Coupled Code Benchmark, Forth Workshop of OECD Kalinin-3 Benchmark, Karlsruhe, Germany, 2012.

(Pasichnyk, 2014) Pasichnyk I., Vlekov K., Final results for Kalinin-3 Exercise 3, AER Group D Meeting, Garching, Germany, 2014.

(Perin, 2012) Perin Y., OECD Kalinin-3 Benchmark: Neutronic Calculations of Exercises 3a and 3b with PARCS, Forth Workshop of OECD Kalinin-3 Benchmark, Karlsruhe, Germany, 2012.

(REL-786-DD-001-02, 2012) REL-786-DD-001-02, Design Documents, Part No. 1: Cross Sections, Revision 2, Kozloduy 6 Full-Scope Replica Control Room Simulator Enhancement with High-Fidelity Two-Phase Thermal Hydraulics and Core Model. Risk Engineering Ltd., Sofia, 2012 (confidential, only in Bulgarian).

(REL-786-DD-002-02, 2012) REL-786-DD-002-02, Design Documents, Part No. 2: Core Model, Revision 2, Kozloduy 6 Full-Scope Replica Control Room Simulator Enhancement with High-

Fidelity Two-Phase Thermal Hydraulics and Core Model. Risk Engineering Ltd., Sofia, 2012 (confidential, only in Bulgarian).

(REL-786-DD-003-01, 2012) REL-786-DD-003-01, Design Documents, Part No. 3: TH Model, Revision 1, Kozloduy 6 Full-Scope Replica Control Room Simulator Enhancement with High-Fidelity Two-Phase Thermal Hydraulics and Core Model. Risk Engineering Ltd., Sofia, 2012 (confidential, only in Bulgarian).

(REL-786-PP-003-00, 2012) REL-786-PP-003-00, Cycle-Specific Cross-Section Update Procedure, Kozloduy 6 Full-Scope Replica Control Room Simulator Enhancement with High-Fidelity Two-Phase Thermal Hydraulics and Core Model. Risk Engineering Ltd., Sofia, 2012 (confidential, only in Bulgarian).

(RELAP5-HD™ Verification Report, 2011) RELAP5-HD™ Verification Report for Real-Time Simulators, GSE Systems, Inc., Sykesville, Maryland 21784, USA, 2011 (proprietary).

(Romas, 2013) Romas A., Modern Simulator – The Optimal Tool for Training, Safety Analysis and Design Verification, 2013 Power Plant Simulation Conference (PowerPlantSim'13), Tampa, FL, USA, January 28 - February 1, 2013.

(Sato, 2010) Sato D., Tsubota S., Yamaji K., Koike H., Matsumoto H., A New Robust Cross Section Representation Methodology for PWR Core Simulator, Advances in Reactor Physics to Power the Nuclear Renaissance (PHYSOR 2010), Pittsburgh, Pennsylvania, USA, May 9-14, 2010.

(Smith, 1986) Smith K., Assembly Homogenization Techniques for Light Water Reactor Analysis, Progress in Nuclear Energy, Volume 17, Issue 3, pp. 303-335, 1986.

(Tereshonok, 2008) Tereshonok V., Stepanov V., Ivchenkov V., Pitilimov V., Nikonov S., Description of a Transient Caused by the Switching-off of One of the Four Operating MCP at Nominal Reactor Power at NPP Kalinin Unit 3, NEA/NSC/DOC(2009)6, OECD 2008.

(Tereshonok, 2009) Tereshonok, V., Nikonov, S., Lizorkin, M., Velkov, K., Pautz, A., Ivanov K. Kalinin-3 Coolant Transient Benchmark – Swiching-off of One of the Four Operating Main Circulation Pumps at Nominal Reactor Power, Specification, First Edition 2008, NEA/NSC/DOC(2009)5, OECD 2009.

(Troyanovsky, 1985) Troyanovsky B., Filipov F., Bulkin A., Steam and gas turbines for nuclear power generating stations, Energoatomizdat, Moscow, USSR, 1985. (Russian language:

Трояновский Б., Филиппов Г., Булкин А., Паровые и газовые турбины атомных электростанций, Энергоатомиздат, Москва, СССР, 1985).

(Watson, 2002) Watson J., Ivanov K., Improved Cross-section Modeling Methodology for Coupled Three-dimensional Transient Simulations, Annals of Nuclear Energy, Volume 29, Issue 8, pp. 937-966, May 2002.

(Yastebenetsky, 2014) Yastebenetsky M., Kharchenko V., Nuclear Power Plant Instrumentation and Control Systems Safety and Security, IGI Global, 2014.

(Zimin, 2005) Zimin V. and Semenov A., Building Neutron Cross-Section Dependencies for Few-Group Reactor Calculations Using Step-Wise Regression, Annals of Nuclear Energy, Volume 32, Issue 1, pp. 119-136, January 2005.

Appendix A. Definitions

Best-estimate	Predicted reference unit performance data derived from engineering evaluation or operational assessment by subject matter experts for specific conditions (ANSI/ANS-3.5-2009, 2009).
Computed values	Parameters representing the state of reference unit systems or components that the simulator mathematical models calculate (ANSI/ANS-3.5-2009, 2009).
Design database	The design documents, performance data, records, assumptions, simplifications, derivations, and other definable data that form the basis of the design of the simulator hardware and software (ANSI/ANS-3.5-2009, 2009).
Full-scope simulator	A simulator incorporating replica operating consoles and panels and detailed modelling of those systems of the reference plant with which the operator interfaces in the actual control room environment (IAEA-TECDOC-1500, 2006).
Initial condition	A set of data that represents the status of the reference unit from which real time simulation can begin (ANSI/ANS-3.5-2009, 2009).
Performance testing	Testing conducted to verify a simulator's performance as compared to actual or predicted reference unit performance (ANSI/ANS-3.5-2009, 2009).
Real-time	Simulation of dynamic performance in the same time base relationships, sequences, durations, rates, and accelerations as the dynamic performance of the reference unit (ANSI/ANS-3.5-2009, 2009).
Reference unit	The specific nuclear power plant unit, identified by a unique docket number, from which the simulator control room configuration, system control arrangement, and simulator design database, are derived (IAEA-TECDOC-1500, 2006).

Reference plant	A specific nuclear power plant from which the simulator control room configuration, system control arrangement, and dynamic operating characteristics are derived (ANSI/ANS-3.5-2009, 2009).
Scenario	Any set of simulator operations performed in accordance with a lesson plan or guide for the purpose of familiarization, training, or examination of operators (ANSI/ANS-3.5-2009, 2009). A series of simulator operations or functions implemented in accordance with a lesson plan or guide for the purpose of familiarization, training, or examination of control room operators (IAEA-TECDOC-1500, 2006).
Simulation	Implementation of a reference plant system or subsystem by using modelling techniques in the simulator development environment. Simulated system performance and fidelity meets defined functional and operating limits based upon reference plant design and operational data (IAEA-TECDOC-1500, 2006).
Stimulation	Implementation of a reference plant system or subsystem using the actual hardware and software installed in the reference plant. Stimulated systems should either have built in support for simulator operational modes or these capabilities should be added by a software control layer as part of the implementation (IAEA-TECDOC-1500, 2006).
Stimulated components	Hardware software components that are integrated with the simulator process via simulator inputs/outputs that perform their functions parallel to, and either independently of or synchronized with, the simulation process (ANSI/ANS-3.5-2009, 2009).

REFERENCES

(ANSI/ANS-3.5-2009, 2009) ANSI/ANS-3.5-2009, Nuclear Power Plant Simulators for Use in Operator Training and Examination, an American National Standard, American Nuclear Society, La Grange Park, Illinois, 2009.

(IAEA-TECDOC-1500, 2006) IAEA-TECDOC-1500, Guidelines for Upgrade and Modernization of Nuclear Power Plant Training Simulators, International Atomic Energy Agency, Vienna, Austria, 2006.

Appendix B. VVER-1000/V320 general description

Russian-style Pressurized Water Reactor VVER-1000/V320 is the 'series' type VVER-1000. The first V320-type unit is commissioned in 1984 (Zaporozhye 1, Ukraine), only 4 years after the prototype VVER-1000 unit, Novovoronezh 5 (STI/PUB/1752, 2016).

Reactor thermal power is 3000 MW and generator power is 1000 MW (e).

The recent book (Andrushechko, 2010) can be used as a handy reference work for general information concerning nuclear power plants with reactors of VVER-1000/V320 series.

Reactor Core

VVER fuel consists of sintered Uranium Dioxide pellets. The fuel pin outer diameter (9.1 mm) is smaller in comparison with common PWR (9.5 mm). Fuel pins are arranged in a triangle lattice with a pitch of 12.75 mm. Thus fuel-to-water volume ratio (about 0.574) is slightly different in comparison with PWR's.

Fuel pins are arranged in a hexagonal fuel assembly without shroud. The assembly pitch (axis-to-axis distance between two fuel assemblies) is 23.6 cm. The fuel assembly contains 312 fuel pins, 18 guide tubes for absorber rods and a central instrument tube.

There are 163 fuel assemblies in the VVER-1000/V320 core. Active height of the core is 3.55 m (hot) and the effective diameter is 3.16 m. Height-to-diameter ratio is higher than optimal from neutronics point of view. Such a proportion is caused by a requirement for railway transport of reactor components.

Absorber elements of are arranged in a cluster of 18. The use of half-length absorber elements was discontinued during mid-1990s and now there is only one type of absorber element used in a VVER-1000/V320 core. 61 control rod drives are positioned on the rector pressure vessel head and perform both reactor power control and SCRAM functions.

Reactor Pressure Vessel

The rector pressure vessel is designed with larger height and smaller diameter in comparison with PWR vessel. Inlet and outlet nozzles are of equal diameter and staggered vertically. These nozzles are symmetrically arranged around the vessel and connect the vessel to the hot and cold leg of the primary coolant loop. Vessel upper head is removable. The vessel bottom is with ellipsoidal shape.

Steam Generators

Horizontal steam generators are typical for all the VVER designs. The horizontal tube bundle of a PGV-1000M steam generator consists of 11 000 steel tubes with an outer diameter of 16 mm (specific coolant mass flow rate of 3 120 $kg \cdot m^{-2} \cdot s^{-1}$).

Nuclear Steam Supply System Main Parameters

The primary pressure is 15.7 MPa. The coolant temperature at rated power of 3000 MW (thermal) is 286 ºC at the inlet and 316 ºC at the outlet of the reactor vessel. Average loop coolant flow rate is 21 350 $m^3 s^{-1}$. For comparison 4-loops Westinghouse PWRs inlet and outlet temperatures are 292.4 ºC and 323.4 ºC and the total coolant mass flow rate is 19 114 $kg \cdot s^{-1}$ (Meyer, 1997).

Steam generator secondary pressure is 6.27 MPa. Steam generators produce saturated steam (steam quality above 99.8 %).

VVER-1000/V320 nuclear steam supply system is designed to operate at constant secondary pressure while typical PWR operates at constant core-average coolant temperature. This causes significant variation of core-average coolant temperature as a function of reactor power. Pressurizer with a volume of 80 m^3 is necessary to absorb changes in coolant density.

Power Conversion System

All the VVER-1000/V320 units are equipped with a single turbo-generator. Various units employ both half speed (1500 rpm, 4-cylinders) or full-speed (3000 rpm, 5-cylinder) turbine sets with a moisture-separator and steam reheat after high-pressure turbine.

Plant Automation

As commissioned, V320 units employed comprehensive plant automation system based on a family of standard cabinets, signal interfaces and integrated circuit boards (the UKTS/KASKAD system). There are multiple types of analogue integrated circuit boards in the family supporting all the variety of plant interlocks, relay circuitry, proportional–integral controllers and control room instrument interfaces.

Another first in V320 units is the use of a digital turbine control system, ASUT-1000. The in-core monitoring system is based on digital computers, too. A digital plant process computer is an integral part of the V320 main control room design.

Throughout service life, V320 units are upgraded and there are now many variations in plant process control and monitoring systems employed.

REFERENCES

(Andrushechko, 2010) Anrushechko S., Afrov A., Vassilev B., Generalov V., Kosourov K., Semchenkov Y., Uraintsev V., Nuclear power generating stations with a VVER-1000 reactor : From reactor physics to evolution of the design, Logos, Moscow, Russia, 2010. (Russian language book: *Андрушечко С., Афров А., Васильев Б., Генералов В., Косоуров К., Семченков Ю., Украинцев В., АЭС с реактором типа ВВЭР-1000: От физических основ эксплуатации до эволюции проекта, Логос, Москва, Россия, 2010*).

(Meyer, 1997) Meyer G., Stokke E., Description of Sizewell B Nuclear Power Plant, Institute for Energy Technology (IFE), OECD Halden Reactor Project, Halden, Norway, 1997.

(STI/PUB/1752, 2016) STI/PUB/1752, Operating Experience with Nuclear Power Stations in Member States (2016 Edition), International Atomic Energy Agency, Vienna, Austria, 2016.

Appendix C. Kozloduy 6 geometry and material composition

There are five different 'alternative' fuel assembly (TVSA) types in the libraries used for Kozloduy 6 simulations presented in this work (Table C-1, Figure C-1).

- Radially-profiled alternative fuel assembly, average enrichment 3.53 % ^{235}U, 6 Gadolinium fuel pins in the inner part of the assembly near 60° degree lines, pellet central hole of 0.14 cm.
- Alternative fuel assembly, average enrichment 3.98 % ^{235}U, 6 Gadolinium fuel pins in the inner part of the assembly near 60° degree lines, pellet central hole of 0.15 cm.
- Alternative fuel assembly, average enrichment 3.98 % ^{235}U, 6 Gadolinium fuel pins in the inner part of the assembly near 60° degree lines, pellet central hole of 0.14 cm.
- Radially-profiled alternative fuel assembly, average enrichment 4.3 % ^{235}U, 6 Gadolinium fuel pins in the inner part of the assembly near 60° degree lines, pellet central hole of 0.15 cm.
- Radially-profiled alternative fuel assembly, average enrichment 4.3 % ^{235}U, 6 Gadolinium fuel pins in the inner part of the assembly near 60° degree lines, pellet central hole of 0.14 cm.

Gadolinium is used as a burnable absorber in the form of Gadolinium Oxide (Gd_2O_3) mixed with Uranium Oxide (UO_2) in three of the 'alternative' fuel assembly types. The content of Gadolinium Oxide in fuel pellets is 5% mass.

Fuel assembly types present in the reactor core are distinguished by a variation in fuel pellet composition (fuel enrichment, burnable poison, etc.) and pellet geometry. The absorber rod contains Dysprosium-Titanium and Boron Carbide parts. Each fuel assembly type is represented as a single fuel assembly in an infinite lattice physics HELIOS calculation. All data of the fuel assemblies needed for modelling purposes is summarized in Table C-2, (Andrushechko, 2010), (Kamenov, 2011), (Naev, 2011).

Two HELIOS main input models in 60° per fuel assembly type are developed: one handling an alternative fuel assembly (Zr-alloy components) without control rods and second for an alternative fuel assembly with control rods inserted.

The specific models of fuel assembly without control rods are as follows.

- Radially-profiled alternative fuel assembly with 6 Gadolinium fuel pins in the inner part of the assembly near 60° degree lines (Figure C-2).
- Alternative fuel assembly with 6 Gadolinium fuel pins in the inner part of the assembly near 60° degree lines (Figure C-3).

Two separate sets are necessary for fuel assemblies with control rods with Boron Carbide or Dysprosium-Titanium absorber rod inserted. The specific models of fuel assembly with control rods are as follows.

- Alternative fuel assembly with 6 Gadolinium fuel pins in the inner part of the assembly near 60° degree lines (Figure C-4).
- Radially-profiled alternative fuel assembly with 6 Gadolinium fuel pins in the inner part of the assembly near 60° degree lines (Figure C-5).

Three reflector models are used: bottom, top and radial (Figure C-6, Figure C-7 and Figure C-8, respectively). Different material compositions, as used in reflector models, are presented in Table C-3, Table C-4 and Table C-5. Material compositions are assumed as mixtures of coolant (water), void, Zirconium alloy and stainless steel 08X18N10T of the reactor baffle and barrel. The hexagonal geometry of VVER-1000 reactor baffle and barrel is reduced to Cartesian geometry

Table C-1: Kozloduy 6 fuel assembly types

Enrichment ^{235}U, wt%	**Central Hole cm**	**Fuel Pin**				**Gadolinium Fuel Pin**		
		Type 1		**Type 2**				
		No.	**^{235}U, wt%**	**No.**	**^{235}U, wt%**	**No.**	**Gd_2O_3, wt%**	**^{235}U, wt%**
3.53	0.14	240	3.6	66	3.3	6	5.0	3.3
3.98	0.15	306	4.4	-	-	6	5.0	3.6
3.98	0.14	306	4.4	-	-	6	5.0	3.6
4.3	0.15	240	4.4	66	4.0	6	5.0	3.6
4.3	0.14	240	4.4	66	4.0	6	5.0	3.6

Table C-2: Kozloduy 6 geometry and material composition data — fuel assemblies

Fuel Pins*	
Fuel pins, number	312
Gadolinium fuel pins, number	6
Fuel pins, lattice	Triangular
Fuel pin pitch, cm	1.275
Cladding, material	Zr-alloy Э110
Cladding, outer diameter, cm	0.91
Cladding, inner diameter, cm	0.773
Pellet, outer diameter, cm	0.757
Pellet, central hole, cm	0.15 / 0.14
Pellet, material	UO_2
Gadolinium pellet, central hole, cm	0.14
Gadolinium pellet, material	$UO_2 + Gd_2O_3$
Gadolinium oxide in fuel pellets, wt%	5.0
Fuel density, g/cm^3	10.4 ÷ 10.7
Stiffeners (angles)	
Number	6
Material	Zr-alloy Э635
Width, cm	5.2
Thickness, cm	0.065
Guide Tubes	
Number	18
Material	Zr-alloy Э635
Outer diameter, cm	1.26
Inner diameter, cm	1.09
Spacer Grids	
Number	15
Material	Zr-alloy Э110
Mass, kg	0.55
Central Water / Instrument Tube	
Number	1
Material	Zr-alloy Э635
Outer diameter, cm	1.3
Inner diameter, cm	1.1

* *Material composition is the same for all the pellets in a fuel pin.*

Table C-3: Kozloduy 6 geometry and material composition data — bottom reflector

Layer	Thickness, mm	Total, mm	Composition
1	23	23	7.0 % 08X18N10T, 58.0 % Water, 35.0 % Zirconium
2	12	35	33.0 % 08X18N10T, 57.0 % Water, 10.0 % Zirconium
3	201	236	33.0 % 08X18N10T, 67.0 % Water, 0.0 % Zirconium

Table C-4: Kozloduy 6 geometry and material composition data — radial reflector

Layer	Thickness, mm	Total, mm	Composition
1	160	160	65.04 % 08X18N10T, 34.96 % Water
2	2.5	162.5	Water
3	65	227.5	08X18N10T
4	8.5	236	Water

Table C-5: Kozloduy 6 geometry and material composition data — top reflector

Layer	Thickness, mm	Total, mm	Composition
1	20	20	10.3386 % 08X18N10T, 47.8021 % Water, 12.689 % Zirconium, 29.1703 % Void
2	195	215	1.1067 % 08X18N10T, 57.034 % Water, 12.689 % Zirconium, 29.1703 % Void
3	15	230	10.3386 % 08X18N10T, 47.8021 % Water, 12.689 % Zirconium, 29.1703 % Void
4	6	236	1.1067 % 08X18N10T, 57.034 % Water, 12.689 % Zirconium, 29.1703 % Void

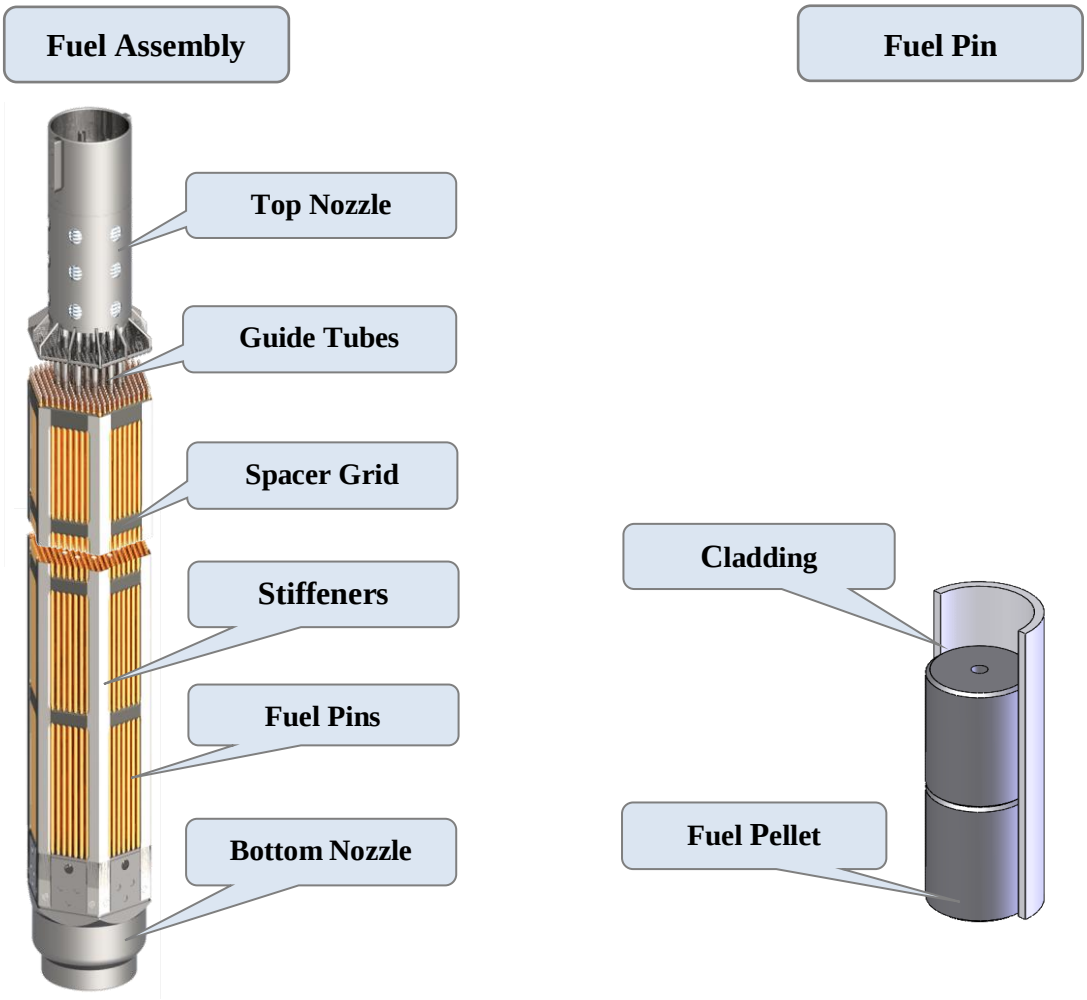

Figure C-1: Three-dimensional scheme of the TVSA type fuel assembly and fuel pin (Kamenov, 2011)

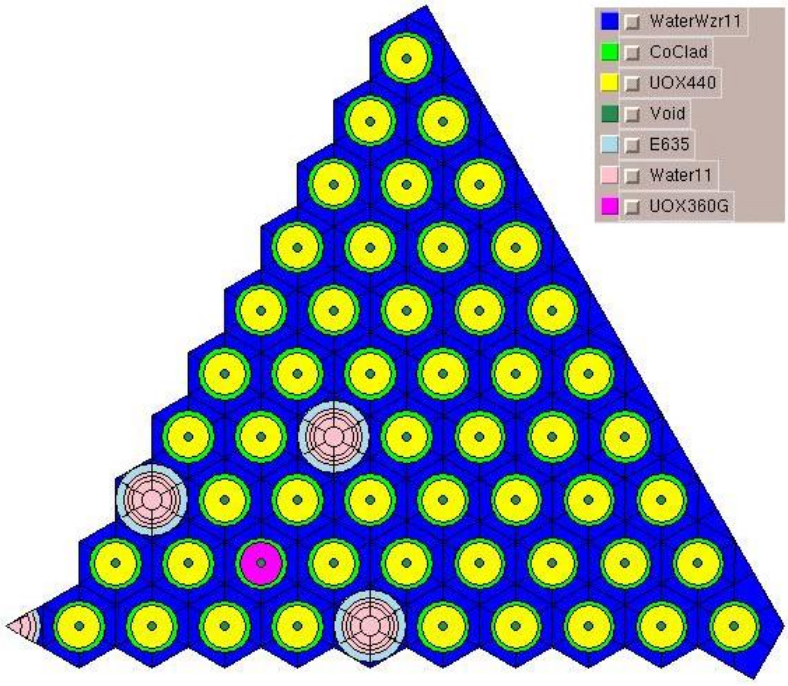

Figure C-2: TVSA model (one-sixth) with 6 Gadolinium fuel pins
(WaterWzr11 — Water; CoClad — Zr-alloy Э110; UOX440 — UO_2; Void —Void; E635 — Zr-alloy Э635; Water11 — Water; UOX360G — UO_2+Gd_2O_3)

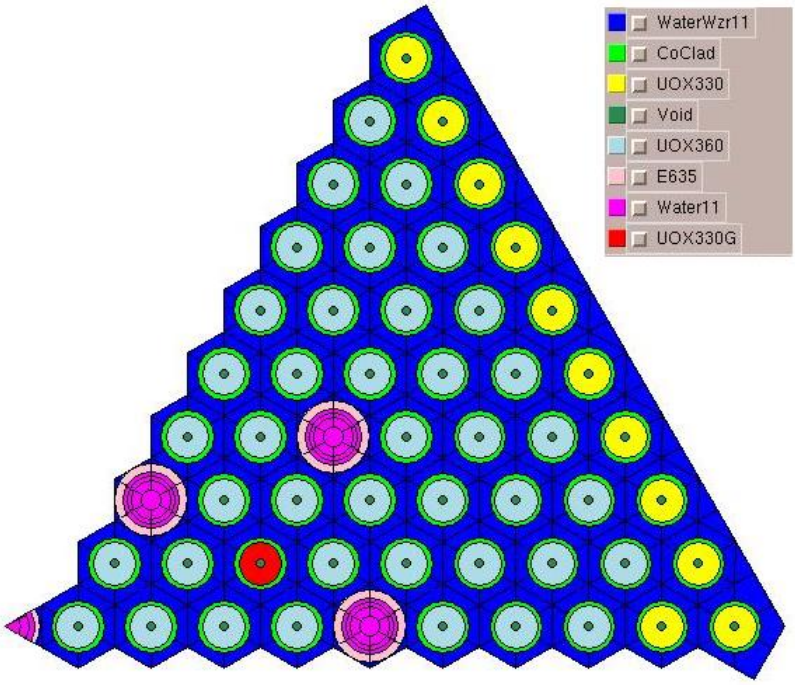

Figure C-3: Radially-profiled TVSA model (one-sixth) with 6 Gadolinium fuel pins
(WaterWzr11 — Water; CoClad — Zr-alloy Э110; UOX330 — UO_2; Void —Void; UOX360 — UO2; E635 — Zr-alloy Э635; Water11 — Water; UOX330G — UO_2+Gd_2O_3)

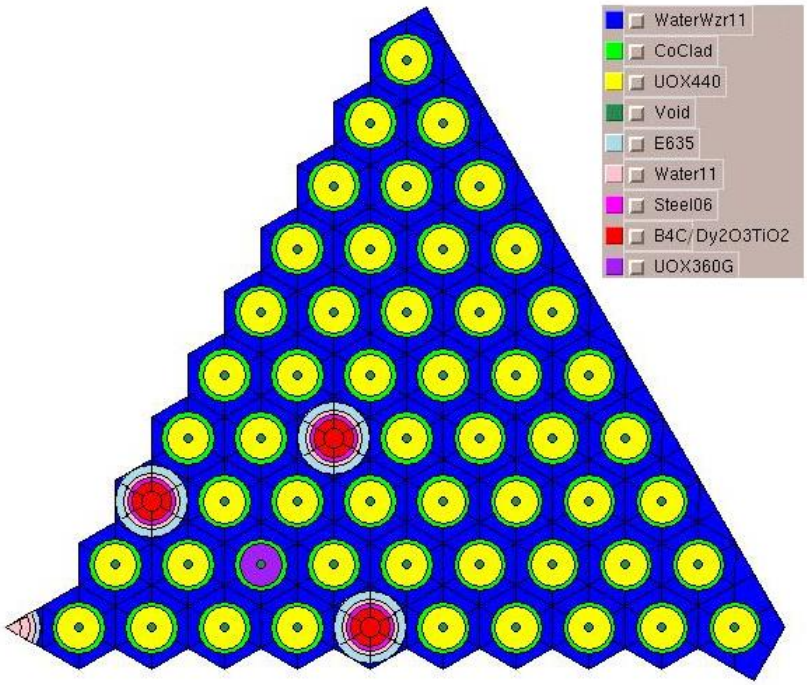

Figure C-4: TVSA model (one-sixth) with 6 Gadolinium fuel pins — rodded (WaterWzr11 — Water; CoClad — Zr-alloy Э110; UOX440 — UO_2; Void —Void; E635 — Zr-alloy Э635; Water11 — Water; Steel06 — 06X18H10T; $B_4C/Dy_2O_3{\bullet}TiO_2$ — B_4C or $Dy_2O_3{\bullet}TiO_2$; UOX360G — $UO_2+Gd_2O_3$)

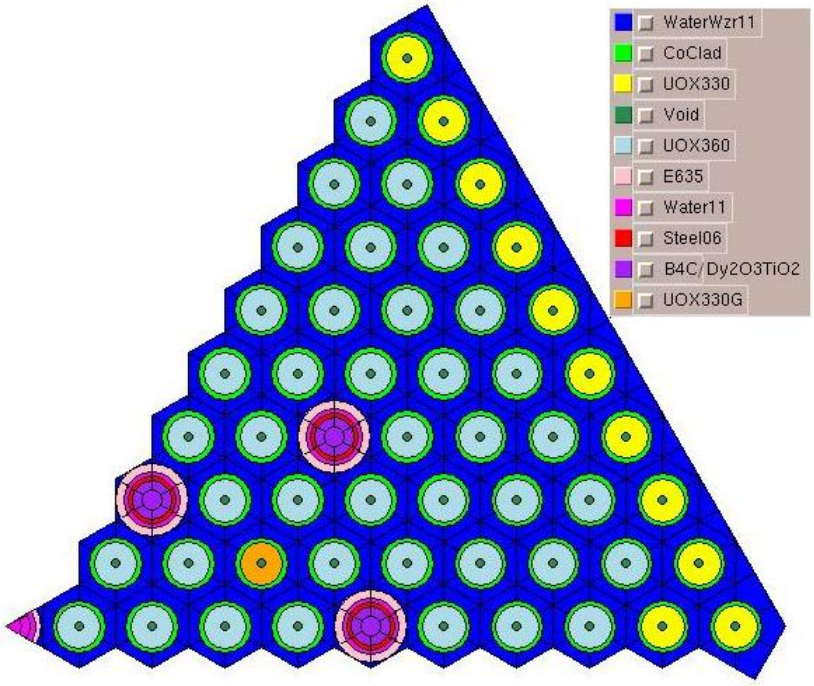

Figure C-5: Radially-profiled TVSA model (one-sixth) with 6 Gadolinium fuel pins — rodded (WaterWzr11 — Water; CoClad — Zr-alloy Э110; UOX330 — UO_2; Void —Void; E635 — Zr-alloy Э635; UOX360 — UO_2; Water11 — Water; Steel06 — 06X18H10T; $B_4C/Dy_2O_3{\bullet}TiO_2$ — B_4C or $Dy_2O_3{\bullet}TiO_2$; UOX330G — $UO_2+Gd_2O_3$)

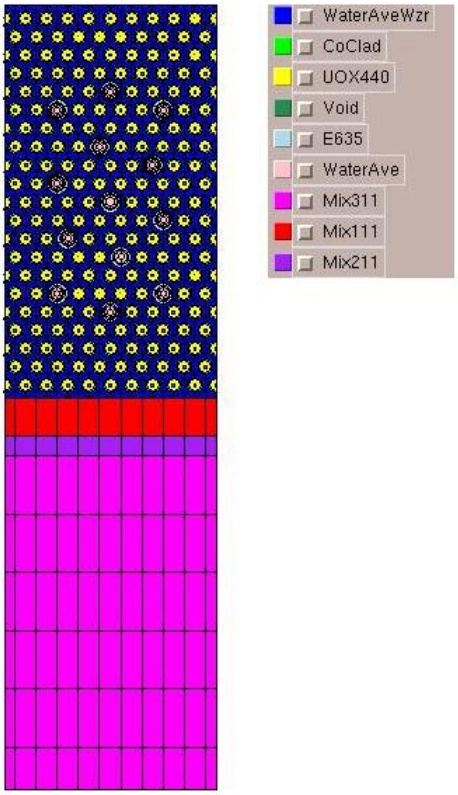

Figure C-6: Bottom reflector model
(WaterAveWzr — Water; CoClad — Zr-alloy Э110; UOX440 — UO2; Void —Void; E635 — Zr-alloy Э635; Water11 — Water; Mix311 — 33.0 % 08X18N10T, 67.0 % Water; Mix111 — 7.0 % 08X18N10T, 58.0 % Water, 35.0 % Zr; Mix211 — 33.0 % 08X18N10T, 57.0 % Water, 10.0 % Zr)

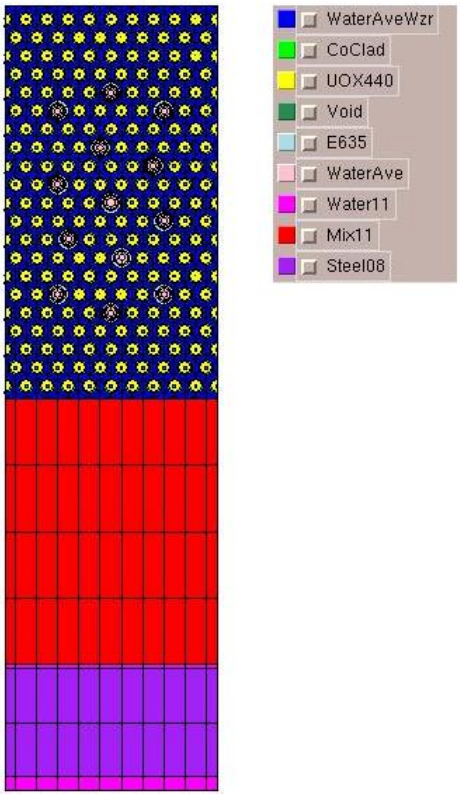

Figure C-7: Radial reflector model
(WaterAveWzr — Water; CoClad — Zr-alloy Э110; UOX440 — UO2; Void —Void; E635 — Zr-alloy Э635; WaterAve — Water; Water11 — Water; Mix11 — 65.04 % 08X18N10T, 34.96 % Water; Steel08 — 08X18N10T)

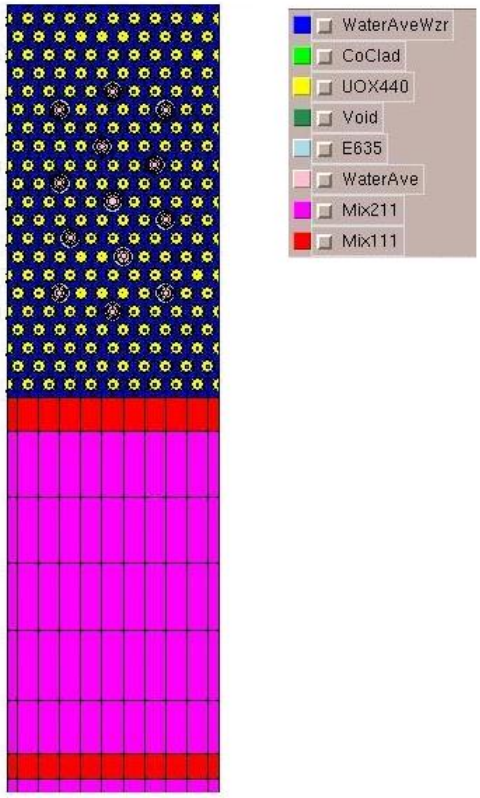

Figure C-8: Top reflector model
(WaterAveWzr — Water; CoClad — Zr-alloy Э110; UOX440 — UO2; Void —Void; E635 — Zr-alloy Э635; WaterAve — Water; Water11 — Water; Mix211 — 1.1067 % 08X18N10T, 57.034 % Water, 12.689 % Zr, 29.1703 % Void; Mix111 —10.3386 % 08X18N10T, 47.8021 % Water, 12.689 % Zr, 29.1703 % Void)

REFERENCES

(Andrushechko, 2010) Anrushechko S., Afrov A., Vassilev B., Generalov V., Kosourov K., Semchenkov Y., Uraintsev V., Nuclear power generating stations with a VVER-1000 reactor : From reactor physics to evolution of the design, Logos, Moscow, Russia, 2010. (from Russian: *Андрушечко С., Афров А., Васильев Б., Генералов В., Косоуров К., Семченков Ю., Украинцев В., АЭС с реактором типа ВВЭР-1000: От физических основ эксплуатации до эволюции проекта, Логос, Москва, Россия, 2010*).

(Kamenov, 2011), Kamenov K., Kamenov A., Hristov D., Experience of TVSA Implementation at Kozloduy NPP, Proceedings of the 9th International Conference WWER Fuel Performance, Modelling and Experimental Support, pp. 51 – 63, Helena Resort, Bulgaria, September 17 - 24, 2011.

(Naev, 2011), Naev I., Tomov A., Activities Promoting The Achievement of High Nuclear Fuel Performance Indicators, Proceedings of the 9th International Conference WWER Fuel Performance, Modelling and Experimental Support, pp. 68 – 73, Helena Resort, Bulgaria, September 17 - 24, 2011.

Appendix D. Kalinin 3 geometry and material composition

There are five different 'alternative' fuel assembly (TVSA) types and one 'standard' fuel assembly (TVS-M) type used, Table D-1 (Tereshonok, 2009).

- Alternative fuel assembly, enrichment 1.3 % ^{235}U.
- Alternative fuel assembly, enrichment 2.2 % ^{235}U.
- Alternative fuel assembly, average enrichment 2.98 % ^{235}U with 9 Gadolinium fuel pins in the inner part of the assembly.
- Radially-profiled alternative fuel assembly, average enrichment 3.9 % ^{235}U with 9 Gadolinium fuel pins in assembly periphery.
- Radially-profiled alternative fuel assembly, average enrichment 3.9 % ^{235}U with 6 Gadolinium fuel pins in assembly periphery near 60° degree lines.
- Standard fuel assembly, enrichment 1.6 % ^{235}U.

Gadolinium is used as a burnable absorber in the form of Gadolinium Oxide (Gd_2O_3) mixed with Uranium Oxide (UO_2) in three of the 'alternative' fuel assembly types. The content of Gadolinium Oxide in fuel pellets is 5% mass.

Fuel assembly types present in the reactor core are distinguished by a variation in fuel pellet composition (fuel enrichment, burnable poison, etc.) and material composition of structural components (Zr-alloy or stainless steel). The absorber rod contains Dysprosium-Titanium and Boron Carbide parts. Each fuel assembly type is represented as a single fuel assembly in an infinite lattice physics HELIOS calculation. All data of the fuel assemblies needed for modelling purposes is summarized in Table D-2. These data are not available in the benchmark specification so they are collected from other sources, (Andrushechko, 2010), (Lavrenyuk, 2008), (Molchanov, 2009), (Molchanov, 2007), (Molchanov, 2005), (Molchanov, 2003), (Samoilov, 2013). Material compositions of Zr-alloy or stainless steel used could be found in the reference books. Presence of isotopes of Hf, Nb, Zr, Fe, Sn etc. is important for evaluation of cross sections.

Four HELIOS main input models in 60° per fuel assembly type are developed: one handling an alternative fuel assembly (Zr-alloy components) without control rods; second for an alternative fuel assembly with control rods inserted; third for a standard fuel assembly (stainless steel components); and forth for a standard fuel assembly with control rods inserted.

Two HELIOS main input models in 120° symmetry per fuel assembly type are developed: one handling an alternative fuel assembly (9 Gadolinium fuel pins) without control rods; second for an alternative fuel assembly (9 Gadolinium fuel pins) with absorber rods inserted.

The specific models of fuel assembly without control rods are as follows.

- Alternative fuel assembly, enrichment 1.3 % ^{235}U (Figure D-1).
- Alternative fuel assembly, enrichment 2.2 % ^{235}U (Figure D-1).
- Radially-profiled alternative fuel assembly, average enriched 3.9 % ^{235}U with 6 Gadolinium fuel pins in assembly periphery (Figure D-2).
- Alternative fuel assembly, average enrichment 2.98 % ^{235}U with 9 Gadolinium fuel pins in inner part of the assembly (Figure D-3).
- Radially-profiled alternative fuel assembly, average enrichment 3.9 % ^{235}U with 9 Gadolinium fuel pins in assembly periphery (Figure D-4).
- Standard fuel assembly, enrichment 1.6 % ^{235}U (Figure D-5), stainless steel components.

Two separate sets are necessary for fuel assemblies with control rods with Boron Carbide or Dysprosium-Titanium absorber rod inserted. The specific models of fuel assembly with control rods are as follows.

- Alternative fuel assembly, enrichment 1.3 % ^{235}U (Figure D-6).
- Alternative fuel assembly, enrichment 2.2 % ^{235}U (Figure D-6).
- Alternative fuel assembly, average enrichment 2.98 % ^{235}U with 9 Gadolinium fuel pins in the inner part of the assembly (Figure D-7).
- Standard fuel assembly, enrichment 1.6 % ^{235}U (Figure D-8).

The reflector models (bottom, top and radial) are the same as used for Kozloduy 6 cases (Appendix A).

Table D-1: Kalinin 3 fuel assembly types

Enrichment ^{235}U, wt%	Comp.	Fuel Pin				Gadolinium Fuel Pin		
		Type 1		Type 2				
		No.	^{235}U, wt%	No.	^{235}U, wt%	No.	Gd_2O_3, wt%	^{235}U, wt%
1.3	Zr-alloy	312	1.3	-	-	-	-	-
1.6	Steel	312	1.6	-	-	-	-	-
2.2	Zr-alloy	312	4.4	-	-	-	-	-
2.98	Zr-alloy	303	3.0	-	-	9	5.0	2.4
3.9	Zr-alloy	240	4.0	66	3.6	6	5.0	3.3
3.9	Zr-alloy	243	4.0	60	3.6	9	5.0	3.3

Table D-2: Kalinin 3 geometry and material composition data — fuel assemblies

	TVSA	TVS-M
Fuel Pins*		
Fuel pins, number	312	312
Gadolinium fuel pins, number	-/6/9	-
Fuel pins, lattice	Triangular	Triangular
Fuel pin pitch, cm	1.275	1.275
Cladding, material	Zr-alloy Э110	Zr+1% Nb
Cladding, outer diameter, cm	0.91	0.91
Cladding, inner diameter, cm	0.773	0.773
Pellet, outer diameter, cm	0.757	0.757
Pellet, central hole, cm	0.15	0.235
Pellet, material	UO_2	UO_2
Gadolinium pellet, material	$UO_2 + Gd_2O_3$	-
Gadolinium oxide in fuel pellets, wt%	5.0	-
Fuel density, g/cm^3	10.4 ÷ 10.7	10.4 ÷ 10.7
Stiffeners (angles)		
Number	6	-
Material	Zr-alloy Э635	-
Width, cm	5.2	-
Thickness, cm	0.065	-
Guide Tubes		
Number	18	18
Material	Zr-alloy Э635	08X18H10T
Outer Diameter, cm	1.26	1.26
Inner Diameter, cm	1.09	1.10
Spacer Grids		
Number	15	15
Material	Zr-alloy Э110	08X18H10T
Mass, kg	0.55	0.55
Central Water / Instrument Tube		
Number	1	1
Material	Zr-alloy Э635	Zr+1% Nb
Outer Diameter, cm	1.3	1.12
Inner Diameter, cm	1.1	0.96

* *Material composition is the same for all the pellets in a fuel pin.*

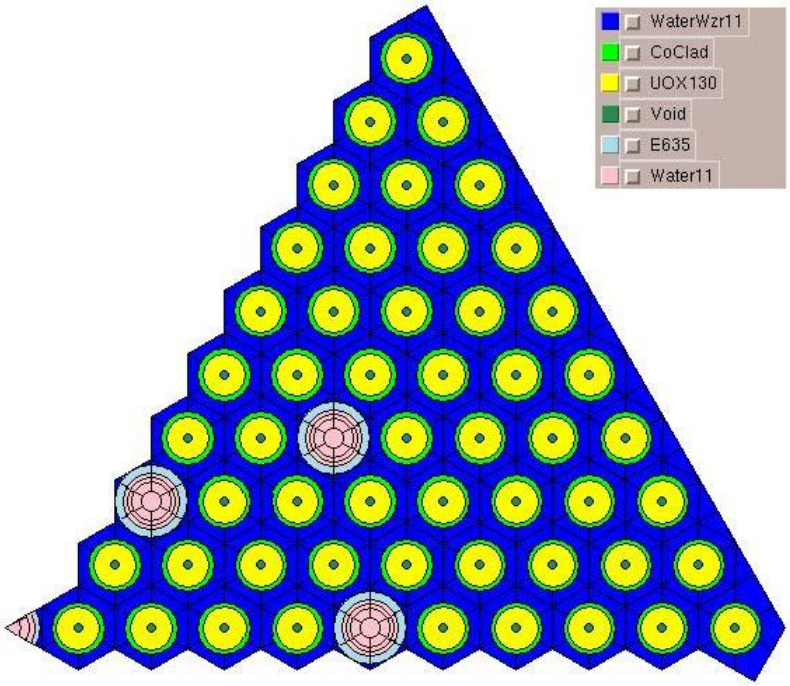

Figure D-1: TVSA model (one-sixth) without Gadolinium fuel pins
(WaterWzr11 — Water; CoClad — Zr-alloy Э110; UOX130 — UO_2; Void —Void; E635 — Zr-alloy Э635; Water11 — Water)

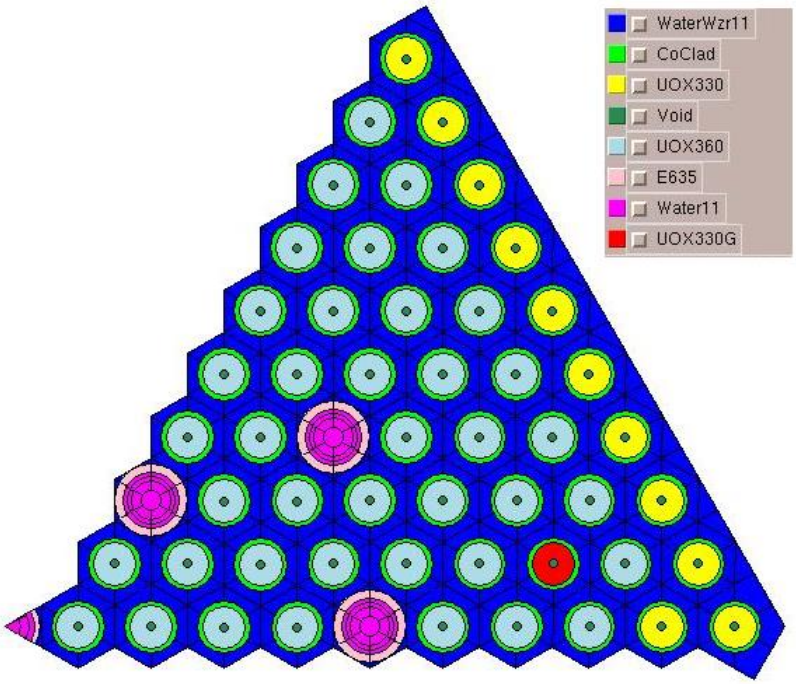

Figure D-2: Radially-profiled TVSA model (one-sixth) with 6 Gadolinium fuel pins
(WaterWzr11 — Water; CoClad — Zr-alloy Э110; UOX330 — UO_2; Void —Void; UOX360 — UO_2; E635 — Zr-alloy Э635; Water11 — Water; UOX330G — UO_2+Gd_2O_3)

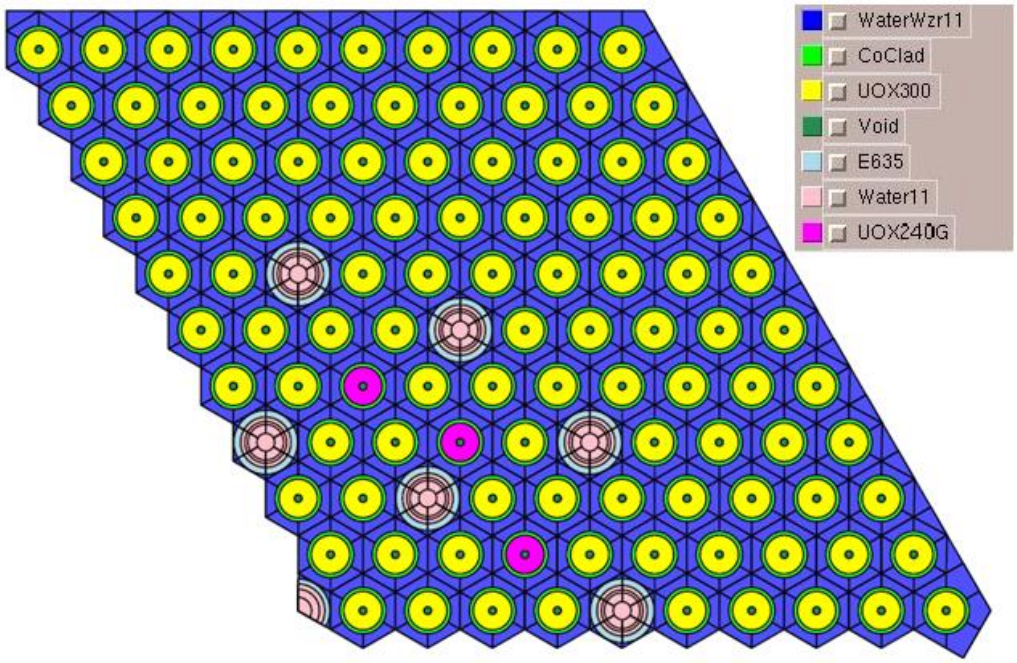

Figure D-3: TVSA model (one-third) with 9 Gadolinium fuel pins
(WaterWzr11 — Water; CoClad — Zr-alloy Э110; UOX300 — UO_2; Void —Void; E635 — Zr-alloy Э635; Water11 — Water; UOX240G — UO_2+Gd_2O_3)

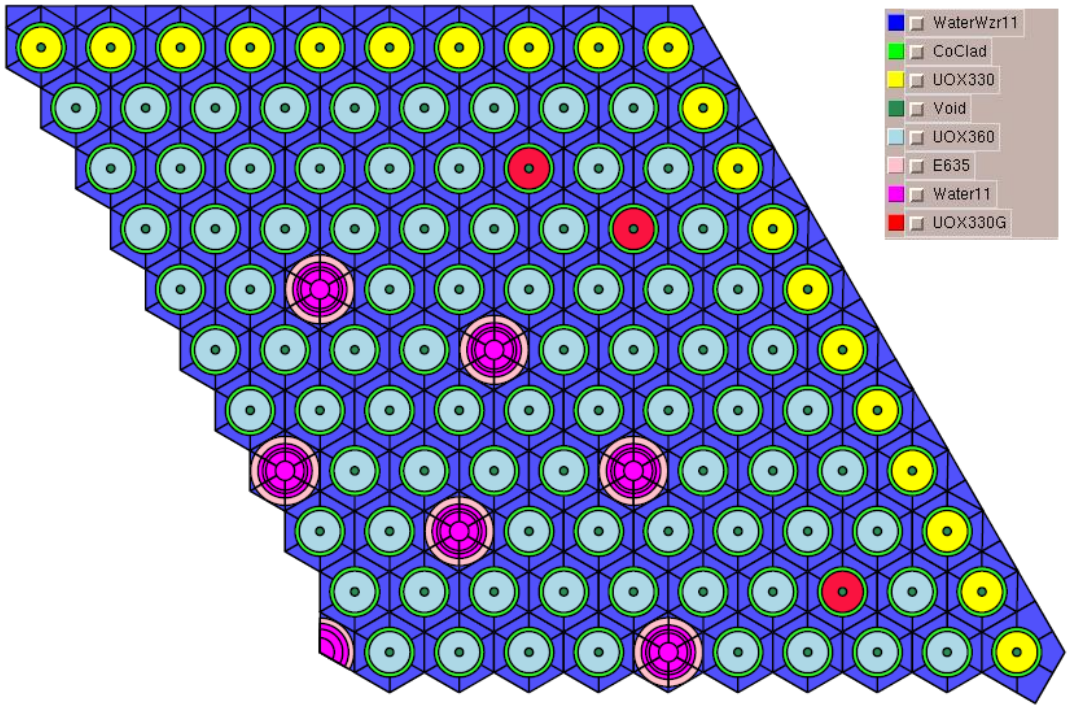

Figure D-4: Radially-profiled TVSA model (one-third) with 9 Gadolinium fuel pins
(WaterWzr11 — Water; CoClad — Zr-alloy Э110; UOX400 — UO_2; Void —Void; UOX360 — UO2; E635 — Zr-alloy Э635; Water11 — Water; UOX330G — UO_2+Gd_2O_3)

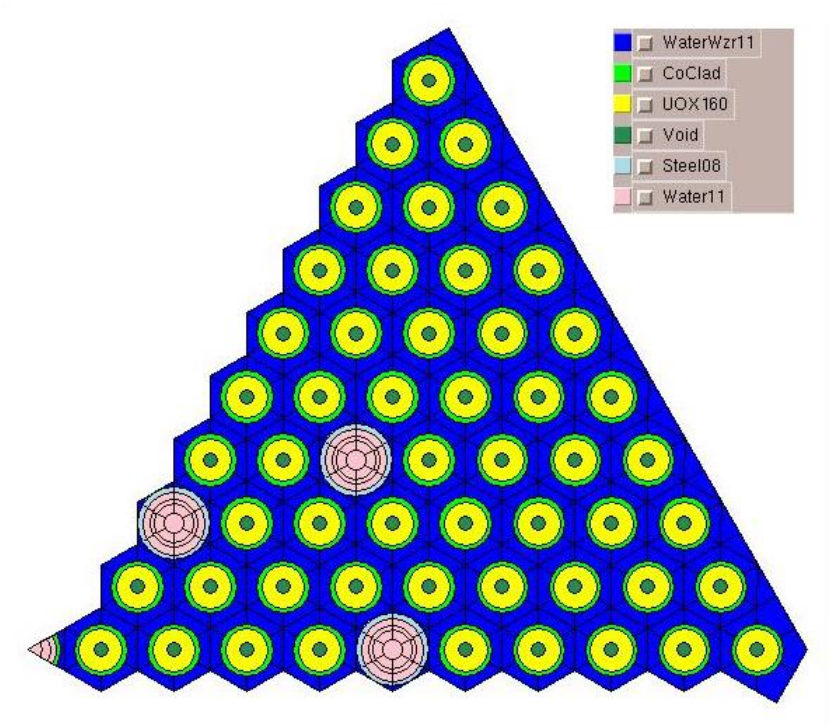

Figure D-5: TVS-M model (one-sixth) without Gadolinium fuel pins
(WaterWzr11 — Water; CoClad — Zr-alloy Э110; UOX160 — UO_2; Void —Void; Steel08 — 08X18H10T; Water11 — Water)

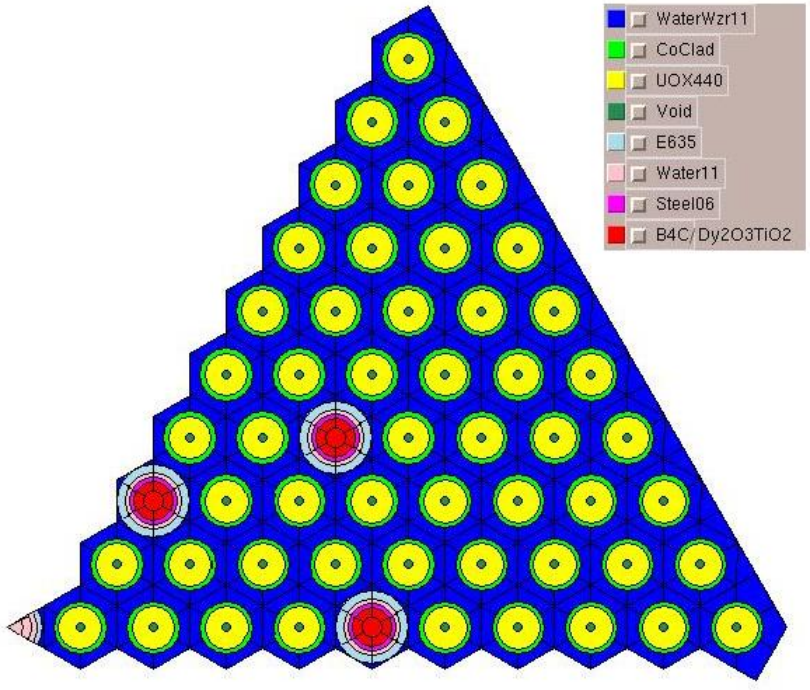

Figure D-6: TVSA model (one-sixth) without Gadolinium fuel pins – rodded
(WaterWzr11 — Water; CoClad — Zr-alloy Э110; UOX440 — UO_2; Void —Void; E635 — Zr-alloy Э635; Water11 — Water; Steel06 — 06X18H10T; $B_4C/Dy_2O_3{\bullet}TiO_2$ — B_4C or $Dy_2O_3{\bullet}TiO_2$)

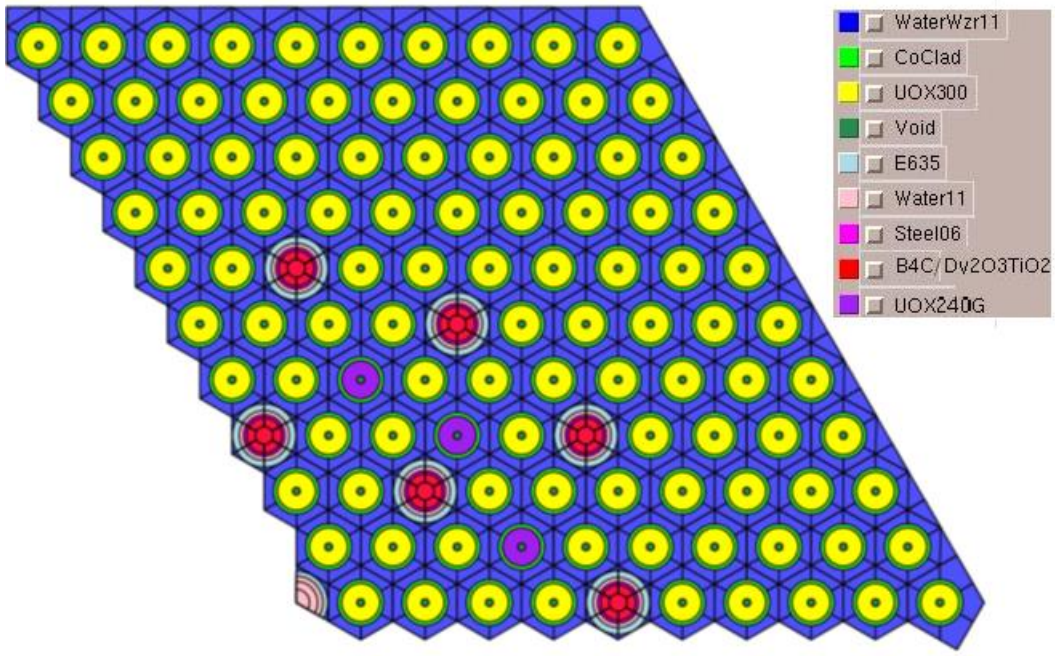

Figure D-7: TVSA model (one-third) with 9 Gadolinium fuel pins – rodded (WaterWzr11 — Water; CoClad — Zr-alloy Э110; UOX300 — UO_2; Void —Void; E635 — Zr-alloy Э635; Water11 — Water; Steel06 — 06X18H10T; B4C/Dy_2O_3•TiO_2 — B_4C or Dy_2O_3•TiO_2; UOX240G — UO_2+Gd_2O_3)

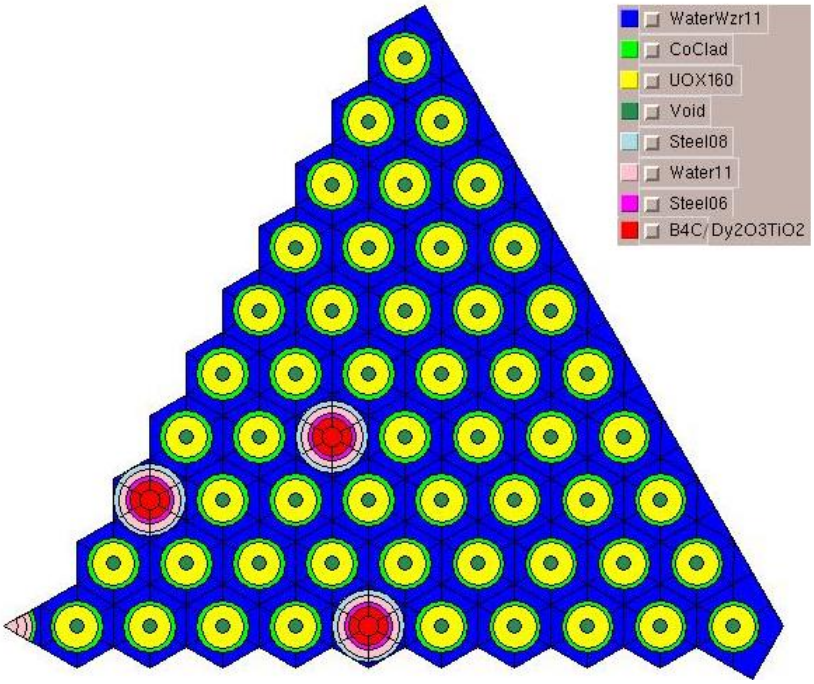

Figure D-8: TVS-M model (one-sixth) without Gadolinium fuel pins — rodded (WaterWzr11 — Water; CoClad — Zr+1% Nb; UOX160 — UO_2; Void —Void; Steel08 — 08X18H10T; Water11 — Water; Steel06 — 06X18H10T; $B_4C/Dy_2O_3TiO_2$ — B_4C or Dy_2O_3•TiO_2)

REFERENCES

(Andrushechko, 2010) Anrushechko S., Afrov A., Vassilev B., Generalov V., Kosourov K., Semchenkov Y., Uraintsev V., Nuclear power generating stations with a VVER-1000 reactor : From reactor physics to evolution of the design, Logos, Moscow, Russia, 2010. (from Russian: *Андрушечко С., Афров А., Васильев Б., Генералов В., Косоуров К., Семченков Ю., Украинцев В., АЭС с реактором типа ВВЭР-1000: От физических основ эксплуатации до эволюции проекта, Логос, Москва, Россия, 2010*).

(Lavrenyuk, 2008) Lavrenyuk P., Molchanov V., Troyanov V., Ionov V., Nuclear Fuel for WWER Reactors: Current Status and Prospects, Proceedings of the 7th International Conference WWER Fuel Performance, Modelling and Experimental Support, pp. 51 – 62, Albena, Bulgaria, September 17 - 21, 2008.

(Molchanov, 2009) Molchanov V., Nuclear Fuel for WWER Reactors: Actual States and Trends, Proceedings of the 8th International Conference WWER Fuel Performance, Modelling and Experimental Support, pp. 43 – 55, Helena Resort, Bulgaria, September 20 - October 4, 2009.

(Molchanov, 2007) Molchanov V., Sharikov A., Samoilov O., Kaldalov V., Shishkin A., Falkov A., Results of WWER-1000 TVSA Operation and Tendencies for Design Development, Proceedings of the 7th International Conference WWER Fuel Performance, Modelling and Experimental Support, pp. 218 – 222, Albena, Bulgaria, September 17 - 21, 2007.

(Molchanov, 2005) Molchanov V., Dolgov A., Samoilov O., Kaidalov V., Romanov A., Levanov L., Petrov I., Aksenov P., Results of Development and Operation Experience of WWER-1000 Alternative FA, Proceedings of the 6th International Conference WWER Fuel Performance, Modelling and Experimental Support, Albena, Bulgaria, September 19 - 23, 2005.

(Molchanov, 2003) Molchanov V., Dolgov A., Samoilov O., Kaydalov V., Kuul V., Levanov L., Africantov I., The results of AFA Operation at Kalinin NPP and Trends of Further Perfection of the Fuel Based on AFA, Proceedings of the 5th International Conference WWER Fuel Performance, Modelling and Experimental Support, pp. 182 – 185, Albena, Bulgaria, September 29 - October 3, 2003.

(Samoilov, 2013) Samoilov O., Kaydalov V., Romanov A., Falkov A., Morozkin O., Sholin Ye., Development of TVSA VVER-1000 Fuel, Proceedings of the 10th International Conference

WWER Fuel Performance, Modelling and Experimental Support, pp. 195 – 198, September 7 - 14, 2013, Sandanski, Bulgaria.

(Tereshonok, 2009) Tereshonok, V., Nikonov, S., Lizorkin, M., Velkov, K., Pautz, A., Ivanov K. Kalinin-3 Coolant Transient Benchmark – Swiching-off of One of the Four Operating Main Circulation Pumps at Nominal Reactor Power, Specification, First Edition 2008, NEA/NSC/DOC(2009)5, OECD 2009.

Appendix E. Kalinin 3 axial power profile for FAs with SPND

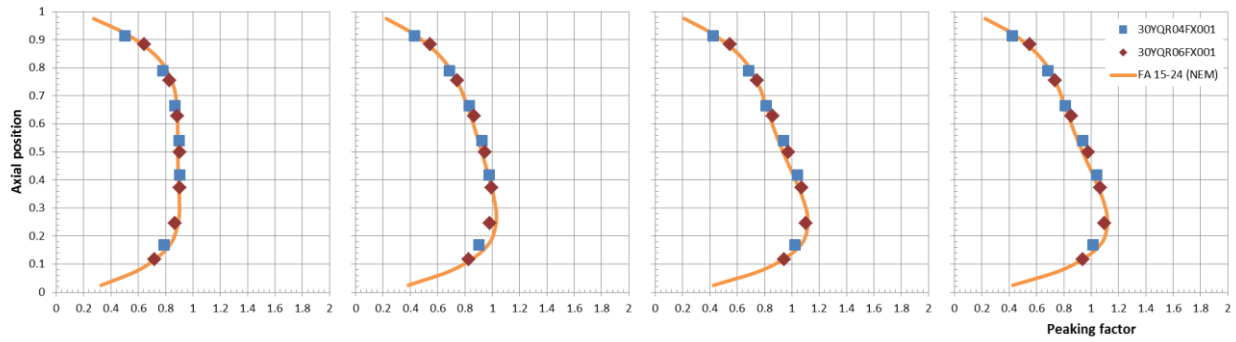

Figure E-1: Axial power profile for FA 1 (15-24) at 0, 45, 90 and 300 s. Data recorded by Kalinin 3 ICMS are shown with symbols — 30YQR04FX001, 30YQR06FX001 (LHR readings normalized to peaking factor).

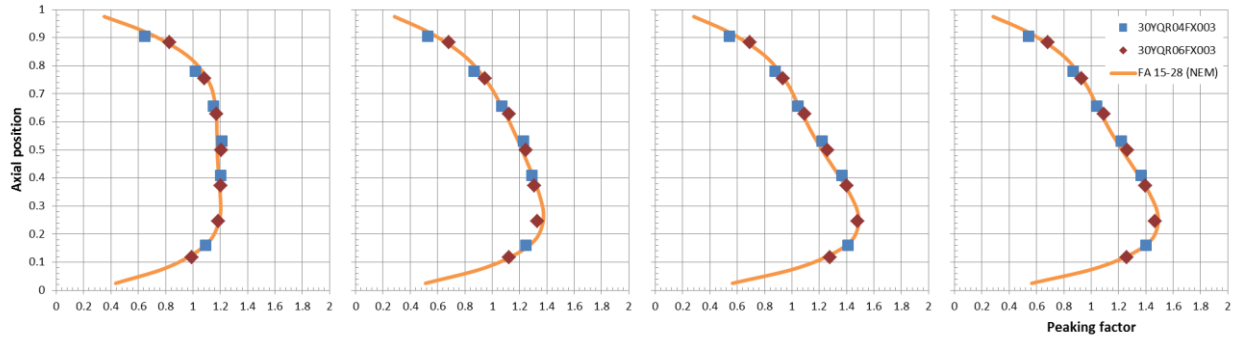

Figure E-2: Axial power profile for FA 3 (15-28) at 0, 45, 90 and 300 s. Data recorded by Kalinin 3 ICMS are shown with symbols — 30YQR04FX003, 30YQR06FX003 (LHR readings normalized to peaking factor).

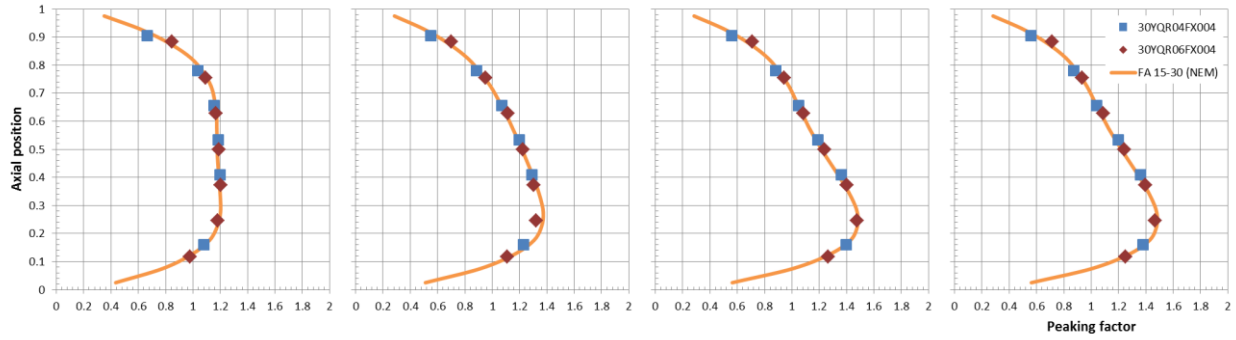

Figure E-3: Axial power profile for FA 4 (15-30) at 0, 45, 90 and 300 s. Data recorded by Kalinin 3 ICMS are shown with symbols — 30YQR04FX004, 30YQR06FX004 (LHR readings normalized to peaking factor).

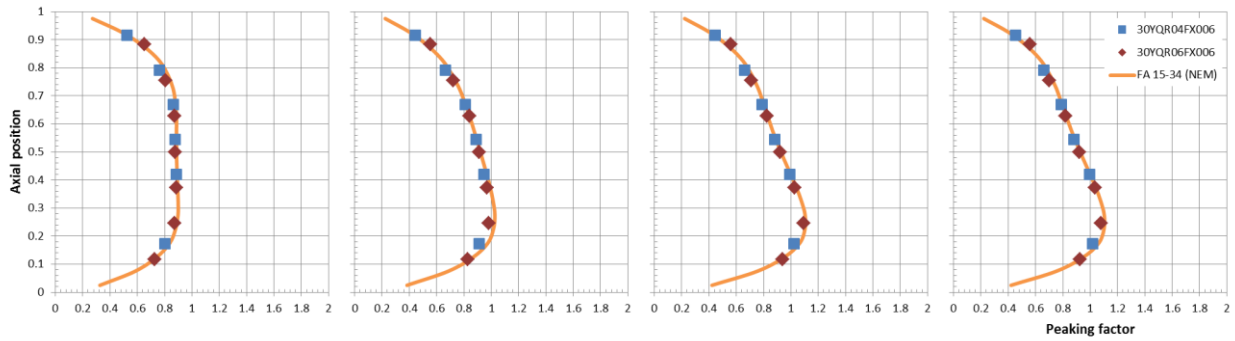

Figure E-4: Axial power profile for FA 6 (15-34) at 0, 45, 90 and 300 s. Data recorded by Kalinin 3 ICMS are shown with symbols — 30YQR04FX006, 30YQR06FX006 (LHR readings normalized to peaking factor).

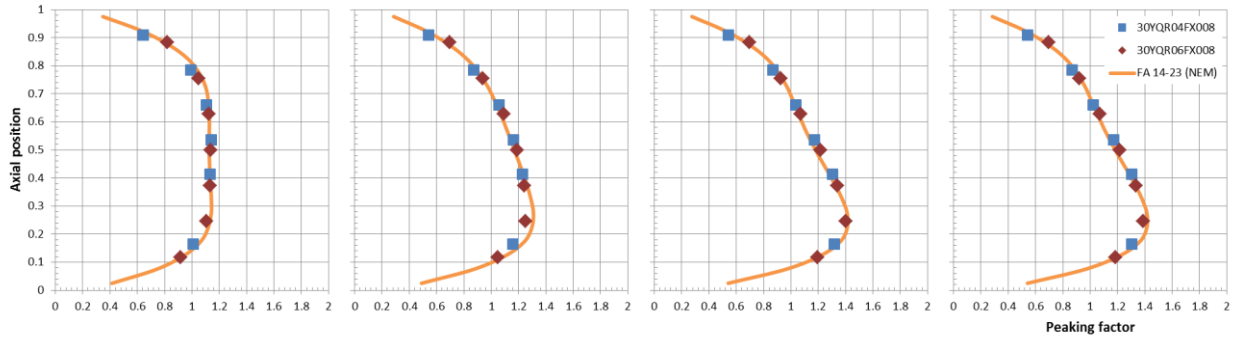

Figure E-5: Axial power profile for FA 8 (14-23) at 0, 45, 90 and 300 s. Data recorded by Kalinin 3 ICMS are shown with symbols — 30YQR04FX008, 30YQR06FX008 (LHR readings normalized to peaking factor).

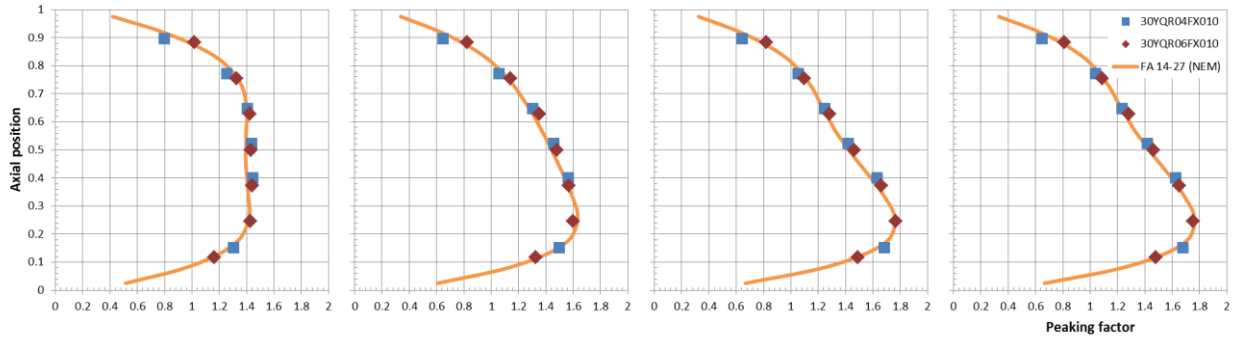

Figure E-6: Axial power profile for FA 10 (14-27) at 0, 45, 90 and 300 s. Data recorded by Kalinin 3 ICMS are shown with symbols — 30YQR04FX010, 30YQR06FX010 (LHR readings normalized to peaking factor).

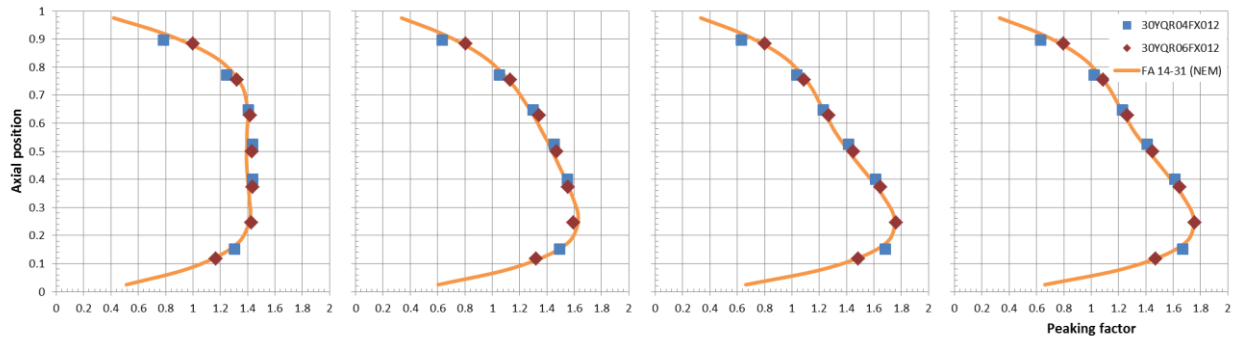

Figure E-7: Axial power profile for FA 12 (14-31) at 0, 45, 90 and 300 s. Data recorded by Kalinin 3 ICMS are shown with symbols — 30YQR04FX012, 30YQR06FX012 (LHR readings normalized to peaking factor).

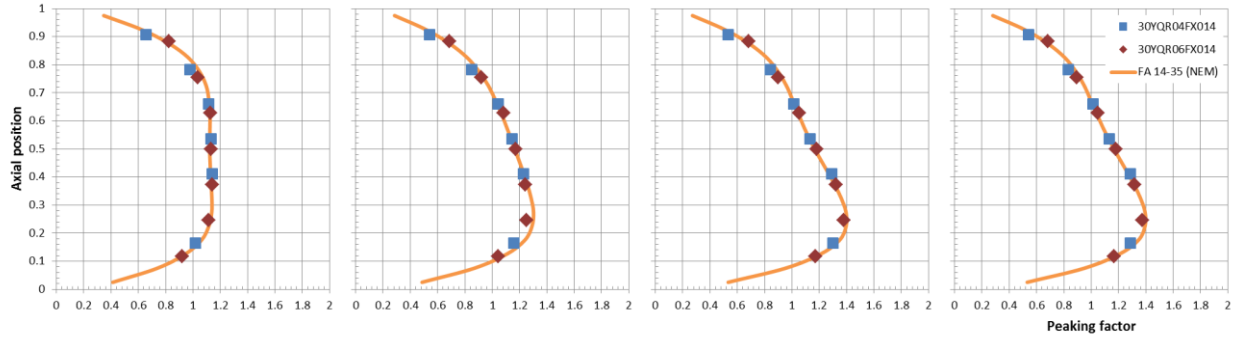

Figure E-8: Axial power profile for FA 14 (14-35) at 0, 45, 90 and 300 s. Data recorded by Kalinin 3 ICMS are shown with symbols — 30YQR04FX014, 30YQR06FX014 (LHR readings normalized to peaking factor).

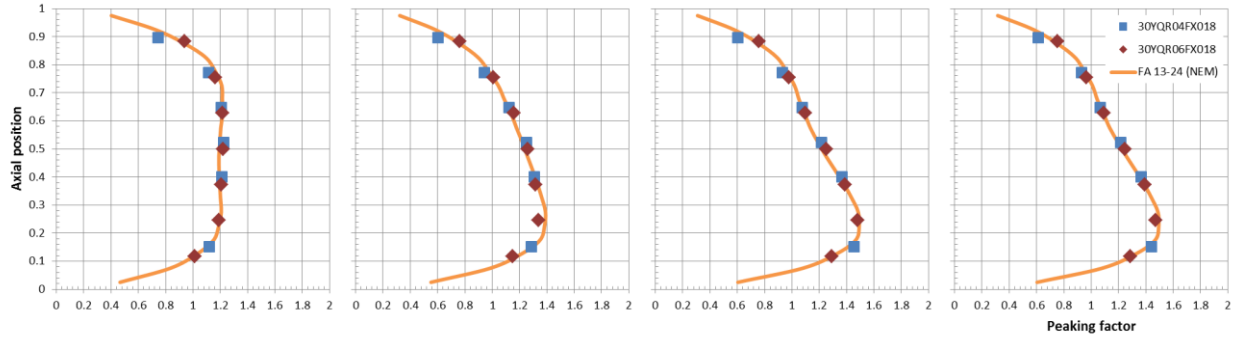

Figure E-9: Axial power profile for FA 18 (13-24) at 0, 45, 90 and 300 s. Data recorded by Kalinin 3 ICMS are shown with symbols — 30YQR04FX018, 30YQR06FX018 (LHR readings normalized to peaking factor).

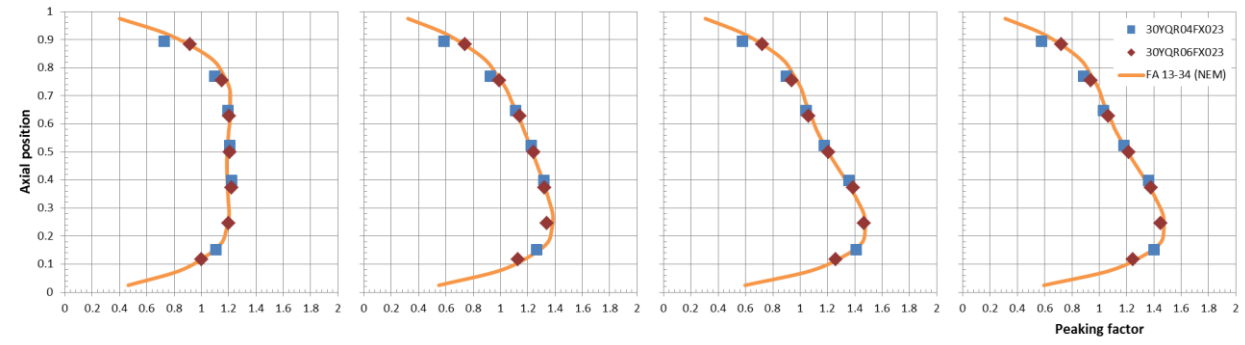

Figure E-10: Axial power profile for FA 23 (13-34) at 0, 45, 90 and 300 s. Data recorded by Kalinin 3 ICMS are shown with symbols — 30YQR04FX023, 30YQR06FX023 (LHR readings normalized to peaking factor).

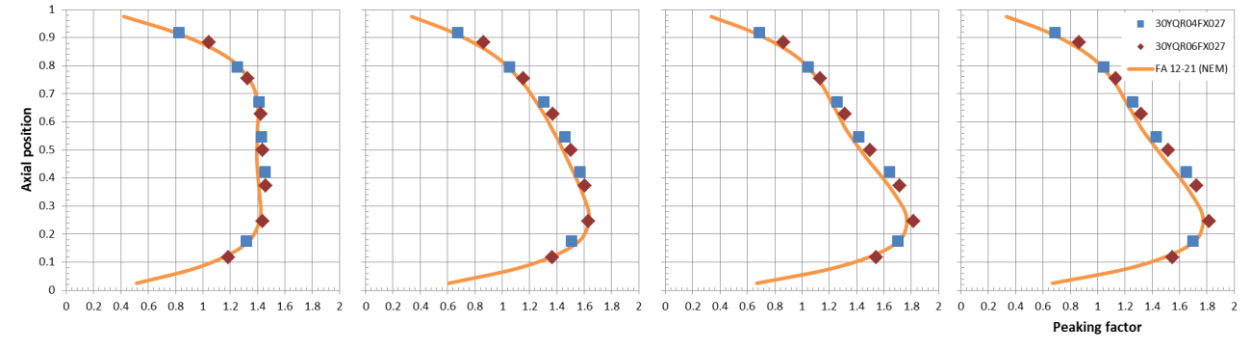

Figure E-11: Axial power profile for FA 27 (12-21) at 0, 45, 90 and 300 s. Data recorded by Kalinin 3 ICMS are shown with symbols — 30YQR04FX027, 30YQR06FX027 (LHR readings normalized to peaking factor).

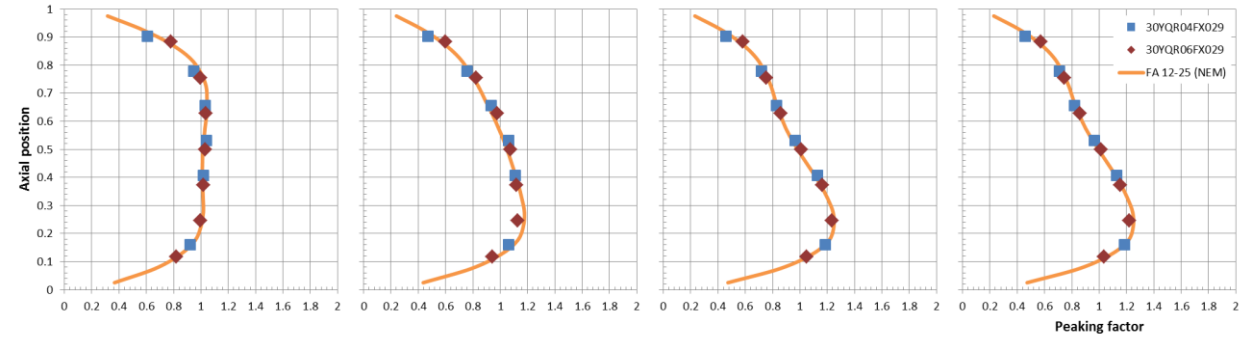

Figure E-12: Axial power profile for FA 29 (12-25) at 0, 45, 90 and 300 s. Data recorded by Kalinin 3 ICMS are shown with symbols — 30YQR04FX029, 30YQR06FX029 (LHR readings normalized to peaking factor).

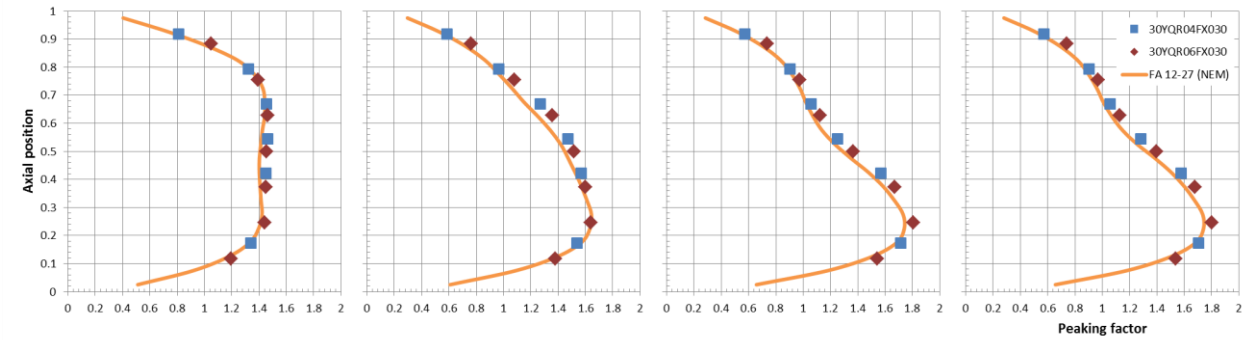

Figure E-13: Axial power profile for FA 30 (12-27) at 0, 45, 90 and 300 s. Data recorded by Kalinin 3 ICMS are shown with symbols — 30YQR04FX030, 30YQR06FX030 (LHR readings normalized to peaking factor).

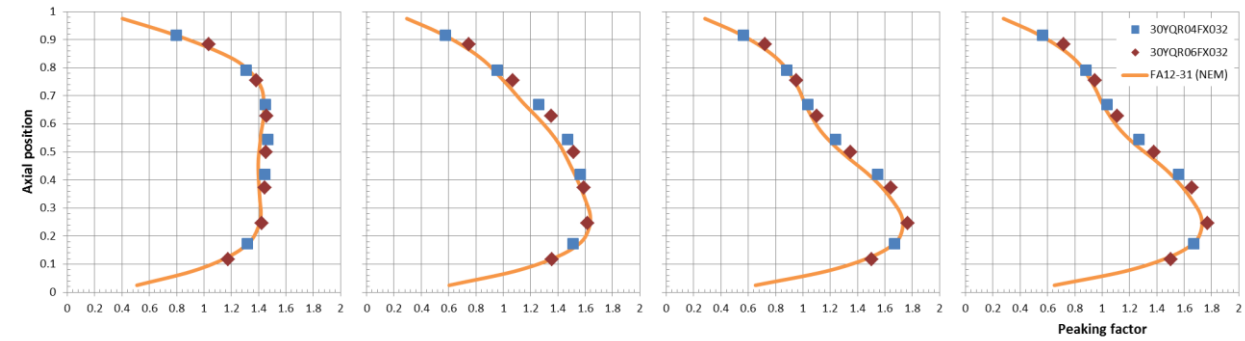

Figure E-14: Axial power profile for FA 32 (12-31) at 0, 45, 90 and 300 s. Data recorded by Kalinin 3 ICMS are shown with symbols — 30YQR04FX032, 30YQR06FX032 (LHR readings normalized to peaking factor).

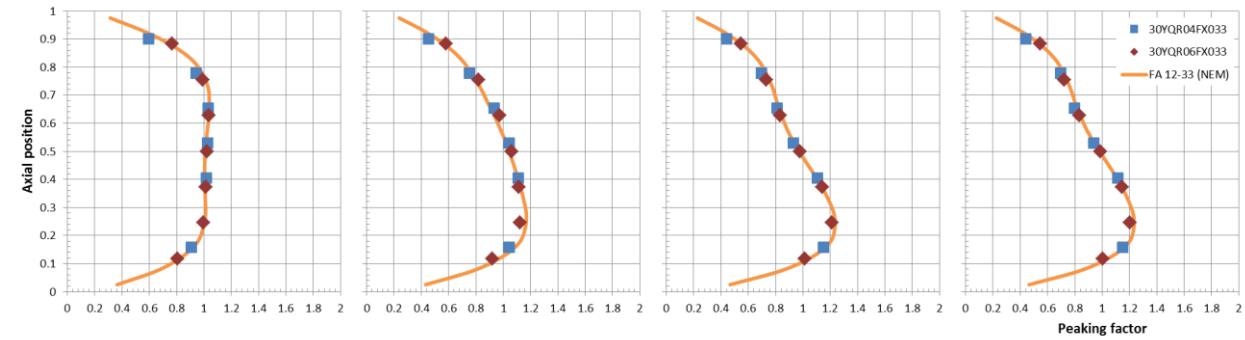

Figure E-15: Axial power profile for FA 33 (12-22) at 0, 45, 90 and 300 s. Data recorded by Kalinin 3 ICMS are shown with symbols — 30YQR04FX033, 30YQR06FX033 (LHR readings normalized to peaking factor).

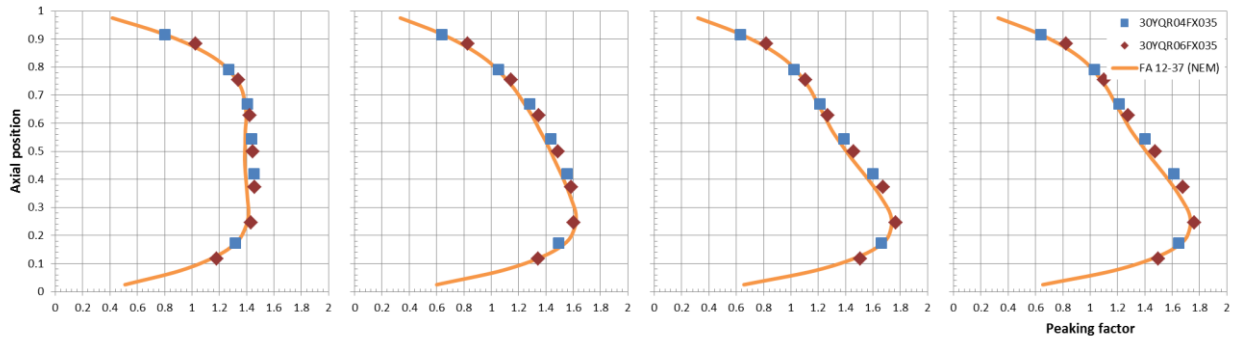

Figure E-16: Axial power profile for FA 35 (12-37) at 0, 45, 90 and 300 s. Data recorded by Kalinin 3 ICMS are shown with symbols — 30YQR04FX035, 30YQR06FX035 (LHR readings normalized to peaking factor).

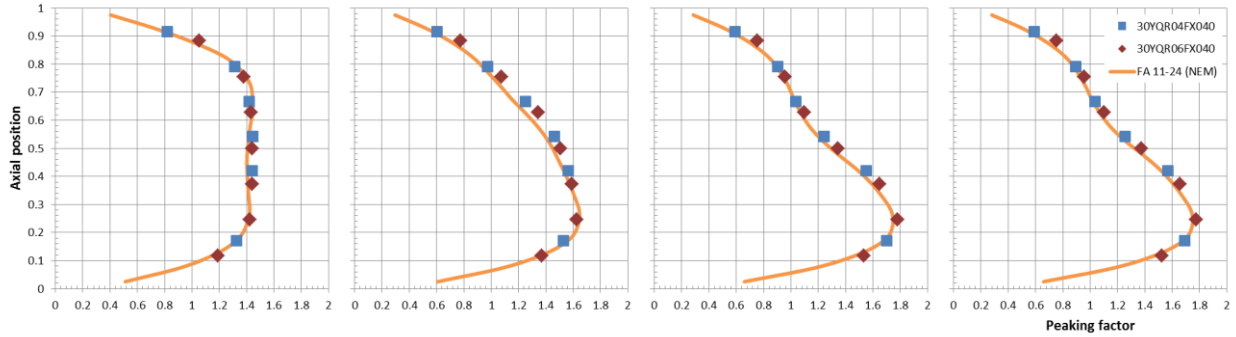

Figure E-17: Axial power profile for FA 40 (11-24) at 0, 45, 90 and 300 s. Data recorded by Kalinin 3 ICMS are shown with symbols — 30YQR04FX040, 30YQR06FX040 (LHR readings normalized to peaking factor).

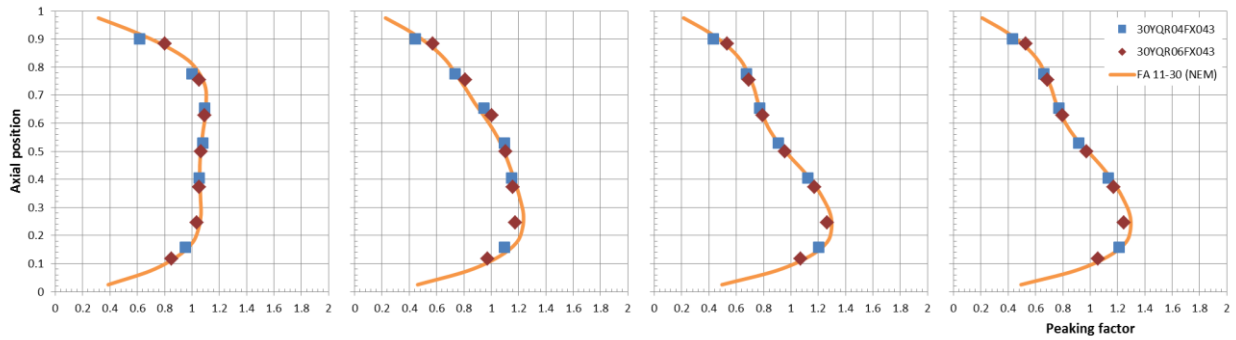

Figure E-18: Axial power profile for FA 43 (11-30) at 0, 45, 90 and 300 s. Data recorded by Kalinin 3 ICMS are shown with symbols — 30YQR04FX043, 30YQR06FX043 (LHR readings normalized to peaking factor).

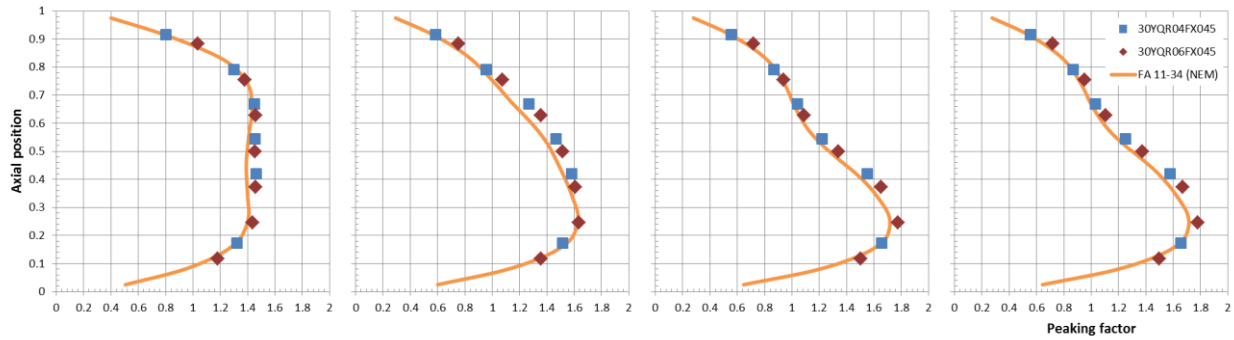

Figure E-19: Axial power profile for FA 45 (11-34) at 0, 45, 90 and 300 s. Data recorded by Kalinin 3 ICMS are shown with symbols — 30YQR04FX045, 30YQR06FX045 (LHR readings normalized to peaking factor).

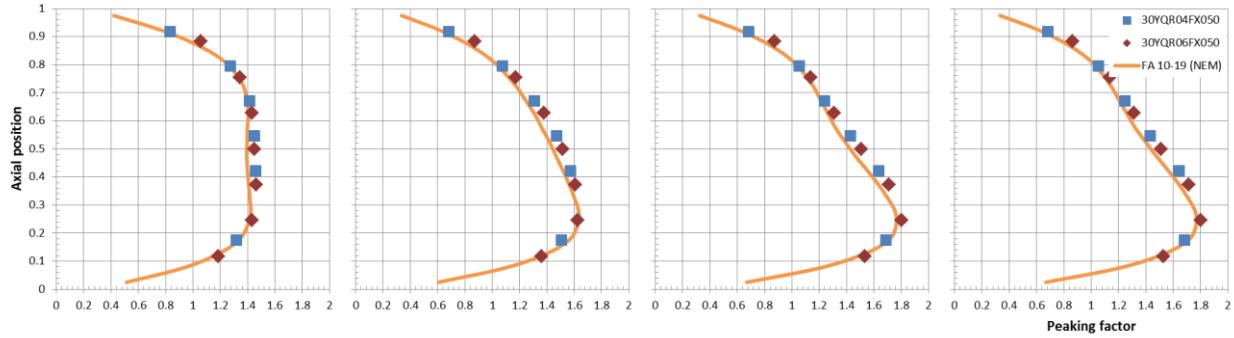

Figure E-20: Axial power profile for FA 50 (10-19) at 0, 45, 90 and 300 s. Data recorded by Kalinin 3 ICMS are shown with symbols — 30YQR04FX050, 30YQR06FX050 (LHR readings normalized to peaking factor).

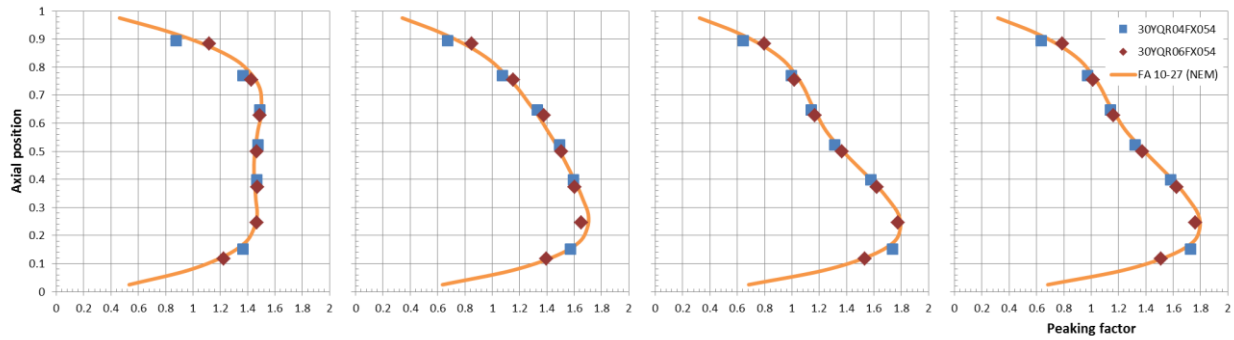

Figure E-21: Axial power profile for FA 54 (10-27) at 0, 45, 90 and 300 s. Data recorded by Kalinin 3 ICMS are shown with symbols — 30YQR04FX054, 30YQR06FX054 (LHR readings normalized to peaking factor).

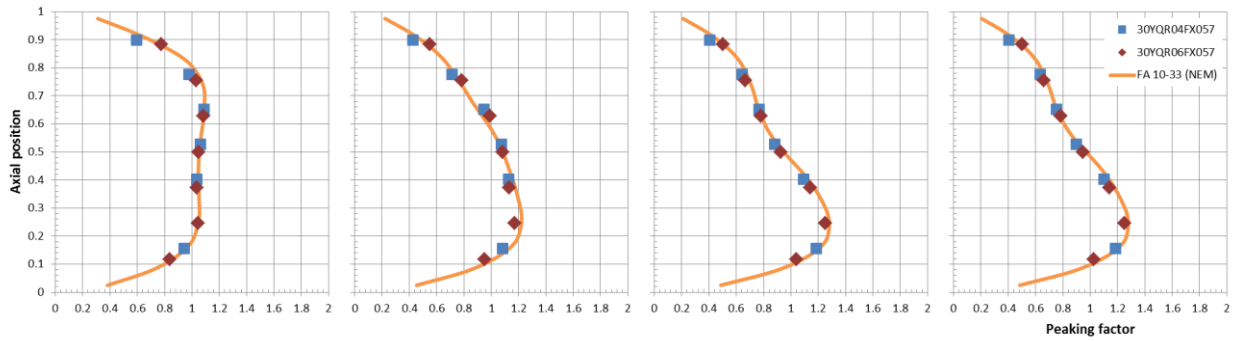

Figure E-22: Axial power profile for FA 57 (10-33) at 0, 45, 90 and 300 s. Data recorded by Kalinin 3 ICMS are shown with symbols — 30YQR04FX057, 30YQR06FX057 (LHR readings normalized to peaking factor).

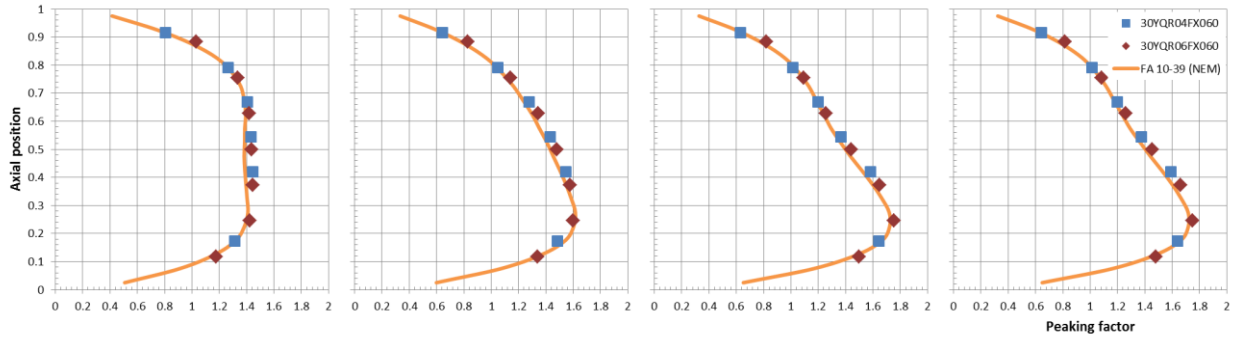

Figure E-23: Axial power profile for FA 60 (10-39) at 0, 45, 90 and 300 s. Data recorded by Kalinin 3 ICMS are shown with symbols — 30YQR04FX060, 30YQR06FX060 (LHR readings normalized to peaking factor).

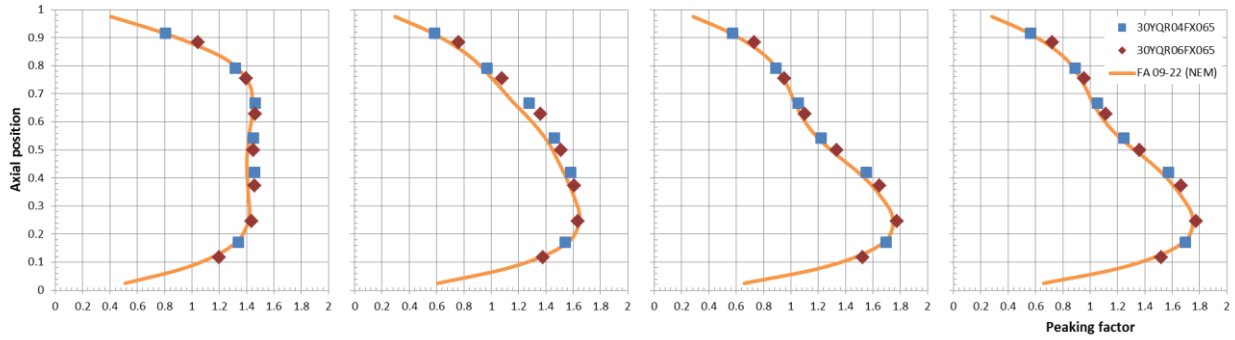

Figure E-24: Axial power profile for FA 65 (09-22) at 0, 45, 90 and 300 s. Data recorded by Kalinin 3 ICMS are shown with symbols — 30YQR04FX065, 30YQR06FX065 (LHR readings normalized to peaking factor).

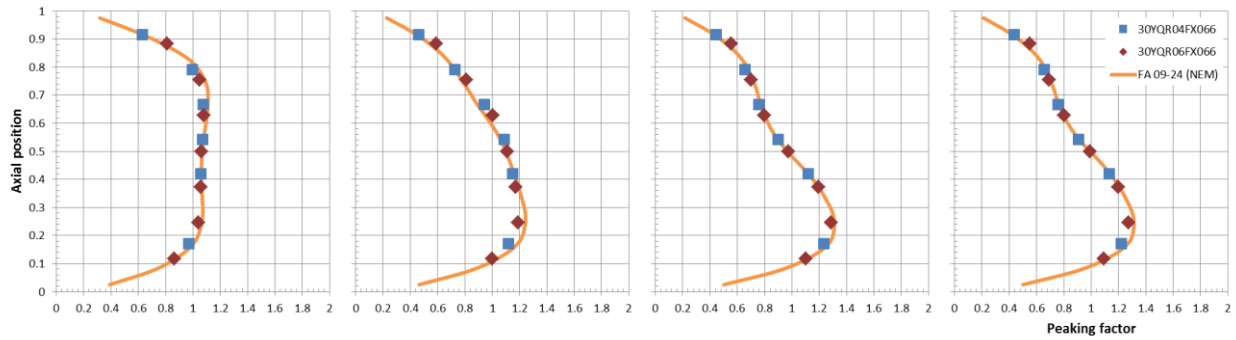

Figure E-25: Axial power profile for FA 66 (09-24) at 0, 45, 90 and 300 s. Data recorded by Kalinin 3 ICMS are shown with symbols — 30YQR04FX066, 30YQR06FX066 (LHR readings normalized to peaking factor).

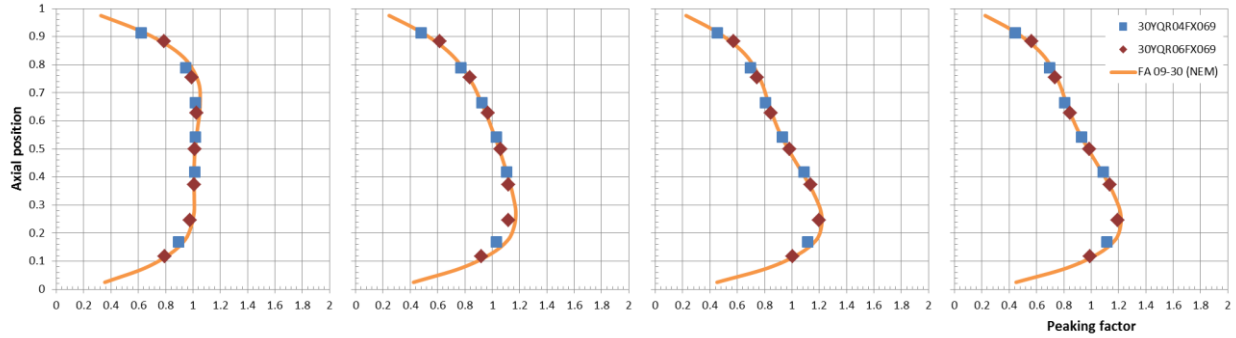

Figure E-26: Axial power profile for FA 69 (09-30) at 0, 45, 90 and 300 s. Data recorded by Kalinin 3 ICMS are shown with symbols — 30YQR04FX069, 30YQR06FX069 (LHR readings normalized to peaking factor).

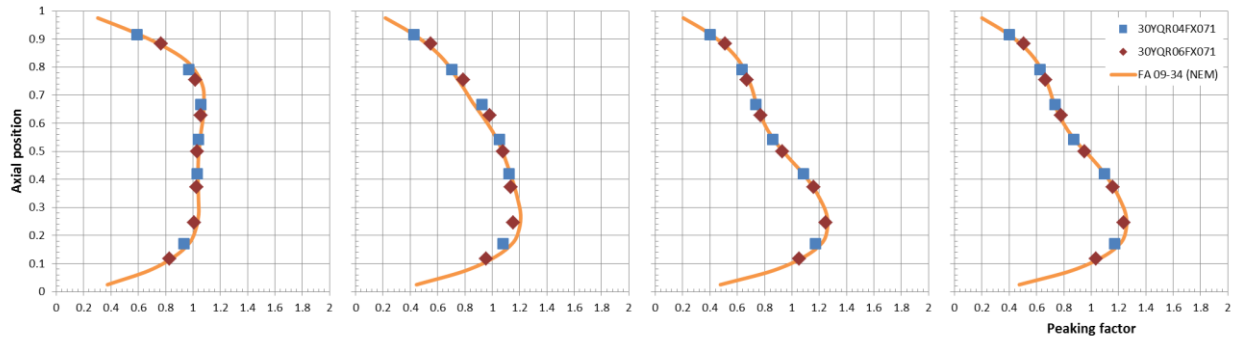

Figure E-27: Axial power profile for FA 71 (09-34) at 0, 45, 90 and 300 s. Data recorded by Kalinin 3 ICMS are shown with symbols — 30YQR04FX071, 30YQR06FX071 (LHR readings normalized to peaking factor).

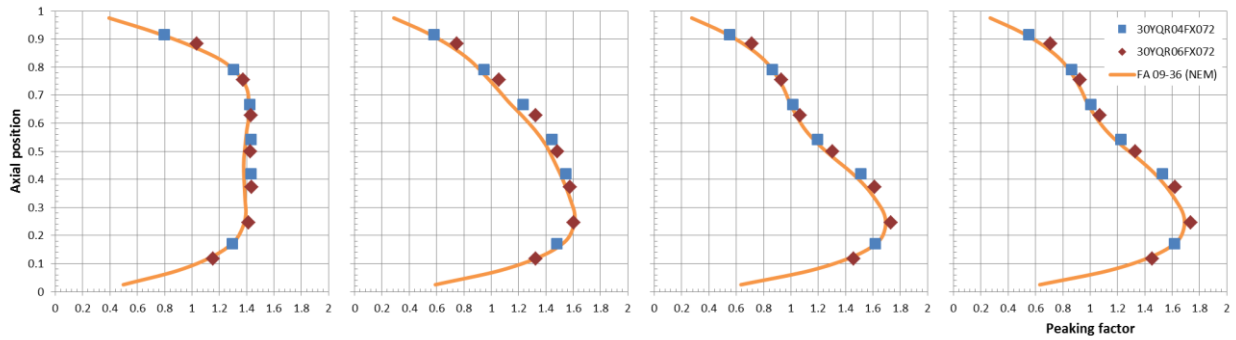

Figure E-28: Axial power profile for FA 72 (09-36) at 0, 45, 90 and 300 s. Data recorded by Kalinin 3 ICMS are shown with symbols — 30YQR04FX072, 30YQR06FX072 (LHR readings normalized to peaking factor).

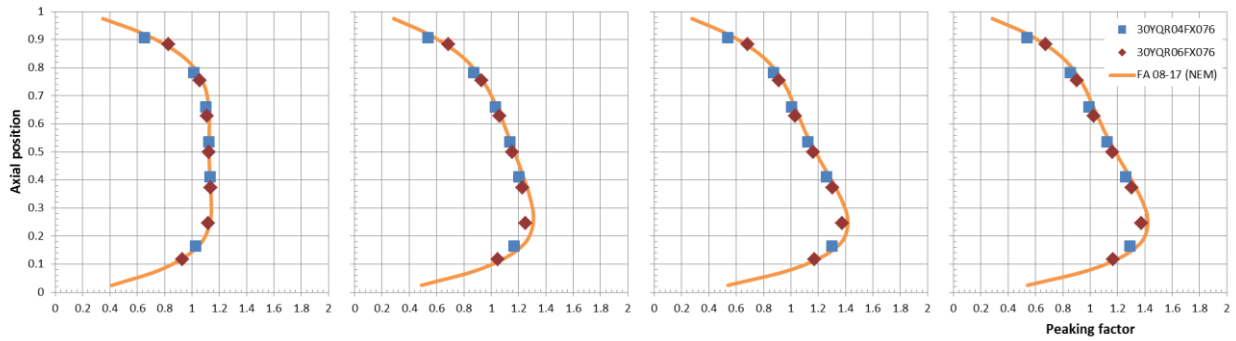

Figure E-29: Axial power profile for FA 76 (08-17) at 0, 45, 90 and 300 s. Data recorded by Kalinin 3 ICMS are shown with symbols — 30YQR04FX076, 30YQR06FX076 (LHR readings normalized to peaking factor).

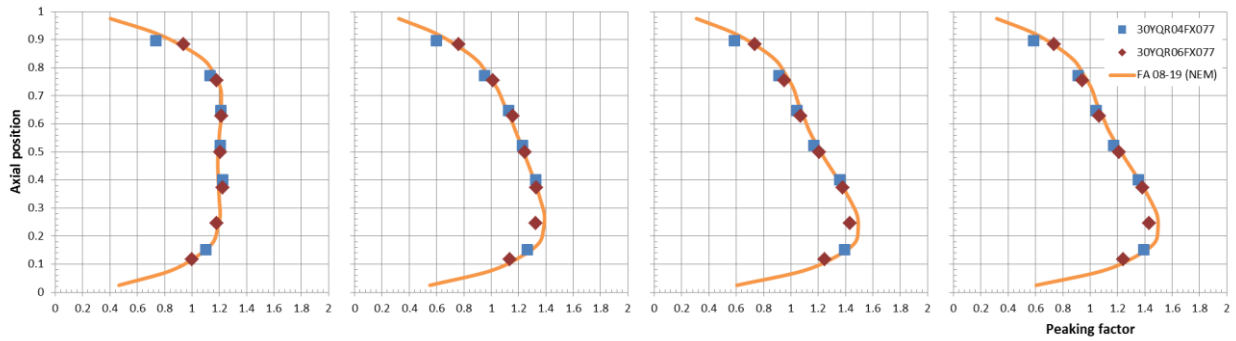

Figure E-30: Axial power profile for FA 77 (08-19) at 0, 45, 90 and 300 s. Data recorded by Kalinin 3 ICMS are shown with symbols — 30YQR04FX077, 30YQR06FX077 (LHR readings normalized to peaking factor).

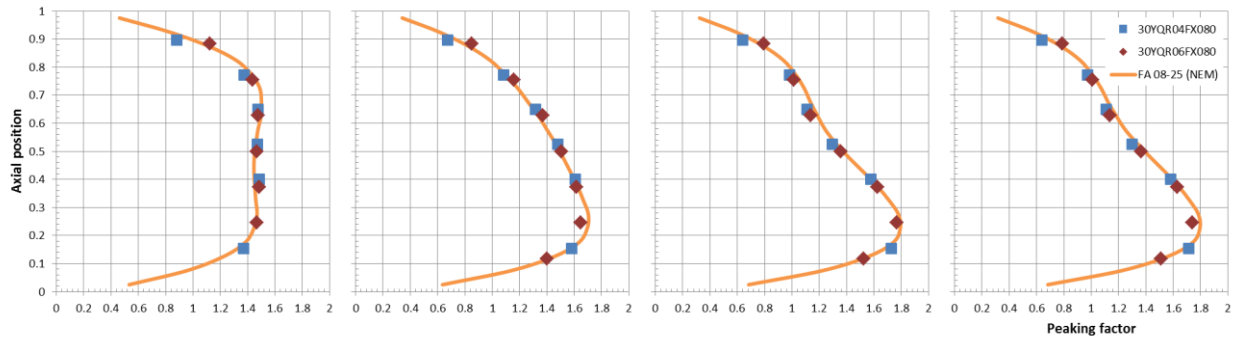

Figure E-31: Axial power profile for FA 80 (08-25) at 0, 45, 90 and 300 s. Data recorded by Kalinin 3 ICMS are shown with symbols — 30YQR04FX080, 30YQR06FX080 (LHR readings normalized to peaking factor).

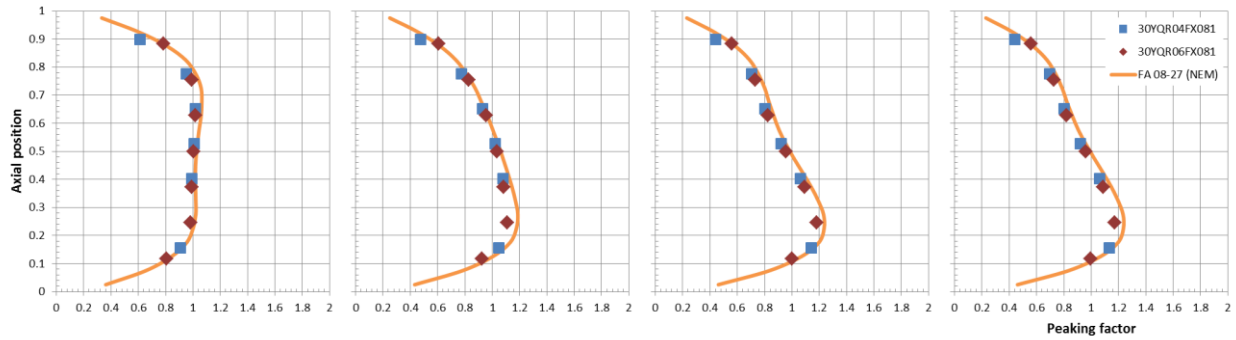

Figure E-32: Axial power profile for FA 81 (08-27) at 0, 45, 90 and 300 s. Data recorded by Kalinin 3 ICMS are shown with symbols — 30YQR04FX081, 30YQR06FX081 (LHR readings normalized to peaking factor).

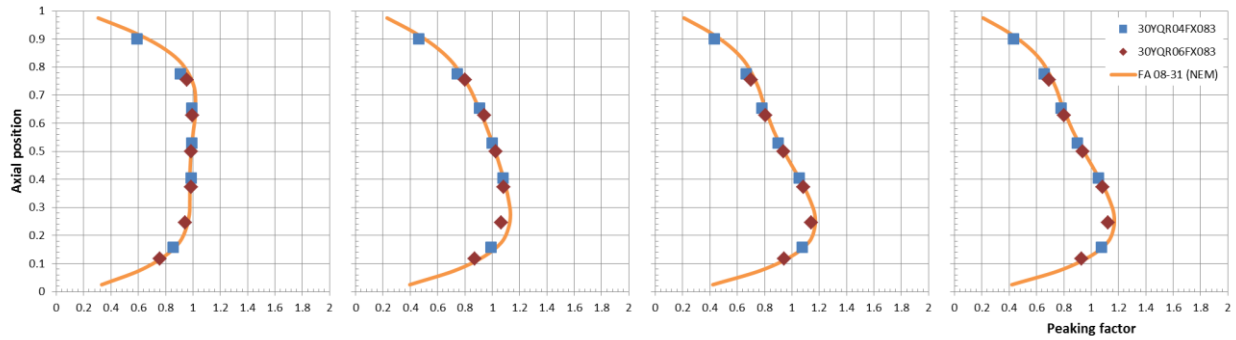

Figure E-33: Axial power profile for FA 83 (08-31) at 0, 45, 90 and 300 s. Data recorded by Kalinin 3 ICMS are shown with symbols — 30YQR04FX083, 30YQR06FX083 (LHR readings normalized to peaking factor).

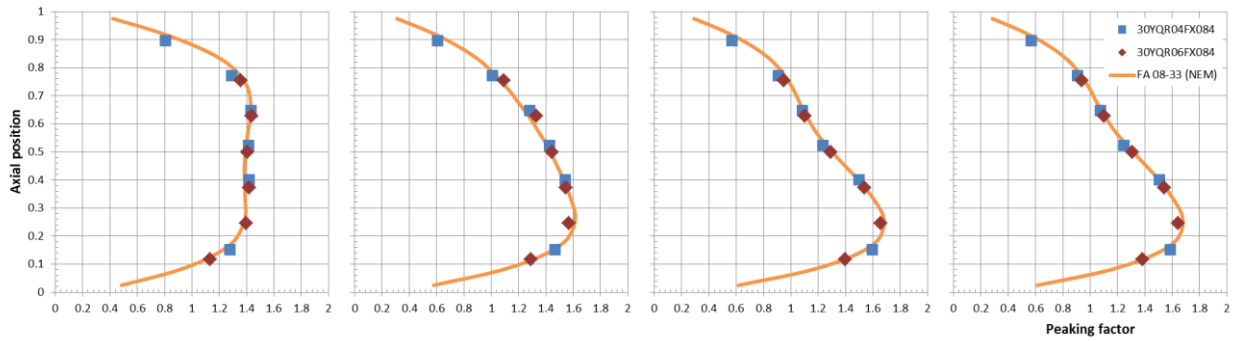

Figure E-34: Axial power profile for FA 84 (08-33) at 0, 45, 90 and 300 s. Data recorded by Kalinin 3 ICMS are shown with symbols — 30YQR04FX084, 30YQR06FX084 (LHR readings normalized to peaking factor).

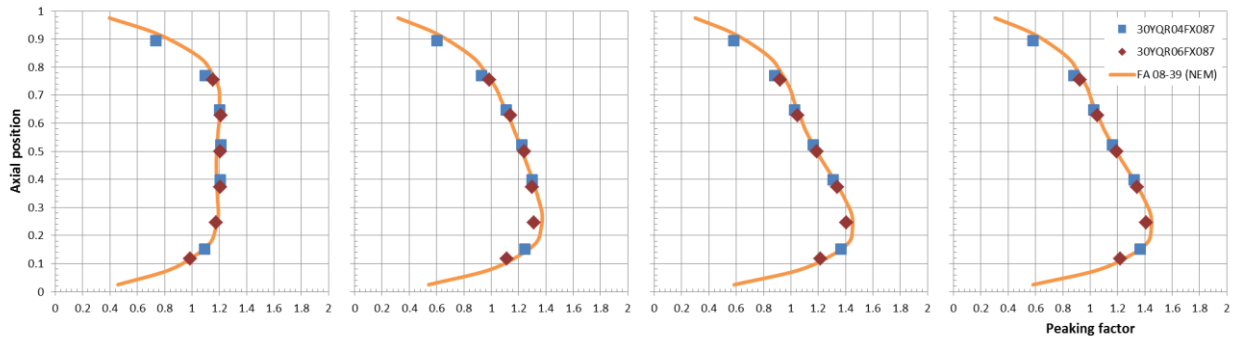

Figure E-35: Axial power profile for FA 87 (08-39) at 0, 45, 90 and 300 s. Data recorded by Kalinin 3 ICMS are shown with symbols — 30YQR04FX087, 30YQR06FX087 (LHR readings normalized to peaking factor).

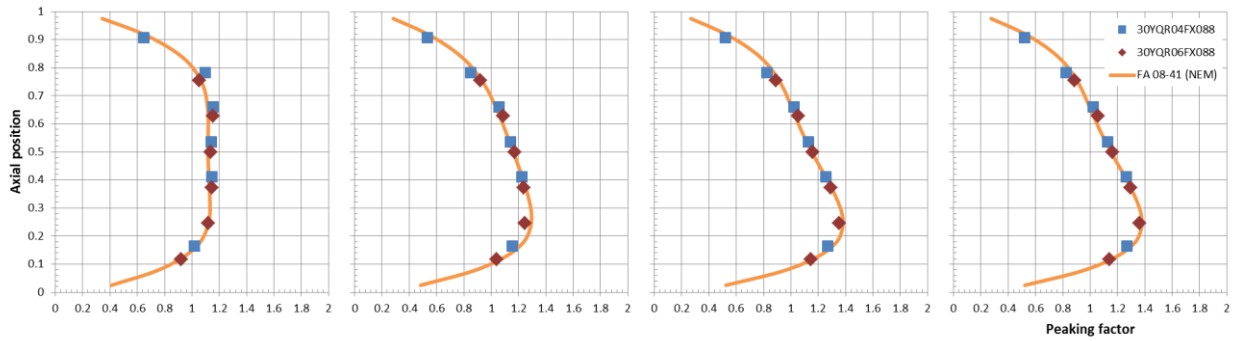

Figure E-36: Axial power profile for FA 88 (08-41) at 0, 45, 90 and 300 s. Data recorded by Kalinin 3 ICMS are shown with symbols — 30YQR04FX088, 30YQR06FX088 (LHR readings normalized to peaking factor).

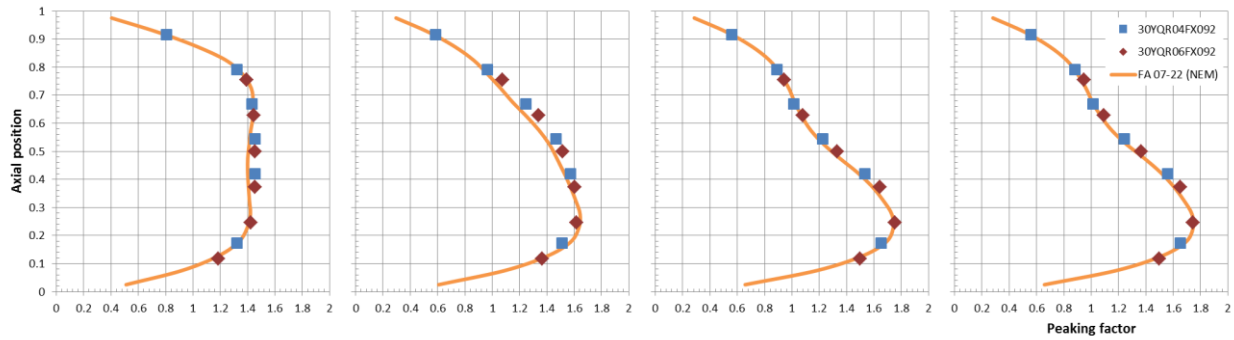

Figure E-37: Axial power profile for FA 92 (07-22) at 0, 45, 90 and 300 s. Data recorded by Kalinin 3 ICMS are shown with symbols — 30YQR04FX092, 30YQR06FX092 (LHR readings normalized to peaking factor).

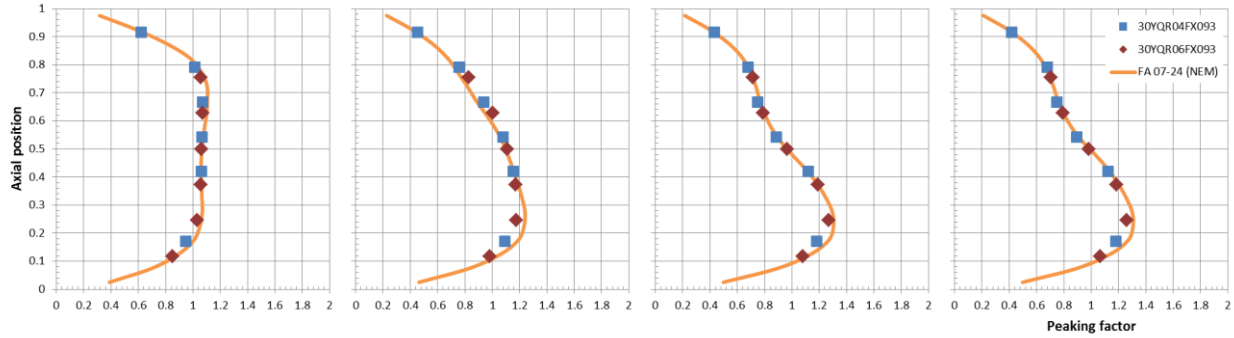

Figure E-38: Axial power profile for FA 93 (07-24) at 0, 45, 90 and 300 s. Data recorded by Kalinin 3 ICMS are shown with symbols — 30YQR04FX093, 30YQR06FX093 (LHR readings normalized to peaking factor).

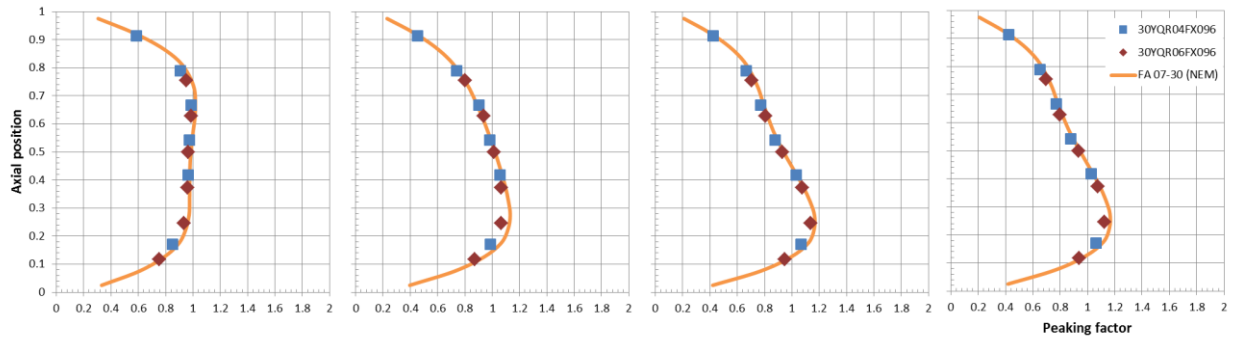

Figure E-39: Axial power profile for FA 96 (07-30) at 0, 45, 90 and 300 s. Data recorded by Kalinin 3 ICMS are shown with symbols — 30YQR04FX096, 30YQR06FX096 (LHR readings normalized to peaking factor).

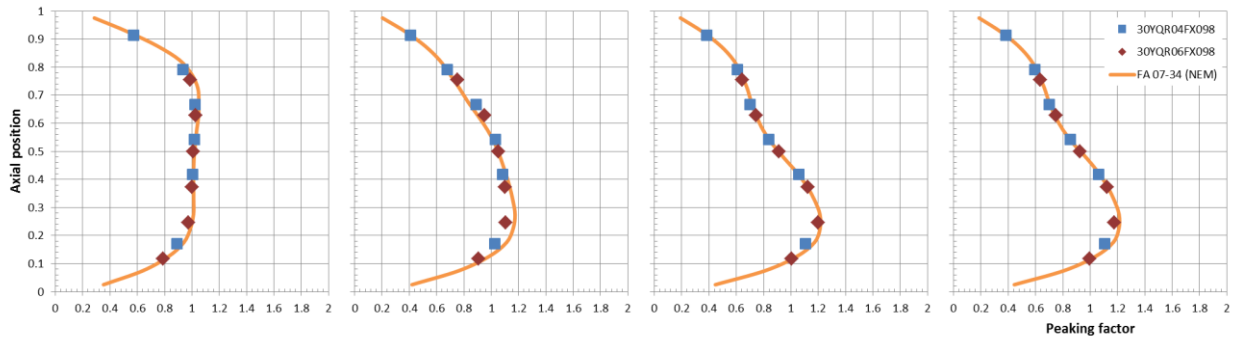

Figure E-40: Axial power profile for FA 98 (07-34) at 0, 45, 90 and 300 s. Data recorded by Kalinin 3 ICMS are shown with symbols — 30YQR04FX098, 30YQR06FX098 (LHR readings normalized to peaking factor).

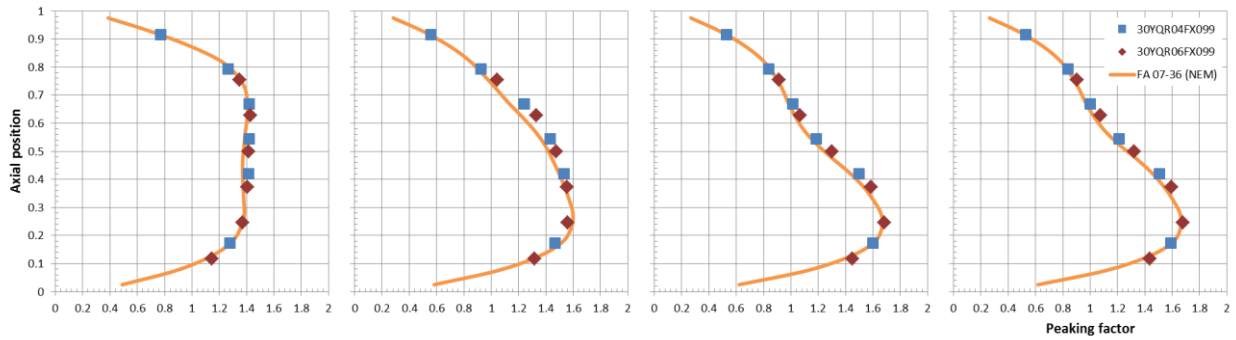

Figure E-41: Axial power profile for FA 99 (07-36) at 0, 45, 90 and 300 s. Data recorded by Kalinin 3 ICMS are shown with symbols — 30YQR04FX099, 30YQR06FX099 (LHR readings normalized to peaking factor).

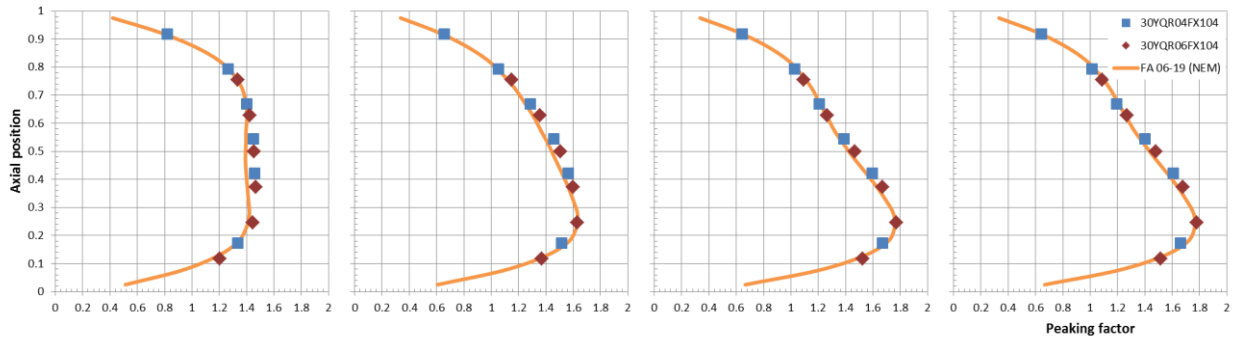

Figure E-42: Axial power profile for FA 104 (06-19) at 0, 45, 90 and 300 s. Data recorded by Kalinin 3 ICMS are shown with symbols — 30YQR04FX104, 30YQR06FX104 (LHR readings normalized to peaking factor).

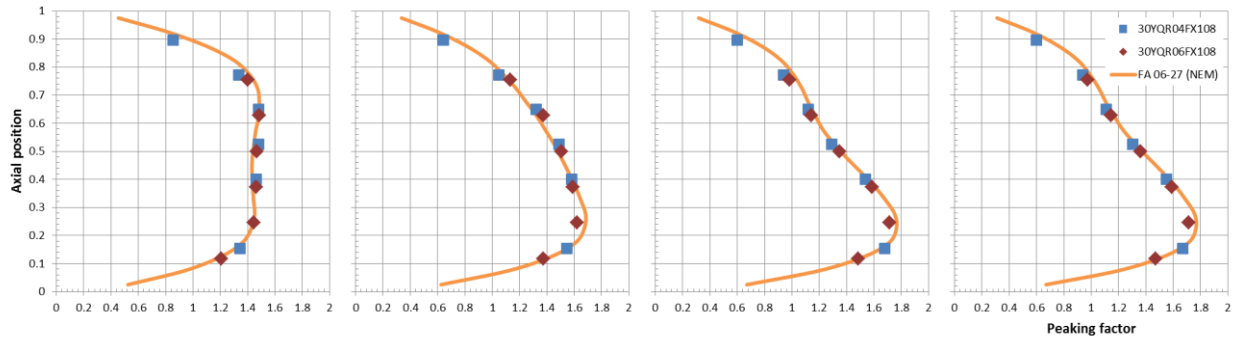

Figure E-43: Axial power profile for FA 108 (06-27) at 0, 45, 90 and 300 s. Data recorded by Kalinin 3 ICMS are shown with symbols — 30YQR04FX108, 30YQR06FX108 (LHR readings normalized to peaking factor).

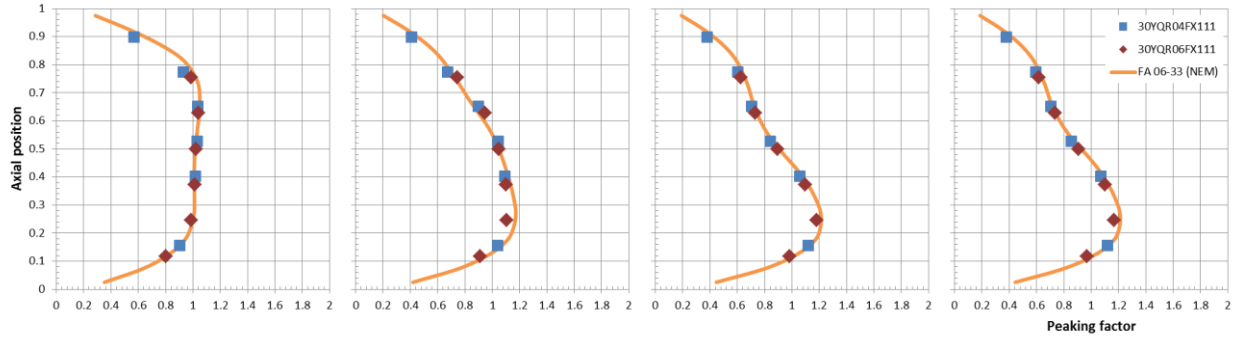

Figure E-44: Axial power profile for FA 111 (06-33) at 0, 45, 90 and 300 s. Data recorded by Kalinin 3 ICMS are shown with symbols — 30YQR04FX111, 30YQR06FX111 (LHR readings normalized to peaking factor).

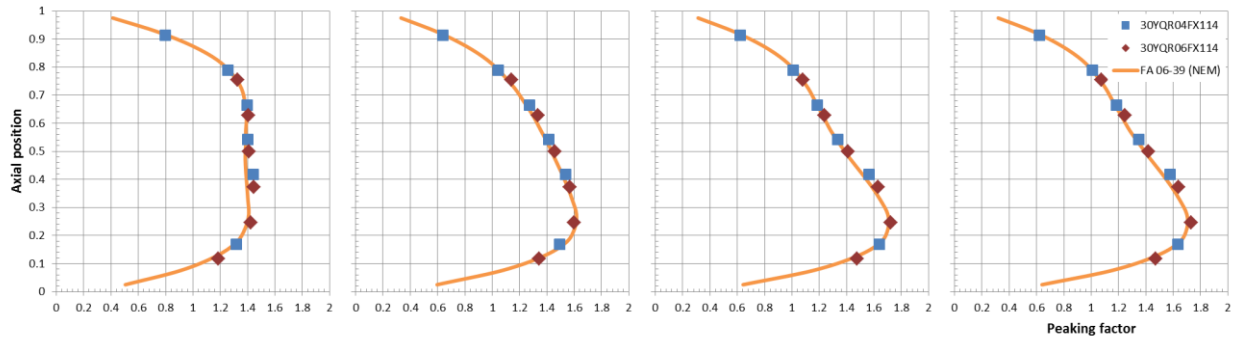

Figure E-45: Axial power profile for FA 114 (06-39) at 0, 45, 90 and 300 s. Data recorded by Kalinin 3 ICMS are shown with symbols — 30YQR04FX114, 30YQR06FX114 (LHR readings normalized to peaking factor).

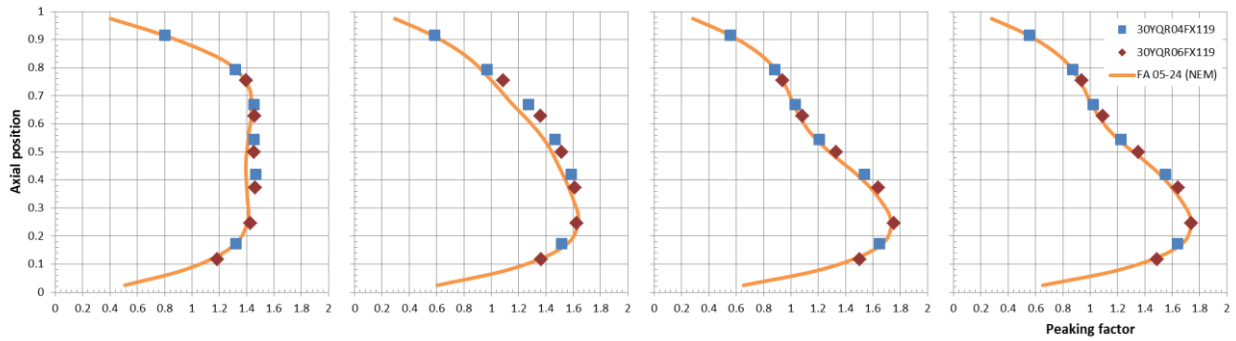

Figure E-46: Axial power profile for FA 119 (05-24) at 0, 45, 90 and 300 s. Data recorded by Kalinin 3 ICMS are shown with symbols — 30YQR04FX119, 30YQR06FX119 (LHR readings normalized to peaking factor).

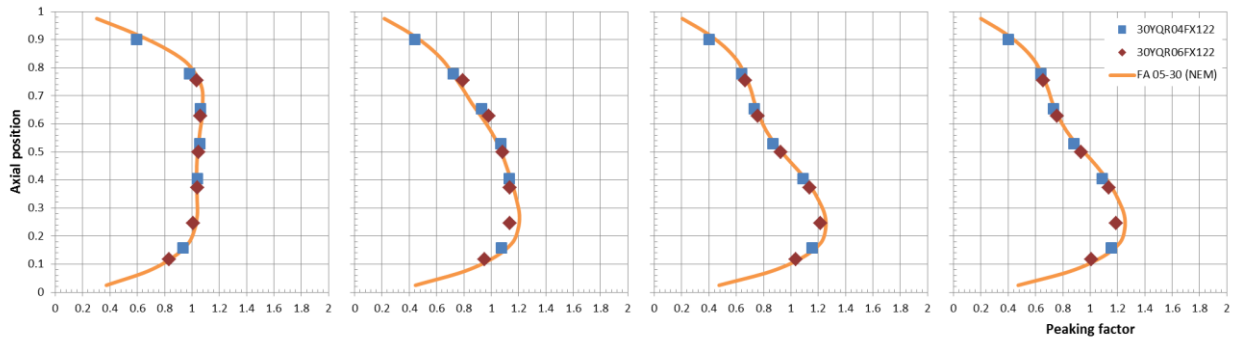

Figure E-47: Axial power profile for FA 122 (05-30) at 0, 45, 90 and 300 s. Data recorded by Kalinin 3 ICMS are shown with symbols — 30YQR04FX122, 30YQR06FX122 (LHR readings normalized to peaking factor).

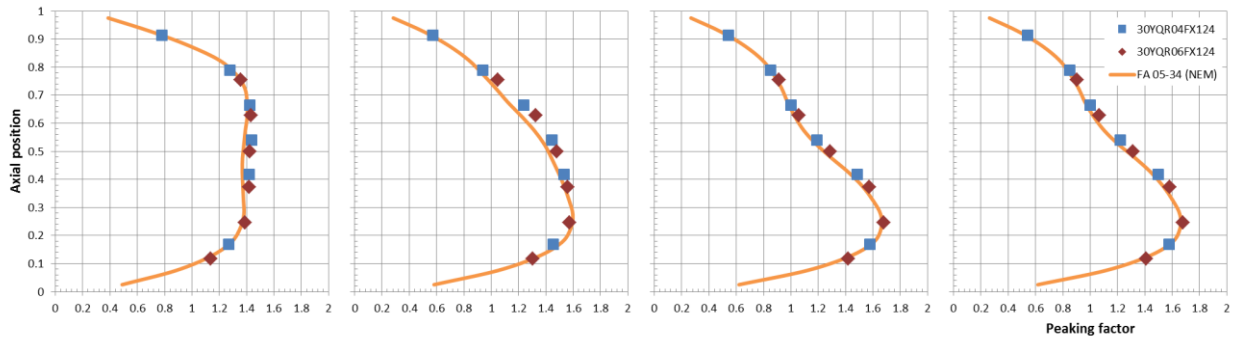

Figure E-48: Axial power profile for FA 124 (05-34) at 0, 45, 90 and 300 s. Data recorded by Kalinin 3 ICMS are shown with symbols — 30YQR04FX124, 30YQR06FX124 (LHR readings normalized to peaking factor).

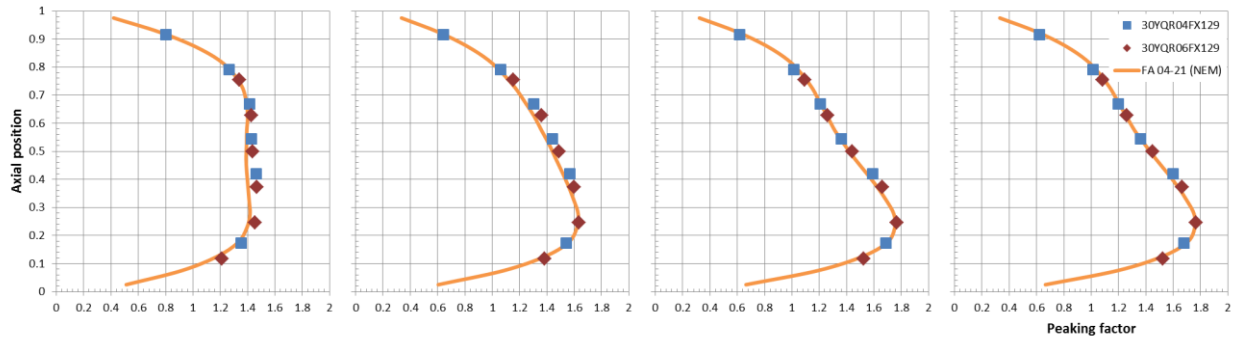

Figure E-49: Axial power profile for FA 129 (04-21) at 0, 45, 90 and 300 s. Data recorded by Kalinin 3 ICMS are shown with symbols — 30YQR04FX129, 30YQR06FX129 (LHR readings normalized to peaking factor).

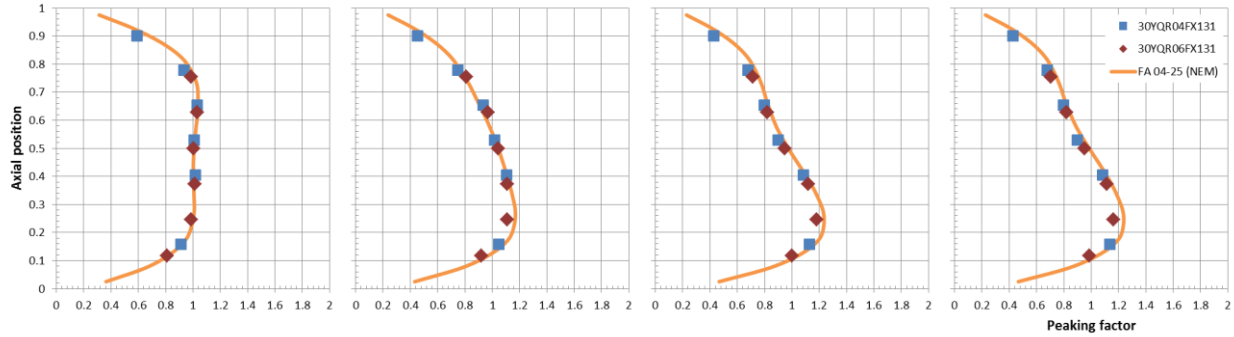

Figure E-50: Axial power profile for FA 131 (04-25) at 0, 45, 90 and 300 s. Data recorded by Kalinin 3 ICMS are shown with symbols — 30YQR04FX131, 30YQR06FX131 (LHR readings normalized to peaking factor).

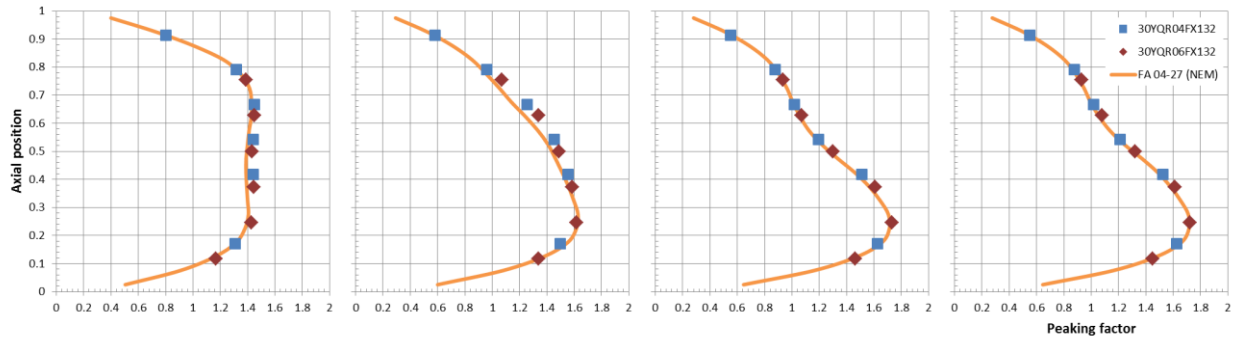

Figure E-51: Axial power profile for FA 132 (04-27) at 0, 45, 90 and 300 s. Data recorded by Kalinin 3 ICMS are shown with symbols — 30YQR04FX132, 30YQR06FX132 (LHR readings normalized to peaking factor).

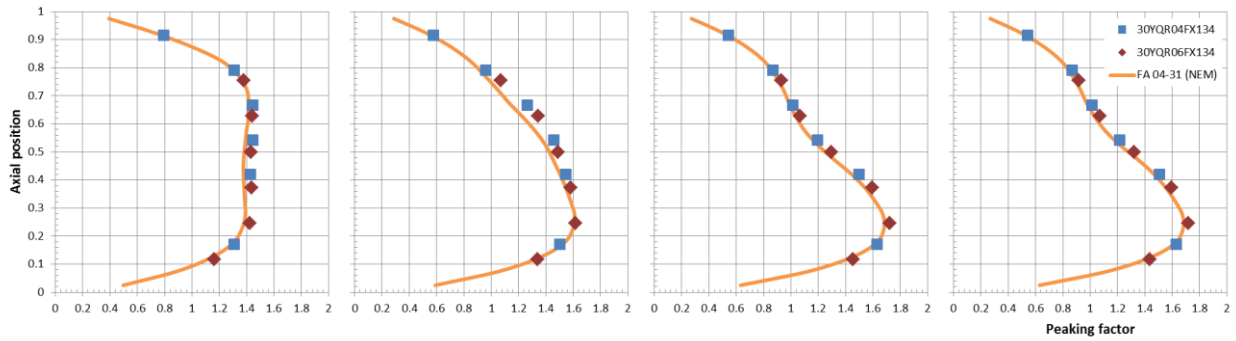

Figure E-52: Axial power profile for FA 134 (04-31) at 0, 45, 90 and 300 s. Data recorded by Kalinin 3 ICMS are shown with symbols — 30YQR04FX134, 30YQR06FX134 (LHR readings normalized to peaking factor).

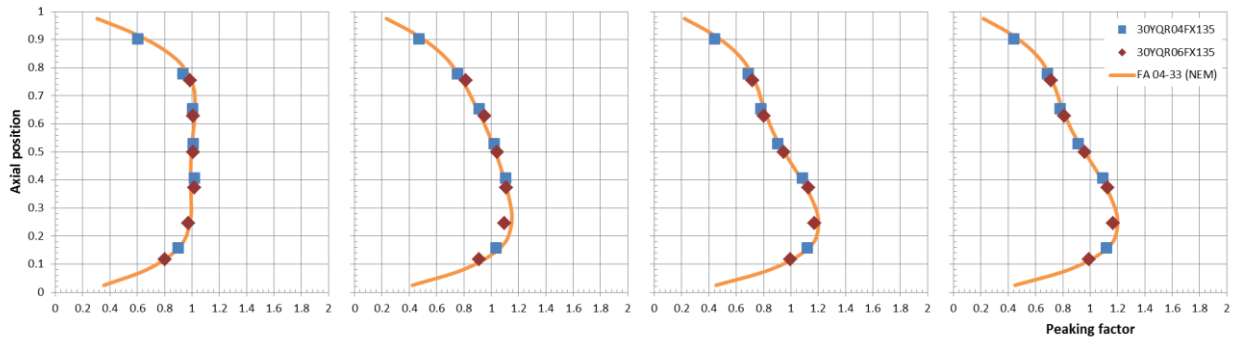

Figure E-53: Axial power profile for FA 135 (04-33) at 0, 45, 90 and 300 s. Data recorded by Kalinin 3 ICMS are shown with symbols — 30YQR04FX135, 30YQR06FX135 (LHR readings normalized to peaking factor).

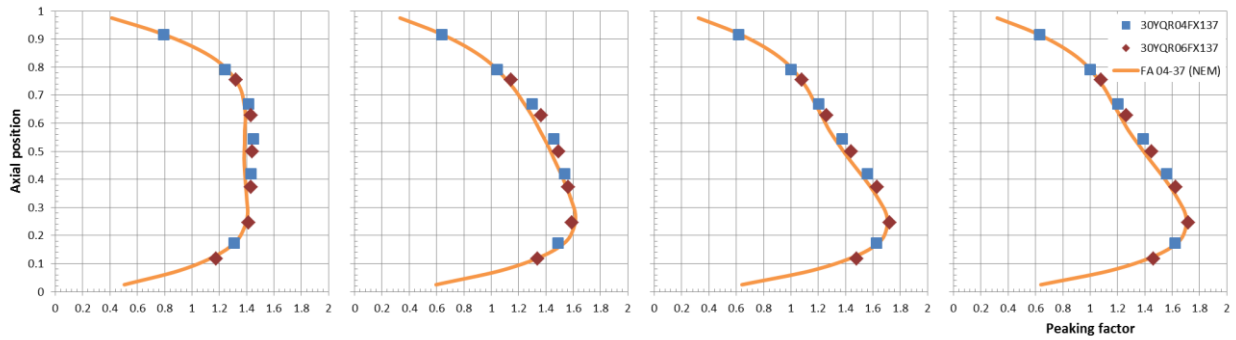

Figure E-54: Axial power profile for FA 137 (04-37) at 0, 45, 90 and 300 s. Data recorded by Kalinin 3 ICMS are shown with symbols — 30YQR04FX137, 30YQR06FX137 (LHR readings normalized to peaking factor).

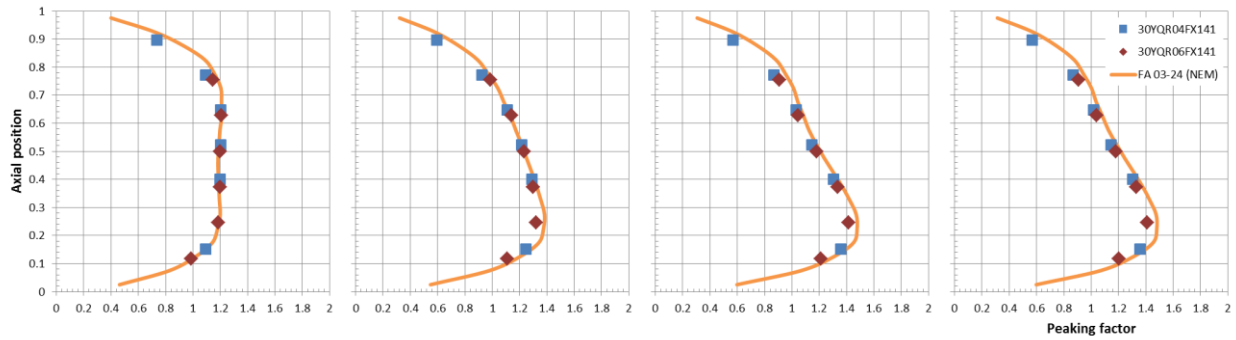

Figure E-55: Axial power profile for FA 141 (03-24) at 0, 45, 90 and 300 s. Data recorded by Kalinin 3 ICMS are shown with symbols — 30YQR04FX141, 30YQR06FX141 (LHR readings normalized to peaking factor).

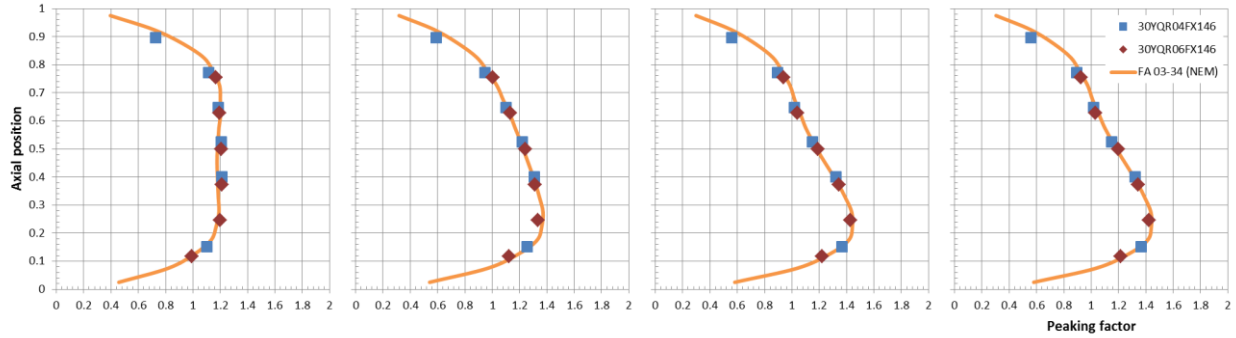

Figure E-56: Axial power profile for FA 146 (03-34) at 0, 45, 90 and 300 s. Data recorded by Kalinin 3 ICMS are shown with symbols — 30YQR04FX146, 30YQR06FX146 (LHR readings normalized to peaking factor).

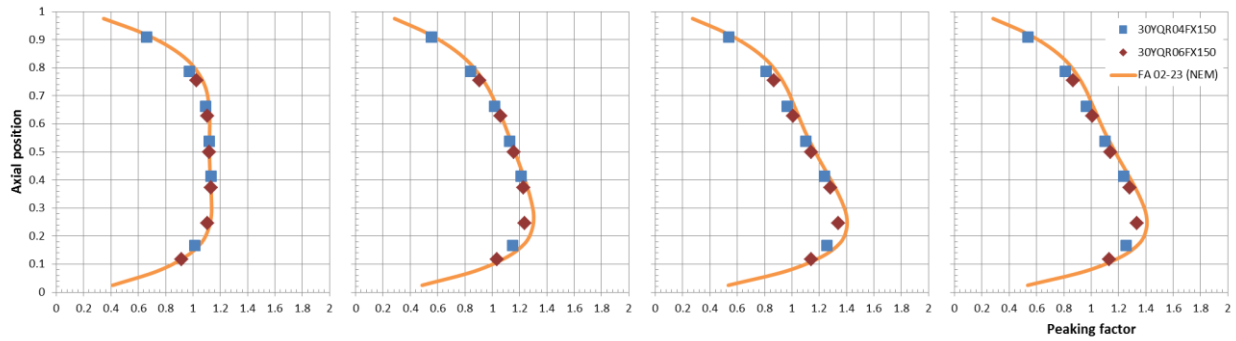

Figure E-57: Axial power profile for FA 150 (02-23) at 0, 45, 90 and 300 s. Data recorded by Kalinin 3 ICMS are shown with symbols — 30YQR04FX150, 30YQR06FX150 (LHR readings normalized to peaking factor).

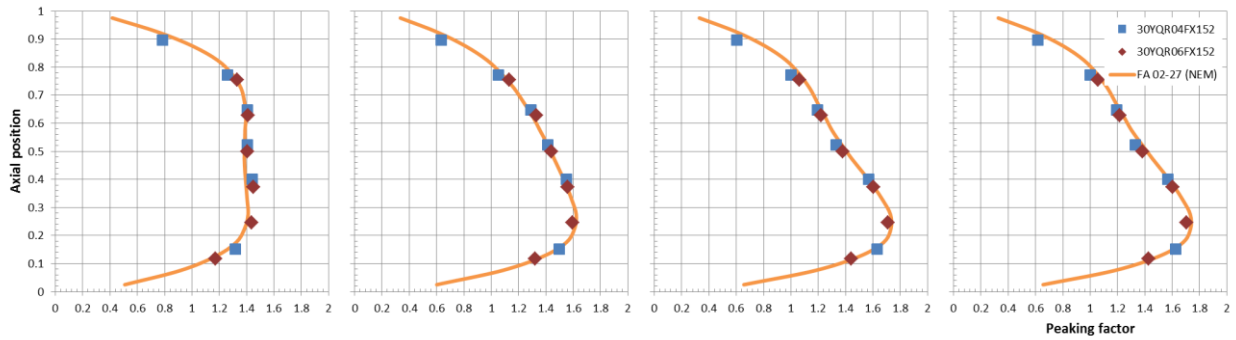

Figure E-58: Axial power profile for FA 152 (02-27) at 0, 45, 90 and 300 s. Data recorded by Kalinin 3 ICMS are shown with symbols — 30YQR04FX152, 30YQR06FX152 (LHR readings normalized to peaking factor).

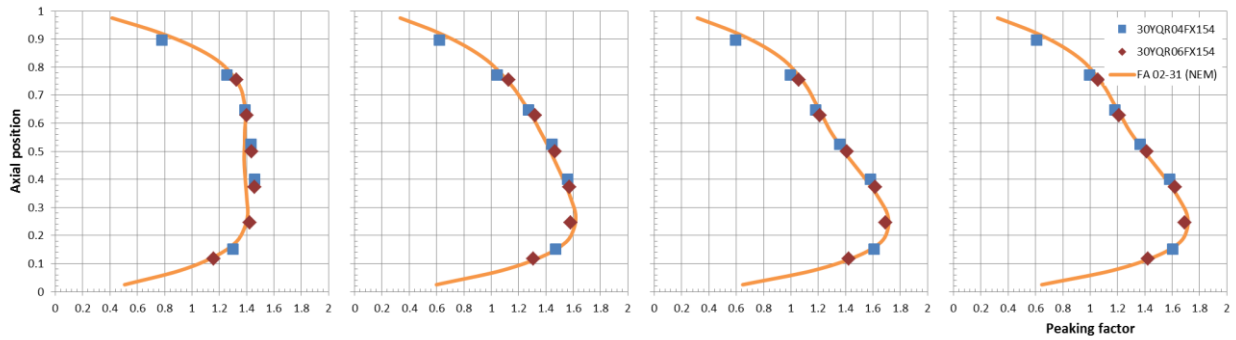

Figure E-59: Axial power profile for FA 154 (02-31) at 0, 45, 90 and 300 s. Data recorded by Kalinin 3 ICMS are shown with symbols — 30YQR04FX154, 30YQR06FX154 (LHR readings normalized to peaking factor).

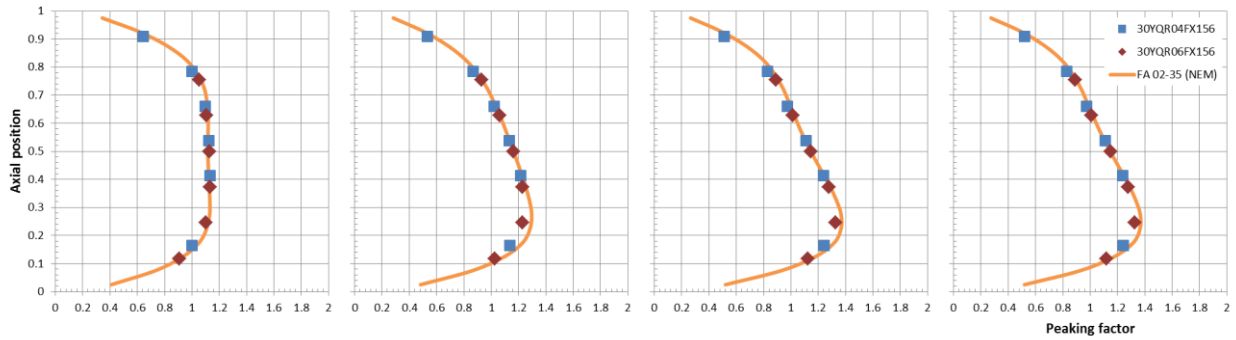

Figure E-60: Axial power profile for FA 156 (02-35) at 0, 45, 90 and 300 s. Data recorded by Kalinin 3 ICMS are shown with symbols — 30YQR04FX156, 30YQR06FX156 (LHR readings normalized to peaking factor).

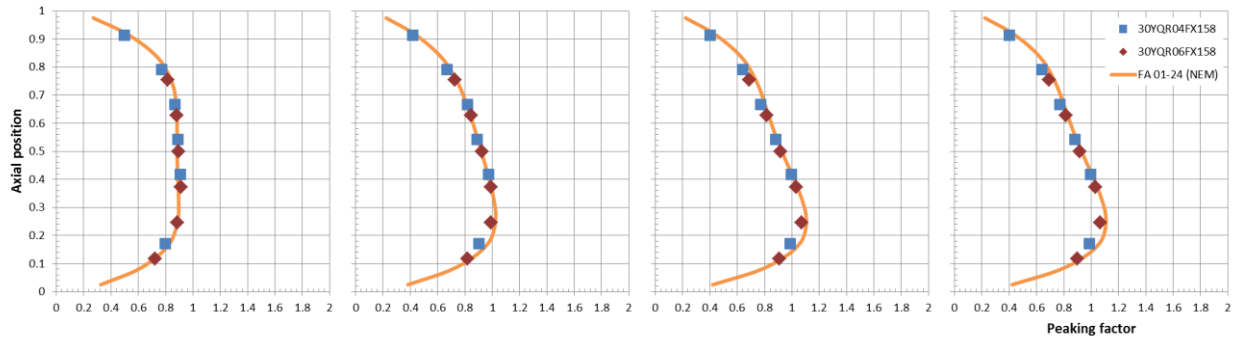

Figure E-61: Axial power profile for FA 158 (01-24) at 0, 45, 90 and 300 s. Data recorded by Kalinin 3 ICMS are shown with symbols — 30YQR04FX158, 30YQR06FX158 (LHR readings normalized to peaking factor).

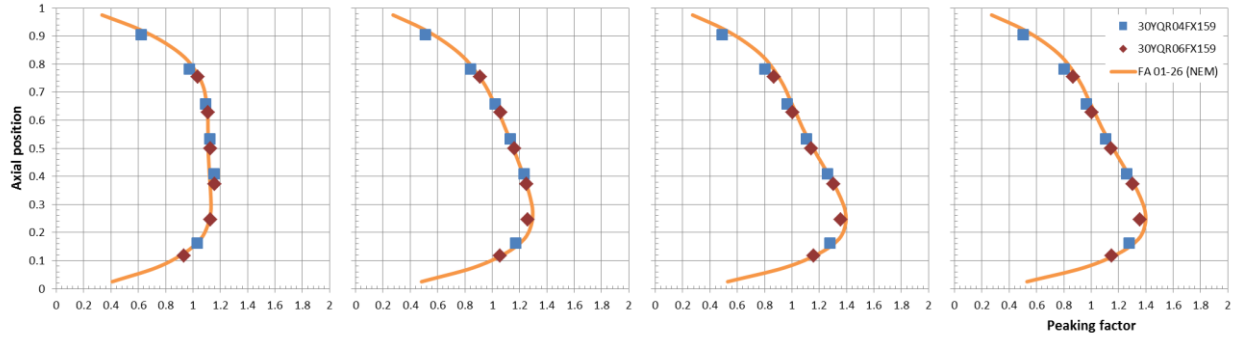

Figure E-62: Axial power profile for FA 159 (01-26) at 0, 45, 90 and 300 s. Data recorded by Kalinin 3 ICMS are shown with symbols — 30YQR04FX159, 30YQR06FX159 (LHR readings normalized to peaking factor).

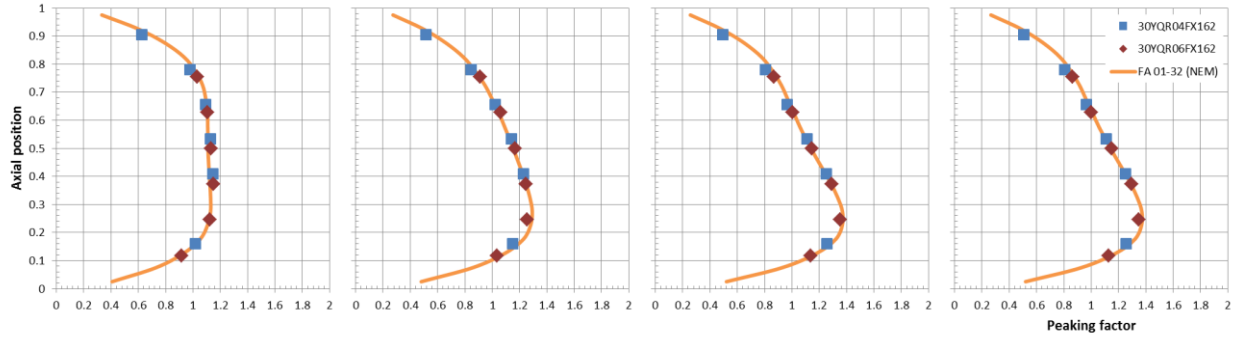

Figure E-63: Axial power profile for FA 162 (01-32) at 0, 45, 90 and 300 s. Data recorded by Kalinin 3 ICMS are shown with symbols — 30YQR04FX162, 30YQR06FX162 (LHR readings normalized to peaking factor).

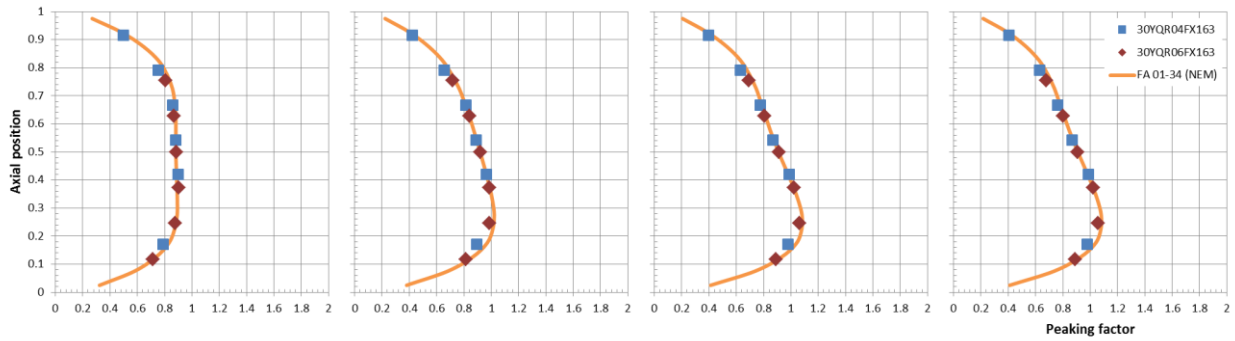

Figure E-64: Axial power profile for FA 163 (01-34) at 0, 45, 90 and 300 s. Data recorded by Kalinin 3 ICMS are shown with symbols — 30YQR04FX163, 30YQR06FX163 (LHR readings normalized to peaking factor).